Identification of a novel cold transduction mechanism in peripheral neurons

Buijs, Tamara

Awarding institution:
King's College London

Identification of a Novel Cold Transduction Mechanism in Peripheral Neurons

Tamara Joëlle Buijs

Thesis submitted to King's College London for the degree of Doctor of Philosophy

2018

Declaration

I declare that the research presented in this thesis is my own work, unless otherwise stated in the text.

Tamara Buijs
September 2018

Abstract

The main aim of this project was to identify the molecular basis of cold transduction in the somatosensory and sympathetic nervous systems. In sensory nerve endings, mechanisms for detecting temperature changes characterised to date depend on Transient Receptor Potential (TRP) ion channels. Temperature changes below 25-30°C are detected by the menthol-sensitive TRPM8 ion channel, but it remains unclear how lower temperatures are detected. Furthermore, the cold-sensitivity of the mustard-sensitive TRPA1 ion channel is a matter of strong debate. The sympathetic nervous system is also directly cold-sensitive but does not express TRPM8 and only expresses TRPA1 in ~3% of neurons, while cold-sensitivity is observed in ~50% of neurons. Therefore, another cold-sensitive mechanism must be present. To identify this mechanism, we used a ratiometric calcium imaging system to measure the responses of acutely dissociated sensory and sympathetic neurons to cold stimuli in the presence of various ion channel antagonists. Results show that members of the store-operated calcium channel family mediate the observed cold-induced calcium entry. Heterologous overexpression of STIM1/Orai1 revealed that these two proteins are sufficient to induce cold-sensitivity.

A second aim of this work was to determine the function of the cold-sensitivity of sympathetic neurons. The sympathetic nervous system is important in regulation of body temperature, and its ability to detect temperature directly may therefore play a role in thermoregulation. To achieve this aim, we used immunohistochemistry to identify expression of proteins associated with neurotransmitter pathways. Results show that nitric oxide synthase is expressed in these neurons. It is possible therefore that sympathetic nerves that innervate blood vessels may release nitric oxide after prolonged cold exposure to cause vasodilation and thus prevent frostbite. The third aim of this work was to develop a method for in vivo calcium imaging of sympathetic ganglia using mice that express genetically encoded calcium indicators to study the temperature sensitivity of sympathetic nerves in vivo. It was found that sympathetic ganglion neurons are spontaneously active and respond to body temperature changes. Overall, this thesis contributes to our understanding of cold transduction mechanisms for the purposes of both conscious temperature sensation and body temperature regulation.

“The beautiful thing about learning is nobody can take it away from you.”

B.B. King

Table of Contents

Table of Figures

Table of Tables

Acknowledgements

Foremost, I would like to express the deepest appreciation to my supervisor Prof. Peter McNaughton for his continued support, reassurance, and wisdom. I have greatly benefited from Peter's faith in my abilities and his optimism for the project, even when my own was waning. He has prepared me for an independent career in academia by encouraging me to formulate my own hypotheses, set up new techniques in the lab, and present my work at international conferences.

I am also grateful to Peter for giving me the opportunity to teach and to supervise the laboratory projects of Josh, Nairuti, and Mario. Similarly, I would like to thank all the academics that have employed me as a tutor on their courses: John Pizzey, Tim Rakow, Andy Grant, Ellie Dommett, Lawrence Moon, Reggie Docherty, Marian Huett, Jon Robbins, Isabella Gavazzi, Paul Francis, and Queelim Ch'ng. I can now proudly call myself an Associate Fellow of the Higher Education Academy.

I would not have been able to develop the *in vivo* Ca^{2+} imaging method presented in Chapter 6 without the help of Dr. Kim Chisholm. She is a pleasure to work with.

I also want to acknowledge Andy Grant, Niki Hamilton-Whitaker, and my colleagues in the McNaughton group for making suggestions when I presented my work in our lab meetings. Special thanks to Bruno for the many stimulating discussions we had about my data; I have thoroughly enjoyed our brainstorming sessions since you joined the project.

Finally, I would like to thank Peter and my second supervisor Prof. Marzia Malcangio for proofreading this thesis and a big thank you to Nat, Elin, Josep, and Andreas for keeping me sane throughout the writing process.

This work would not have been possible without the financial support of the Wellcome Trust, BBSRC, and Pfizer Inc.

List of Acronyms and Abbreviations

Abbreviation	Meaning
$[Ca^{2+}]_i$	Intracellular calcium concentration
˚C	Degree Celsius
µm	Micrometre
µM	Micromolar
2-APB	2-aminoethoxydiphenyl borate
4-AP	4-aminopyridine
A	Ampere
Ab	Antibody
ADP	Adenosine diphosphate
AITC	Allyl isothiocyanate AM Acetoxymethyl ester
ANKTM	Ankyrin repeat/transmembrane containing ion channel
ANO1	Anoctamin 1, calcium activated chloride channel
APTES	(3-Aminopropyl)triethoxysilane
ATP	Adenosine triphosphate
AVA	Arterio-venous anastomoses
BAT	Brown adipose tissue
BCTC	N-(4-tertiarybutylphenyl)-4-(3-cholorphyridin-2yl) tetrahydropyrazine-1(2H)-carbox- amide
BDNF	Brain-derived neurotrophic factor
BF	Brightfield
Ca^{2+}	Calcium
Ca_V	Voltage-gated calcium channel
CB	Canabinoid receptor
cDNA	complementary Deoxyribonucleic Acid
CGRP	Calcitonin-gene related peptide
ChAT	Choline acetyl transferase
CICE	Cold-induced Ca^{2+} entry
CIVD	Cold-induced vasodilation

CMFHBSS	Calcium- and magnesium-free Hank's balanced salt solution
CMH	C-fiber Mechano-Heat sensitive nociceptor
CNS	Central nervous system
CNTF	Ciliary neurotrophic factor
COX	Cyclooxygenase
DAG	Diacylglycerol
DAPI	4',6-diamidino-2-phenylindole
DBH	Dopamine-β-Hydroxylase
DH	Dorsal horn
DMEM	Dulbecco's modified eagle medium
DMH	Dorsomedial hypothalamus
DMSO	Dimethyl sulfoxide
DNA	Deoxyribonucleic acid
dNTP	Deoxyribonucleotide triphosphate
DPBS	Dulbecco's phosphate buffered saline
DPX	Distrene, Plasticisier, Xylene
DRG	Dorsal root ganglia
dTRP	Drosophila Transient Receptor Potential
EC50	Half maximal effective concentration
EDTA	Ethylenediaminetetraacetic acid
EGFP	Enhanced Green Fluorescent Protein
ER	Endoplasmic reticulum
F	Faraday's constant 9.65 x 10^4 s A/mol
FBS	Fetal bovine serum
FGF	Fibroblast growth factor
GABA	Gamma-aminobutyric acid
GDNF	Glial cell line derived neurotrophic factor
GFP	Green fluorescent protein
GLUT	Vesicular glutamate transporter
GPCR	G-protein coupled receptor
GTP	Guanosine Triphosphate

H&E	Haematoxylin and eosin
HBSS	Hank's balanced salt solution
HCl	Hydrogen chloride
HCN	Hyperpolarization-Activated Cyclic Nucleotide-modulated channel
HCN2	HCN channel 2
HEK293	Human embryonic kidney 293 cell line
HEPES	4-(2-hydroxyethyl)-1-piperazineethanesulfonic acid
I	Current
IB4	Isolectin B4
IC50	Half maximal inhibitory concentration
IL	Interleukin
IML	Intermediolateral nucleus
IMS	Industrial methylated spiril
IP	Intraperitoneal
IP_3	Inositol trisphosphate
I-V	Current-voltage
K^+	Potassium
K2P	Two-pore domain potassium channel
KCl	Potassium chloride
KCNQ	Voltage-gated potassium channel
kD	Kilo Dalton
K_d	Dissociation constant
KH_2PO_4	Potassium dihydrogen phosphate
K_{ir}	Inward-rectifier potassium channel
KO	Knockout
K_V	Voltage-gated potassium channel
L	Litre
LPBd	Dorsal subnucleus of lateralparabrachial nucleus
LPBel	External lateral subnucleus of lateralparabrachial nucleus
M	Molar
ML204	4-Methyl-2-(1-piperidinyl)quinoline

MnPO	Median preoptic nucleus
mol	Mole
MPO	Medial preoptic area
mRNA	Messenger Ribonucleic Acid
n	Amount of solute in moles
Na^+	Sodium
Na_2HPO_4	Sodium hydrogen phosphate
NaCl	Sodium chloride
NADH	Reduced Nicotinamide adenine dinucleotide
$NaHCO_3$	Sodium carbonate
NANC	Non-adrenergic non-cholinergic
NaOH	Sodium hydroxide
Na_v	Voltage-activated sodium channel
NCKX	Na/Ca-K exchanger
NCX	Na^+/Ca^{2+} exchanger
NFCI	Non-freezing cold injury
NGF	Nerve growth factor
nM	Nanomolar
nNOS	Neuronal nitric oxide synthase (NOS1)
NO	Nitric oxide
nSOCE	Neuronal SOCE
NT	Neurotrophic factor
P	Postnatal day (age)
pA	Picoampere
PBS	Phosphate buffered saline
PC	Paravertebral Chain
PC12	Rat adrenal pheochromocytoma 12 cells
PCa/PNa	Permeability of calcium / permeability of sodium
PCR	Polymerase chain reaction
PFA	Paraformaldehyde
PGE	Prostaglandin E
pH	Per Hydrogen

PI3K	Phosphatidylinositol-3-kinase
PIP2	Phosphatidylinositol 4, 5-bisphosphate
PKA	Protein kinase A
PKC	Protein kinase C
PLA2	Phospholipase A2
PLC	Phospholipase C
PMA	Phorbol, 12-myristate, 13-acetate
PMCA	Plasma membrane calcium ATPase
PMT	Photo-Multiplier tube
PNS	Peripheral nervous system
POAH	Preoptic/anterior hypothalamus
PPAR-γ	Peroxisome proliferator-activated receptor-γ
PPG	Pterygopalatine ganglion
PTK	Protein Tyrosine Kinase
Q_{10}	The change in current resulting from a 10˚C change in temperature for a given ion channel
qPCR	Quantitative polymerase chain reaction
r	Radius
RA	Retinoic acid
rMR	rostral medullary raphe region
RNA	Ribonucleic Acid
ROI	Region of interest
ROS	Reactive oxygen species
RPM	Revolutions per minute
RT-qPCR	Reverse transcription quantitative polymerase chain reaction
RTX	Resiniferatoxin
SARAF	SOCE-associated regulatory factor
SCG	Superior cervical ganglion
SCG	Superior cervical ganglion
SD	Standard deviation
SDS	Sodium dodecyl sulphate

SDS-PAGE	SDS Polyacrylamide Gel Electrophoresis
SEM	Standard Error of the Mean
SG	Stellate ganglion
shRNA	Short hairpin RNA
siRNA	Small Inhibitory Ribonucleic Acid
SP	Substance P
Src	Sarcoma Kinase
STIM	Stromal interaction molecule
TALK	TWIK-related alkaline-activated K^+ channel
TASK	TWIK-related acid-sensitive K^+ channel
TEA	Tetraethylammonium
TG	Trigeminal ganglia
TH	Tyrosine hydroxylase
THIK	TWIK-related halothane-inhibited K^+ channel
TIFF	Tagged image file format
TM	Trans-membrane domain
TNF-α	Tumor necrosis factor α
TREK	TWIK-related K^+ channel
TRESK	TWIK-related spinal cord K^+ channel
TRP	Transient receptor potential
TRPA	Transient receptor potential ankyrin
TRPA1	TRP, subfamily Ankyrin 1
TRPC	TRP, subfamily Canonical
TRPC5	Transient Receptor Potential Canonical 5
TRPM	TRP, subfamily Melastatin
TRPM2	Transient Receptor Potential Melastatin 2
TRPM3	Transient Receptor Potential Melastatin 3
TRPM4	Transient Receptor Potential Melastatin 4
TRPM6	Transient Receptor Potential Melastatin 6
TRPM8	Transient Receptor Potential Melastatin 8
TRPV	TRP, subfamily Vanilloid
TRPV1	Transient Receptor Potential Vanilloid Channel 1

TRPV2	Transient Receptor Potential Vanilloid Channel 2
TRPV3	Transient Receptor Potential Vanilloid Channel 3
TRPV4	Transient Receptor Potential Vanilloid Channel 4
TTX	Tetrodotoxin
TWIK	Two-pore domain weak inwardly rectifying K^+ channel
UCP1	Uncoupling Protein 1
UV	Ultraviolet V
Vm	Membrane potential
VR1	Vanilloid receptor; TRPV1
WT	Wild type
z	Ionic charge
π	Pi constant = 3.14

Chapter 1 Introduction

All biological processes are affected by temperature and it is therefore crucial for animals to regulate the temperature of their bodies. Beside thermoregulating, animals also need to avoid noxious temperatures to prevent tissue damage. Especially low temperatures that cause water to freeze and form ice crystals that can pierce cells, and high temperatures that cause denaturation of proteins and chemical instability, need to be avoided.

Warm-blooded endotherms such as mammals maintain a stable elevated body temperature by regulating metabolic mechanisms, whereas cold-blooded ectotherms such as reptiles generate less heat and are more dependent on their environment for thermoregulation (Tattersall *et al.*, 2012). This makes the body temperature of reptiles variable (poikilothermic) while most larger mammals carefully maintain their body temperature within 0.5˚C of 37˚C (homeothermic), independent of environmental temperature, by using their autonomic nervous system (Ivanov, 2006). It has been estimated that almost 50% of mammalian energy expenditure is dedicated to thermoregulation alone (Landsberg, 2012). In both cases the ability of an animal to sense the temperature of its environment and to regulate its internal temperature is critical for direct survival and reproductive success (Horowitz *et al.*, 2015).

Animals need to be able to detect the environmental temperature so that they can remain in their thermoneutral zone to ensure an optimal functioning of the biochemical and physiological processes in their bodies. The thermoneutral zone is the external temperature range at which an animal can keep its body temperature stable without regulatory changes in metabolic heat production or evaporative heat loss. It varies per animal, as they are adapted to adverse environmental conditions common to their habitat. For a naked, resting human, the thermoneutral zone is 26 – 36°C (Silva, 2006).

To achieve a stable body temperature, temperature is sensed by peripheral and visceral thermosensors and relayed to the hypothalamus, which is thought to compare the input to its set point of 37˚C using local thermosensors, and will regulate the temperature of the body accordingly by promoting either thermogenesis or heat loss (Morrison, 2011).

In this introductory chapter, we will review what is currently known about thermosensation and thermoregulation, with a focus on cold transduction and cold defence mechanisms.

1.1 Thermoregulation

Humans, like most mammals, are homeothermic. This means that we keep our body temperature constant, using the vital homeostatic function of thermoregulation.

There are two main types of thermoregulation: conscious behavioural thermoregulation and subconscious thermoregulation, which is executed by the autonomic nervous system. Behavioural thermoregulation is primarily based on conscious perception of skin temperature and is the first response in line due to the speed, low energy expenditure, and minimal water loss required. Thermoregulatory behaviours in animals include huddling together in a group and moving into the shade. Humans can choose from a wider range of behavioural thermoregulatory responses ranging from turning on the air conditioning system to drinking a hot beverage. Since behavioural thermoregulation is a voluntary response, the neural pathways associated with it are complex and not yet understood (Romanovsky 2007).

Like many homeostatic processes, subconscious thermoregulation is controlled by the hypothalamus in the brain. The hypothalamus receives information about core and skin temperature and controls how much heat is lost and generated by the body. When body temperature drops, it can be increased in several ways, such as activation of skeletal muscle (shivering), and constriction of the cutaneous vasculature to conserve heat (vasoconstriction). To decrease body temperature, sweat glands are activated to cause evaporative heat loss, and arteries in the skin dilate to increase heat dissipation (Romanovsky 2007). These processes waste a lot of energy (shivering) or dehydrate the body (sweating), whereas constriction and dilation of blood vessels carry little bodily cost. This is carried out solely by the sympathetic division of the autonomic nervous system, as the parasympathetic division does not innervate the cutaneous vasculature (Guidry and Landis, 2000) as shown in Figure 1.

Thermoregulation requires energy expenditure and therefore food intake, especially in low environmental temperatures. However, food is not always available in cold habitats. Therefore, some mammals (heterotherms) reduce their metabolic rate substantially to enter a state of torpor or hibernation in these conditions. In these states body temperature is intentionally decreased such that thermoregulation requires less energy and energy conservation is maximised in cold environments (Geiser, 2004).

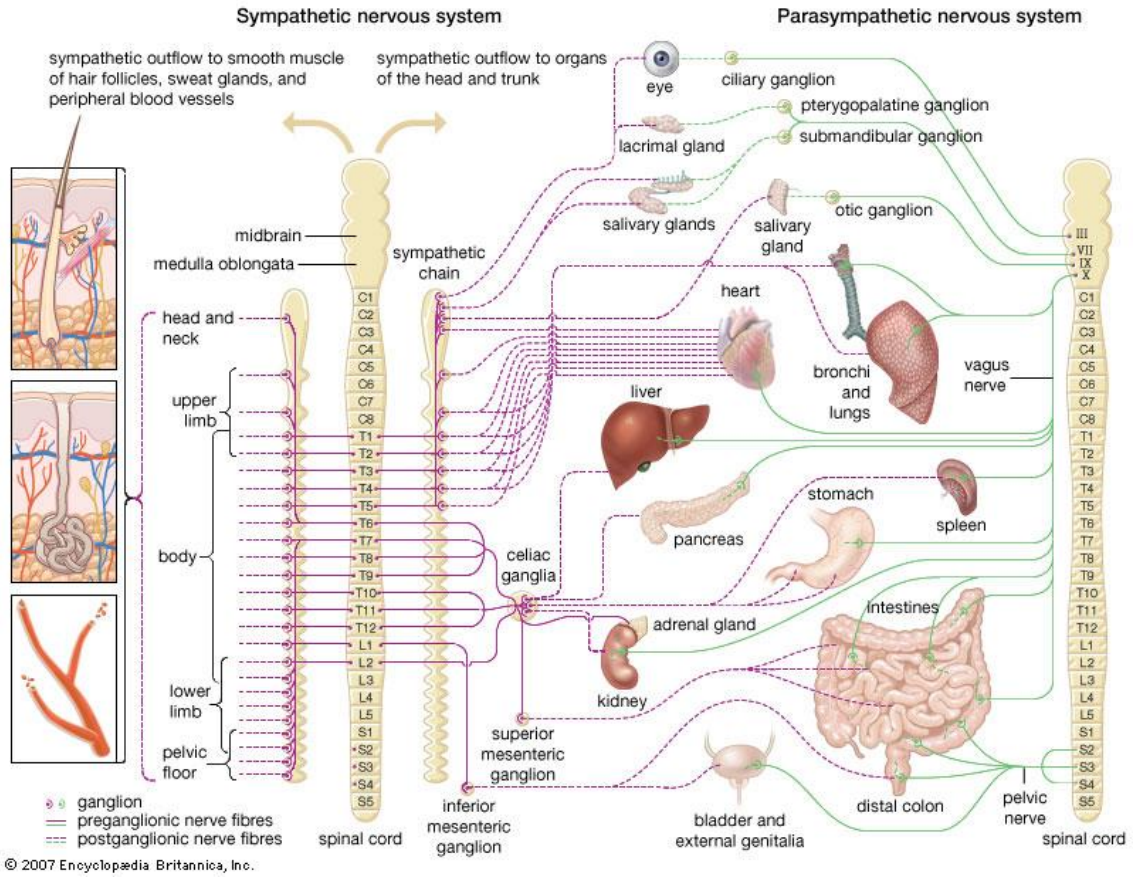

Figure 1 Schematic depiction of the autonomic nervous system.
The sympathetic (purple) and parasympathetic (green) branches of the autonomic nervous system innervate the viscera. The smooth muscle of hair follicles, sweat glands, and peripheral blood vessels is exclusively innervated by the sympathetic branch for the thermoregulatory purposes of piloerection, sweating, and vasoconstriction respectively. Figure from www.britannica.com/science/thermoreception/media/591718/119698.

1.1.1 The Sympathetic Nervous System

The sympathetic nervous system consists of pre- and postganglionic neurons. The cholinergic preganglionic neurons, whose cell bodies are located in the intermediolateral column of the spinal cord, synapse in the sympathetic ganglia, where they release acetylcholine onto the noradrenergic postganglionic neurons. The sympathetic ganglia start in the neck, and continue down alongside the vertebra as the 'paravertebral chain ganglia' (McCorry, 2007). The first sympathetic ganglion is called the superior cervical ganglion (SCG) and innervates the head and neck. The inferior cervical ganglion and upper thoracic ganglion are often fused to form the stellate ganglion (SG), which innervates the heart, brown adipose tissue, and upper limbs (Morrison, 2004; Narouze, Vydyanathan and Patel, 2007).

Postganglionic sympathetic neurons are mostly noradrenergic in nature. A small proportion are cholinergic sudomotor neurons that innervate sweat glands. The connective tissue around bones called the periosteum is also innervated by cholinergic

neurons (Apostolova and Dechant, 2009). Around half of the SCG neurons are vasomotor neurons, meaning that they innervate blood vessels.

There are species-specific differences in the sympathetic innervation of the vasculature, for example, cats and dogs have cholinergic fibres that cause vasodilation in the limb muscle vasculature, but rats and mice do not (Guidry and Landis, 2000). Similarly, cholinergic cutaneous vasodilator neurons are exclusive to humans (Smith and Johnson, 2016). Around 1% of postganglionic sympathetic neurons have a glutamatergic phenotype and have a similar gene expression pattern to sensory neurons (Furlan *et al.*, 2016).

1.1.2 Cold-Sensitivity of Sympathetic Nerves

Preganglionic sympathetic fibres of the rat that form the splanchnic nerve fire spontaneous rhythmic discharges which can be inhibited by temperatures below 16°C (Su and Su, 2013). In contrast, postganglionic sympathetic neurons of the mouse can be directly activated by cold below 16°C (Smith *et al.*, 2004; Munns, AlQatari and Koltzenburg, 2007). Sympathetic ganglia isolated from rat, guinea pig, rabbit, and dog are also directly cold-activated (Alkadhi, 2008).

Around 60% of mouse sympathetic neurons express a cold-sensitive ion channel whose activation results in an influx of Ca^{2+}. The channel is not activated by agonists of the proposed Transient Receptor Potential (TRP) ion channel cold sensors TRPM8 (menthol) or TRPA1 (mustard oil) and cannot therefore be either TRPM8 or TRPA1 (Munns, AlQatari and Koltzenburg, 2007). We will aim to identify the molecular basis of this cold-induced Ca^{2+} influx in Chapter 3.

1.1.3 Current Consensus Model of Thermoregulation

Rodents are a relevant model of human thermoregulation, because they show the same thermal reflex responses and use the same thermal effectors as humans, except for sweating. In the mouse, evaporative heat loss is achieved via activation of the salivary glands and a behavioural response that involves licking of the fur (Morrison 2016). Mice do sweat from their footpads (Anderson, Bergner and Murphy, 2006), which may function to increase the grip of their paws when running away and could be used as a model of human sweating.

The study of rodents has led to the formation of the current consensus model of thermoregulation depicted in Figure 2. Skin temperature is sensed by the nerve endings of first-order DRG neurons, which synapse onto second-order neurons in the dorsal horn. Information about warmth and coolness are kept separately as "labelled lines" represented by the orange and blue lines respectively. These neurons then synapse onto third-order neurons located in the lateral parabrachial nucleus. Here the information is transmitted to the preoptic area by glutamatergic neurons.

Neurons carrying information about warmth (orange) inhibit glutamatergic interneurons (dark green) in the median preoptic subnucleus (MnPO), which excite warm-sensitive neurons in the medial preoptic area (MPA). In contract, neurons carrying information about coolness (blue) excite GABAergic interneurons (red) in the MnPO, which then inhibit warm-sensitive neurons in the MPA.

For cutaneous vasoconstriction (CVC), warm-sensitive neurons cease to inhibit sympathetic premotor neurons in the rostral raphe pallidus, which are tonically excited by the MnPO (dotted light green). The premotor neurons then activate sympathetic preganglionic neurons (green), which synapse onto sympathetic postganglionic neurons that innervate blood vessels (red).

For brown adipose tissue (BAT) thermogenesis, inhibition of warm-sensitive neurons switches off inhibition of neurons in the dorsomedial hypothalamus and dorsal hypothalamic area (DMH/DA), which are tonically excited by the MnPO (dotted light green). These neurons then activate sympathetic premotor neurons, which synapse onto sympathetic preganglionic neurons in the intermediolateral nucleus (IML) of the spinal cord. These neurons activate sympathetic postganglionic neurons (orange) that innervate BAT.

For shivering thermogenesis, inhibition of warm-sensitive neurons switches off inhibition of neurons in the DMH/DA, which are tonically excited by the MnPO (dotted light green). These neurons then activate premotor neurons in the rostral raphe pallidus (rRPa), which synapse onto alpha and gamma motor neurons (blue) in the ventral horn (VH) of the spinal cord that innervate skeletal muscle.

In fever states, prostaglandin E2 (PGE_2) can inhibit warm-sensitive neurons in the MPA directly to activate cold defence mechanisms.

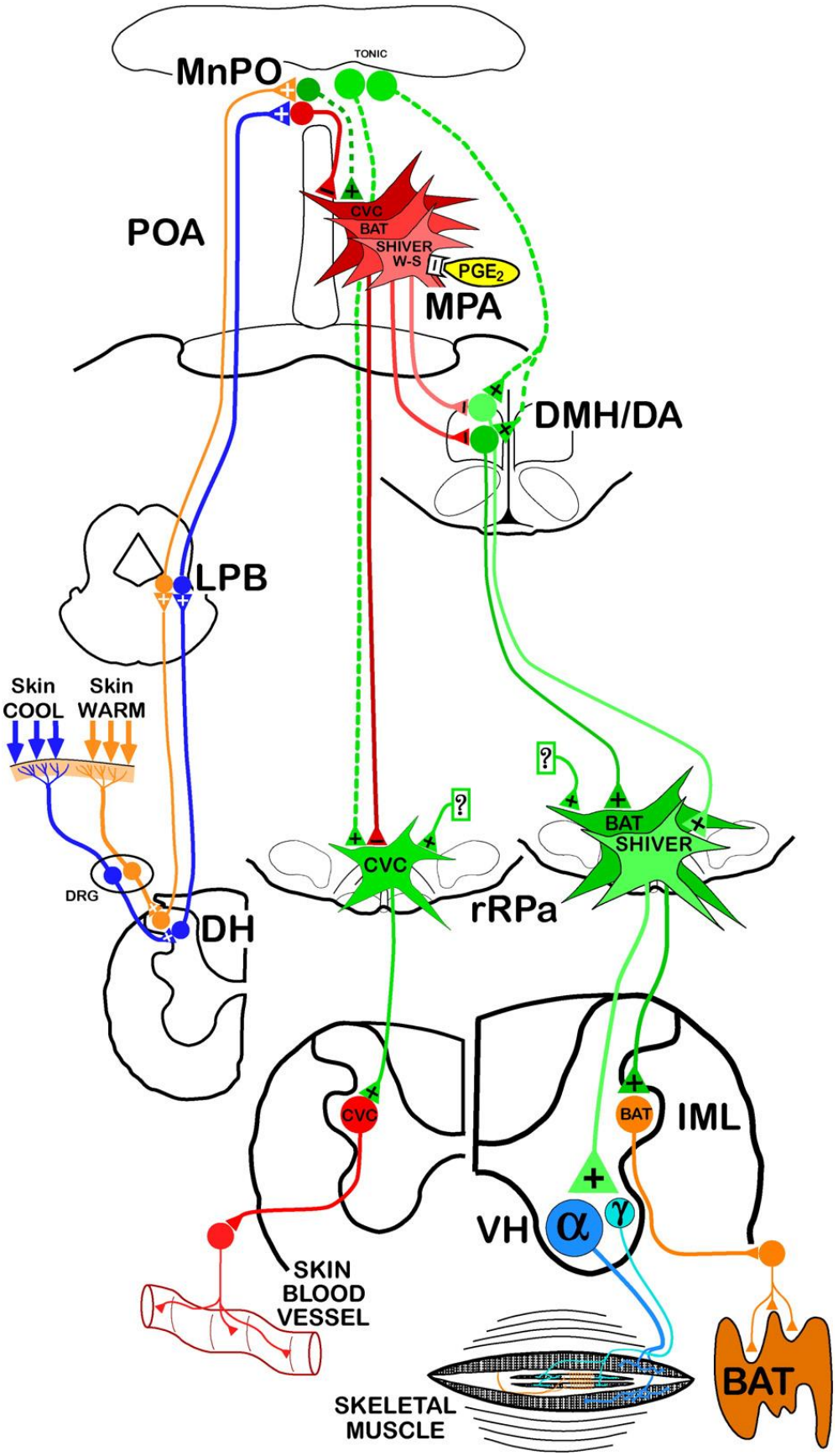

Figure 2 Current consensus model of thermoregulation.
DRG = Dorsal Root Ganglion; DH = Dorsal Horn; LPB = Lateral Parabrachial Nucleus; POA = PreOptic Anterior Hypothalamus; MnPO = Median PreOptic Subnucleus; CVC = Cutaneous VasoConstriction; BAT = Brown Adipose Tissue; W-S = Warm-Sensitive Neurons; PGE_2 = ProstaGlandin E_2; MPA = Medial Preoptic Area; DMH/DA = dorsomedial hypothalamus and dorsal hypothalamic area; rRPA = rostral raphe pallidus; IML = intermediolateral nucleus; γ = gamma motorneurons; α = alpha motorneurons; VH = Ventral Horn. Figure from Morrison (2016).

1.1.4 Thermosensation for the Purpose of Thermoregulation

Information about body temperature comes from cutaneous, visceral, and central thermoreceptors. Thermosensory afferents express ion channels, whose ionic conductance is temperature-dependent, and thus transduce thermal information. Higher-order neurons that transmit this information to the brain also express thermosensors themselves and may integrate this information about local temperature with the information about peripheral temperature to provide an optimal thermoregulatory response. For example, second-order neurons located in lamina I of the dorsal horn of the spinal cord that transmit information about temperature also respond linearly to local heat and cold themselves, irrespective of peripheral input from cutaneous thermosensors (Craig, 2003).

1.1.5 Heat defence mechanisms

Under normothermic conditions, heat production and dissipation are in balance. An increase of ambient temperature or internal heat production due to metabolism or exercise results in hyperthermia. To protect themselves from hyperthermia, endothermic mammals employ two mechanisms of heat dissipation: convection *via* cutaneous vasodilation, and evaporation *via* sweating, salivation, or panting. A brief overview of these autonomic responses to hyperthermia will be presented here.

1.1.5.1 Evaporative Heat Loss

Mammals use a variety of strategies to achieve evaporative heat loss. Cooling via wet body surfaces is mediated by sweating in mammals such as humans and horses, and salivation combined with fur licking behaviour in mammals such as mice and kangaroos or combined with increased breathing rate (panting) in mammals such as dogs and sheep.

In humans, sweating is mediated by signals from the hypothalamus to sympathetic postganglionic cholinergic sudomotor nerves with periglandular nerve endings that release ACh onto M3 muscarinic receptors on eccrine sweat glands (Uno, 1977). Several co-transmitters have been proposed, including adenosine triphosphate (ATP), vasoactive intestinal peptide (VIP), calcitonin gene-related peptide (CGRP), nitric oxide (NO), galanin, and NA, but their roles in the sweat response are not fully understood. The amount of sweat released in response to sympathetic stimulation

depends on the density of sweat glands in the skin. There is great regional variation of sweat gland density, with the highest density observed on the forehead and lower back in humans (Smith and Johnson, 2016).

The primary driver of evaporative heat loss is brain temperature (Vanbeaumont and Bullard, 1965; Nadel, Bullard and Stolwijk, 1971; Smiles, Elizondo and Barney, 1976; DiPasquale, Buono and Kolkhorst, 2003; Shibasaki, Wilson and Crandall, 2006). Additionally, local heating contributes to sweating in three ways. Mild warming <40˚C of the skin increases sweat production via increased release of ACh by the sudomotor nerve and sensitivity of the sweat gland (Bullard, Banerjee and Mac Intyre, 1967; MacIntyre *et al.*, 1968; Ogawa, 1970; Ogawa and Asayama, 1986; Ogawa and Sugenoya, 1993). Local heat >42˚C directly activates sweat glands independent of cholinergic activation (Isekutz, Hetenyi and Diosy, 1950; Lloyd, 1961). Local sudomotor axon reflexes also enhance sweating via activation of presynaptic muscarinic receptors, which evoke antidromic action potentials that recruit the other branches of the nerve and activate other sweat glands nearby (Namer *et al.*, 2004; Illigens and Gibbons, 2009).

1.1.5.2 Development of Sudomotor Neurons

The development of the sympathetic nervous system continues after birth and functional neurotransmission is not observed until postnatal week two in the rat (Hirst and McLachlan, 1984). Sudomotor nerves switch from a noradrenergic to a cholinergic phenotype during postnatal development (Cane and Anderson, 2009). When noradrenergic sudomotor neurons synapse onto sweat glands, they release noradrenaline, which causes the sweat glands to release growth factors such as ciliary neurotrophic factor (CNTF), leukaemia inhibitory factor (LIF), and glial cell line-derived neurotrophic factor (GDNF). This then converts the chemical phenotype of the sympathetic neurons from noradrenergic to cholinergic (Loy *et al.*, 2011). However, in primates, these neurons continue to express noradrenaline-synthesising enzymes (Weihe *et al.*, 2005). It is unknown whether this is also the case in mice. We will explore this in Chapter 2.

1.1.5.3 Cutaneous Vasodilation

There are two types of cutaneous vasodilation. Passive vasodilation is caused by a reduction in vasoconstrictor nerve activity, which results in vasodilation because of ongoing NO release from vascular endothelial cells, while active vasodilation is under control of sympathetic cholinergic vasomotor nerves (Smith and Johnson, 2016). NO is a gaseous intercellular messenger that freely diffuses into the smooth muscle cells of the vascular wall, where it binds to soluble guanylyl cyclase (GC). Soluble GC then synthesises the second messenger cyclic guanosine monophosphate (cGMP) resulting in smooth muscle relaxation and vasodilation (Arnold *et al.*, 1977).

The existence of active neurogenic vasodilation mediated by ACh and co-transmitters has been controversial but is now believed to be unique to human hairy skin (Smith and Johnson, 2016). This makes evolutionary sense, considering that human skin is not covered in fur and therefore better suited to mediate heat dissipation than the skin of furry mammals such as dogs. Furthermore, humans use sweating to dissipate heat and the same nerve may innervate both the cutaneous vasculature and eccrine sweat glands. Active vasodilation and sweating are possibly activated by the same nerve, because the sweat response cannot occur in isolation. It requires both the increased heat from vasodilation to ensure sweat evaporation and the increased blood plasma availability to produce the necessary fluid component of sweat (Smith and Johnson, 2016). Moreover, patients with congenital anhidrotic ectodermal dysplasia do not exhibit active vasodilation and their skin completely lacks eccrine sweat glands (Brengelmann *et al.*, 1981). This can be explained by the fact that cholinergic neurons are dependent on factors released from sweat glands to become cholinergic, as discussed previously.

In humans, cholinergic vasodilator nerves can greatly increase skin blood flow. Under normothermic conditions, total skin blood flow ranges from 250 to 500 mL/min, but can be increased to 7 L/min during extreme heat stress (Johnson, Minson and Kellogg, 2014). Vasodilation is mediated by cholinergic nerves, but release of ACh alone is not enough to achieve the full vasodilation response observed in conditions of heat stress (Kellogg *et al.*, 2007). Possibly ACh is released in combination with co-transmitters such as VIP or NO. VIP is expressed in cholinergic nerve endings and microdialysis of a VIP antagonist resulted in a 42% reduction of hyperthermia-induced vasodilation (Kellogg *et al.*, 2010). However, cystic fibrosis patients - whose nerves lack VIP - exhibit normal

vasodilatory responses to whole body heating (Kellogg *et al.*, 2007). Further studies are needed to fully elucidate the role of VIP in active vasodilation.

NO has been implicated in activate vasodilation in several studies (Kellogg, Johnson and Kosiba, 1989; Kimura *et al.*, 2013). Some found that neuronal sources of NO are responsible (Kellogg, Zhao and Wu, 2008), whereas others found that endothelial NO is the main contributor to vasodilation (Mcnamara *et al.*, 2014). Further studies are needed to fully elucidate the role of NO in active vasodilation.

1.1.6 Cold Defence Mechanisms

Since the body temperature of endotherms is usually higher than the ambient temperature, most thermoreceptors are involved in sensing cold and most thermoeffector organs trigger cold defence mechanisms (Morrison, 2016). We will now review the mechanisms employed by the body to protect itself from hypothermia, in order of increasing energy cost.

1.1.6.1 Cutaneous Vasoconstriction (CVC)

When ambient cold causes the temperature of the body to drop below its set point, cutaneous vasoconstriction (CVC) is the first line of defence. In rodents, the main body part responsible for CVC is the hairless tail (Rand, Burton and Ing, 1965). Humans exhibit CVC throughout their extremities.

The thermoregulatory centre in the hypothalamus will signal to glutamatergic and serotonergic premotor neurons in the rRPa and parapyramidal (PaPy) regions of the ventromedial medulla to excite preganglionic sympathetic neurons in the IML of the thoracolumbar spinal cord, which in turn excite postganglionic sympathetic vasomotor nerves to release NA and neuropeptide Y (NPY) and increase CVC (Morrison 2016). This will reduce the amount of blood flow and consequently heat dissipation from the skin and result in a net increase in body temperature due to conservation of metabolic heat production in the body core.

CVC is mediated by noradrenergic neurons that release noradrenaline onto α adrenoceptors of smooth muscle cells in the blood vessel walls of cutaneous blood vessels and arteriovenous anastomoses (AVAs). AVAs are blood vessels linking arterioles and venules in the skin whose constriction and/or activation has a large effect on skin blood flow as they control blood flow to the capillary beds (Figure 3). AVAs contain smooth

muscle that is heavily innervated by the sympathetic nervous system. A recent study has shown that TRPA1 is involved in cutaneous vasoconstriction by activating NA release through an unknown mechanism and increasing reactive oxygen species (ROS), which increase vasoconstriction *via* a phosphorylated myosin light chain (MLC) induced increase in Ca^{2+} (Aubdool *et al.*, 2014).

Vascular smooth muscle also expresses some β2 adrenoceptors, which can cause muscle relaxation and vasodilation when activated by NA, but these receptors are greatly outnumbered by α adrenoceptors in the cutaneous vasculature, so the vasodilatory effect is negligible (Conti *et al.*, 2013).

At normothermic body temperature, sympathetic nerve fibres constantly release NA onto resistance arteries, causing the so-called 'vasoconstrictor tone' (McCorry, 2007). When ambient heat causes the temperature of the body to be above its set point, sympathetic tone is decreased and passive vasodilation resulting from a background release of NO from vascular endothelial cells increases heat dissipation, resulting in a reduction of body temperature. Vasoconstrictor sympathetic neurons can also be activated by local orthostatic pressure changes via a sympathetic axon reflex (Low, 1993).

In furry mammals, CVC is often accompanied by piloerection or "goose bumps". Sympathetic nerves activate the smooth muscle cells surrounding hair follicles, which raises the hairs up from the skin and traps warm air (Furlan *et al.*, 2016).

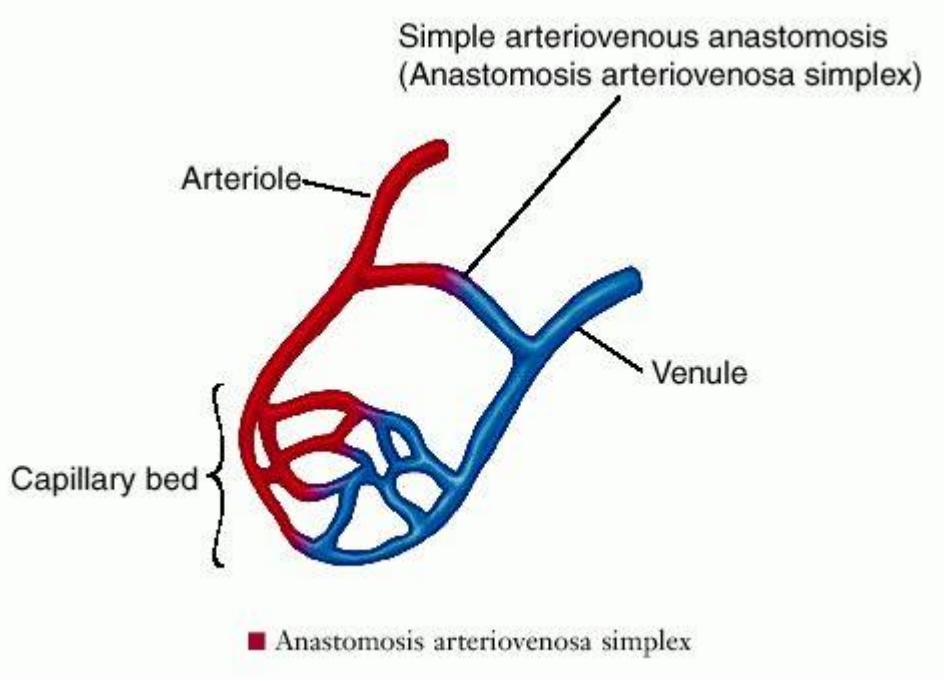

Figure 3 The structure of an arteriovenous anastomosis (AVA).
An AVA is a shunt between an arteriole and a venule in the skin. It contains smooth muscle tissue in the blood vessel wall, which can constrict and dilate to control blood flow to the cutaneous capillary bed. Figure source: Dorland's Medical Dictionary for Health Consumers (2007).

1.1.6.2 Shivering Thermogenesis

When CVC and piloerection fail to return the temperature of the body to 37±0.5°C, mammals can rapidly increase metabolic heat production by shivering. Shivering generates heat via repeated quick contractions of skeletal muscle, which is innervated by alpha motor neurons that fire in bursts. These neurons are excited by somatic premotor neurons in the rRPa, which are excited by cutaneous cold sensors *via* the LPB and hypothalamus (Morrison, 2016).

1.1.6.3 Brown Adipose Tissue (BAT) Thermogenesis

A second major source of metabolic heat production is brown adipose tissue (BAT) thermogenesis. There are three types of adipose tissue: white adipose tissue, inducible beige adipose tissue and BAT. Thermogenesis is the sole function of BAT. White fat stores energy and is not usually involved in thermogenesis but does play a role in thermic insulation e.g. in the walrus, which is protected from environmental cold by a thick layer of subcutaneous fat aptly termed "blubber". Beige adipose tissue can perform both functions.

The main depot of BAT is interscapular BAT located on the top of the back in most mammals. It is most relevant in smaller mammals and infants, which have a high surface-

to-volume ratio and thus dissipate heat more easily (Lim *et al.*, 2012). BAT is also present in humans, where its activity is reduced in overweight or obese individuals (van Marken Lichtenbelt *et al.*, 2009). The authors concluded that decreased BAT may contribute to obesity, but this may be a consequence rather than a cause of obesity, as it could be explained by the lower surface-to-volume ratio in obese individuals, which reduces their need for BAT thermogenesis.

The pathway of BAT thermogenesis is as follows: cold exposure results in activation of glutamatergic and serotonergic sympathetic premotor neurons in the rRPA, which excite preganglionic neurons in the IML that synapse onto postganglionic neurons in the paravertebral chain. Their nerves then release NA onto ß3-receptors on brown adipocytes, activating lipases, which provide fatty acids as fuel for mitochondria; and activates the proton channel UCP1 (Uncoupling Protein 1), which dissipates the mitochondrial pH gradient and so causes the mitochondria to generate heat instead of ATP (Bartness, Vaughan and Song, 2010).

Surprisingly, white and beige fat can be directly activated by environmental cold (4°C) independent of sympathetic nerve activity. This causes induction of UCP1 and triggers a thermogenic programme in these adipocytes. Interestingly, this direct effect of cold on adipocytes does not apply to brown adipocytes (Lim *et al.*, 2012). The cold-sensitive mechanism responsible for this phenomenon has not yet been identified, but is not mediated by TRPM8, TRPA1, TRPV1, or TRPV4 in mice (Ye *et al.*, 2013). In humans, cold activation of TRPM8 may underlie the local thermogenic mechanism (Rossato et al. 2014).

UCP1 is not just present in BAT of mammals. UCP1-mediated mitochondrial thermogenesis is present in many lower species, such as deep-water fish. Even plants use a UCP1-mediated thermogenic strategy (Silva, 2006).

1.1.7 Cold-Induced Vasodilation (CIVD)

High body temperature is not the only cause of vasodilation in the skin. In fact, local **cold** can directly cause vasodilation, called cold-induced vasodilation (CIVD). The local cold must be severe, e.g. less than 15 ˚C water temperature, and core body temperature has to be normothermic for CIVD to occur (Keatinge, 1957; Chen, 1996). CIVD does not have a thermoregulatory function but is a mechanism for prevention of cold injuries such as frost bite and non-freezing cold injury (NFCI). Cold inhibits nerve

conduction (Vanggaard, 1975; Zimmermann *et al.*, 2007) and the resulting reduced pain sensation could lead to frostbite if CIVD did not occur (Daanen and Van Der Struijs, 2005). CIVD can be trained. For example, fish filleters, whose hands are continuously cold, have a stronger CIVD reaction (Nelms and Soper, 1962).

The cutaneous blood vessels involved in CIVD are likely to be arterio-venous anastomoses (AVAs), which are the cutaneous blood vessels that are most heavily innervated by the sympathetic nervous system. AVAs constrict in hypothermic states to reduce total skin blood flow and dilate in hyperthermic states to increase total skin blood flow. In humans, AVAs can be found in the fingers, toes, lips, nose, cheeks, and elbows, and their numbers can increase during local acclimatisation to cold (Hale & Burch 1960).

CIVD can be observed by directly measuring the increase in blood flow or the resulting increase in skin surface temperature. AVAs can greatly influence skin blood flow. Spealman found a resting finger blood flow of 5.9cc per 100cc hand volume per minute at a temperature of 35˚C. After cooling the hand to 15°C vasoconstriction occurred, and the blood flow was decreased to 0.9cc per 100cc hand volume per minute. At 5˚C CIVD occurred and the blood flow increased again to 4.3cc per 100cc hand volume per minute (Spealman, 1945).

CIVD was first described by Thomas Lewis in 1930, who hypothesised that it was mediated by a somatosensory axon reflex, because he observed that CIVD is still present shortly after sympathectomy, but lost after complete degeneration of peripheral nerves (Lewis, 1930). This hypothesis was later challenged when electrical stimulation, which normally causes axon reflexes, was found not to promote CIVD (Daanen and Ducharme, 2000). However, it is possible that the electrical stimulation used in this study only affected somatosensory, but not autonomic neurons. Further studies are needed to determine the involvement of sympathetically-mediated axon reflexes in CIVD.

A 1986 study by Johnson et al. showed that noradrenergic transmission is disrupted during CIVD (Johnson *et al.*, 1986). Therefore, most scientists in the field believe that CIVD is merely caused by sympathetic withdrawal and the resulting decrease in noradrenaline release (Flouris and Cheung, 2010). A recent study has shown that TRPA1 is involved in restoration of blood flow following brief (5 min) cold exposure by causing the production of NO, and release of neuropeptides substance P, and CGRP

from sensory neurons (Aubdool *et al.*, 2014). This type of vasodilation is not the same as CIVD, which only occurs during prolonged cold-exposure. Further studies are needed to determine if TRPA1 plays a role in CIVD.

1.1.8 Raynaud's Phenomenon

Raynaud's phenomenon is a pathological vasoconstriction in areas that contain AVAs, such as the fingertips. It can be triggered by exposure to cold or emotional stress, suggesting the involvement of the sympathetic nervous system, but the underlying pathology is not known. Raynaud's patients also exhibit an attenuated CIVD response, but their vasculature responds normally to CGRP, histamine and PGE2 (Brain *et al.*, 1990). Possibly the mechanism responsible for CIVD is defective in these patients, resulting in a loss of balance between CIVD and CVC, resulting in excessive CVC. If so, pharmacological activation of CIVD may provide an effective treatment for Raynaud's phenomenon, because it would target exclusively the affected areas, rather than bringing about a generalised vasodilation with unwanted side-effects on the cardiovascular system.

1.2 Thermosensation

The somatosensory neurons that sense internal and external temperature are pseudo-unipolar cells and have their cell bodies in the dorsal root ganglia (DRG) located alongside the spinal cord. They relay the temperature information detected mostly by thermosensory ion channels in their cutaneous nerve endings to the spinothalamic tract and via the thalamus for conscious perception of skin temperature (Morrison, 2016).

Activation of thermal transduction mechanisms in sensory nerve endings leads to depolarisation and consequently action potential firing mediated by voltage-gated sodium (Nav) channels along the axon. These action potentials carry information about the intensity and duration of the stimulus to the spinal cord.

According to the "labelled lines" theory of sensory perception, sensory nerves each encode only one type of information e.g. information about heat and cold are carried by different nerves (Craig, 2002). This theory is based on a discovery that was made more than a century ago that specific places in the human skin either detect warm or cold stimuli (Blix, 1882). Information about warmth is coded in a graded fashion i.e. how many neurons are activated and how strongly they are activated. Information about cold is coded in a combinatorial fashion i.e. which neurons are activated, and which are not (Wang *et al.*, 2018).

Most thermosensory afferents are only excited by thermal stimuli over a specific range of temperatures. However, 50% of nerve fibres are polymodal, conducting more than one type of information (Wang *et al.*, 2018). For example, mechanosensory Merkel cells are potentiated by cold (Iggo and Muir, 1969). This underlies the illusion that cold objects feel heavier than warm objects, called the Weber phenomenon (Spray, 1986). Similarly, some nerves can be activated by multiple painful stimuli e.g. noxious cold and noxious heat. This can produce the physiological illusion of paradoxical cold: when cold-sensitive fibres are activated by noxious heat above 45˚C (Long, 1977). There is evolutionary logic behind this, as it is more important to withdraw from a damaging stimulus than to know the exact temperature of said stimulus.

Cold activation of peripheral nerves can produce one of two sensations. Moderate innocuous cold produces a sensation of coolness, and noxious cold produces a sensation of painful cold. Information about cold is conducted by thinly myelinated A-fibres and unmyelinated C-fibres. There are two types of cold-sensitive C-fibre in the rat. Low

threshold fibres that are activated around 28˚C and fire action potentials at a high rate presumably produce a sensation of coolness. High threshold fibres that are activated around 5˚C and fire action potential at a slow rate presumably produce a sensation of pain. This last type is also heat and mechanosensitive (Grossmann *et al.*, 2009).

1.2.1 Cold Transduction Mechanisms

Most sensory transduction is mediated by ion channels. For example, mechanosensation is mediated by Piezo ion channels (Coste *et al.*, 2010). The main sensors of temperature in the nervous system are ion channels of the TRP (transient receptor potential) family (Caterina, 2007). TRP channels all have six transmembrane domains and are permeable to cations, such as Ca^{2+} and Na^{+} (Julius, 2013). When TRP channels are activated by temperature, they open to allow cations into the cell, which depolarises the membrane and leads to action potentials that are then conveyed to the brain.

Temperature-sensitivity of ion channels can be determined by measuring their multiplicative constant Q_{10} value, which is defined as the change in current resulting from a 10˚C change in temperature. Most non-thermosensitive ion channels have a Q_{10} value of 1 to 3, but many TRP channels have a Q_{10} of more than three. According to this definition, heat-sensitive TRP channels include TRPV1-4 and TRPM2-5, and the cold-sensitive TRP channels are TRPM8, TRPA1 and TRPC5 (Wang and Siemens, 2015). These channels are activated at different temperatures. An overview of some of these thermosensitive TRP channels and their agonists is presented in Figure 4.

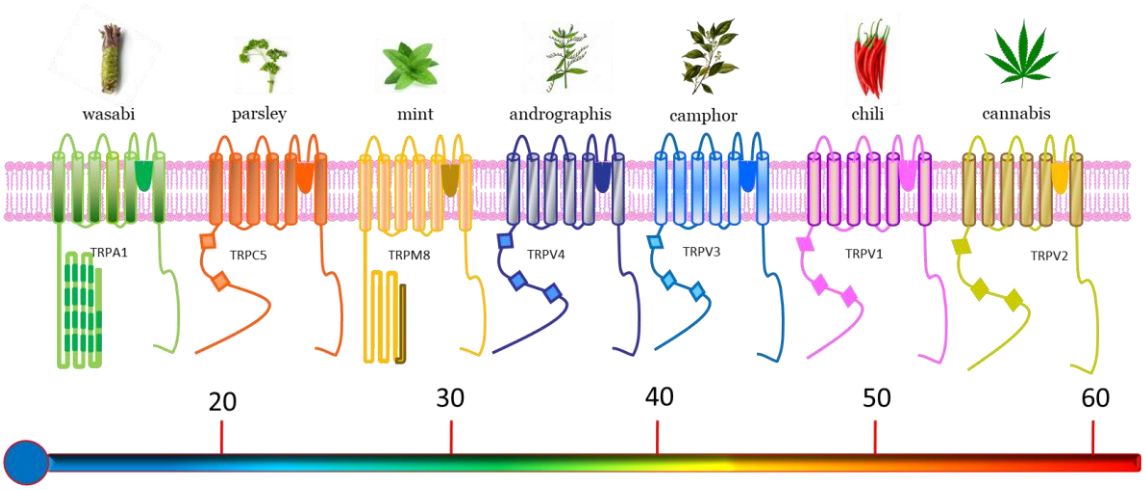

Figure 4 Schematic depiction of seven mammalian thermoTRP channels.
ThermoTRPs display distinct thermal thresholds from very hot (TRPV2) to cold (TRPA1). Each thermoTRP is also activated by specific natural compounds, which are also known to induce the relevant thermal and pain sensations in humans. Figure modified from (Mak, Zhang and McNaughton, 2010).

Apart from TRP channels, a few other ion channels can be activated by changes in temperature, such as the chloride channel anoctamin-1 (ANO-1)(Cho *et al.*, 2012), two-pore domain potassium channels (K2P)(Maingret *et al.*, 2000; Dawon Kang, Choe and Kim, 2005), endothelial sodium channels (ENaC)(Askwith *et al.*, 2001), and store-operated calcium channels (SOCE)(Xiao *et al.*, 2011). All candidate cold transduction mechanisms proposed in the literature to date will now be reviewed.

1.2.1.1 Transient Receptor Potential Melastatin 8 (TRPM8)

TRPM8 is an outwardly rectifying nonselective cationic channel with a single channel conductance of 83pS that can be activated by cold between 30˚C to 15˚C with a Q_{10} value of 24 and has a Ca^{2+}/Na^{+} ion selectivity ratio of P_{Ca}/P_{Na} = 0.97-3.3 (Bautista *et al.*, 2007; Harding *et al.*, 2018). TRPM8 activation requires phosphatidylinositol 4,5-bisphosphate (PIP_2) to be present in the plasma membrane (Rohács *et al.*, 2005). Agonists of TRPM8 include the natural compound menthol from mint and icilin (Peier *et al.*, 2002). Icilin can only activate the channel when intracellular Ca^{2+} is elevated, unlike cold and menthol (Chuang, Neuhausser and Julius, 2004). TRPM8 is inhibited by the TRPV1 blockers N-(4-Tertiarybutylphenyl)-4-(3-cholorphyridin-2-yl)tetrahydropyrazine -1(2H)-carbox-amide (BCTC), its derivative thio-BCTC, and capsazepine (Behrendt *et al.*, 2004).

TRPM8 was first cloned from prostate epithelium. It is also expressed in tumours of breast, colon, lung, and skin origin (Tsavaler *et al.*, 2001), DRG and trigeminal ganglion (McKemy, Neuhausser and Julius, 2002), nodose ganglion (Zhang *et al.*, 2004), and pulmonary arterial and aortic smooth muscle (Yang *et al.*, 2006).

TRPM8 is voltage-gated and can be activated by depolarisation. Cold can activate the channel by shifting its voltage-dependent activation curve to the level of the resting membrane potential (Voets *et al.*, 2004). Activation of TRPM8 by cold is increased with high pH (Andersson, Chase and Bevan, 2004). Direct activation of TRPM8 by cold was confirmed *via* overexpression in hippocampal neurons, which renders them cold-sensitive (de la Peña *et al.*, 2005).

A significantly reduced number of neurons responded to cooling and/or menthol in TRPM8 knockout (KO) mice (14.9% *versus* 7.6%). The remaining cold-sensitive neurons therefore use another mechanism (Dhaka *et al.*, 2007). TRPM8 activation

causes Na^+ and Ca^{2+} to enter the cell. Na^+ entry depolarises the membrane and opens Ca_V channels and triggers action potentials. Most Ca^{2+} entry observed upon activation of TRPM8 is mediated by these Ca_V channels, and not by TRPM8 itself. In fact, the resulting Ca^{2+} increase is nearly abolished by voltage clamping the cell at a negative holding potential (Reid, Babes and Pluteanu, 2002) or in the absence of external Na^+ that initiates action potential firing (Viana, de la Peña and Belmonte, 2002).

TRPM8 also plays a role in cold thermosensation *in vivo.* TRPM8 deficient mice spent more time at 5˚C than at room temperature in the thermal place preference test (Colburn *et al.*, 2007). However, some report that these mice can still feel noxious cold (Bautista *et al.*, 2007). Others have reported that TRPM8 is required for both neural and behavioural responses to noxious cold (Knowlton *et al.*, 2010). A later study again contradicts this finding using TRPM8/TRPA1 double KO mice, which display no deficits in noxious cold sensation (Brenner *et al.*, 2014). Thus, TRPM8 plays a clear role in thermosensation, but its role in the detection of noxious cold temperatures needs further study.

Besides thermosensation, TRPM8 is also involved in thermoregulation. TRPM8 agonists caused a transient increase in body temperature when injected subcutaneously in rats (Ruskin, Anand and LaHoste, 2007), when applied to the skin of mice (Tajino *et al.*, 2007), and when injected intramuscularly in rats (Ding *et al.*, 2008). Furthermore, inhibition of TRPM8 decreased core body temperature and attenuated autonomic and behavioural cold defences in rat, mouse, and human (Almeida *et al.*, 2012; Gavva *et al.*, 2012). This thermoregulatory effect is mediated by peripheral TRPM8, because intravenous administration of TRPM8 antagonists is more effective than intrathecal or intracerebroventricular administration (Almeida *et al.*, 2012).

In conclusion, TRPM8 is an important cold sensor in rodents and humans for the purposes of thermosensation and thermoregulation, but its role in nociception remains unclear, and it is not the only sensor of cold.

1.2.1.2 Transient Receptor Potential Ankyrin 1 (TRPA1)

TRPA1 is a moderately outwardly rectifying nonselective cationic channel with a single channel conductance of 87-100 pS that can be activated by cold below 17˚C in expression systems with a Q_{10} value of 6 and has a Ca^{2+}/Na^+ ion selectivity ratio of P_{Ca}/P_{Na} = 0.84 (Harding *et al.*, 2018). Agonists of TRPA1 include many natural

compounds, such as eugenol, gingerol, Δ^9-tetrahydrocannabinol (THC), thymol, and allyl isothiocyanate (AITC) from mustard oil (Story *et al.*, 2003; Harding *et al.*, 2018). Foods containing these compounds, such as mustard, elicit a noxious burning sensation in the mouth (but not a sensation of cold) when ingested, suggesting that TRPA1 is involved in nociception but not responsible for the conscious perception of cold in humans.

Apart from natural compounds, elevated intracellular Ca^{2+} is also a direct agonist of the channel (Doerner *et al.*, 2007; Zurborg *et al.*, 2007). TRPA1 gating is inhibited by immunopharmacological ligands such as resolvin D1 and the channel can be blocked by the ion Gd^{3+} and common TRP channel blocker ruthenium red (Harding *et al.*, 2018). TRPA1 was first cloned from cultured fibroblasts (Jaquemar, Schenker and Trueb, 1999). The channel is widely expressed, including in tissues such as DRG, heart, intestine, lung, skeletal muscle, and pancreas (Stokes *et al.*, 2006).

15 years ago, the group of Ardem Patapoutian reported that TRPA1 was cold-sensitive (Story *et al.*, 2003), but the dispute over whether TRPA1 is indeed directly cold-sensitive is still ongoing today. The channel was first found to be sensitive to cold below 17˚C when expressed in CHO (Chinese hamster ovary) cells (Story *et al.*, 2003). A year later, Babes and colleagues found that there are two populations of cold-sensitive neurons in the DRG (responding between 32-12˚C); one population was sensitive to menthol and the other population was not sensitive to menthol, but also not sensitive to TRPA1 agonist mustard oil (Babes, Zorzon and Reid, 2004). This suggests that there are two mechanisms of cold transduction: TRPM8 and an unknown mechanism that is not TRPA1. The identity of this mechanism will be explored in Chapter 3.

The same year, David Julius' laboratory reported that TRPA1 was expressed by 46.5% of DRG neurons, but only 3.6% of DRG neurons responded to a noxious cold stimulus. If TRPA1 is cold-sensitive, that should render all neurons expressing the channel cold-sensitive. Furthermore, 96% of TRPA1-expressing rat trigeminal neurons did not respond to a 5˚C cold stimulus in this study as measured by *in vitro* Ca^{2+} imaging (Jordt *et al.*, 2004). Moreover, the cold-sensitive neurons of TRPM8 KO mice did not respond to the TRPA1 agonist mustard oil, showing that TRPA1 does not underlie their cold responses (Bautista *et al.*, 2007). Similarly, only a small percentage of cold-sensitive mouse trigeminal neurons were activated by TRPA1 agonists (Madrid *et al.*, 2009). Recombinant TRPA1 when overexpressed in human embryonic kidney (HEK293)

cells also failed to respond to a 5˚C cold stimulus (Jordt *et al.*, 2004). This last finding was confirmed by another group the following year (Nagata, 2005), but contradicted again later (Sawada *et al.*, 2007).

TRPA1 can be directly activated by $[Ca^{2+}]_i$ (Doerner *et al.*, 2007; Zurborg *et al.*, 2007). Therefore, some of these contradictory findings could be explained by an indirect activation of TRPA1 *via* a background Ca^{2+} influx during cooling. Such a background cold response has been observed in most heterologous cell types, but not in sensory neurons (Caspani and Heppenstall, 2009). This explanation was challenged by the Voets laboratory, who found that TRPA1 still responds to cold with an increased current in the absence of extracellular Ca^{2+} and with intracellular calcium chelator BAPTA in the patch pipette, thus showing a direct effect of cold on TRPA1 (Karashima *et al.*, 2009). Of note, the same study showed that this direct activation of TRPA1 by cold is not accompanied by any detectable Ca^{2+} increase using the standard fluorescent Ca^{2+} reporter dye Fura-2, while agonist-induced TRPA1 activation was clearly visible. This is a puzzling observation but consistent with findings that many sensory neurons that respond to TRPA1 agonists do not seem to respond to cold in Ca^{2+} imaging experiments using Fura-2.

Another explanation for the discrepancy between TRPA1 expression and cold-sensitivity of sensory neurons was provided by the observation that voltage-gated potassium ($K_V1.2$) channel blockers increased the percentage of cold-sensitive neurons in the DRG (Memon *et al.*, 2017). This effect was observed in neurons expressing TRPA1, but also in neurons not expressing TRPA1.

K_V channels could attenuate the cold-sensitivity of TRPA1-expressing neurons in two ways. Firstly, if most of the Ca^{2+} influx after TRPA1 activation is mediated by Ca_V channels (cf. TRPM8), K_V channels could prevent this part of the Ca^{2+} influx by hyperpolarising the membrane. Secondly, if TRPA1 is activated by cold *via* a shift in its voltage-dependent activation curve (cf. TRPM8), K_V channels could prevent activation by hyperpolarising the membrane as well.

The study by Memon *et al.* suggests that this last mechanism is not at play and that the observed Ca^{2+} influx in cold-sensitive and TRPA1-expressing DRG neurons is in fact mediated by TRPA1. Only 8% of TRPA1 expressing DRG neurons responded to a 30s 4°C cold stimulus, but the amplitude of the cold-induced Ca^{2+} influx in these neurons was decreased after application of a selective TRPA1 antagonist (Memon *et al.*, 2017).

Unfortunately, the authors did not provide data regarding the size of this decrease, which makes it difficult to conclude that TRPA1 was solely responsible for the observed Ca^{2+} influx. Therefore, these results do not prove that TRPA1 is directly cold-sensitive and the results could still be explained by an indirect activation of TRPA1 *via* a small cold-induced Ca^{2+} influx mediated by another Ca^{2+} channel as suggested previously.

Thus far, *in vitro* experiments addressing the cold-sensitivity of TRPA1 remain inconclusive. Additionally, in vivo studies using TRPA1 KO mice also report conflicting results. The first study using TRPA1 KO mice reported no deficits in cold thermosensation (Bautista *et al.*, 2006). TRPA1 KO mice were indistinguishable from WT littermates in the two-plate choice test (Bautista *et al.*, 2007). Others have reported that TRPA1 did contribute to cold sensation, but only in females (Kwan *et al.*, 2006), or only in males (Winter *et al.*, 2017). Another study found a small increase in withdrawal latency at temperatures between 12 to 23°C in female TRPA1 KO mice using the extended cold plantar assay (eCPA), but not in males. However, there was no significant difference between the responses of both male and female TRPA1/TRPM8 double KO mice to their TRPM8 KO littermates (Brenner *et al.*, 2014).

Others report that TRPA1 KO mice did exhibit a partial deficit in cold thermosensation, but only during some cold stimulus protocols (Karashima *et al.*, 2009). TRPA1 may not contribute to cold-sensation, but contribute exclusively to cold hypersensitivity (del Camino *et al.*, 2010), or may not be required for any neural or behavioural responses to cold (Knowlton *et al.*, 2010).

In rats, TRPA1 agonist cinnamaldehyde applied to the skin did not sensitise noxious cold evoked hind limb withdrawal. It did sensitise noxious heat withdrawal mediated by C-fibres. Altering the temperature of the receptive field did not modulate TRPA1 agonist evoked-activity in cutaneous primary afferents, in either normal or inflamed skin. In addition, block of TRPA1 did not inhibit cold-evoked activity in any sensory nerves (Dunham *et al.*, 2010). This suggests that TRPA1 does not play a role in thermosensation. Furthermore, an in vivo Ca^{2+} imaging study of the DRG showed no difference in responses to mild or intense cooling between TRPA1 KO and WT mice (Ran, Hoon and Chen, 2016). The Voets group, who previously reported that TRPA1 is cold-sensitive *in vitro*, has now reported that it is in fact heat-sensitive and does not contribute to cold thermosensation *in vivo* (Vandewauw *et al.*, 2018). TRPA1 is also heat-sensitive in chicken (Saito *et al.*, 2014).

Taken together, these studies suggest that TRPA1 does not contribute to cold-sensation in somatosensory neurons and is therefore not involved in the conscious detection of cold. However, TRPA1 is cold-sensitive in rat vagus nerve (Fajardo *et al.*, 2008) and may therefore contribute to unconscious thermoregulation. Some studies report an effect of TRPA1 agonists on body temperature (Mori *et al.*, 2013; Gentry, Andersson and Bevan, 2015), but this is contradicted by others (Chen *et al.*, 2011), and doubts have been raised about the specificity of the compounds used. For example, mustard oil also activates TRPV1 (Everaerts *et al.*, 2011), so the observed effects of TRPA1 agonists on body temperature may not be mediated by TRPA1.

TRPA1-selective antagonists caused analgesia but had no effect on core body temperature in mice (Chen *et al.*, 2011; Gentry, Andersson and Bevan, 2015). Similarly, TRPA1 KO mice showed no difference in skin or core body temperature compared to wild-types (de Oliveira *et al.*, 2014). In contrast, paracetamol causes hypothermia in rodents, which has been shown to be mediated by TRPA1 (Gentry, Andersson and Bevan, 2015).

In conclusion, the evidence presented above suggests that TRPA1 plays a role in some types of nociception but its role in thermosensation and thermoregulation remains unclear.

1.2.1.3 Transient Receptor Potential Canonical 5 (TRPC5)

TRPC5 is a nonselective cationic channel that has a Ca^{2+}/Na^{+} ion selectivity ratio of P_{Ca}/P_{Na} = 9, carries a current with double rectification, and is activated in expression systems by temperatures between 25-37˚C with a Q_{10} value of 10 (Okada *et al.*, 1998; Katharina Zimmermann *et al.*, 2011).

TRPC5 can be activated by GPCR agonists, lysophospholipids, lanthanides, Rosiglitazone, and Ca^{2+} store depletion (Beech, 2007). Antagonists include lanthanum and 2-APB (Okada *et al.*, 1998; Xu *et al.*, 2005). Phosphokinase C (PKC) also has an inhibitory effect on TRPC5 and mediates desensitisation following receptor activation (Beech, 2007).

TRPC5 was first cloned from mouse brain (Philipp *et al.*, 1998), but is expressed in many tissues including pituitary gland, heart, liver, muscle (Riccio *et al.*, 2002), and DRG (Jang *et al.*, 2012; Vandewauw, Owsianik and Voets, 2013).

A function for the cold-sensitivity of TRPC5 has not yet been identified. The channel was found to contribute to cold sensation *in vitro*, but TRPC5 KO mice displayed no difference in temperature preference compared to WT mice (Zimmermann *et al.*, 2011a), suggesting that the ion channel is not involved in thermosensation. However, the temperature-preference of these mice was measured over only a five-minute period and this may not have been long enough to detect any defects in thermosensation. Comparable work in our lab has established that a protocol of at least ten minutes is required to detect a deficit in heat-sensation using TRPM2 knock-out mice (Tan and McNaughton, 2016). Therefore, TRPC5 could still be involved in thermosensation despite the initial findings by Zimmermann *et al.* (2011a).

1.2.1.4 Two-Pore Domain Potassium Channels (K2P)

The K2P family consists of 15 genes which together make an important contribution to the native K^+ background leak currents observed in many neurons. There are several subfamilies of K2P channels, including the weakly inward rectifying K^+ channel (TWIK), the acid-sensitive K^+ channel (TASK), the TWIK-related K^+ channel (TREK), and the TWIK-related arachidonic acid stimulated K^+ channel (TRAAK) (Enyedi and Czirjak, 2010).

K2P channels are not voltage-gated. Instead, their open probability is affected by a large variety of chemical and physiological stimuli, including neurotransmitters, post-translational modifications, second messengers, mechanical stretch and temperature. The main function of K2P channels is to control membrane excitability by setting the resting membrane potential. They also determine the frequency and morphology of action potentials (Harding *et al.*, 2018).

The first K2P channel subunit was cloned from the genome of the budding yeast Saccharomyces cerevisiae (Ketchum *et al.*, 1995). In mammals, K2P channels are expressed in many excitable tissues including the hypothalamus, sensory nervous system, sympathetic nervous system, heart and skeletal muscles, and non-excitable cell types including the pancreas, vascular endothelium and some immune cells (Medhurst *et al.*, 2001).

K2P channels are involved in modulating the perception of cold, heat, and pain (Pollema-Mays *et al.*, 2013). Of the K2P channels, TREK-1, TREK-2, and TRAAK are thermosensitive (Maingret *et al.*, 2000; Kang, Choe and Kim, 2005). TREK-1 has a

single channel conductance of 90pS and is activated by heat with a Q_{10} value of ~7 (Maingret *et al.*, 2000) and can be blocked by Ba^{2+}, quinidine, phosphokinase A (PKA), and PKC (Goldstein *et al.*, 2005; Ma *et al.*, 2011). Phosphorylation switches the phenotype of the channel between leak and voltage-dependent activation (Bockenhauer, Zilberberg and Goldstein, 2001).

TREK-2 is an open rectifier with a single channel conductance of 100pS that can be activated by heat and blocked by quinidine, PKA, and PKC (Lesage *et al.*, 2000). The whole-cell currents of recombinant TREK-2 expressed in COS-7 cells increased ~20 fold between 24 to 42˚C with an activation threshold of 25˚C (Kang, Choe and Kim, 2005). This means that TREK-2 is normally open at physiological temperatures but closes below 24˚C, thus causing a net depolarisation of the cell when exposed to cold.

TRAAK is an open rectifier with a single channel conductance of 46pS, whose open probability can be increased by heat above 31˚C and can be blocked by Gd^{3+} (Goldstein *et al.*, 2005; Kang, Choe and Kim, 2005). This means that TRAAK is normally open at physiological temperatures but closes below 30˚C, causing a net depolarisation of the cell when exposed to mild cold.

In rat primary sensory neurons, inhibition of a background potassium conductance (presumably mediated by K2P channels) was shown to contribute to cold transduction with a Q_{10} value of 2-4, which is ten-fold lower than the Q_{10} of TRPM8 (Reid and Flonta, 2001). In another study, deletion of TREK-1 or TRAAK alone did not affect cold-sensitivity, but a double KO increased the percentage of cold-sensitive DRG neurons from 24 to 54% (Noël et al. 2009). This suggests that these channels may function to inhibit cold transduction as follows. Activity of TREK-1 and TRAAK hyperpolarises the neuron and inhibits the activation of cold-sensors. During cooling, the channels close, and thus the neuron is activated by cold. Notably, this mechanism mostly affects neurons that do not express TRPM8 or TRPA1 (Noël *et al.*, 2009).

Co-expression of K2P channels with thermosensors may suggest a role for these channels in thermosensation. In DRG neurons, TREK-1 is co-expressed with the cold sensor TRPM8 (Usoskin *et al.*, 2015). Additionally, TREK-1 is co-expressed with a cold-sensitive cationic channel called cyclic nucleotide-gated alpha 3 (CNGA3) in Grünenberg ganglion neurons, located in the vestibule of the murine nose (Stebe *et al.*, 2013). These neurons transduce coolness via a cGMP cascade (Mamasuew *et al.*, 2010).

Thus, *in vitro* experiments suggest a role for TREK-1, TREK-2, and TRAAK channels in thermosensation. KO mice have been generated to establish the function of these channels *in vivo*. TREK-2 KO mice have a somewhat enhanced sensitivity to moderately cool temperatures (20°C *versus* 25°C)(Pereira *et al.*, 2014). TREK-1 and TRAAK KO mice have no obvious phenotype (Heurteaux *et al.*, 2004; Noël *et al.*, 2009), but these mice do exhibit an increased thermal hyperalgesia in inflammatory states (Alloui *et al.*, 2006). Furthermore, TREK-1/TRAAK double KO mice are more sensitive to cold in the cold plate assay and temperature preference test (Noël *et al.*, 2009). This suggest that these channels play a role in desensitisation of cold thermal afferents.

Inhibition of a background K^+ current would be an atypical method of sensory transduction, but it is a common method for neuromodulation. Therefore, we suspect that K2P channels play a role in the modulation of cold-sensitivity but may not constitute a cold-transduction mechanism in isolation.

1.2.1.5 Epithelial Sodium Channels (ENaC)

Temperature modulates taste sensation (McBurney, Collings and Glanz, 1973; Green and Frankmann, 1988). Cationic epithelial sodium (ENaC) channels are expressed in the tongue, where they function as taste receptors (Li, Blackshaw and Snyder, 1994; Ugawa *et al.*, 1998; Boughter and Gilbertson, 1999; Lin *et al.*, 1999). ENaC channels are also expressed in the DRG, where they may play a role as mechanosensors (Waldmann *et al.*, 1997; Price *et al.*, 2000). Askwith *et al.* have found that the constitutively active Na^+ current of these channels was potentiated by cold 23-25˚C with a Q_{10} value of 4.4 in heterologous cells and DRG neurons, but only in the presence of protons (Askwith *et al.*, 2001). Therefore, these channels may play a role in cold transduction. The authors also proposed that ENaC channels may mediate the increased firing rates in response to cooling observed in the thermoregulatory area of the hypothalamus (Boulant and Dean, 1986).

The findings of Askwith *et al.* are inconsistent with the finding that the ENaC antagonist Amiloride did not affect cold-activated currents in DRG neurons (Reid and Flonta, 2001).

1.2.1.6 Store-Operated Calcium Entry Channels (SOCE)

SOCE channels consist of a hexameric combination of Orai1-3 subunits that is directly gated by Stromal Interaction Molecule 1 (STIM1) or STIM2 proteins (Hou *et al.*, 2012) and can be activated by cooling from 37 to 25˚C (Bailong Xiao *et al.*, 2011). The etymology of "Orai" comes from Greek mythology, where the Orai is the keeper of the gate of heaven. STIM1 and Orai1 are expressed in all tissue types (Thul *et al.*, 2017) and all STIM and Orai isoforms are expressed in the DRG and TG (Manteniotis *et al.*, 2013). SOCE channels are particularly important in non-excitable cells, where they constitute the main Ca^{2+} entry pathway and function to refill intracellular Ca^{2+} stores of the endoplasmic reticulum (ER) in a process called store-operated calcium entry (SOCE) (Lu and Fivaz, 2016).

We can find the origins of the concept of SOCE in Putney 1986 (Putney, 1986). Upon activation by a Gq Protein-Coupled Receptor (GPCR), Ca^{2+} is released from stores by inositol triphosphate (IP_3) and the stores are then refilled as a direct consequence. Ca^{2+} is pumped into the ER by the sarcoplasmic-endoplasmic reticulum Ca^{2+} ATPase (SERCA) pump (Thastrup *et al.*, 1990).

The ionic current associated with store refilling is called I_{CRAC} for Ca^{2+} release-activated Ca^{2+} current (Hoth and Penner, 1992). It is highly selective for Ca^{2+} and thus strongly inwardly rectifying with a positive reversal potential. I_{CRAC} is undetectably small: <1pA/pF (Vig *et al.*, 2006). Noise analysis has estimated that the single-conductance of the CRAC channel is only ~24 fS (Zweifach and Lewis, 1993). This is minute compared to e.g. an L-type Ca_V, which has a single-channel conductance of 28pS (Umemiya and Berger, 1995). The ER Ca^{2+} sensors STIM1 and STIM2 were discovered relatively recently in 2005 and the CRAC channel subunit proteins Orai1, Orai2, and Orai3 were discovered a year later (Feske *et al.*, 2006; Vig *et al.*, 2006; Zhang *et al.*, 2006).

Figure 5 shows the current consensus model of SOCE, which is as follows: STIM1, a single-pass membrane protein resident in the ER contains a Ca^{2+} binding EF hand domain on the luminal side that is bound to Ca^{2+} at rest and interacts with the sterile alpha motif (SAM) to ensure a stable monomeric state of STIM1. When a GPCR is activated by a ligand e.g. adenosine triphosphate (ATP), phosphatidylinositol 4,5-bisphosphate (PIP2) is cleaved by phospholipase C (PLC), which generates IP_3 and diacylglycerol (DAG). IP_3 then diffuses through the cytosol to bind and open IP_3

receptors in the ER membrane, which triggers Ca^{2+} release. When Ca^{2+} is released from the ER, it dissociates from the intraluminal EF hand domain of STIM1, which causes a conformational change in the protein. STIM1 then forms dimers, which subsequently oligomerise. This leads to an extension of the coiled-coil (CC) cytoplasmic domains of STIM1 causing translocation to the plasma membrane and formation of ER-PM junctions, where STIM1 can recruit and open Orai channels directly (Prakriya and Lewis, 2015).

STIM1 has also been found to activate an Orai1/TRPC complex via electrostatic interactions (Cheng *et al.*, 2013), but there is conflicting evidence suggesting that TRPC channels are not involved in SOCE (Dehaven *et al.*, 2009; Wang *et al.*, 2010). STIM1 can also inhibit Ca_V channels (Park, Shcheglovitov and Dolmetsch, 2010; Youjun Wang *et al.*, 2010).

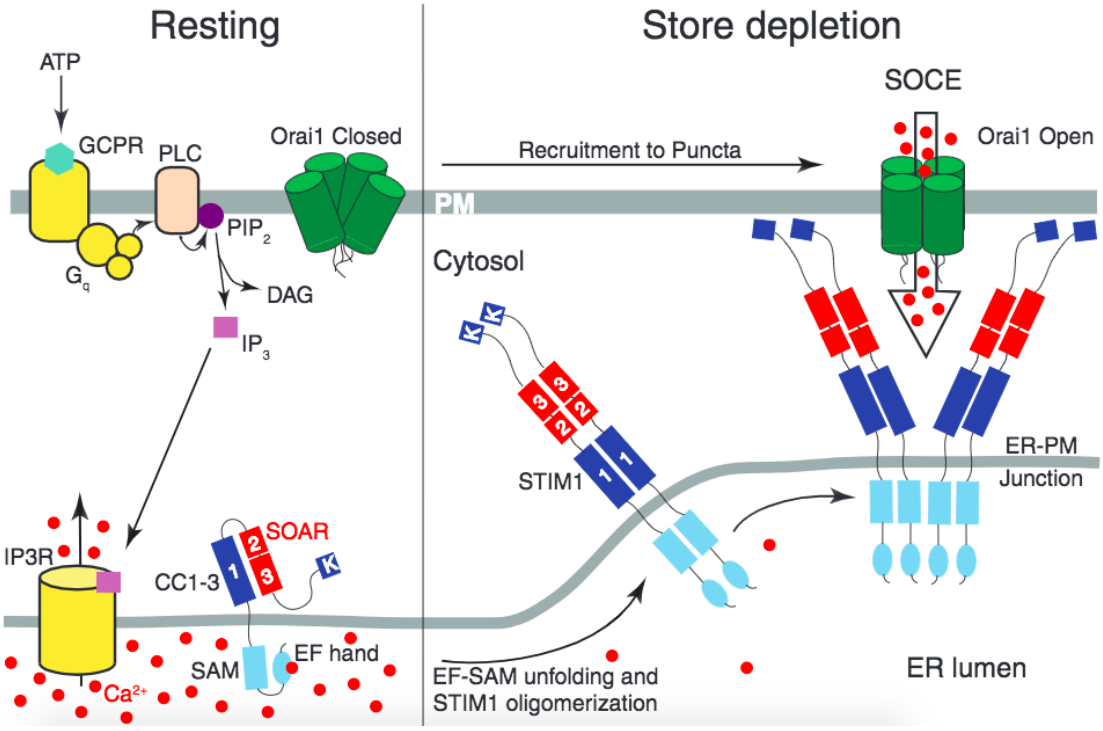

Figure 5 Current consensus model of SOCE.
ATP = adenosine triphosphate; GCPR = G-coupled protein receptor (GCPR); PLC = phospholipase C; PIP_2 = phosphatidylinositol 4,5-bisphosphate; IP_3 = inositol trisphosphate; DAG = diacylglycerol; SAM = sterile alpha motif; CC1-3 = coiled-coil domains; SOAR2-3 = STIM/Orai activating regions. Figure from (Nelson and Roe, 2018).

SOCE is involved in various biological processes, such as Ca^{2+} homeostasis, cell differentiation, gene regulation, and apoptosis (Parekh & Putney 2005). Furthermore, STIM and Orai are not just involved in SOCE. For example, STIM1 can bind cytoskeletal microtubules and so remodel the ER (Grigoriev *et al.*, 2008; Smyth *et al.*, 2012). Orai1/3 heteromers are STIM1-gated but store depletion independent and can be activated by arachidonic acid (Thompson and Shuttleworth, 2013), or by its metabolite Leukotrine-C4 (Zhang *et al.*, 2013). Orai1 can also be constitutively activated by Golgi calcium transporter Secretory Pathway Ca^{2+} ATPase (SPCA2) in calcium-transporting epithelia, in a store-independent and STIM1-independent fashion (Feng *et al.*, 2010). Mutations in SOCE channels cause severe phenotypes, such as immunodeficiency because T cell activation depends on a Ca^{2+} influx via SOCE channels (Feske *et al.*, 2006) and male infertility because sperm motility is dependent on SOCE-mediated Ca^{2+} signals (Davis *et al.*, 2016).

STIM1-mediated SOCE can be enhanced by heating to 40˚C and inhibited by cooling to 34˚C in the rat pheochromocytoma (PC12) cell line (Thompson, Pabelick and Prakash, 2009). A later study by Xiao *et al.* has shown that mild heating of cells induced clustering of STIM1 independently of store-depletion. However, this clustering did not lead to enhanced SOCE as the interaction between STIM1 and Orai1 was inhibited by heat, but could be induced by subsequent cooling (Xiao *et al.*, 2011). Figure 6 summarises how STIM1-mediated Ca^{2+} influx can be induced by cooling to room temperature after heating to 39°C. Further research is required to determine whether this Ca^{2+} influx would also happen directly in response to cooling, or only in response to cooling after heating to >39°C. A recent study by Bailong Xiao that is currently unpublished has suggested an *in vivo* role for the thermosensitivity of STIM1, showing that it contributes to the optimal preference temperature of mice.

In conclusion, studies suggest that STIM1 is thermosensitive, but whether it is activated by cold or heat remains unclear.

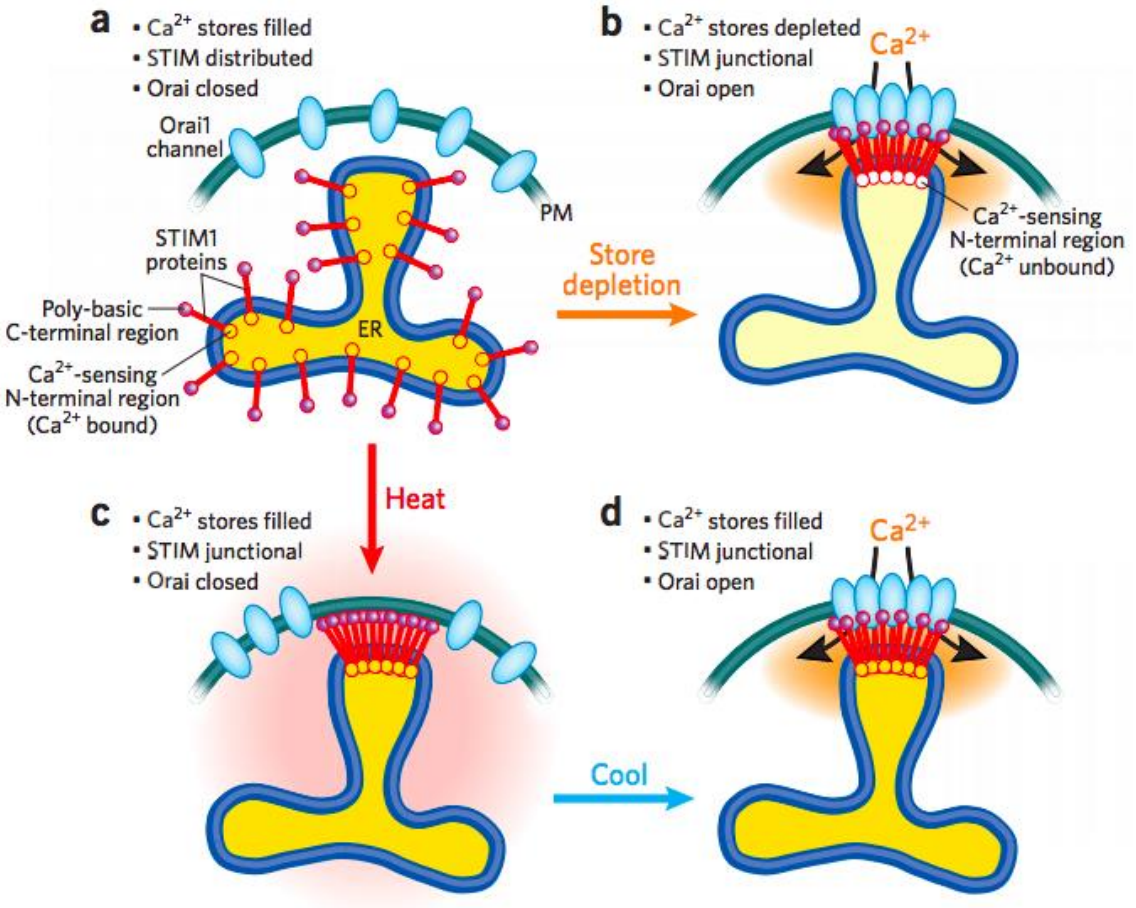

Figure 6 SOCE can be activated by cooling after heating.
a) ER-resident STIM is in a monomeric state while bound to Ca^{2+} at rest. b) Ca^{2+} store depletion is sensed by STIM, which multimerises and opens Orai. c) Heat can also multimerise STIM but does not open Orai. d) Cold can open Orai, but only when multimerised STIM1 is present at ER-plasma membrane junctions. Figure from Mancarella, Wang and Gill (2011).

1.3 Aims

Many sensory and sympathetic neurons respond to cold with an increase in Ca^{2+} that is not mediated by TRPM8 or TRPA1 (Babes, Zorzon and Reid, 2004; Smith *et al.*, 2004; Reid, 2005; Bautista *et al.*, 2007; Munns, AlQatari and Koltzenburg, 2007; Noël *et al.*, 2009). The molecular basis of this cold transduction mechanism is still elusive. Furthermore, the function of sympathetic cold-sensitivity has not been studied. Therefore, the general aims of this thesis are to identify the molecular basis of a novel cold transduction mechanism in sympathetic and sensory neurons, and to find clues about the function of this mechanism in sympathetic neurons.

More specifically, in Chapter 2 we aim to correlate the thermal and neurotransmitter phenotype of sympathetic neurons with the use of *in vitro* Ca^{2+} imaging and immunocytochemistry. This will provide information about a possible function of local thermosensitive mechanisms expressed in sympathetic nerves. For example, if the population of vasomotor neurons overlaps with the population of cold-sensitive neurons, that could mean that the cold sensors play a role in vasoconstriction.

In Chapter 3, we will use *in vitro* Ca^{2+} imaging in combination with pharmacology for our second aim to identify the mechanisms underlying cold transduction in the sensory and sympathetic nervous systems. Isolated dorsal root and superior cervical ganglion neurons in culture will be used as a model of the otherwise inaccessible axon terminal. Several candidates will be ruled out before discovering that STIM and Orai form a novel cold-transduction mechanism in peripheral neurons.

The aim of Chapter 4 is to determine which members of the SOCE family are involved in cold transduction, employing the different techniques of gene silencing and heterologous overexpression. We will find that combined overexpression of STIM1 and Orai1 is sufficient for a cold-induced Ca^{2+} influx to occur.

We then explore in Chapter 5 whether sympathetic neurons could cause CIVD by releasing vasodilators using immunohistochemistry and find that neuronal nitric oxide synthase is widely expressed in these neurons. This may suggest a role of the local cold transduction mechanism in CIVD.

Finally, in Chapter 6 we aim to develop a novel *in vivo* Ca^{2+} imaging method of the sympathetic nervous system that could be used to determine whether the novel thermosensitive mechanisms are expressed in the nerve terminal and generate antidromic action potential firing in vasomotor nerves.

Chapter 2 Correlation of Sympathetic Thermal and Neurotransmitter Phenotypes

2.1 Introduction

The sympathetic division of the autonomic nervous system is responsible for executing many thermoregulatory functions, including activation of BAT and vasoconstriction to increase body temperature. Cold detected by the sensory nervous system indirectly mobilises these responses. Remarkably, murine postganglionic sympathetic neurons are also directly activated by cold stimuli in culture (Smith *et al.*, 2004; Munns, AlQatari and Koltzenburg, 2007). Munns, AlQatari and Koltzenburg have speculated that the cold-sensitivity of sympathetic afferents may trigger an axon reflex and mediate local release of NA or ATP, or that this phenomenon could be responsible for the cold hypersensitivity often observed in sympathetically maintained pain via an activation of sensory afferents by NA.

Heat also directly activates murine postganglionic sympathetic neurons in culture (Tan and McNaughton, 2016). Since these nerves are involved in thermoregulation, we hypothesised that their inherent thermosensitivity may serve a thermoregulatory function. As described in the general introduction (section 1.1.1), there are two main types of sympathetic neurons: cholinergic neurons projecting to sweat glands and periosteum, and noradrenergic neurons projecting to blood vessels, salivary glands, brown adipose tissue (BAT), etc. Around 50% of mouse sympathetic ganglion neurons are Neuropeptide Y (NPY)-expressing noradrenergic vasomotor neurons that innervate the smooth muscle of blood vessels (Gibbins, 1991).

Cholinergic activation of sweat glands results in a decrease in body temperature, whereas noradrenergic nerves cause vasoconstriction which results in a net increase in body temperature. A proportion of sympathetic neurons express the heat-sensitive ion channels TRPM2 and TRPV2, and a proportion of sympathetic neurons express an unidentified cold-sensitive ion channel (Smith *et al.*, 2004; Munns, AlQatari and Koltzenburg, 2007; Furlan *et al.*, 2016; Tan and McNaughton, 2016).

A possible function for these thermosensory ion channels expressed in sympathetic neurons may be suggested by the neurotransmitter phenotype of the neurons in which they are expressed. In this chapter, we hypothesise that sympathetic neurons expressing

the recently identified TRPM2 warmth-sensitive mechanism have a cholinergic phenotype and thus project to sweat glands to dissipate heat, while neurons expressing the novel cold-sensitive mechanism express a noradrenergic phenotype and innervate blood vessels to conserve heat by vasoconstriction.

To test this hypothesis, we used single cell Ca^{2+} imaging to determine the thermal responses of cultured sympathetic neurons *in vitro*, followed by histological staining for choline acetyl transferase (ChAT), a cholinergic biosynthetic enzyme, and tyrosine hydroxylase (TH), a biosynthetic enzyme in the noradrenergic pathway. A correlation between thermal response and neurotransmitter phenotype suggests a thermoregulatory function for the novel thermally activated mechanisms.

2.2 Materials and Methods

2.2.1 Animals

All experimental protocols were conducted in accordance with the Guide for Care and Use of Laboratory Animals (Institute of Laboratory Animal Research, 2011). Adult male and female 1 – 3-month-old FVB/N transgenic mice with GFP (green fluorescent protein) encoded under the ChAT (choline acetyl transferase) promoter were used for all experiments in this chapter (Grybko et al. 2011). This transgenic mouse is a targeted knock-in.

2.2.2 Retrograde Tracing

In order to label sympathetic neurons innervating the blood vessels and eccrine sweat glands in the paw, mice were anaesthetised via inhalation of 2% isoflurane and injected with 5μL 2% w/v Fast Blue (FB; Polysciences Inc.) retrograde tracer dye in PBS into the glabrous skin of both front paws using a 10μL Hamilton syringe (Hamilton) and 30 gauge needle (Anderson, Bergner and Murphy, 2006). FB is a long lasting fluorescent tracer dye that is taken up into axons and retrogradely transported into cell bodies, which for sympathetic nerves innervating the paw are located in the stellate ganglion. The stellate ganglion also innervates other structures such as the heart, lungs, and ribs. This method allows for identification of neurons innervating the paw skin specifically. The optimal time for labelling was established experimentally.

2.2.3 Dissection

Mice were killed by cervical dislocation and decapitated prior to dissection. For harvesting of SCG, the skin of the throat, the underlying salivary glands and trachea were removed to expose the common carotid artery. The SCG is attached to the bifurcation of this artery (Figure 7). For harvesting of SG and paravertebral chain ganglia, the skin of the chest and underlying ribs were removed. Then, all organs residing in the ribcage were removed to expose the SG, which is located at the base of the first rib. The paravertebral chain was then followed down to locate the other sympathetic ganglia of the paravertebral chain. For collection of DRG to use as control tissue, the vertebral column was removed and placed in phosphate buffered saline (PBS,

Sigma). The vertebral column was then cut in half along the dorso-ventral axis and the spinal cord was removed to expose the DRG. DRG of all levels were used. SCG, SG and DRG were used from the same mouse whenever possible to reduce the number of animals used and to make the DRG more valid as a control tissue. All ganglia were temporarily stored in sterile PBS for up to 30 minutes during dissection when used for immunohistochemistry and in Hibernate-A medium (Life Technologies) when used for cell culture. Hibernate-A medium is optimised for use at ambient CO_2 levels.

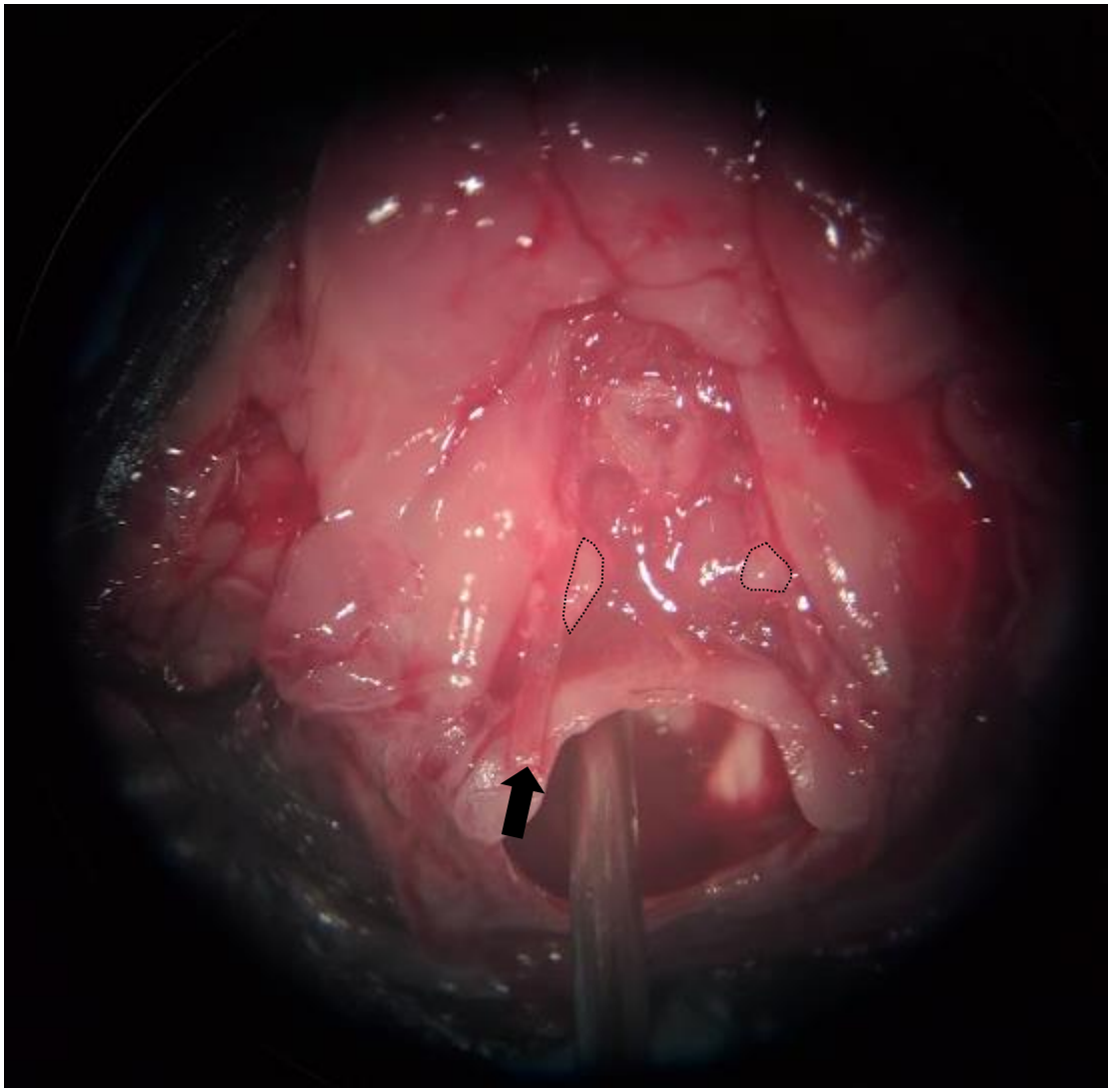

Figure 7 Dissection of the superior cervical ganglia from an adult mouse.
Inferior aspect of the isolated head after decapitation. A needle (visible a the bottom of the image) was placed through the cranium to pin down the head. The trachea has been displaced upward and excess tissue removed from the dissection field, exposing the SCG (dotted outlines). The cut carotic artery (arrowhead) is clearly visible and can be followed upward to locate the SCG.

2.2.4 Tissue Preparation

Ganglia were fixed with 4% w/v paraformaldehyde (PFA; Sigma) in PBS for ten minutes at room temperature and soaked in 20% w/v sucrose (Fisher) in PBS overnight at 4°C to prevent the formation of ice crystals during freezing. The next day, ganglia were embedded in CryoEmbed and frozen by placing the embedded ganglia on a weighing boat floating on liquid nitrogen. Ganglia were stored at -80°C or immediately sliced into 10µm sections with a cryostat (Bright Instruments) at -23°C and placed on Superfrost Plus microscope slides (Thermo Scientific). Slides were blocked for 30 minutes at room temperature with a solution that consisted of 5% v/v normal goat or donkey serum (Jackson Immunoresearch) in PBS with 0.1% v/v Triton X (Sigma). Normal serum from goat or donkey was used for blocking depending on the host of the secondary antibodies used. Slides were incubated in this blocking buffer for 30 minutes to one hour at room temperature. Finally, slides were washed three times in PBS on a rocking platform for five minutes each time.

2.2.5 Immunohistochemistry

All slides were labelled with fluorescent antibodies using the two-step indirect staining method. Primary antibodies (Table 1) in PBS with 0.1% v/v Triton X were added overnight at room temperature. Anti-GFP antibody was used to stain for ChAT in transgenic mice that express GFP under the ChAT promoter (Grybko *et al.*, 2011). Slides were washed three times in PBS on a rocking platform and incubated with secondary antibodies at dilution factor 1:1000 (

Table 2) in PBS for two hours at room temperature. In some experiments, DAPI (4',6-diamidino-2-phenylindole) (AnaSpec) or Hoechst 33258 (Sigma) was added to the secondary antibody solution to stain nuclei blue. After staining, Fluosave™ reagent (CalBiochem) and glass coverslips (VWR International) were added to the slides. Then, slides were stored at 4°C in the dark until imaged using an Axioplan2 microscope (Zeiss) and Axiovision software (Zeiss). Images were exported as Tagged Image File Format (TIFF) files.

Table 1 Primary antibodies

Antibody	Reference	Source	Dilution
Rabbit anti-TH	Ab152	Millipore	1:500
Chicken anti-GFP	Ab13970	Abcam	1:1000
Mouse anti-βIIITubulin	G712A	Promega	1:1000
Rabbit anti-DBH	SAB2701977	Sigma	1:300

Table 2 Secondary antibodies

Antibody	Reference	Source	Conjugate
F(ab')2-Goat anti-Rabbit IgG (H+L)	A11069	Life Technologies	Alexa Fluor® 350
Goat anti-Chicken IgY (H+L)	A11039	Life Technologies	Alexa Fluor® 488
Chicken anti-Rabbit IgG (H+L)	A21441	Invitrogen	Alexa Fluor® 488
Donkey anti-Rabbit IgG (H+L)	A21207	Invitrogen	Alexa Fluor® 594
Goat anti-Mouse IgG (H+L)	A21049	Invitrogen	Alexa Fluor® 350
Goat anti-Mouse IgG2a	A21131	Life Technologies	Alexa Fluor® 488
Donkey anti-Mouse IgG (H+L)	A21202	Life Technologies	Alexa Fluor® 488
F(ab')2-Goat anti-Mouse IgG (H+L)	A11020	Life Technologies	Alexa Fluor® 594

2.2.6 Haematoxylin and Eosin

Haematoxylin and eosin stain (H&E) was performed by Carl Hobbs according to the standard Wolfson CARD protocol. Embedding medium was removed from SCG sections by submerging them twice in xylene on a rocking platform for ten minutes. Then, sections were rinsed four times in absolute ethanol on a rocking platform for 30 seconds and rinsed in tap water for one minute. Nuclei were stained with Haemalum for five minutes and slides were rinsed in running tap water until clear. Then, slides were dipped five times into 0.5% w/v hydrochloric acid (HCl) in 70% v/v industrial methylated spirit (IMS) and quickly returned to running tap water for one minute to

allow nuclei to turn blue. Slides were counterstained with 0.5% w/v eosin for ten minutes and rinsed in tap water until clear. Then, slides were rinsed briefly in deionised water and dried in an oven at 60°C for one hour. Slides were then rinsed twice in xylene and mounted using DPX mounting medium (Distrene, Plasticisier, Xylene). H&E stained slides were imaged using an Axioskop microscope (Zeiss) and Axiovision software.

2.2.7 Primary Cell Culture of DRG, SCG and SG Neurons

Ca^{2+} and Mg^{2+}-free Hank's Balanced Salt Solution (CMFHBSS) was prepared according to Table 3 and the pH was adjusted with 1M sodium hydroxide (NaOH) and 5% w/v hydrogen chloride (HCl) solution to 7.4 as determined by a pH210 microprocessor pH meter (Hanna Instruments) and stored in frozen aliquots. Ganglia were placed in 5mL Eppendorf tubes and centrifuged at 1000 rpm for three minutes. Then, the supernatant was aspirated off and papain (Sigma) solution was added through a filter (2mg/mL papain in CMFHBSS). Ganglia were incubated at 37°C in a shaking water bath for 30 minutes at 100rpm.

The cell solution was then centrifuged at 1000 rpm for three minutes and the supernatant was aspirated off and collagenase (VWR) solution was added through a filter (2.5mg/mL collagenase IV in CMFHBSS). Cells were incubated in a 37°C shaking water bath for 30 minutes at 100 rpm. Then, the cell solution was centrifuged at 1000 rpm for ten minutes. The supernatant was removed and Neurobasal-A medium (Life Technologies) was added. Neurobasal-A medium was previously supplemented with 0.25% v/v L-Glutamine 200mM (Invitrogen), 2 % v/v B-27 Supplement (Invitrogen) and nerve growth factor (NGF) at 50ng/mL and warmed to 37 °C.

The cell solution was then triturated with a P200 pipette until a homogeneous turbid solution was obtained, showing that complete mechanical dissociation had been achieved. At this time, a sample was taken for cell counting. Then, the solution was centrifuged at 1000rpm for ten minutes. The supernatant was aspirated off and Neurobasal-A medium was added at a volume of 20µl per coverslip. These coverslips had been previously sterilised with ethanol and the letter F had been etched in with a diamond scribe to allow for cell localisation between calcium imaging and epifluorescence imaging after staining. Cover slips were also coated for one hour with 40ng/mL laminin (Fisher Scientific) in 0.01% w/v Poly-L-Lysine solution (Sigma),

washed twice with distilled water, air dried, and put in the wells of 4-well plates (Nunc). Cells were incubated at 37°C for 30 minutes to let them adhere before wells were filled with pre-warmed Neurobasal-A medium. Cells were incubated at 37°C for 18-36 hours until fixation or calcium imaging.

Table 3 Calcium- and Magnesium-free HBSS (CMFHBSS)

	mM	**Source**
KCl	5.33	Sigma
KH_2PO_4	0.44	VWR
$NaHCO_3$	4.17	BDH
NaCl	137.93	Fisher
Na_2HPO_4	0.34	Sigma
D-Glucose	5.56	Fisher

2.2.8 Immunocytochemistry

Coverslips were fixed with 4% PFA w/v and 15% w/v sucrose solution in PBS for 20 minutes at room temperature and slides were washed three times in PBS on a rocking plate. Blocking buffer consisting of 3% w/v BSA and 0.1% v/v Triton X in PBS was added for one hour and slides were washed again. Primary antibodies were added in PBS with 0.1% v/v Triton X for one hour at room temperature or overnight at 4°C. The next day, slides were washed three times, and secondary antibodies were added at 1:1000 dilution factor in PBS for one hour at room temperature. Finally, slides were washed and Fluosave and glass coverslips (VWR International) were added. Slides were stored in the dark at 4°C until imaging was performed using an Axioplan2 microscope (Zeiss) and Axiovision software (Zeiss). Images were exported as TIFF files.

2.2.9 Calcium Imaging

Cells for Ca^{2+} imaging were prepared as described above (see 2.2.7). Hank's Balanced Salt Solution (HBSS, Table 4) and high KCl solutions were prepared from 10x stock solution and D-Glucose was added on the day of the experiment. The pH was adjusted to 7.4 using 5M NaOH solution and the osmolality was on average 277 mOsm/L as measured by an Advanced Micro-Osmometer (Advanced Instruments). HBSS was heated to 60 ° C overnight to prevent the formation of air bubbles in the perfusion system.

Acetoxymethylester Fura-2 solution was prepared on the day of the experiment and consisted of 5μM Fura-2 AM (Life Technologies) with 0.02% v/v pluronic acid (Life Technologies) and 0.1% v/v dimethyl sulfoxide (DMSO, Sigma).

Fura-2 is a ratiometric fluorescent Ca^{2+} dye with a maximum fluorescence emission of ~510nm. The portion of Fura-2 that is bound to Ca^{2+} will fluoresce most when excited at 340nm, whereas the portion of free Fura-2 will emit most light when excited at 380nm. This makes Fura-2 a ratiometric dye, which means that the ratio of the fluorescence signals obtained at different wavelengths can be used to estimate the concentration of Ca^{2+}, independent of the concentration of the dye itself. Unfortunately, Fura-2 emission is affected by temperature differently at 340nm and 380nm excitation. This causes an upward artifact in the $F_{340/380}$ trace during heating ramps, and a downward artifact during cooling (Oliver *et al.*, 2000). Consequently, the amplitudes of heat responses reported in this thesis are overestimated, and the amplitudes of cold responses are underestimated.

Fura-2 AM has an acetoxymethylester group attached to it which makes the dye cell permeable. This group is cleaved off by endogenous esterases after diffusing into the cell, which prevents the dye from leaking out of the cell and exposes the Ca^{2+} binding anionic sites. Cells were loaded with Fura-2 solution in Neurobasal-A medium for 30 minutes before imaging. Coverslips were placed on a chamber platform (Warner Instrument Corp., Figure 8) filled with 37˚C HBSS and placed on the stage of a Nikon Eclipse Ti microscope. Cells were perfused with 32-37˚C HBSS for at least 5 minutes before the start of the experiment and the perfusion speed (3mL/min) and baseline temperature were kept constant throughout the day. HBSS was aspirated by a suction catheter placed in a separate part of the bath that communicates with the main part via a small tunnel.

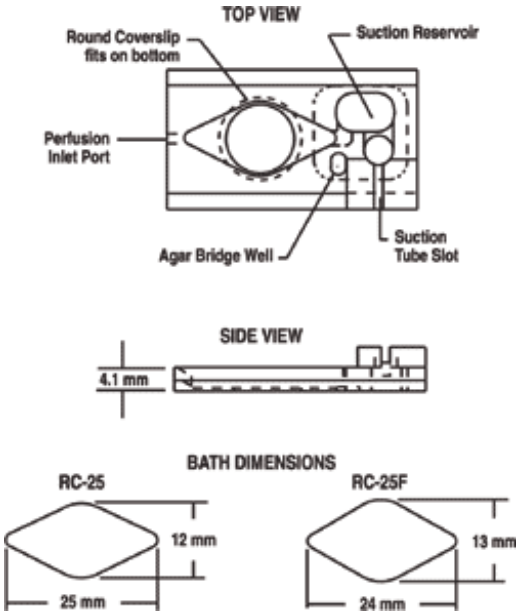

Figure 8 Warner Instruments Chamber Platform
Schematic of the chamber platform used during calcium imaging. The coverslip with cells was clamped underneath the chamber platform. The bath has a volume of 369μL. With the flow speed set to 3mL/min, this means the solution in the bath is replaced every 7.38 seconds. Figure from https://warneronline.com/img_lg/line/250/rc-25.gif

A Peltier device (Pedcool) linked to a custom-built temperature controller (CVScientific) was used to apply cold and heat ramps during the experiments. The Peltier device itself was cooled using a water cooling pump (XSPC). Temperature protocol traces were recorded separately beforehand. Cold ramps to ~5°C were applied for 2 minutes each time. At the end of each experiment, a high K^+ solution was added to depolarise all the living neurons on the coverslip (Table 5) and thus confirm neuronal identity. A high intensity arc lamp and monochromator (Cairn) was used to excite the sample and an iXon EMCCD camera (Andor) was used to record fluorescence signals. In concert, WinFluor software (University of Strathclyde) was used to record the fluorescence over time at a frame rate of one frame per second, alternating between capturing an image at 340nm excitation and 380nm excitation, with an exposure time of 100ms per frame. This way, one $F_{340/380}$ ratio image was obtained every two seconds. Images were exported as TIFF files.

Table 4 Hank's Balanced Salt Solution (HBSS)

	mM	**Source**
$CaCl_2$	1.8	Sigma
$MgCl_2$	1	Sigma
KCl	4	Sigma
NaCl	140	Fisher
Hepes	10	Sigma
D-glucose	4	Fisher

Table 5 High KCl HBSS

	mM	**Source**
$CaCl_2$	1.8	Sigma
$MgCl_2$	1	Sigma
KCl	50	Sigma
NaCl	94	Fisher
Hepes	10	Sigma
D-glucose	4	Fisher

2.2.10 Optimisation

The calcium imaging technique was optimised in several ways. The chamber platform was leaky, so Vaseline was added around the edges of the coverslip to prevent leakage onto the microscope objective. To ensure a constant perfusion rate, flow controllers were added to the perfusion system and the perfusion rate was matched for all solution chambers. Stopcocks were added to the perfusion system that allows access of an extra syringe, which can be used to flush the system before and after experiments to eliminate bubbles as well as wash the tubing.

The Peltier controller available in the lab at the start of this project could not cool below ~10°C. This was a problem because many cold-sensitive neurons have a threshold of activation below 10°C. It also produced a temperature recording with many artifacts (Figure 9). Therefore, a new Peltier controller was purchased from CVScientific and used for all experiments reported in this thesis. See Figure 18 for an example of a temperature trace generated by the new system.

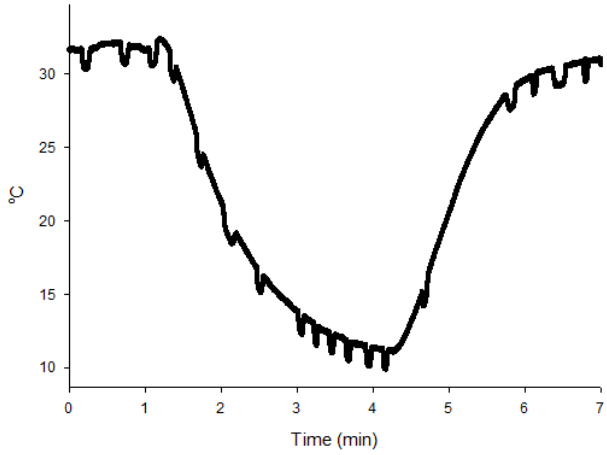

Figure 9 Typical temperature trace of the old Peltier controller.
Representative recording of temperature change in the bath during a cold ramp from 32 °C to 11°C. Cooling below 10°C was not possible. Dips in the trace are an artefact of unknown origin.

The main obstacle that was encountered during application of cold ramps was the formation of condensation on the bottom of the coverslip. This reduced the fluorescence intensity and made it impossible to image the cellular responses to cold (Figure 10). Several attempts were made to reduce this condensation. First, a dehumidifier was placed in the room. Second, coverslips were silanized with (3-Aminopropyl) triethoxysilane (APTES) to make them hydrophobic. Several different silanisation protocols were tried. Third, silica-dried air was blown onto the bottom of the coverslip. None of these methods satisfactorily prevented condensation from forming. Therefore, a 20x water immersion objective was purchased from Nikon, which eliminated the possibility of condensation because there is no air in between the coverslip and the objective.

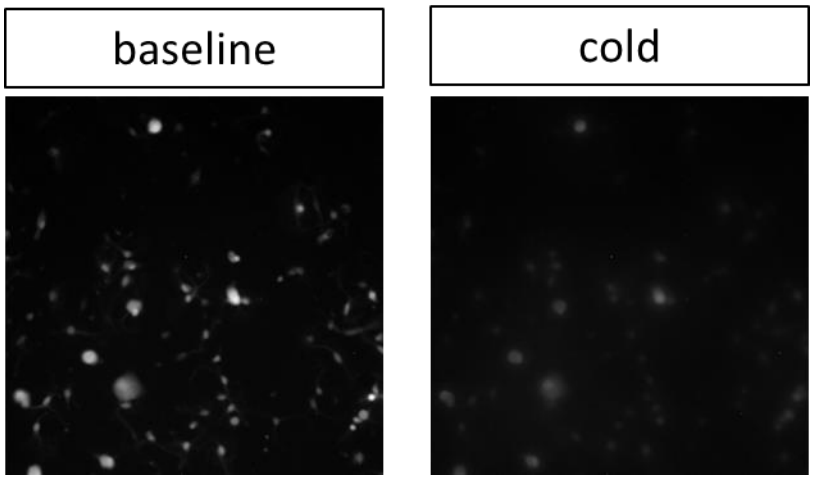

Figure 10 Condensation during cooling greatly decreased the Fura-2 signal.
Representative images of DRG neurons plated on glass coverslips, labelled with Fura2-AM dye, and excited at 340nm wavelength. At baseline (left) cells looked bright, but during cold ramps (right) condensation formed on the glass between the cells and the microscope objective, which greatly decreased the observed signal. Similar results were obtained after a dehumidifier was placed in the room; after the glass coverslips were silanised to make them more hydrophobic, and silica-dried air was blown onto the glass coverslips during imaging.

2.2.11 Data Analysis

FIJI (ImageJ) software was used to measure the fluorescence intensity per cell over time, and background fluorescence of the coverslip. Average background values were calculated from five unoccupied regions of the field of view and subtracted from each frame using Excel software. The ratio of the fluorescence at 340nm and 380nm excitation was calculated from the subtracted traces.

Cell cultures from peripheral ganglia consist of both neuronal and non-neuronal cells, such as glia, and application of a high K^+ solution was used to activate Ca_V channels and thus identify neurons. Any cell with a $F_{340/380}$ ratio increase of >1 in response to K^+ application was identified as neuronal. All other cells were excluded from further analysis. Additionally, neurons with a high Ca^{2+} baseline were excluded. This exclusion criterion is based on the knowledge that a healthy cell maintains a very low (~100nm) level of Ca^{2+}, which corresponds to the observed baseline $F_{340/380}$ mode of 0.7. Therefore, any cell with a maximum $F_{340/380}$ value of >1.5 during the baseline period was assumed to be functioning abnormally and excluded from further analysis (Figure 11). These exclusion criteria never resulted in exclusion of more than 10% of neurons.

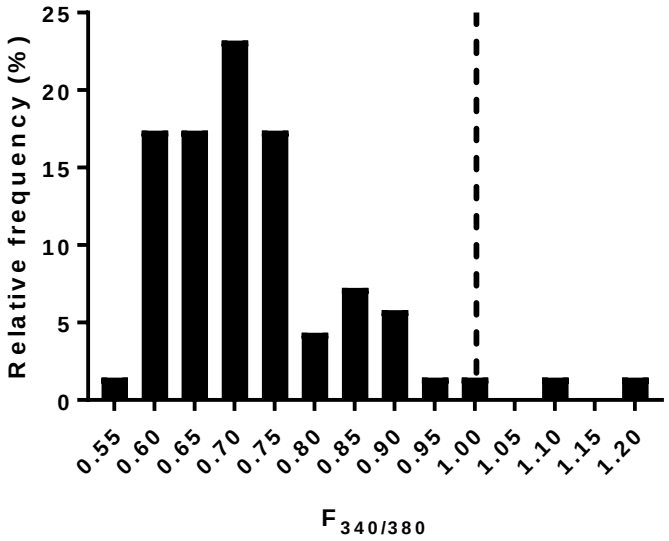

Figure 11 SCG neuron $F_{340/380}$ at baseline.
Frequency histogram showing the baseline values of SCG neurons at 32°C. The modal baseline is 0.7. Dotted line indicates threshold for exclusion.

As discussed previously, Fura-2 fluorescence is affected by temperature changes (Oliver *et al.*, 2000). To exclude false positives and negatives from the data, we therefore took concurrent measurements in glia present in the cell cultures and defined thresholds for heat and cold response as mean $F_{340/380}$ increase in glial cells + 3.09 SD. This eliminated 99.9% of false positives and negatives from the data, however it is based on the assumption that glia do not experience a change in $[Ca^{2+}]_i$ in response to temperature change (method from Tan & McNaughton 2016).

To determine the phenotype of sympathetic neurons, neurons were labelled with fluorescent antibodies and mean pixel intensity was measured for each neuron. Then, the mean pixel intensity of the three neurons with the lowest pixel intensity was calculated and the threshold was defined as 2*mean + 6*SEM (method from Tsantoulas et al. 2017). This method was found to be the most similar to a separate manual quantification of the data performed on three individual coverslips.

2.3 Results

2.3.1 Characterisation of Neurotransmitter Phenotypes in Peripheral Ganglia

To observe the general size and shape of mouse sympathetic ganglia, the superior cervical ganglion (SCG), which innervates the face and back of the head, was dissected. This ganglion was used because it is the largest of the sympathetic ganglia and it is conveniently located behind the bifurcation of the common carotid artery and therefore relatively easy to locate and dissect out. A haematoxylin and eosin (H&E) stain was performed to look at the general size and shape of the ganglion. Figure 12 shows a longitudinal and transverse section of typical SCGs, which have an elongated shape. Visible structures include the preganglionic fibres, neuronal cell bodies and their corresponding postganglionic fibres, as well as many glial cells. The neuronal fibres are much more prominent and cover the cells in longitudinal sections. Therefore, transverse sections were favoured in most subsequent figures, which allow for a clearer view of the cell bodies.

There is great variability in the shape of the SCG both between animals and within the same animal. For instance, the ganglia in Figure 12 are from the same animal, but the one displayed on the left has a more elongated shape, while the one on the right has a more rounded shape. A transverse section of the ganglion on the left would look about half the size on this scale.

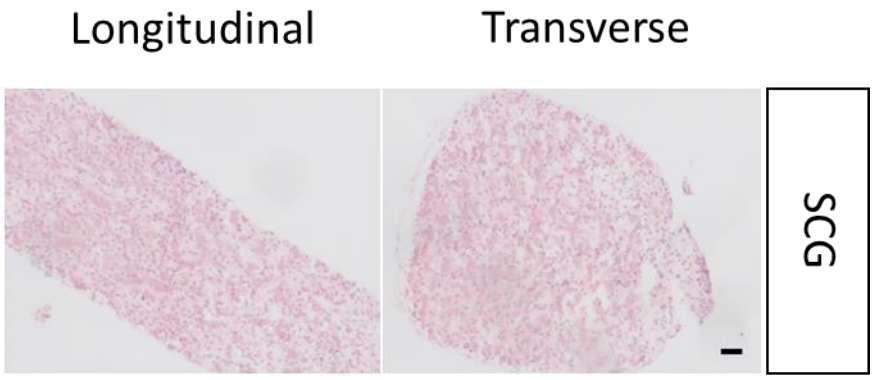

Figure 12 Hematoxylin and eosin stain shows the structure of mouse superior cervical ganglion (SCG).
Representative images of longitudinal (left) and transverse (right) sections of adult mouse SCG that were stained with hematoxylin (blue) and eosin (pink) marking DNA in nuclei and cytoplasmic protein in cell bodies respectively. Both ganglia are from the same animal. Visible structures include the preganglionic fibres, as well as the postganglionic cell bodies and fibres. It is not possible to distinguish between pre- and postganglionic fibres in these images. In some animals the SCG has a more extended shape as the longitudinal section on the left shows, and in some animals the shape is more rounded. Transverse sections were favoured in most subsequent figures because the preganglionic fibres are less prominent in those images. n=1. Scale bar = 50 μm.

Sympathetic neurons are known to be mostly noradrenergic in phenotype and should therefore stain positive for Tyrosine Hydroxylase. To confirm accurate dissection of sympathetic ganglia, the superior cervical ganglion, stellate ganglion and two subsequent paravertebral ganglia as well as dorsal root ganglia were dissected and stained with antibodies to identify TH expression (Figure 13). As expected, most sympathetic neurons - but only a small number of DRG neurons - were labelled, which also confirms specificity of the antibody.

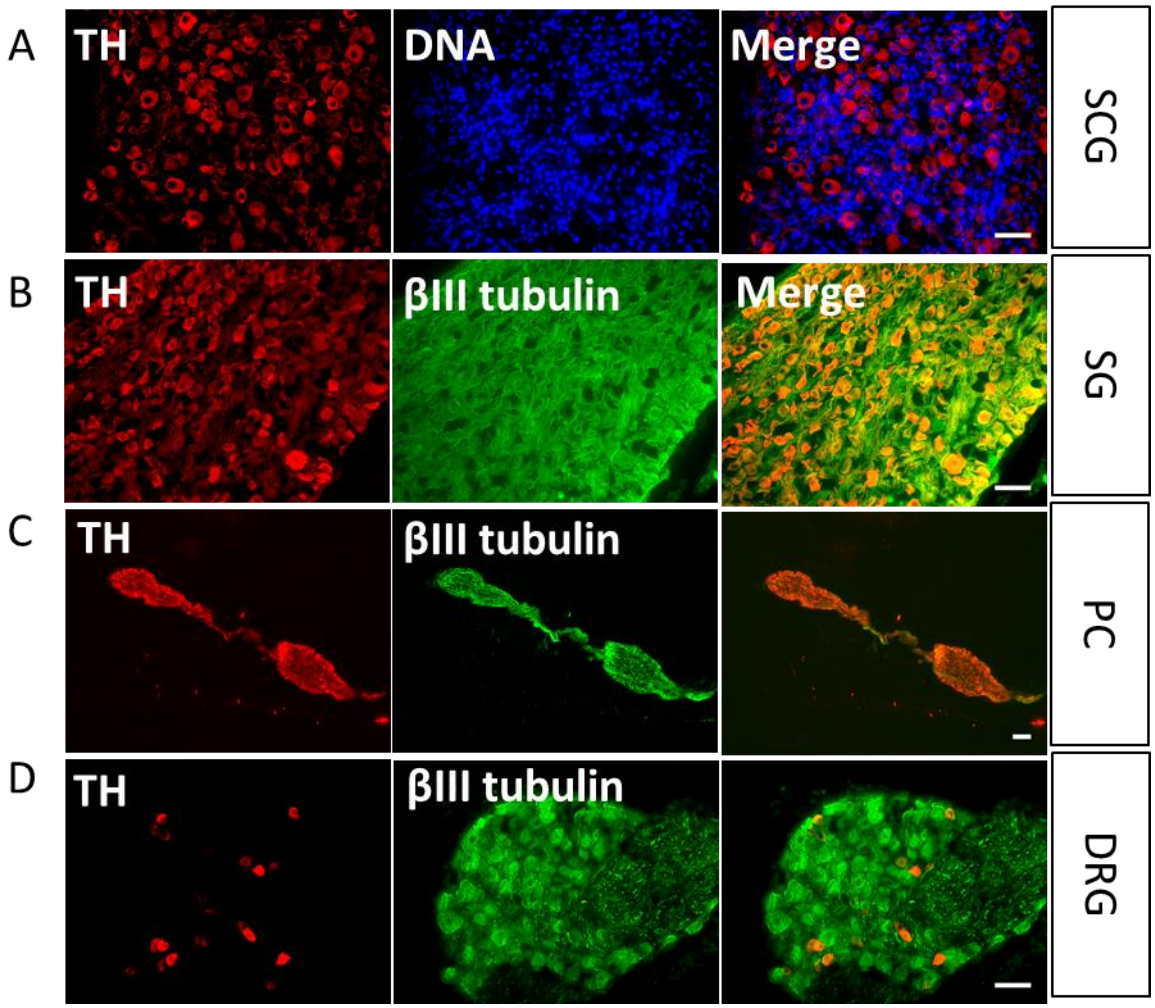

Figure 13 Expression of Tyrosine Hydroxylase (TH) confirms sympathetic and sensory phenotypes of dissected ganglia.
Fluorescence images showing adult mouse SCG (A) n=2, SG (B) n=3, PC (Paravertebral Chain) (C) n=1, and DRG (D) n=3 sections that were stained for TH (red) to label noradrenergic/dopaminergic neurons and βIII Tubulin to label all neurons respectively. TH is widely expressed in SCG, SG, and paravertebral chain, confirming their sympathetic phenotype. DRG sections are from the same animal and function as a positive control. TH is expressed in a subset of DRG neurons as expected. Rabbit anti-TH (1:500 was used in combination with donkey anti-rabbit 594; mouse anti-βIII Tubulin (1:1000) was used in combination with goat anti-mouse 488 (1:1000. Nuclei of both neurons and glia are shown in blue by 4',6-diamidino-2-phenylindole staining (DAPI, 1:50,000). Scale bar = 50 μm.

Along with noradrenergic neurons, sympathetic ganglia also contain cholinergic neurons expressing the synthetic enzyme for acetylcholine: choline acetyltransferase (ChAT) (Nagatsu, Levitt and Udenfriend, 1964). The aim of this chapter is to test the hypothesis that there is a correlation between the temperature sensitivity of these cells and their neurotransmitter subtype. Therefore, we first characterised the distribution of these cells in the SCG with immunohistochemical methods.

The commercially available antibodies for ChAT are suboptimal for use in the peripheral nervous system as they bind to a region of the protein that is present in central ChAT but is spliced out of peripheral ChAT (Tooyama and Kimura, 2000). Therefore, we used transgenic mice that express GFP under the ChAT promoter, and we labelled cholinergic neurons with antibodies for GFP instead. Despite this, no cholinergic neurons could be identified in the SCG and all cells seem to express TH and are therefore noradrenergic in nature (Figure 14A).

Preganglionic fibres of the sympathetic nervous system are all cholinergic and stain for GFP in these images (Figure 14A), providing reassurance that the ChAT stain was specific. A possible reason for the failure to identify ChAT-expressing neurons in mouse SCG could be that this ganglion does not innervate any skin that contains sweat glands in the mouse and cholinergic neurons are therefore rare (Anderson et al. 2006).

The stellate ganglion (SG), which innervates the heart, ribs, and forelimbs, including some sweat glands in glabrous skin of the paw, contains the largest number of cholinergic neurons (Apostolova and Dechant, 2009). Therefore, the same experiment was repeated on sections of the stellate ganglion (Figure 14B). The stellate ganglion does indeed contain cholinergic neurons, albeit very few.

Three neuronal subtypes can be identified in these images: most cells are purely noradrenergic and do not express ChAT; some cells are purely cholinergic and do not express TH; some cells express both ChAT and TH. These subtypes represent noradrenergic and cholinergic neurons as expected, and a third subtype of neurons, which may be noradrenergic neurons in the process of converting into cholinergic neurons (see general introduction section 1.1.5.2).

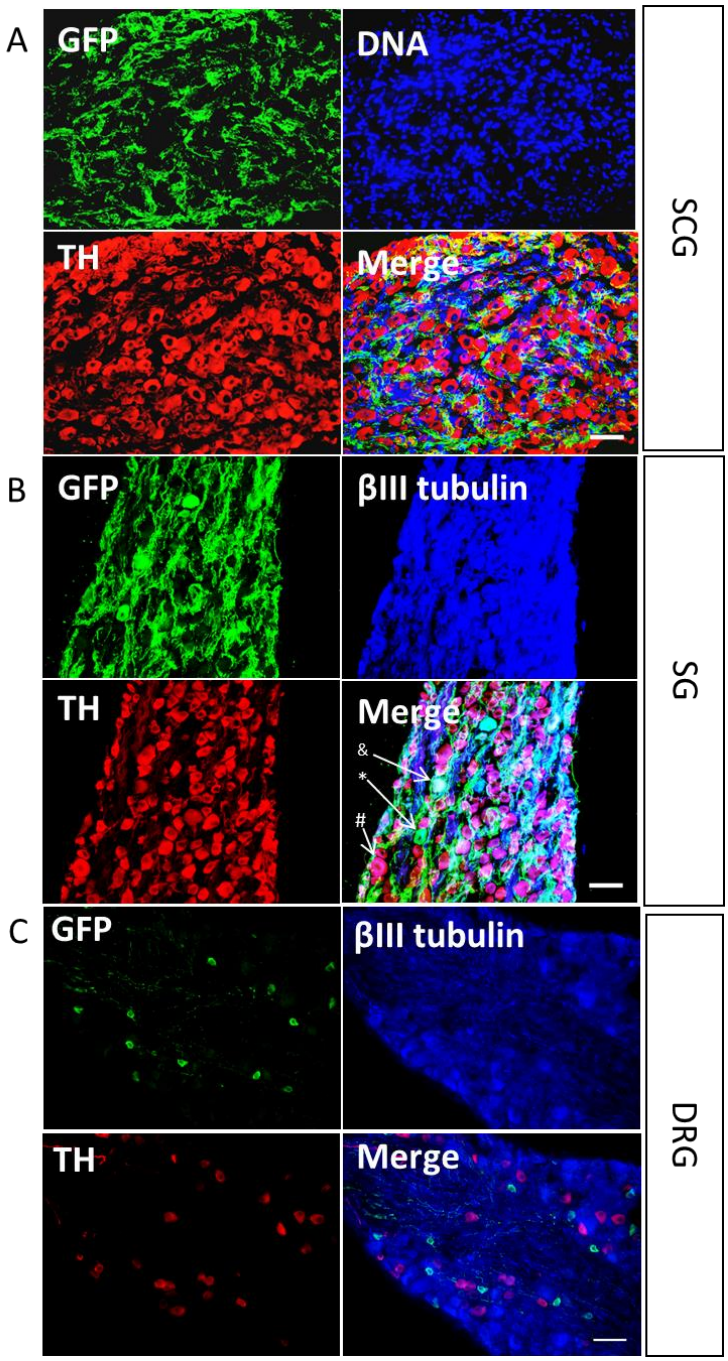

Figure 14 The SCG does not contain cholinergic neurons, but the Stellate ganglion (SG) and Dorsal Root Ganglion do.

A) Fluorescence images showing adult ChAT-GFP mouse SCG sections that were stained for GFP, which marks ChAT (green) and TH (red) to label cholinergic and noradrenergic neurons respectively. Many cholinergic preganglionic fibres are visible, but no cell bodies. Chicken anti-GFP antibody (1:1000) was used in combination with goat anti-chicken Alexa Fluor 488 (1:1000); rabbit anti-TH (1:500 was used in combination with donkey anti-rabbit 594; Nuclei of both neurons and glia are shown by 4',6-diamidino-2-phenylindole staining (DAPI, blue, 1:50,000). n=4. Scale bar = 50 μm. B) Fluorescence images showing adult ChAT-GFP mouse SG sections that were stained for GFP to mark ChAT (green), TH (red), and βIII Tubulin (blue) to label cholinergic, noradrenergic/dopaminergic, and all neurons respectively. Three types of neurons are visible: purely cholinergic neurons (*), purely noradrenergic neurons (#), and neurons that coexpress ChAT and TH (&). Cholinergic neurons are scattered randomly throughout the SG. n=5. Scale bar = 50 μm. C) Fluorescence images showing adult ChAT-GFP mouse DRG sections that were stained for GFP to mark ChAT (green), TH (red), and βIII Tubulin (blue) to label cholinergic, noradrenergic/dopaminergic, and all neurons respectively. ChAT and TH are expressed in distinct neuronal populations, which also shows that there is little non-specific binding of the antibodies. The neurons expressing ChAT are smaller in size than the TH-expressing neurons. Chicken anti-GFP antibody (1:1000) was used in combination with goat anti-chicken Alexa Fluor 488 (1:1000); rabbit anti-TH (1:500 was used in combination with donkey anti-rabbit 594; mouse anti-βIII Tubulin (1:1000) was used in combination with goat anti-mouse 350 (1:1000). n=7. Scale bar = 50 μm.

Experiments to determine the correlation between temperature sensitivity and neurotransmitter type required isolated neurons. Therefore, SG neurons were dissociated using the protocol described in methods. Figure 15 shows these cells under control conditions, i.e. without prior Ca^{2+} imaging. Cultured SG neurons show the same phenotypic subdivision as previously seen in tissue sections, namely cholinergic, noradrenergic, and cholinergic/noradrenergic, i.e. ChAT/TH co-expressing cells.

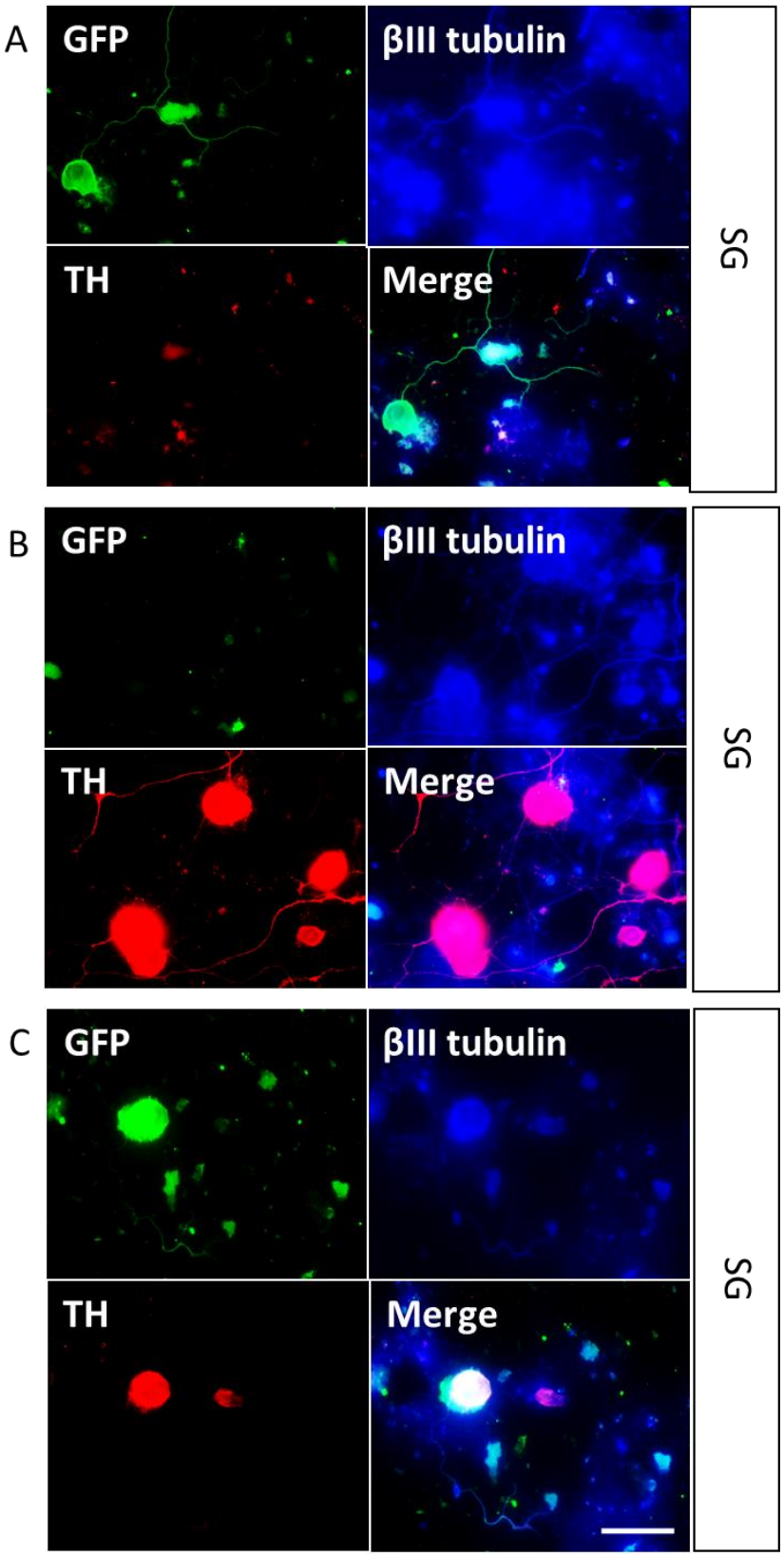

Figure 15 Cultured stellate ganglion neurons show the same phenotypic subdivision into TH+ (noradrenergic), ChAT+ (cholinergic) and TH/ChAT co-expressing cells as previously seen in tissue sections.
Fluorescence images showing cultured SG neurons from adult ChAT-GFP mouse that were stained for GFP to mark ChAT (green), TH (red), and βIII Tubulin (blue) to label cholinergic, noradrenergic, and all neurons respectively. SG neurons from adult mice were fixed one day after isolation. Neuronal subtypes include cholinergic (A), noradrenergic/dopaminergic (B), and neurons that have both phenotypes (C). These three subtypes were also seen in tissue sections. Chicken anti-GFP antibody (1:500) was used in combination with goat anti-chicken Alexa Fluor 488 (1:1000); rabbit anti-TH (1:500 was used in combination with donkey anti-rabbit 594; mouse anti-βIII Tubulin (1:500) was used in combination with goat anti-mouse 350 (1:1000). n=4. Scale bar = 50 μm.

It is not possible to detect the difference between noradrenergic postganglionic neurons and dopaminergic interneurons (Takaki *et al.*, 2015) in the sympathetic nervous system using an antibody against tyrosine hydroxylase, as TH is involved in the synthesis of both dopamine and noradrenaline (Figure 16). Therefore, an antibody against dopamine-ß-hydroxylase was tested. This way only noradrenergic neurons would be stained for. Unfortunately, this antibody was not of good quality and failed to clearly label neurons, indicated by the lack of visible neuronal arbours (Figure 17).

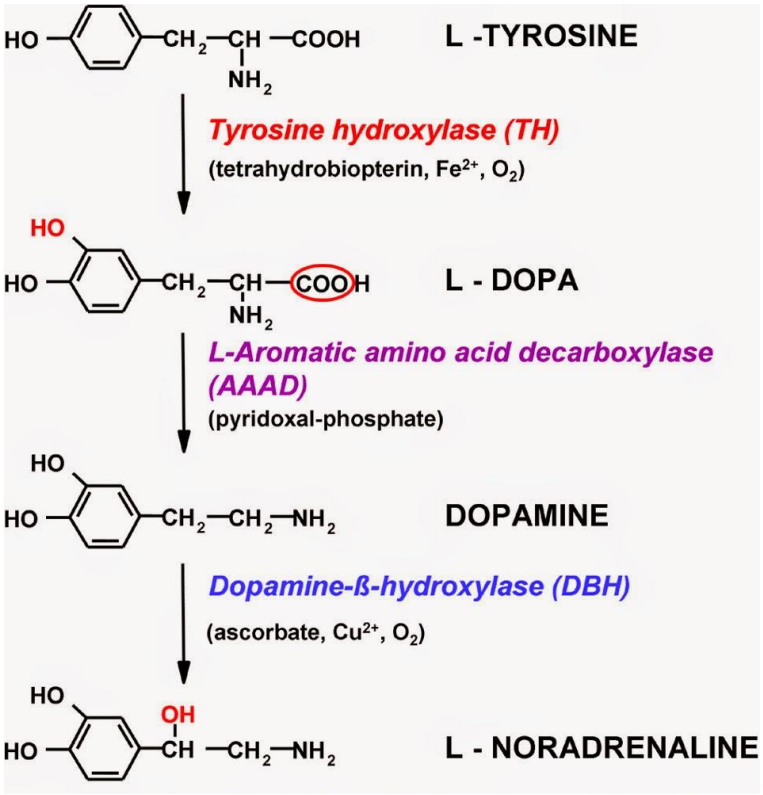

Figure 16 Noradrenaline synthesis pathway.
An antibody against tyrosine hydroxylase cannot be used to distinguish between dopaminergic and noradrenergic neurons, because this enzyme is located upstream of both neurotransmitters. Only an antibody against DBH could be used to exclusively label noradrenergic neurons. Image modified from Kuhar MJ, Couceyro PR, Lambert PD. Biosynthesis of Catecholamines. In: Siegel GJ, Agranoff BW, Albers RW, et al., editors. Basic Neurochemistry: Molecular, Cellular and Medical Aspects. 6th edition. Philadelphia: Lippincott-Raven; 1999.

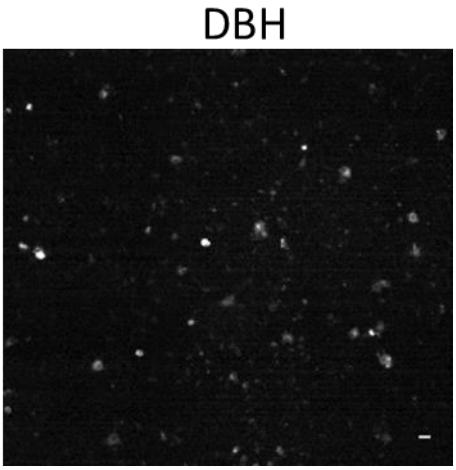

Figure 17 The antibody for DBH did not provide good quality images
Fluorescence images showing culture SG neurons from adult GFP-ChAT mice that were stained for DBH to label noradrenergic neurons. SG neurons from adult mice were fixed one day after isolation. The quality of the DBH stained images was not high enough for use in further experiments. Rabbit anti-DBH (1:300) was used in combination with donkey anti-rabbit 594 (1:1000). DBH staining was also tested at 1:1000 and 1:500 dilution, which did not improve the image quality (data not shown) n=1. Scale bar = 20µm. Experiment performed by BSc student Nairuti Patel.

2.3.2 Sympathetic Neurons can be Activated by Cold and Heat

Cultured sympathetic neurons can respond to both cold (Munns, AlQatari and Koltzenburg, 2007) and heat (Tan and McNaughton, 2016). To confirm these findings, cold and heat ramps were applied to a primary culture of SCG neurons and their responses were measured using calcium imaging as described in the methods section. Figure 18 shows the responses of different neurons to heat and cold. Sympathetic neurons can be subdivided in four categories according to these responses: heat-sensitive; cold-sensitive; cold- and heat-sensitive; or temperature-insensitive. The percentages of each subtype in SCG and SG are summarised in Table 6.

In order to mitigate any effect of the order of the heat and cold ramps, both orders were tested and found not to influence the percentage of neurons responding to either stimulus. The percentage of heat-sensitive neurons in the SCG reported here (16.1%) is lower than the percentage reported in the literature (58%) (Tan and McNaughton, 2016). This may be due to the ~10°C difference in baseline temperature. The SCG neurons were heated to 47°C in both cases, but in our case were heated from skin temperature at baseline, rather than room temperature. The percentage of cold-sensitive neurons in the SCG reported here (18.3%) is similar to the percentage reported in the literature (20%) (Smith et al., 2004).

Table 6 Proportion of neurons belonging to each subtype in SCG and SG

	Heat	Cold	Both	Neither
SCG (n = 218)	16.1%	18.3%	2.8%	78.4%
SG (n = 396)	14.1%	21.5%	2.5%	66.9%

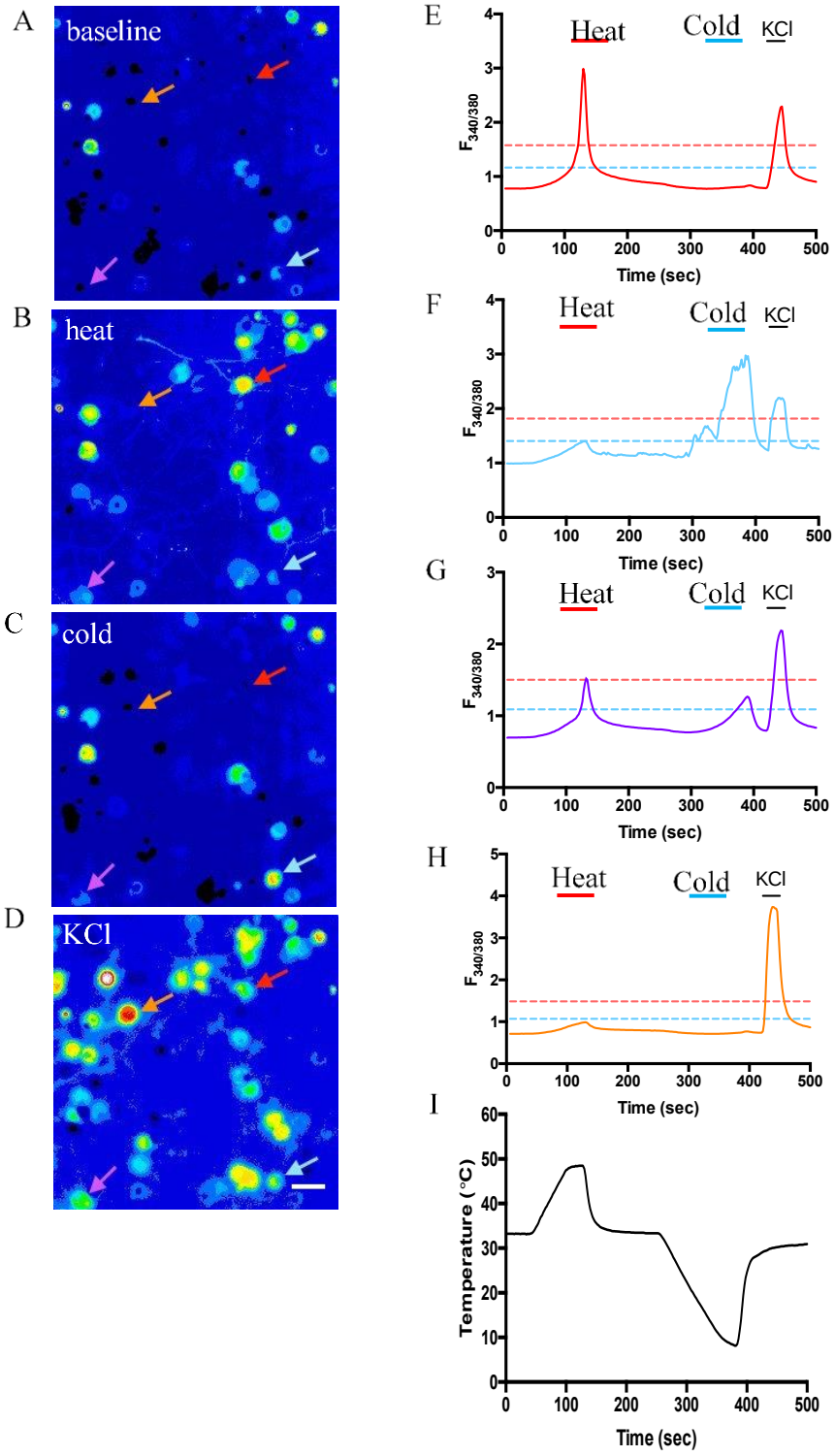

Figure 18 Sympathetic neurons can sense both heat and cold.
A-D) pseudocolour $F_{340/380}$ images showing intracellular Ca^{2+} levels of SG neurons at baseline (A) and during application of heat (B), cold (C), and 50mM K^+ (D). Scale bar = 30µm. E-H) Representative traces of the four neurons with arrows in images A-D. The colours of the traces correspond to the arrows on images A-D. There are four different types of neurons: those responding to heat only (E), those responding to cold only (B), those responding to both heat and cold (G) and those responding to neither stimulus (H). A pulse of K^+ is applied at the end of the experiment to confirm neuronal identity. Heat and and cold thresholds are shows as dotted lines in red and blue respectively and were calculated as the mean $F_{340/380}$ + 3.09 SD of glia on the same coverslips. I) Temperature protocol. Data analysis performed by BSc student Joshua Taussig.

Another way to visualise the responses of neurons to temperature changes is by plotting the $F_{340/380}$ together with the temperature at each timepoint (Figure 19). These graphs clearly show the temperature thresholds at the inflections points as well as the temperatures of peak response. Data is shown for representative cold-sensitive (A), heat-sensitive (B) and heat- and cold-sensitive (C) neurons.

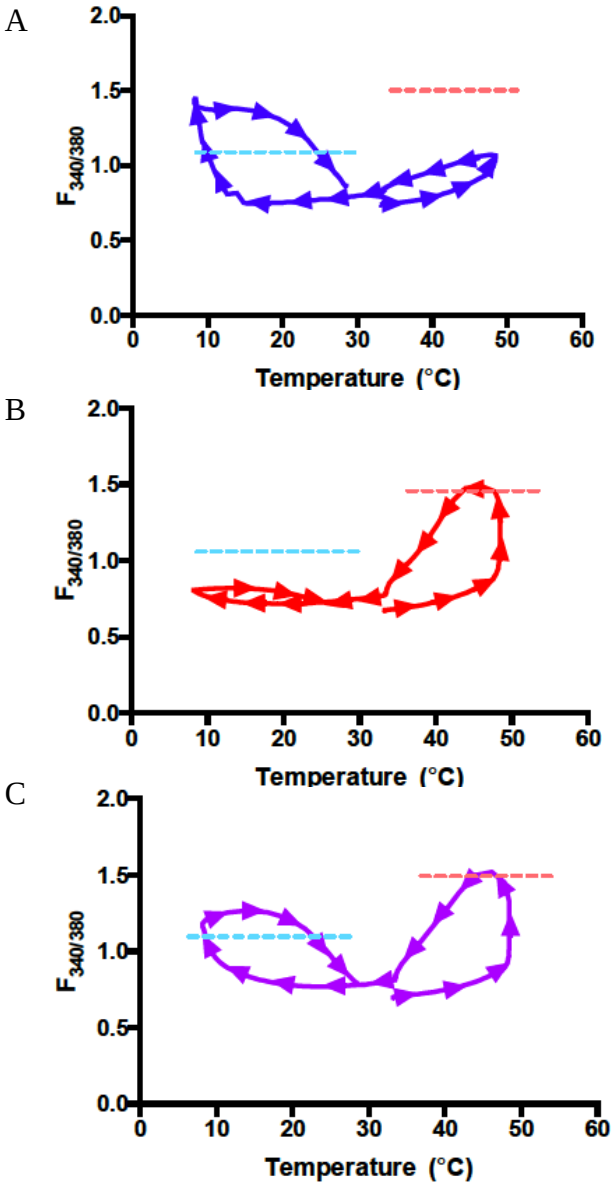

Figure 19 Sympathetic neurons responding to different temperatures
A-C) Graphs showing examples of a neuron responding to cold (A), heat (B), and both stimuli (C). Arrows indicate the direction of the passage of time. Dotted lines mark the thresholds for cold (blue) and heat (red) responses used in data analysis (calculated as in Figure 18). Data analysis performed by BSc student Joshua Taussig.

The aim of this experiment was to determine the proportion of neurons responding to heat and/or cold. However, this data can also be used to estimate the activation threshold temperatures for each neuron. This was defined as the temperature at which the $F_{340/380}$ increase passed the threshold value of the mean of glial cell responses +3.09SD. Using this method, the average response threshold was 46.6 ± 0.31°C for heat responses and 12.1 ± 0.50°C for cold responses (data presented as mean ± SEM). These results are consistent with the reported thresholds in the literature of 11.8-16.9°C (Munns, AlQatari and Koltzenburg, 2007). The Frequency histograms in Figure 20 show that the modal response threshold was 48°C for heat, which is only 2°C below the maximum temperature reached by the ramp. This could be interpreted as a reason to increase the maximum stimulus temperature. However, very few neurons were activated at 49°C, so this was not deemed necessary. In contrast, the modal cold activation threshold was at the lower end of the cold stimulus. This suggests that our data underestimates the proportion of neurons responding to cold.

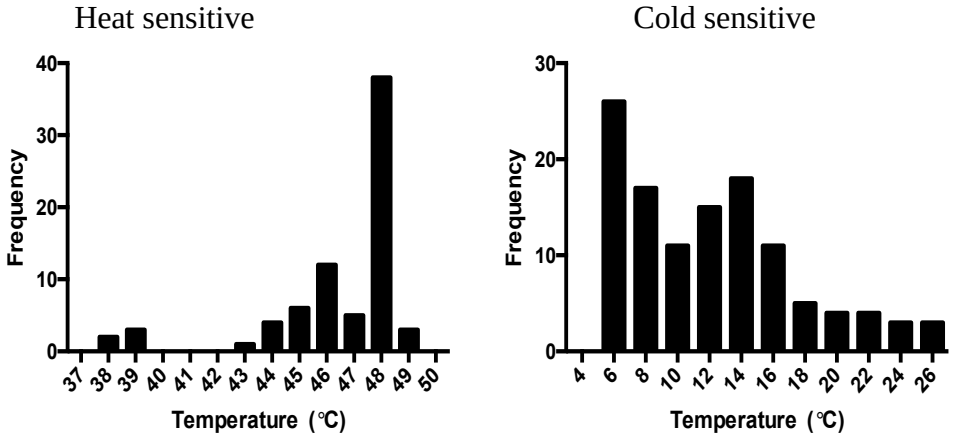

Figure 20 Frequency histograms of responses to heat and cold.
Frequency histograms showing a somewhat bimodal distribution of heat (n=74) and cold (n=120) response thresholds. The mode for heat responses was 48°C and for cold responses 6°C. Data analysis performed by BSc student Joshua Taussig.

As described in the methods section, the mice used for these experiments express GFP in cholinergic neurons. We had hoped that these neurons would be visible on our Ca^{2+} imaging setup. However, even with maximal gain it was not clear which neurons were expressing GFP and which were not (Figure 21). Furthermore, our previous discovery that neurons can carry both a noradrenergic and a cholinergic phenotype (Figure 14 and Figure 15) made it necessary to perform immunocytochemistry on the neurons after calcium imaging.

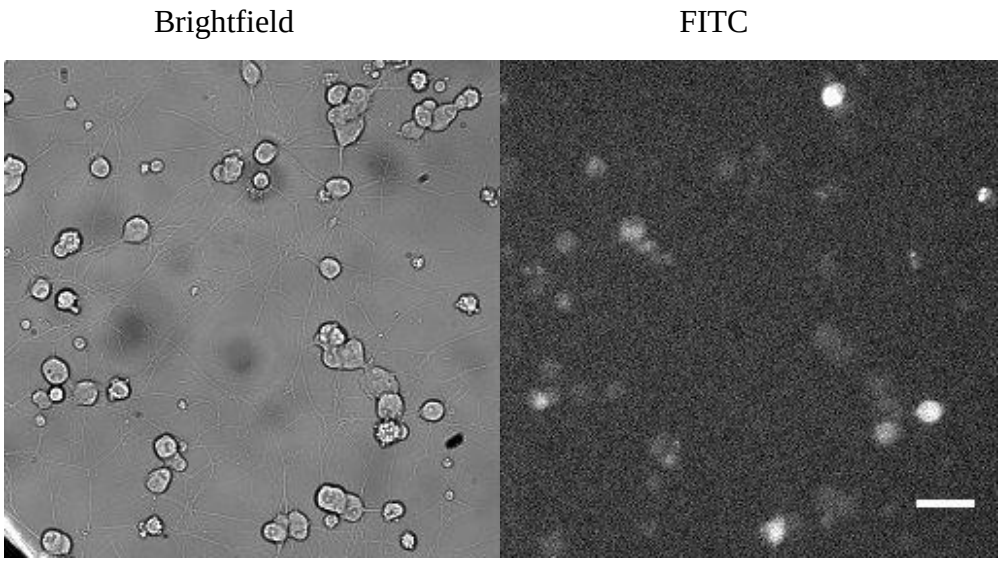

Figure 21 Endogenous GFP expression was not clearly visible on our calcium imaging setup.
Representative images of live cells taken using the brightfield (left) and FITC (right) emission filters without prior antibody labelling. The FITC image was taken at maximum gain, but shows no clear distinction between cholinergic and non-cholinergic neurons. Scale bar = 30μm.

After Ca^{2+} imaging, coverslips were fixed and stained with antibodies against ßIIItubulin, TH and GFP to label all neurons, noradrenergic neurons, and cholinergic neurons respectively. Quantitative analysis of 1459 neurons on 8 coverslips showed that 84.7±2.1% of neurons in the stellate ganglion were exclusively noradrenergic, 15.4±5.9% were exclusively cholinergic, 11.0±2.0% co-express both phenotypes, and 11.0±2.0% were found to be non-adrenergic non-cholinergic neurons (NANC). These findings roughly match the recent scientific literature, which reports 83-91% noradrenergic, 2.5-5% cholinergic, and 4-14.5% NANC neurons (Masliukov *et al.*, 2012, 2013, 2014, 2015). Notably, we have found a somewhat larger percentage of cholinergic neurons. One explanation for this may be that we used a mouse expressing GFP in cholinergic neurons and an antibody for GFP, which is possibly a more sensitive method than using antibodies for cholinergic markers ChAT and vesicular acetylcholine transporter (VAChT). The discrepancy could also be due to different analysis methods or the species and age of the mice. The population of cholinergic neurons in the sympathetic ganglia increases until postnatal day 10, and then decreases until day 60 (Masliukov *et al.*, 2015). The mice used in this study were aged between 14-44 days, which may provide another explanation for the higher number of cholinergic neurons identified.

Because the neurons were grown on coverslips that had the letter “F” etched into them, we could use the brightfield images to locate the area of the coverslip that corresponded

to the field-of-view visible on the calcium imaging microscope. The Ca^{2+} imaging data images were then made partially transparent and rotated and overlaid on the immunocytochemistry data to locate the correct field-of-view (Figure 22). This allowed each neuron to be classified according to both their temperature sensitivity and their neurotransmitter phenotype.

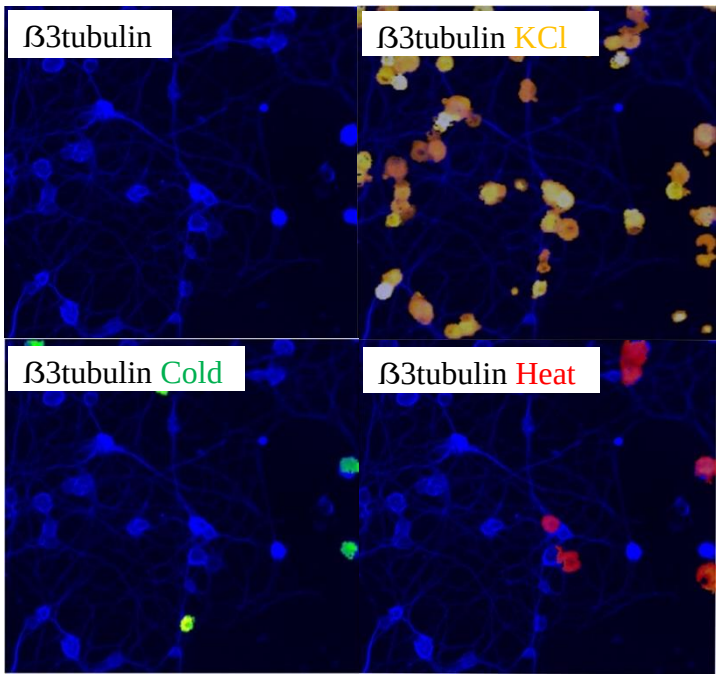

Figure 22 Image overlays allowed for correllation of the calcium imaging and immunocytochemical data. Representative fluorescence images showing cultured SG neurons from adult ChAT-GFP mice that were stained for βIII Tubulin (blue) to label all neurons and overlaid with calcium imaging data during 50mM K^+ application (yellow), cold (green) and heat ramps (red) n=7. Mouse anti- βIII Tubulin (1:500) was used in combination with goat anti-mouse 350 (1:1000). Some neurons are visible on the calcium imaging data but not the immunocytochemical data, which indicates that they were lost during the fixation or staining process. Data analysis performed by BSc student Joshua Taussig.

2.3.3 Correlation of Temperature Sensitivity and Neurotransmitter Phenotype

If our hypothesis is true that cholinergic neurons can sense heat, to promote sweating and noradrenergic neurons can sense cold, to promote vasoconstriction, then the results of this experiment should show that all heat-sensitive neurons are cholinergic, and all cold-sensitive neurons are noradrenergic. We found that in the SG 2.9% of heat-sensitive neurons were exclusively cholinergic (cf. 3.3% in general population) and 82.6% of cold-sensitive neurons were exclusively noradrenergic (cf. 72.6% in general population). This suggests that heat-sensitive neurons were not more likely to be exclusively cholinergic and cold-sensitive neurons were only somewhat more likely to

be exclusively noradrenergic (Table 7). Unfortunately, the n of this experiment was too low to perform a valid Chi squared (χ^2) test to determine whether this observed difference is statistically significant.

A paper that was published after this study was performed showed that TRPM2 is highly expressed in noradrenergic neurons of the mouse sympathetic nervous system, except for vasomotor neurons, but it is not expressed in cholinergic neurons and could therefore not mediate heat responses in these neurons (Furlan *et al.*, 2016). This is consistent with our findings. The same paper does report that another heat-sensitive ion channel with a higher temperature threshold of 52˚C (TRPV2) is highly expressed in all cell types of the sympathetic nervous system, including cholinergic neurons. We heated the neurons to 49˚C, so would not have activated any TRPV2-expressing neurons here.

Table 7 Observed phenotypic frequencies of SG neurons.

	Observed frequency (%)			
	Population (n = 1459)	Heat-sensitive (n=35)	Cold-sensitive (n=23)	Polymodal (n=8)
Noradrenergic	84.71	94.29	91.30	100.00
Exclusively noradrenergic	72.57	77.15	82.60	87.50
Cholinergic	15.42	20.00	8.70	12.50
Exclusively cholinergic	3.28	2.90	0.00	0.00
Noradrenergic and cholinergic	12.14	17.14	8.70	12.50
NANC	11.00	2.86	8.70	0.00

2.3.4 Retrograde Tracing Labels Vaso- and Sudomotor Neurons

It is important to note that our hypothesis only pertains to those sympathetic nerves that innervate the glabrous skin of the paw, as this is the only area that contains both eccrine sweat glands and blood vessels in the mouse. Furthermore, noradrenergic neurons innervate targets with opposing effects on thermoregulation, for example, salivary glands, which function to cool down the mouse via fur licking, and brown adipose tissue, which causes heat production. Therefore, we decided to use retrograde tracing to identify the subpopulation of neurons that innervate the glabrous skin of the paw and repeat the above experiment.

Initially, two mice were injected with 5µL 5% Fast Blue (FB) dye in PBS in each paw. Unfortunately, these mice did not survive, which may have been due to the paw licking behaviour and consequent dye ingestion we observed after injection. Therefore, the concentration of dye was lowered to 2% and mice were kept under anaesthesia for 20 minutes after injection to allow the dye to be absorbed and paws were cleaned. Figure 23 shows that FB is detectable in the stellate ganglion six days after injection, but not after three days. Since FB was injected into the paw, presumably only vasomotor and sudomotor neurons are labelled in this image.

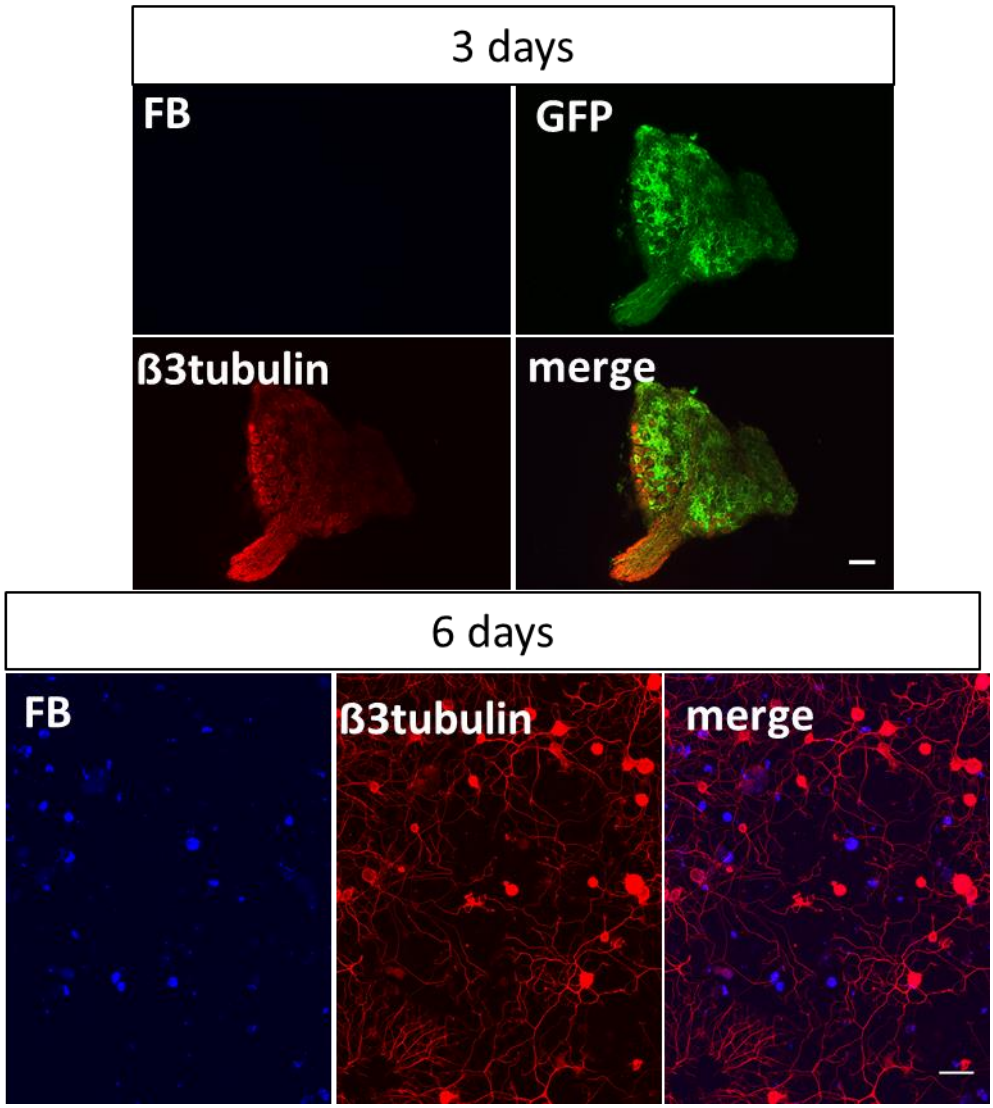

Figure 23 Fast Blue needed between 4 and 6 days to reach the stellate ganglion.
Representative fluorescence images showing a SG section (top) and cultured SG neurons (bottom) from adult ChAT-GFP mice that were stained for βIII Tubulin (red) to label all neurons and GFP to label cholinergic neurons (top only). FB was detectable after six days, but not yet after three days (n=1). Mouse anti- βIII Tubulin (1:1000 top; 1:500 bottom) was used in combination with goat anti-mouse 594 (1:1000). Chicken anti-GFP antibody (1:500) was used in combination with goat anti-chicken Alexa Fluor 488 (1:1000). Scale bar = 50µm.

Having shown that the retrograde tracing method using FB was effective, neurons were loaded with Fura-2 for Ca^{2+} imaging. Unfortunately, this resulted in considerable bleed-through from the Fura-2 fluorescence into the blue channel. This was unexpected, because previous experiments showed that Fura-2 did not appear in the green channel, which overlaps much more with the emission spectrum of Fura-2 than the blue channel does. However, the overlap in **excitation** wavelength of the blue channel and Fura-2 was not considered.

As shown in Figure 24, there is a complete overlap of the excitation of calcium bound Fura-2 and Fast Blue. Furthermore, these images were taken with an exposure time of

100ms, whereas a 2000ms exposure time was needed previously to detect Fast Blue. This makes the FB tracer dye incompatible with Fura-2 dye, as FB cannot be detected once cells are loaded with Fura-2.

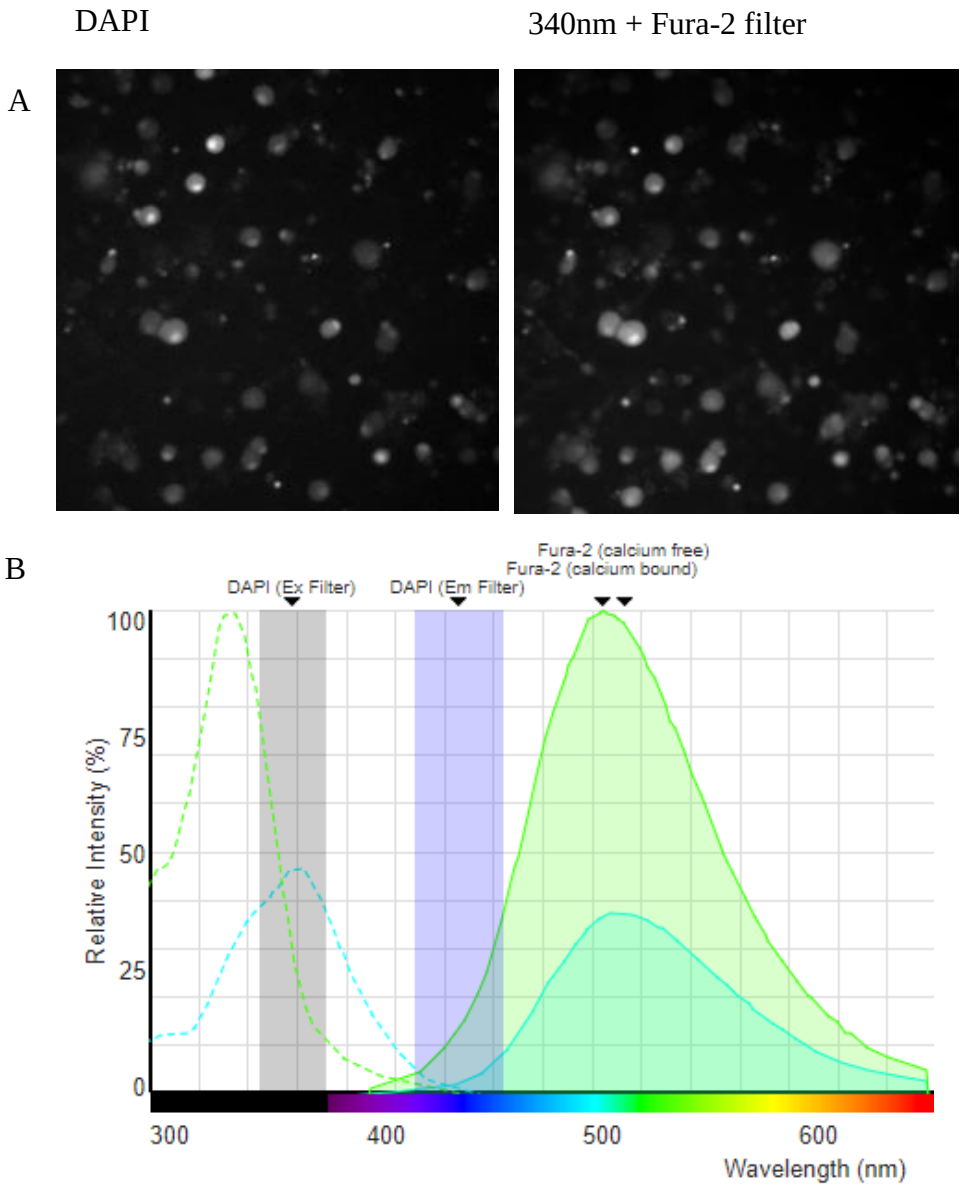

Figure 24 DAPI excitation filter and Fura-2 excitation overlap.
A) Images taken on the calcium imaging setup show that all neurons were visible in the blue DAPI channel, not just the subset of neurons labelled with Fast Blue. B) Fluorescence spectra of Fura-2 and DAPI blue channel filters showing an overlap of excitation wavelengths.

One way forward would be to either use a different tracer dye, or a different Ca^{2+} indicator dye. However, the project was discontinued at this point. The main reason for this was the extremely low-throughput nature of the work. Out of 19 coverslips that were used for Ca^{2+} imaging, only 7 could be used for further analysis as it was impossible to locate the correct field-of-view on the other ones. Furthermore, analysis of 1459

neurons on these 7 coverslips only yielded one heat-sensitive cholinergic neuron. Another reason to discontinue the work was that the data collected in this chapter did not support the hypothesis. Moreover, the observation that sympathetic neurons respond to noxious cold only below 15˚C may be incongruent with our initial hypothesis, because a mechanism that causes vasoconstriction to conserve body heat would be more likely to sense innocuous cold (just below normal skin temperature) instead of noxious cold.

2.4 Conclusion

Previous work has shown that murine sympathetic nerve fibres can respond with an increase in Ca^{2+} to both hot and cold stimuli, though it was not clear whether individual fibres can be polymodal and respond to both stimuli (Munns, AlQatari and Koltzenburg, 2007; Tan and McNaughton, 2016). This begged the question of what the function is of this temperature sensitivity. One of the functions of the sympathetic nervous system is regulation of body temperature, so perhaps these local thermosensitive mechanisms contribute to this process.

We have employed Ca^{2+} imaging in combination with immunocytochemistry to correlate thermal and neurotransmitter phenotypes respectively. We hypothesised that noradrenergic vasoconstrictor neurons would be activated by cold, and cholinergic sudomotor neurons (innervating sweat glands) would be activated by heat. Around half of noradrenergic neurons are vasomotor neurons and half of cholinergic neurons are sudomotor. However, we found no clear correlation between the variables of heat- and cold-sensitivity and noradrenergic or cholinergic phenotype.

The percentage of noradrenergic neurons that are cold-sensitive may be much larger when looking at only those nerves innervating the blood vessels, so we attempted retrograde tracing to identify this population. This method needed further optimisation, but the project was discontinued due to the low yield. Nevertheless, a future study that groups these neurons more specifically depending on their target organ could produce interesting results. SCG neurons express subtype-specific neuropeptides that could be used as markers e.g. NPY, which is a specific marker for vasomotor neurons (Chubb and Anderson, 2010). This way thermosensitivity can be correlated with target tissue. We can hypothesise that neurons which innervate target tissues that are involved in dissipating heat, such as salivary glands whose activation causes fur licking behaviours and subsequent heat loss, would respond to heat, and that neurons which innervate target tissues that are involved in conserving or producing heat, such as blood vessels and BAT, would respond to cold.

2.5 Limitations

The main caveat of this work is the use of the mouse as a model organism for human thermoregulation. Mice are small and furry animals, while humans are large and have a

negligible amount of hair on their bodies. The main difference between mice and men is that mice do not seem to sweat for the purpose of thermoregulation. The only other mammal that sweats to dissipate heat is the horse, a model which was not available to us. In contrast, mice have very few eccrine sweat glands that are mainly limited to the glabrous skin of the paw, and are used to promote grip while running in stressful situations rather than for thermoregulation (Taylor *et al.*, 2012). This might explain the absence of cholinergic neurons (that innervate sweat glands) in the mouse SCG, which projects to the head. The SG, which projects to the paw, does contain cholinergic neurons, albeit very few. Unfortunately, the number of cholinergic neurons proved too low for the hypothesis to be statistically tested.

Chapter 3 Cold Transduction in Peripheral Neurons

3.1 Introduction

The previous chapter confirms earlier findings that sympathetic neurons are cold-sensitive, but these neurons do not express TRPM8 or TRPA1 and it remains unknown which protein is responsible for the observed cold-induced Ca^{2+} influx (Smith *et al.*, 2004; Munns, AlQatari and Koltzenburg, 2007). Additionally, several studies have reported a population of cold-sensitive DRG neurons that does not express TRPM8 or TRPA1 (Babes, Zorzon and Reid, 2004; Munns, AlQatari and Koltzenburg, 2007; Ran, Hoon and Chen, 2016). The aim of this chapter is to identify a novel cold-sensor using pharmacology and calcium imaging of DRG and SCG neurons.

Figure 25 shows the ways in which intracellular [Ca^{2+}] is thought to be increased. These proteins are candidate cold-sensors because they could increase Ca^{2+} levels in response to cold.

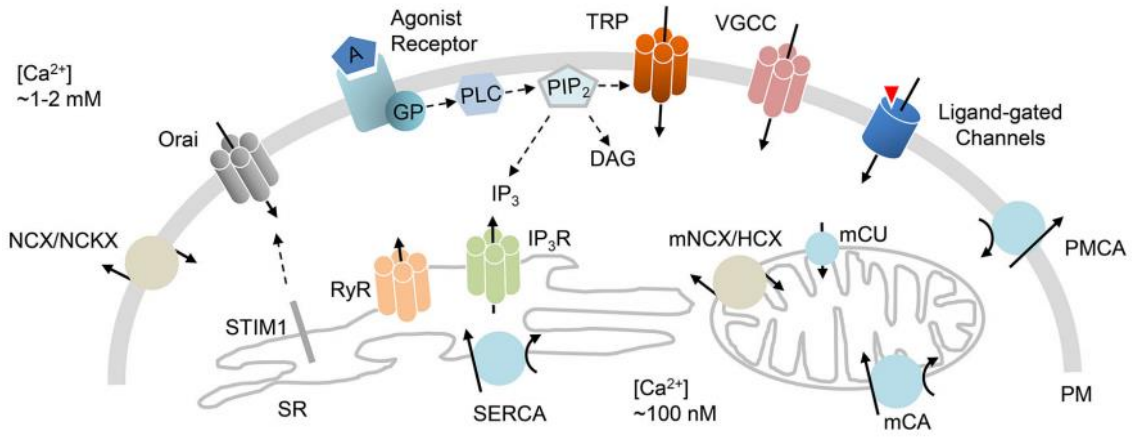

Figure 25 Candidate cold sensors.
Diagramme showing all the proteins responsible for increasing intracellular [Ca^{2+}]. NCX= Na^+/Ca^{2+} exchanger; NCKX = Na/Ca-K exchanger; A = agonist; GP= G protein; PLC = Phospholipase C; PIP_2 = Phosphatidylinositol 4,5-bisphosphate; DAG = Diacylglycerol; IP_3 = Inositol Triphosphate; SERCA = Sarco/Endoplasmic Reticulum Ca^{2+}-ATPase; RyR = Ryanodine Receptor; STIM1 = Stromal Interaction Molecule 1; SR = Sarco/Endoplasmic Reticulum; TRP = Transient Receptor Potential channel; VGCC = Voltage-Gated Ca^{2+} Channel; PMCA = Plasma membrane Ca^{2+}-ATPase; PM = Plasma Membrane; mCA = mitochondrial Ca^{2+}-ATPase; mCU = mitochondrial Ca^{2+} Uniporter; mNCX = mitochondrial Na^+/Ca^{2+} exchanger; HCX = H^+/Ca^{2+} Exchanger. Figure from Harraz & Altier 2014.

Before the start of this project, TRPM8 and TRPA1 had already been ruled out as cold-sensors in SCG neurons (Smith *et al.*, 2004; Munns, AlQatari and Koltzenburg, 2007). In addition, earlier data from the McNaughton lab by Dr. Tan that is currently unpublished ruled out several more candidates. I will briefly summarise this work first. Cold responses in SCG neurons are not affected by the absence of Na^+ in the extracellular solution (Figure 26). This eliminates the involvement of the Na^+/Ca^{2+} exchanger (NCX) and Na/Ca-K exchanger (NCKX).

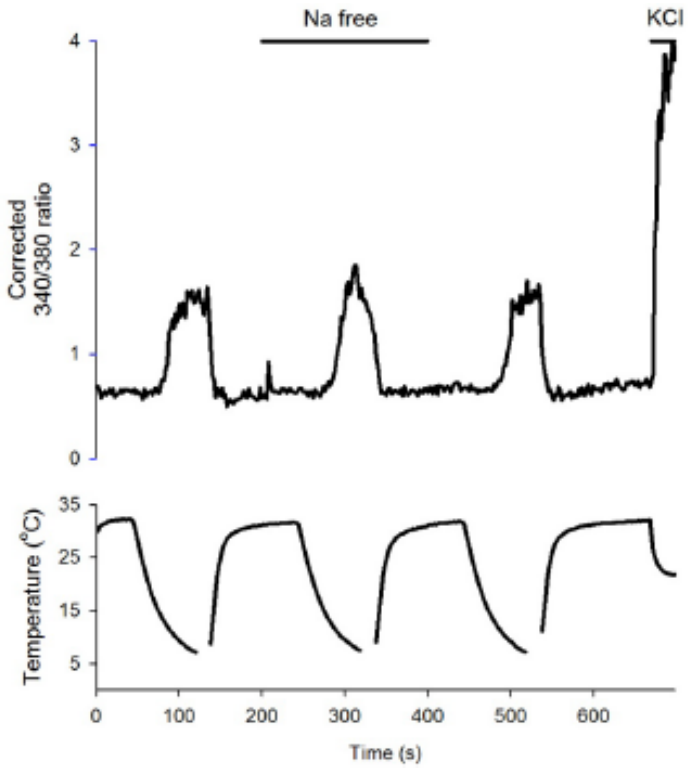

Figure 26 Cold responses in SCG neurons is not changed in the absence of sodium in the extracellular solution. Representative trace showing the typical pattern of intracellular Ca^{2+} in SCG neurons in response to cold (temperature protocol shown at the bottom) in different extracellular solutions. The trace shows a cold-sensitive neuron whose response is not changed in Na^+-free (sodium chloride replaced with choline chloride) extracellular solution. The trace shown are typical of all SCG neurons in the culture (n=111). Interruption in the temperature trace occurred because of power supply overload. Figure and legend from (Tan 2014).

Concurrent patch clamp and Ca^{2+} imaging recordings showed that cold causes an **early** Ca^{2+} influx, followed by depolarisation and a **late** Ca^{2+} influx during Ca^{2+}-dependent action potentials, and that the initial depolarisation is not Ca^{2+}-dependent (Figure 27). We will henceforth refer to this early Ca^{2+} influx mechanism as Cold-Induced Calcium Entry (CICE) and refer to both mechanisms together as Cold-Induced Ca^{2+} influx.

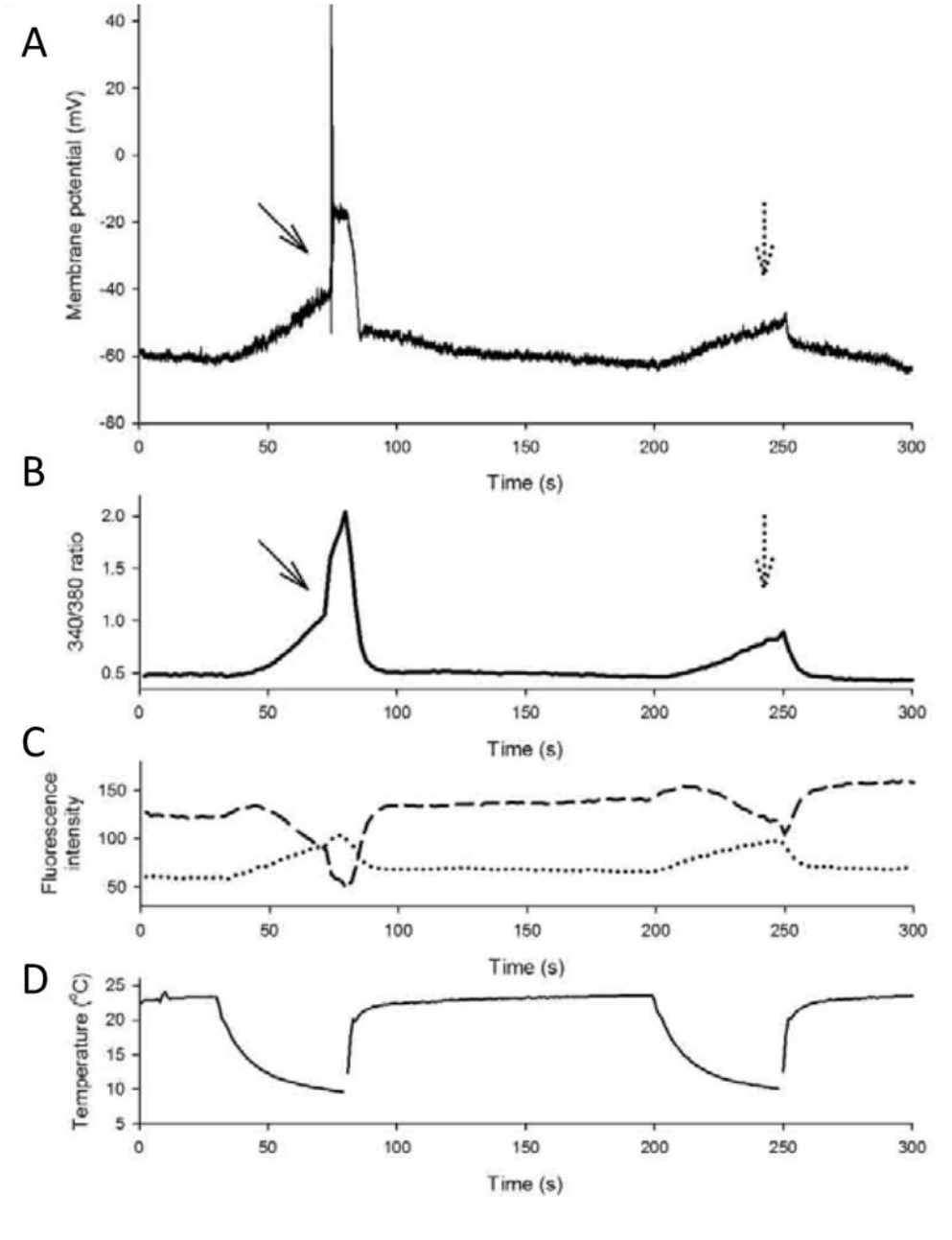

Figure 27 Concurrent patch clamp recording and Ca^{2+} imaging of a cold-sensitive SCG neuron during cold stimuli. A) Membrane potential recording during two cold stimuli. The cold-sensitive neuron depolarized gradually during both cold stimuli, and action potentials were elicited during the first cold stimulus. B) 340/380 ratio of the simultaneous calcium imaging recording showing the calcium influx during cold stimuli. C) The dotted line shows the 340 nm fluorescence intensity and the dashed line shows the 380 nm fluorescence intensity of the simultaneous Ca^{2+} imaging result. The Ca^{2+} influx precedes the action potential firing. Firing of action potentials causes further Ca^{2+} entries (solid arrow), which is absent during the second cold stimulus (dotted arrow). Similar results were obtained in 3 SCG neurons. D) Interruption in the temperature trace occurred because of power supply overload. Figure and legend from (Tan 2014).

Figure 27 showed that the depolarisation that leads to Ca^{2+} influx is not Ca^{2+}-dependent. Instead, cold suppresses a K^+ current, evidenced by the current-voltage (IV) curve in Figure 28, which shows a reversal potential that is negative to -50mV. This is characteristic of a K2P channel such as TREK1 (Figure 29). K2P channels are known

to be inhibited by cold (Viana et al. 2002; Lesage et al. 2000; Noël et al 2009; Pereira et al. 2014), which could explain the observed depolarisation.

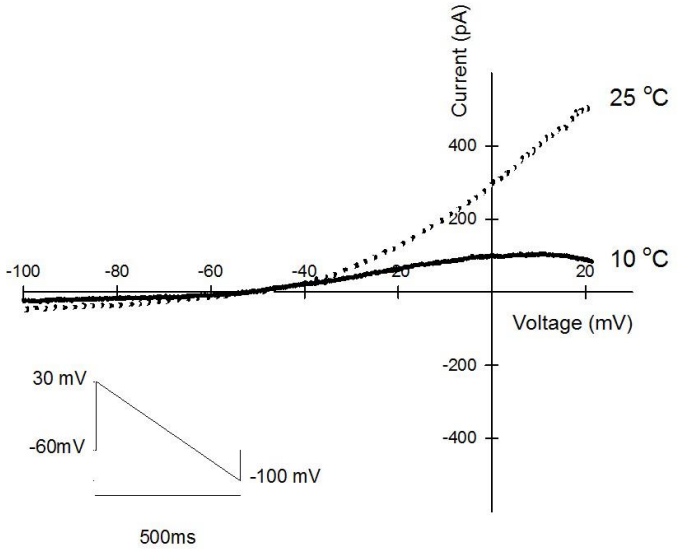

Figure 28 Current–voltage relations of SCG neurons at 25˚C and 10˚C.
The current-voltage relations were obtained by applying a voltage ramp passing from +30 mV to -100 mV in 500 msec at 25˚C and then at 10˚C. The dotted line shows the current-voltage relation of a SCG neruon obtained at 25˚C, and the solid line shows that obtained at 10˚C. The current-voltage relation is reduced at all voltages at 10˚C. TTX (2 μM), $CdCl_2$ (100 μM), and TEA(10 mM) and 4-AP (5 mM) were added to the extracellular solution to block voltage-gated sodium channels, calcium channels, and potassium channels, respectively. Similar results were obtained in 10 SCG neurons. Figure and legend from (Tan 2014).

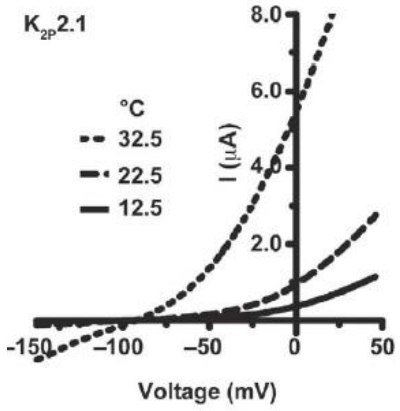

Figure 29 Cold inhibits TREK-1.
IV curve of TREK-1 at different temperatures. Cold inhibits the current at all voltages. Figure adapted from (Bagriantsev et al. 2012).

Figure 28 and Figure 29 showed that cold inhibits K2P channels, which causes depolarisation and subsequent **late** Ca^{2+} influx through Ca_V channels. However, when an SCG neuron is voltage-clamped at -60mV, the **early** cold-induced Ca^{2+} entry (CICE) is still present, which rules out the involvement of fully activated Ca_V channels

in CICE (Figure 30B). Thus, the whole cold-induced Ca^{2+} influx is not exclusively mediated by K2P-mediated depolarisation and subsequent activation of Ca_V channels. Surprisingly, CICE is not accompanied by any detectable inward current (Figure 30A). This means that Ca^{2+} is likely to enter through an electroneutral mechanism and rules out VGCC, TRP and Ligand-gated channels as candidate cold-sensors (Figure 25).

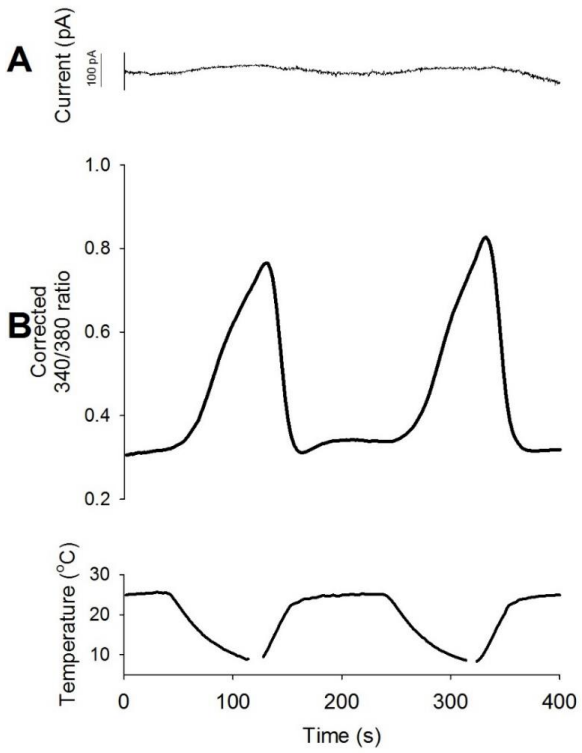

Figure 30 No detectable inward currents but persistent calcium influx during cold stimuli in SCG neurons.
A) A trace showing no inward current induced by cold can be detected when the SCG neurons was voltage-clamped at -60 mV. B) Simultaneous calcium imaging shows influx of calcium into the SCG neuron during cold stimuli (temperature protocol shown at the bottom). Similar results were obtained in 10 SCG neurons. Interruption in the temperature trace occurred because of power supply overload. Figure and legend from (Tan 2014).

Figure 30 showed that the **early** Ca^{2+} influx is not accompanied by any detectable inward current. However, the electrophysiology rig used for these experiments produces ~10pA noise, which means that CICE could produce a current that is too small to be detected. An undetectable inward Ca^{2+}-current of merely 1pA could result in a substantial increase in $[Ca^{2+}]_i$, which can be estimated in several steps as follows:

$$Ca^{2+}\ entry\ (mole\ flow\ rate)\ =\ \frac{I}{z * F}$$

$$I = 10^{-12}A$$

$$z\ =\ 2\ electrons\ for\ Ca^{2+}$$

$$F = 9.65 \cdot 10^{-4}\ sA/mol$$

$$\frac{10^{-12}}{2 * 9.65 \cdot 10^{-4}} = 5.18 \cdot 10^{-18}\ mol/s$$

1pA of Ca^{2+} current equals an increase of $5.18 \cdot 10^{-18}\ mol/s$, but most Ca^{2+} ions will be quickly sequestered into the ER or bound by cytoplasmic proteins (Miller, 1991). Only one in every 100 Ca^{2+} ions are free to contribute to a rise in intracellular [Ca^{2+}] in neurons (Roussel *et al.*, 2006), so the measurable Ca^{2+} influx is reduced to 5.18 x 10^{-20} moles per second. Mouse SCG neurons are roughly spherical and ~20μm in diameter (Ruit *et al.*, 1990), and therefore have a cell volume of:

$$sphere\ volume\ (V) = \frac{4}{3}\pi r^3$$

$$\pi = 3.14$$

$$r = 10\mu m$$

$$sphere\ volume = \frac{4}{3}3.14 \cdot 10^3 = 4.19 \cdot 10^{-12}L$$

Now, whole cell free Ca^{2+} influx can be calculated as the concentration change per second:

$$concentration\ change\ per\ second(c) = \frac{n}{V}\ per\ second$$

$$n = 5.18 \cdot 10^{-20}\ mol$$

$$V = 4.19 \cdot 10^{-12}L$$

$$concentration\ change = \frac{5.18 \cdot 10^{-20}}{4.19 \cdot 10^{-12}} = 1.24 \cdot 10^{-8}\ M/s$$

As described in methods (section 2.2.9), cold stimuli were applied for 2 minutes each time, during which the cells are cooled below their activation threshold for ~80 seconds. The total concentration can be calculated as:

$$80 * 1.24 \cdot 10^{-8} = 9.92 \cdot 10^{-7}M = 992nM$$

So that would increase the $[Ca^{2+}]i$ from ~100nM at rest to ~1092nM at peak response, which is an 11-fold increase.

To summarise, at the start of this project it was known that neurons of the sympathetic nervous system are directly cold-sensitive, and that cooling activates two separate mechanisms. First, CICE, which seems to be electrically silent i.e. no inward current is detected in voltage-clamp experiments (Figure 30). This Ca^{2+} entry is not mediated by NCX, NCKX, TRP, VGCC or Ligand-gated channels. Second, a **late** Ca^{2+} influx. This mechanism consists of depolarisation that is likely mediated by cold-induced K2P channel inhibition, and resultant activation of Ca_V channels and firing of action potentials.

The aim of this chapter is to discover which protein mediates the **early** cold-induced Ca^{2+} entry (CICE), which seems electroneutral because it is not accompanied by a detectable current. There are four hypotheses that will be tested:

Hypothesis 1: Cold could activate a GPCR and so release Ca^{2+} from intracellular stores or cold could trigger Ca^{2+} release from intracellular stores directly (see Figure 25). This hypothesis will be tested by the removal of extracellular Ca^{2+}. If the cold response is still present in the absence of extracellular Ca^{2+}, that suggests that the Ca^{2+} is released from intracellular stores.

Hypothesis 2: Ca^{2+} could be exchanged for another cation by a pump, such as the Plasma Membrane Calcium ATPase (PMCA), which exchanges one Ca^{2+} ion for two H^+ ions and is thought to operate in an electroneutral fashion (Thomas, 2009). All biochemical processes are suppressed by cold and enzymes such as PMCA are no exception. Therefore, the activity of PMCA could be suppressed by cold, which would mean that net $[Ca^{2+}]$ would increase because the influx of Ca^{2+} through leakage pathways is likely to be much less affected by cold (Figure 31). This hypothesis will be tested using an antagonist of PMCA. If the cold response is potentiated by inhibition of PMCA, that suggests that PMCA suppression underlies CICE.

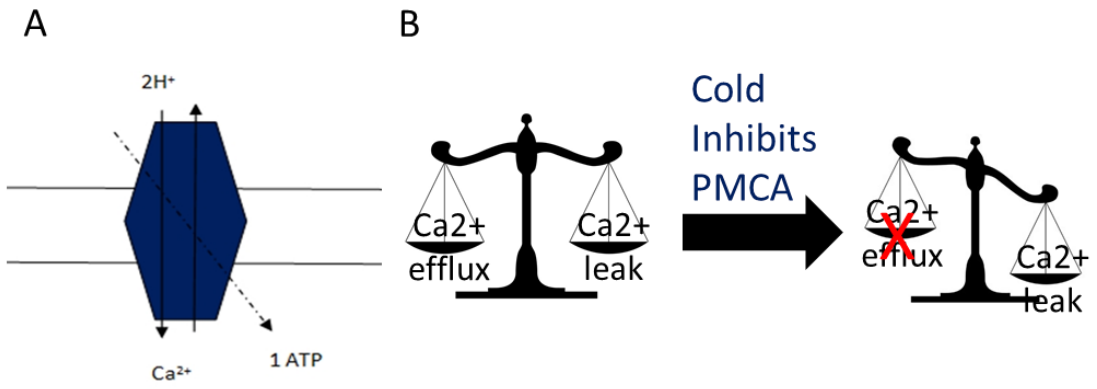

Figure 31 PMCA could be responsible for the observed Ca^{2+} influx.
A) Graphical representation of PMCA, which uses one ATP molecule to exchange one Ca^{2+} ion for two protons. B) graphical representation of the hypothesis that cold inhibits PMCA, which would lead to a net influx of Ca^{2+} into the cell.

Hypothesis 3: CICE could be mediated by a leak from Ca_V channels, which would only produce a very small current. This leak is called the window current, referring to the "window" between the activation and inactivation curve (Figure 32). Cold could increase the window current of these channels, either through a depolarising shift of the inactivation curve or through a hyperpolarising shift of the activation curve. The kinetics of T-type Ca_V have been shown to be affected differently by 21°C and 37°C (Iftinca *et al.*, 2006). Possibly the window current is much larger at temperatures below 10°C. We will test this with the use of various Ca_V blockers. If the blockers fully block the cold responses, this will indicate that Ca_V channels mediate CICE in a voltage-independent manner.

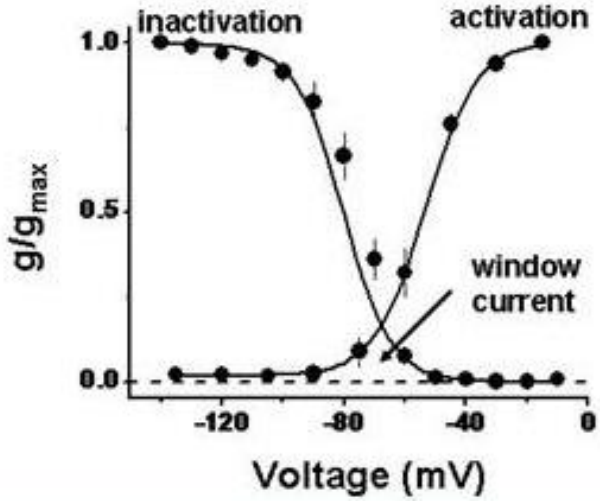

Figure 32 Ca_V channels carry a window current.
There is a small influx of Ca^{2+} mediated by tonically activated Ca_V channels when the membrane potential is between -50mV and -90mV i.e. at resting Vm. This window current could be increased by either a leftward hyperpolarising shift of the activation curve or a rightwards depolarising shift of the inactivation curve, which could be influenced by temperature. g/gmax= relative conductance. Figure from (Iftinca, 2011).

Hypothesis 4: Ca^{2+} might enter through a highly selective Ca^{2+} channel that carries a whole-cell current of <10pA. The only Ca^{2+} channel that matches this description is the Orai Ca^{2+} channel family, which have an extremely low conductance (see general introduction section 1.2.1.6). STIM could be activated by cold and open Orai channels during cold stimuli. We will test this hypothesis with the use of Orai channel inhibitors. If they block the cold-responses, this will support the idea that STIM and Orai channels are involved.

3.2 Materials and methods

3.2.1 Animals and Dissection

Adult male and female C57BL/6J mouse SCG and DRG were used for all experiments in this chapter. See Chapter 2 for remaining methods relating to isolation of neurons.

3.2.2 Ca^{2+} Imaging and Data Analysis

All agonists and antagonists used in this chapter were prepared as a 1000x stock solution in dimethyl sulfoxide (DMSO) and stored at -20˚C. On the morning of the experiments, stock solutions were diluted in HBSS and pH adjusted to 7.4 using HCl or NaOH. Most agonist and antagonist specificity information for this chapter can be found in the IUPHAR/BPS Guide to PHARMACOLOGY (Harding *et al.*, 2018). See chapter 2 for remaining methods relating to calcium imaging and data analysis.

The cold response threshold was defined as the mean maximal increase of the negative control (zero Ca^{2+} condition) plus 3.09 SD, because 99.8% of a population lies within 3.09 SD of the mean, assuming a normal distribution (Figure 34F). Using this method, all cells that responded to cooling with an $F_{340/380}$ increase of >0.2 were identified as cold-sensitive.

3.3 Results and Discussion

3.3.1 Cold Responses Are Not Mediated by Any Known Cold-Sensitive TRP Channel in SCG Neurons

We began by confirming experiments from the Koltzenburg group, which show that the cold-sensitivity of SCG neurons is not mediated by either of the known cold-sensitive TRP channels TRPM8 or TRPA1 (Munns, AlQatari and Koltzenburg, 2007). Additionally, TRPC5 has more recently been proposed as a cold-sensor (Zimmermann *et al.*, 2011a).

We stimulated SCG neurons with a cold ramp to 3˚C and agonists for TRPM8, TRPA1 and TRPC5 in order to measure overlap of cold-sensitivity and TRP channel expression. Menthol (300μM) was used to activate TRPM8 (Andersson, Chase and Bevan, 2004). Menthol also activates TRPV3 (Macpherson *et al.*, 2006). Allyl isothiocyanate (50μM AITC) was used to activate TRPA1 (Bandell *et al.*, 2004). Peroxisome proliferator-activated receptor-γ (PPAR-γ) agonist Rosiglitazone (100μM) was used to activate TRPC5 (Majeed *et al.*, 2011). Rosiglitazone also inhibits TRPM2 and TRPM3 (Majeed *et al.*, 2011).

Figure 33A shows the response of a typical SCG neuron to cold and TRP channel agonists. While 44% of SCG neurons responded to cold with an $F_{340/380}$ increase of >0.2, only 5% responded to cold and to at least one TRP channel agonist (cold-sensitive and TRPM8/TRPA1/TRPC5 (red) in Figure 33B). None of the SCG neurons responded to menthol, indicating that TRPM8 and TRPV3 are not expressed in these neurons (Figure 33C). 10% of cold-sensitive SCG neurons responded to AITC or Rosiglitazone, indicating that they express TRPA1 and/or TRPC5 (Figure 33C). This means that at least 90% of cold-sensitive SCG neurons are likely to express one or both of the two novel mechanisms mentioned above i.e. CICE through an unidentified mechanism and Ca^{2+} influx resulting from K2P inhibition and activation of Ca_V channels. Therefore, SCG neurons were used in this study to identify the molecular identity of CICE.

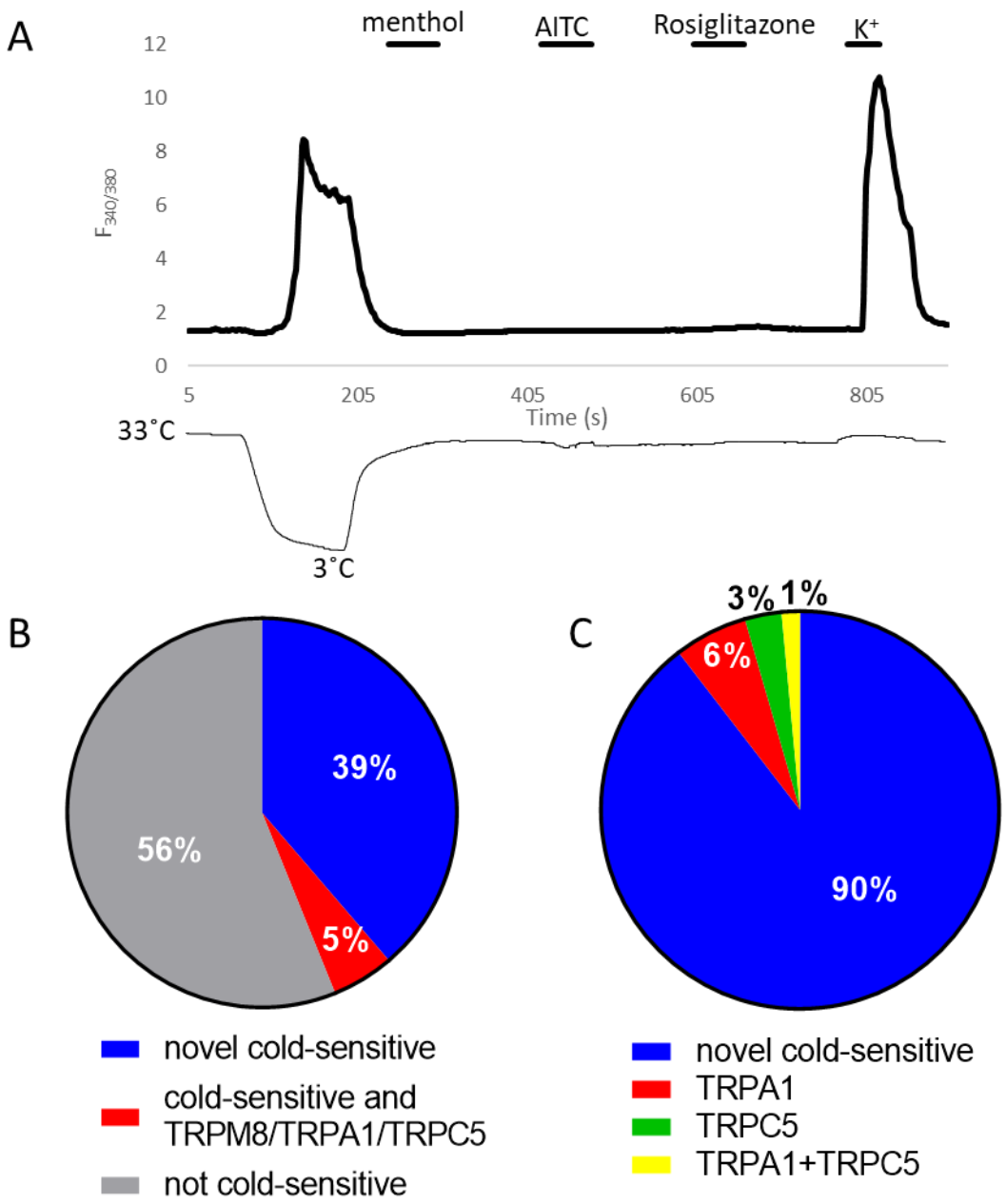

Figure 33 SCG neurons express novel cold-sensitive mechanisms.
Representative trace showing an SCG neuron that is cold-sensitive, but does not express TRPM8, TRPA1 or TRPC5. The temperature trace is shown below. B) Pie chart showing the percentage of SCG neurons that are both cold-sensitive and express either TRPM8, TRPA1, or TRPC5 (red); and novel cold-sensitive SCG neurons that do not express any of these channels (blue). n=155 neurons imaged on three separate days. 39% of SCG neurons express novel cold-sensitive mechanisms (blue). C) Pie chart showing the different populations of cold-sensitive neurons by expression of TRPM8, TRPA1, and TRPC5. n=67 neurons imaged on three separate days. None of the neurons imaged responded to TRPM8 agonist menthol. 10% of cold-sensitive neurons ressponded to TRPA1 and/or TRPC5 agonists AITC and Rosiglitazone (red, green, yellow). 90% of cold-sensitive neurons do not express TRPM8 or TRPA1 or TRPC5 (blue).

3.3.2 Cold Does Not Cause Release of Ca^{2+} from Intracellular Stores in SCG Neurons

To test whether the observed cold-induced Ca^{2+} influx comes from outside or inside the cell, we applied a cold stimulus to SCG neurons in the absence of extracellular Ca^{2+} (Figure 34). Neurons were cooled from 31˚C to 6˚C four times for two minutes each time. Extracellular Ca^{2+} was absent during the first cold ramp and there was no observable increase in $F_{340/380}$ signal (Figure 34A and B). There is a rise in Ca^{2+} during the second cold-ramp after Ca^{2+} was reintroduced. This means that Ca^{2+} enters through the plasma membrane upon cooling.

The dip in the trace during the first cold ramp is caused by the intrinsic temperature sensitivity of Fura-2 as discussed in methods (section 2.2.9), which becomes apparent due to the lack of response in the absence of extracellular Ca^{2+}. SCG neurons are somewhat desensitised by repeated cold ramps as shown in Figure 34. The most common or modal response to cold was an $F_{340/380}$ increase of 0.6, and only 12.5% of neurons responding with an $F_{340/380}$ increase of >2.

Having established that the there was no cold-induced release of Ca^{2+} from internal stores, the response to a cold ramp applied while the cells are in Ca^{2+}-free HBSS was used as a negative control, and to determine the cold-response threshold used for all further experiments in this chapter. This cold response threshold was defined as the mean maximal increase of the negative control plus 3.09 SD, because 99.8% of a population lies within 3.09SD of the mean assuming a normal distribution (Figure 34F). Using this method all cells that responded to cooling with an $F_{340/380}$ increase of >0.2 were identified as cold-sensitive (71% of SCG neurons on this day).

The result that Ca^{2+} is not released from intracellular stores means that cold must activate a Ca^{2+} influx pathway and rules out the following candidates: GPCR, SERCA, RyR, mCA, mCU, mNCX, HCX (Figure 25). Remaining candidates for CICE are PMCA, an increased VGCC window current, and activation of STIM/Orai channels.

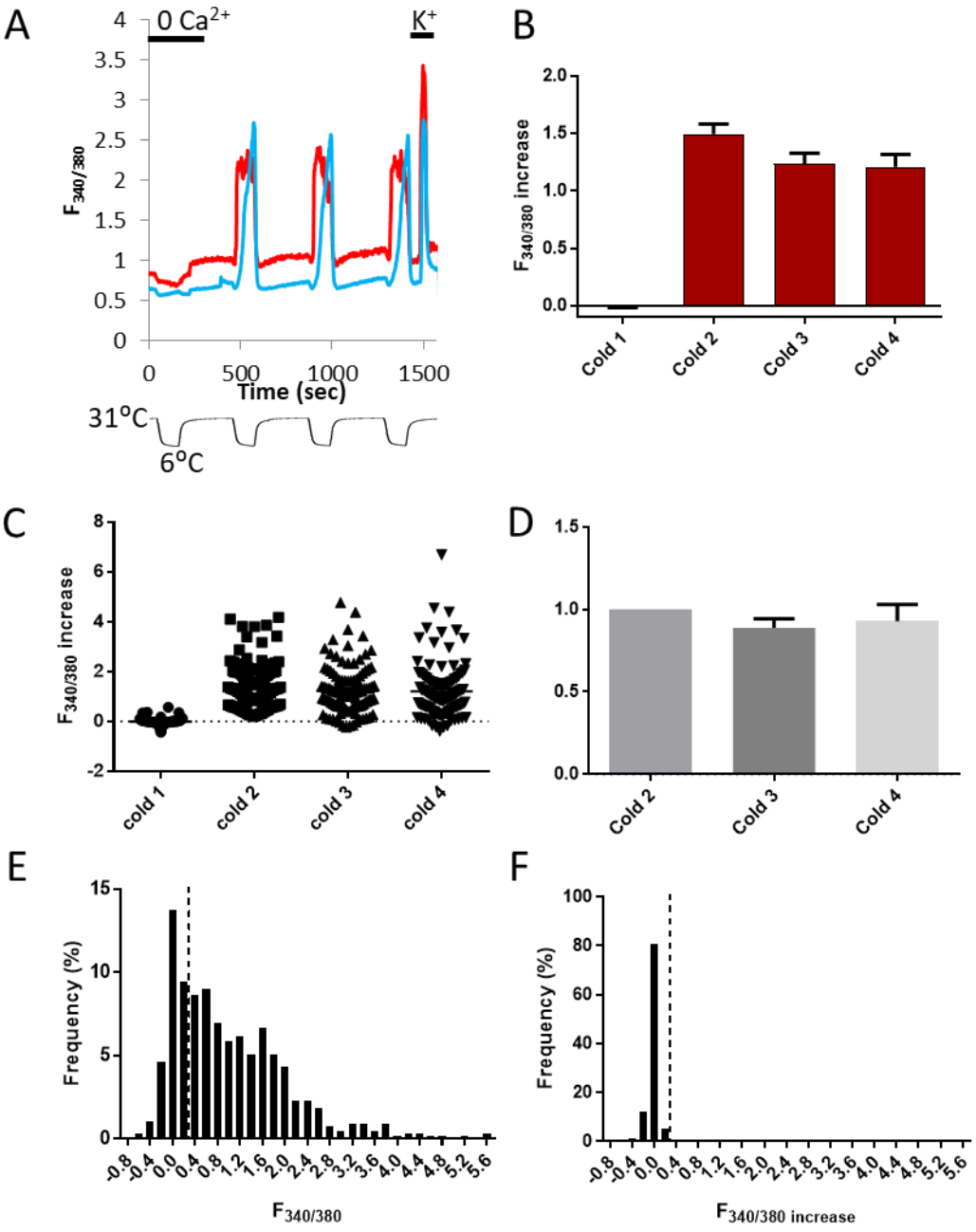

Figure 34 The CICE is absent when the extracellular solution contains no Ca^{2+}.
A) Representative traces showing cold-responses of SCG neurons in the absence and presence of Ca^{2+}. The dip in the trace that is apparent during the first cold ramp is caused by the intrinsic temperature sensitivity of Fura-2. The temperature trace is shown below. B) Bar graph summarising results of 110 cold-sensitive neurons on 3 coverslips. Ca^{2+} was absent during the first cold ramp. C) Scatter plot showing cold-responses in absence and presence of extracellular Ca^{2+}. Cold-response amplitude was highly variable. D) Bar graph showing normalised cold-responses. The cold-response amplitude was consistent between cold ramps. E-F) Frequency histograms showing the amplitude of cold responses in the presence (E) and absence (F) of extracellular Ca^{2+} (n=648). Dotted lines indicate the threshold for definition of a cold-sensitive neuron as determined by the mean+3.09SD increase of $F_{340/380}$ in response to cold in the absence of extracellular Ca^{2+}. Using this method, 71% of SCG neurons were cold-sensitive. The modal response to cold was an $F_{340/380}$ increase of 0.6. Only 12.5% of neurons show an increase of >2 in response to cold.

3.3.3 PMCA is Not Responsible for CICE in SCG Neurons

Next, we tested whether inhibition of the plasma membrane Ca^{2+} ATPase (PMCA) may be responsible for CICE. It could either be inhibited by cold or start operating in reverse-mode. The possibility of operating in reverse-mode has been shown for NCX, but may also apply to PMCA (Hirota, Pertens and Janssen, 2007).

To test this hypothesis, three cold ramps were applied to SCG neurons and Eosin, an antagonist of PMCA, was applied during the second cold ramp. Eosin (10μM) is a potent inhibitor of PMCA that does not affect NCX (Gatto *et al.*, 1995). If PMCA inhibition underlies SCG cold-sensitivity, then further inhibition of PMCA by Eosin would potentiate cold-responses. If PMCA reverse-mode underlies SCG cold-sensitivity, then inhibition of PMCA by Eosin would inhibit cold-responses.

Figure 35 shows that cooling SCG neurons from 30°C to 7°C in the presence of Eosin did not have any effect on cold-response amplitude. This result eliminates PMCA as a candidate cold-sensor. The remaining candidate cold sensors are an increased VGCC window current, and activation of STIM/Orai channels (Figure 25).

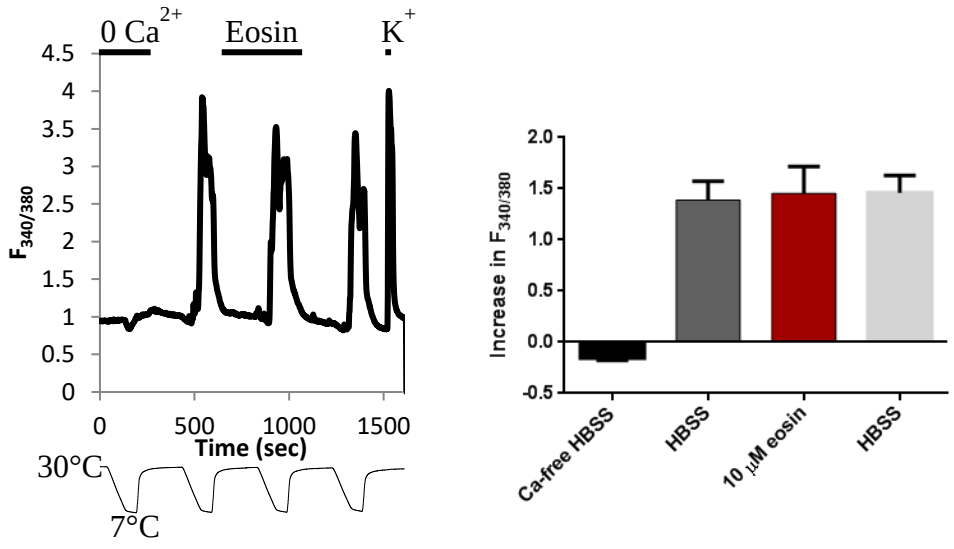

Figure 35 Eosin did not block cold responses in SCG neurons
Left: Representative trace showing the effect of PMCA antagonist Eosin (10μM) on cold-induced Ca^{2+} influx in SCG neurons. The temperature trace is shown below. Right: Bar graph summarising results (mean+SEM) of 61 neurons. There is no significant difference after application of Eosin as determined by a repeated measures one-way ANOVA and Dunnett's multiple comparisons test. Data from Dr. Bruno Vilar.

3.3.4 CICE is Not Mediated by an Increased Ca_V Window Current in SCG Neurons

Next, we tested whether an increased window current from Ca_V channels may be responsible for CICE. To test this, three cold ramps were applied to SCG neurons and antagonists with varying selectivity for voltage gated Ca^{2+} channels were applied during the second cold ramp. These antagonists all block the other cold response mechanism too, which is mediated by K2P channel inhibition and subsequent depolarisation and activation of Ca_V channels.

The first antagonist tested was cadmium (Cd^{2+}), which blocks almost all Ca^{2+} permeable proteins, including Ca_V (Williams *et al.*, 1994; Hobai *et al.*, 1997; Scholze *et al.*, 2001) and STIM-Orai channels (Yamashita *et al.*, 2017), and is also an activator of TRPA1 (Andersson *et al.*, 2009; Miura *et al.*, 2013).

A high concentration (250μM) Cd^{2+} caused an irreversible rise in baseline Ca^{2+} levels (data not shown), presumably due to block of NCX (Hobai *et al.*, 1997). A lower concentration of Cd^{2+} (100μM) did not have this effect; cooling SCG neurons from 34˚C to 6˚C in the presence of Cd^{2+} reversibly decreased cold-response amplitudes by 87% (Figure 36).

Therefore, the cold-induced Ca^{2+} influx must be mediated by a Ca^{2+}-permeable ion channel located in the plasma membrane. It also confirms earlier observations showing that TRPA1 is not responsible for the cold-induced Ca^{2+} influx in SCG neurons, as Cd^{2+} is an activator of TRPA1 and would have potentiated cold-responses rather than blocked them.

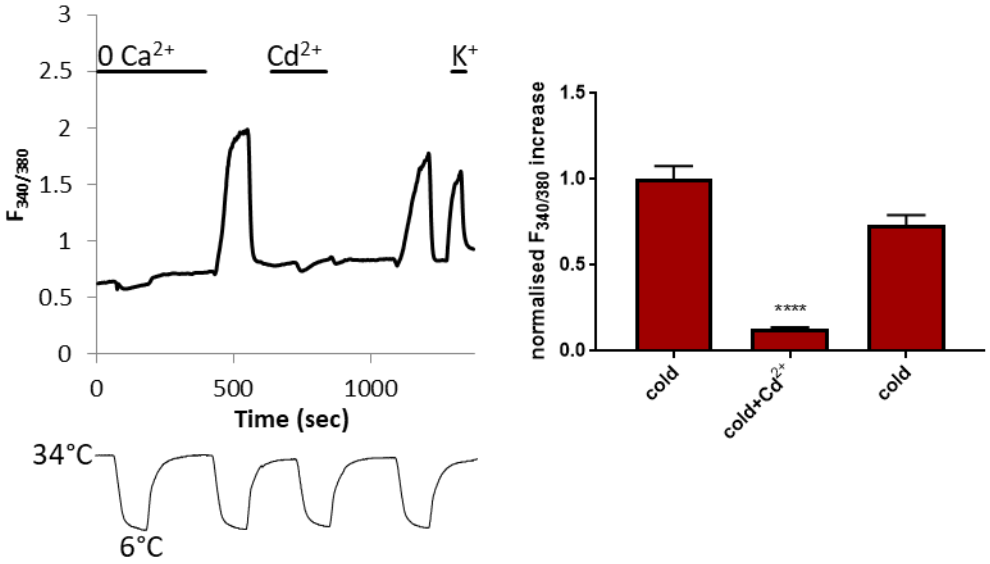

Figure 36 Cd^{2+} blocked cold responses in SCG neurons.
Left: Representative trace showing the effect of Ca^{2+} channel blocker Cd^{2+} (100μM) on cold-induced Ca^{2+} influx in SCG neurons from C57BL/6 mouse pups that were sacrificed via IP injection with pentobarbital and femoral artery exsanguination. The dip in the trace that is apparent during the first cold ramp was caused by the intrinsic temperature sensitivity of Fura-2. The temperature trace is shown below. Right: Bar graph summarising normalised results (mean+SEM) of 60 cold-sensitive (cold-induced $F_{340/380}$ increases of >0.3) neurons on 8 coverslips. There was a significant difference ($p<0.0001$) in cold response amplitude after application of Cd^{2+} as determined by a repeated measures one-way ANOVA and Dunnett's multiple comparisons test.

The second antagonist tested was gadolinium (Gd^{3+}), which is somewhat more selective than Cd^{2+} but still blocks many Ca^{2+} permeable proteins, including Ca_V (Biagi and Enyeart, 1990) and Orai channels (Yeromin *et al.*, 2006). Gd^{3+} also blocks TREK/TRAAK channels (Goldstein *et al.*, 2005), and is an activator of TRPC5 (Harding *et al.*, 2018).

Like Cd^{2+}, Gd^{2+} (100μM) abolished SCG neuron cold-responses. Cooling SCG neurons from 35˚C to 5˚C in the presence of Gd^{3+} reversibly decreased cold-response amplitudes by 82% (Figure 37).

Therefore, the cold-induced Ca^{2+} influx must be mediated by a Ca^{2+}-permeable ion channel located in the plasma membrane such as Ca_V or Orai channels. It also confirms our earlier finding that TRPC5 is not responsible for the cold-induced Ca^{2+} influx in SCG neurons, because Gd^{3+} is an activator of TRPC5 and would have potentiated cold-responses rather than blocked them.

There are several spikes visible on the first cold-response in Figure 37. This may be an indication that there are indeed two separate mechanisms active: CICE, which is more gradual, and an indirect Ca^{2+} influx, characterised by K2P inhibition and Ca^{2+}-mediated action potentials, which may show up as spikes on the trace. There are no spikes visible

after wash-off of Gd^{3+}, but the K^+ response three minutes later is also relatively small. This may mean that the Ca_V-mediated spiking mechanism is still somewhat blocked by Gd^{3+}. Possibly Gd^{3+} washes off the CICE mechanism faster.

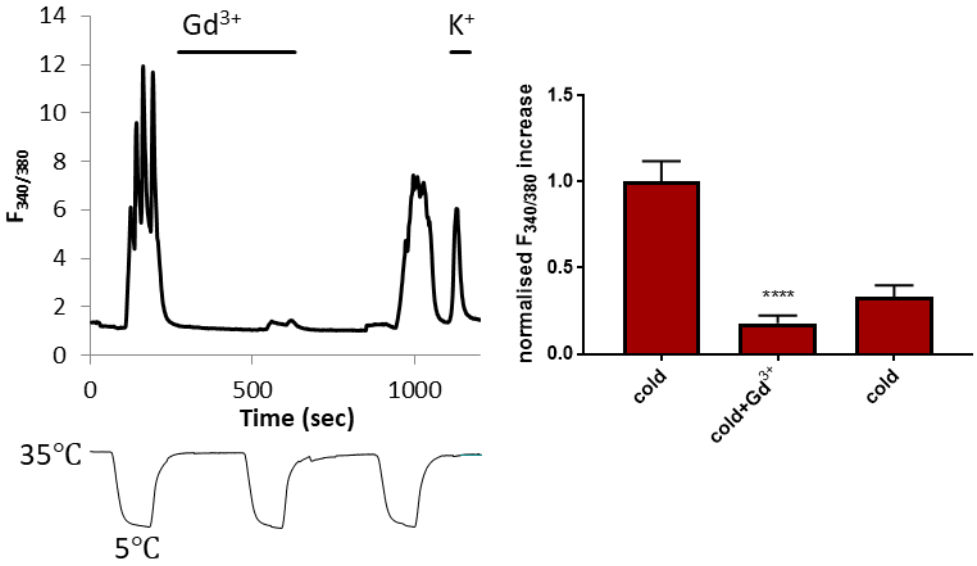

Figure 37 Gd^{3+} blocked cold responses in SCG neurons.
Left: Representative trace showing the effect of Ca^{2+} channel blocker Gd^{3+} (1μM) on cold-induced Ca^{2+} influx in SCG neurons from adult C57BL/6 mice sacrificed via cervical dislocation and decapitation. The temperature trace is shown below. Right: Bar graph summarising normalised results (mean+SEM) of 78 cold-sensitive neurons on 12 coverslips, imaged on 2 separate days. There was a significant difference ($p<0.0001$) in cold response amplitude after application of Gd^{3+} as determined by a repeated measures one-way ANOVA and Dunnett's multiple comparisons test.

To look more specifically at whether CICE is mediated by an increased window current from Ca_V channels, rather than activation of Orai channels, Ca_V selective antagonists were tested next. Ca_V channels can be activated by application of K^+, which causes depolarisation. We first tested the effect of different dihydropyridine Ca_V channel antagonists with varying selectivity profiles on this K^+-induced Ca^{2+} influx to determine which type of Ca_V is predominant in SCG neurons. Antagonists tested were the non-selective Ca_V blockers Bepridil, Benidipine, and Nickel; and the L-type selective antagonists Nifedipine and Verapamil (Triggle, Langs and Janis, 1989; Miljanich and Ramachandran, 1995; Nadal *et al.*, 1995; Kochegarov, 2003).

None of the compounds used had an effect on baseline Ca^{2+}. The non-selective Ca_V blockers Bepridil, Benipidine, and Nickel caused an inhibition of K^+ responses of 40-66%, but the L-Type specific Ca_V blockers Nifedipine and Verapamil caused a greater inhibition of K^+ responses of 60-85% (Figure 38). This suggests that L-type Ca_V channels are predominant in SCG neurons.

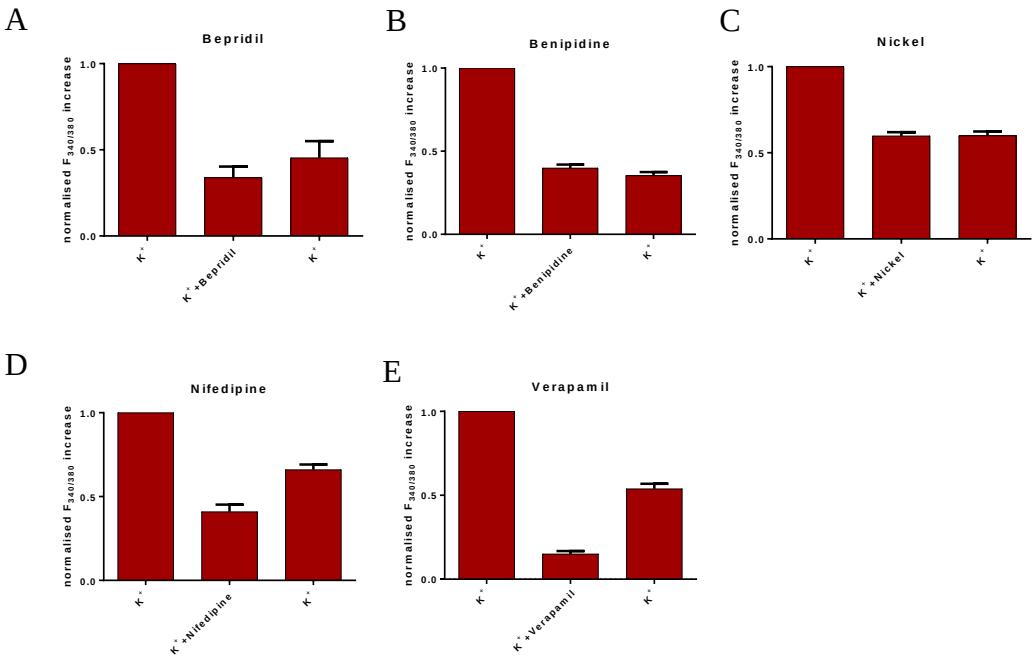

Figure 38 Determining efficacy of various Ca_V blockers on K^+-induced calcium influx.
Bar graphs summarising normalised results (mean+SEM) of the effect of various Ca_V blockers on K^+-induced Ca^{2+} influx at 30°C in SCG neurons from adult C57BL/6 mice sacrificed via cervical dislocation and decapitation. A) Non-selective Ca_V blocker Bepridil (10μM) caused an inhibition of K^+ responses of >66% (n=26). B) Non-selective Ca_V blocker Benipidine (10μM) caused an inhibition of K^+ responses of >60% (n=38). C) Non-selective Ca_V blocker Nickel (100μM) caused an inhibition of K^+ responses of >40% (n=72). D) L-Type Ca_V blocker Nifedipine (10μM) caused an inhibition of K^+ responses of >60% (n=20). E) L-Type Ca_V blocker Verapamil (100μM) caused an inhibition of K^+ responses of >85% (n=51). Data from Dr. Bruno Vilar.

Having found that voltage-gated Ca^{2+} influx was mainly mediated by L-type Ca_V, the effects of L-type Ca_V antagonists Nifedipine and Verapamil were tested on the cold-induced Ca^{2+} influx. Nifedipine was tested first, which blocks all L-type Ca_V channels indiscriminately (there were no isoform specific pharmacological agents available) and should have almost no effect on Orai channels (2% inhibition at 10μM) (Ishikawa *et al.*, 2003). Nifedipine is also a direct agonist of TRPA1 (Fajardo *et al.*, 2008). Direct application of Nifedipine to SCG neurons did not increase Ca^{2+} levels, further showing that TRPA1 is not expressed in these neurons (Figure 39A).

Figure 39 A and B show that Nifedipine (10μM) effectively inhibited the K^+-induced Ca^{2+} influx by >60%, so it should also inhibit Ca_V activation evoked by K2P channel inhibition. If CICE is also mediated by (an increased window current and leak from) Ca_V channels, it should fully block the cold-responses. Figure 39 C and D show that Nifedipine did not have a significant effect on average cold-response amplitude. This suggests that SCG cold responses are not mediated by Ca_V channels.

However, Nifedipine did have some effect on cold-responses: it partially inhibited large responses, probably because it inhibits some of the K2P channel inhibition evoked Ca^{2+} influx as expected, but it also **potentiated** some responses. As shown in Figure 39D, the largest cold response is clearly blocked by Nifedipine, and the smallest cold response is greatly potentiated. This potentiation therefore seems to target the CICE mechanism and made it difficult to determine the exact contribution of the two mechanisms to cold responses (CICE and the K2P inhibition-mediated Ca^{2+} influx). A different L-type Ca_V antagonist was tested next to determine whether this phenomenon was common to the whole class of dihydropyridines that target Ca_V channels.

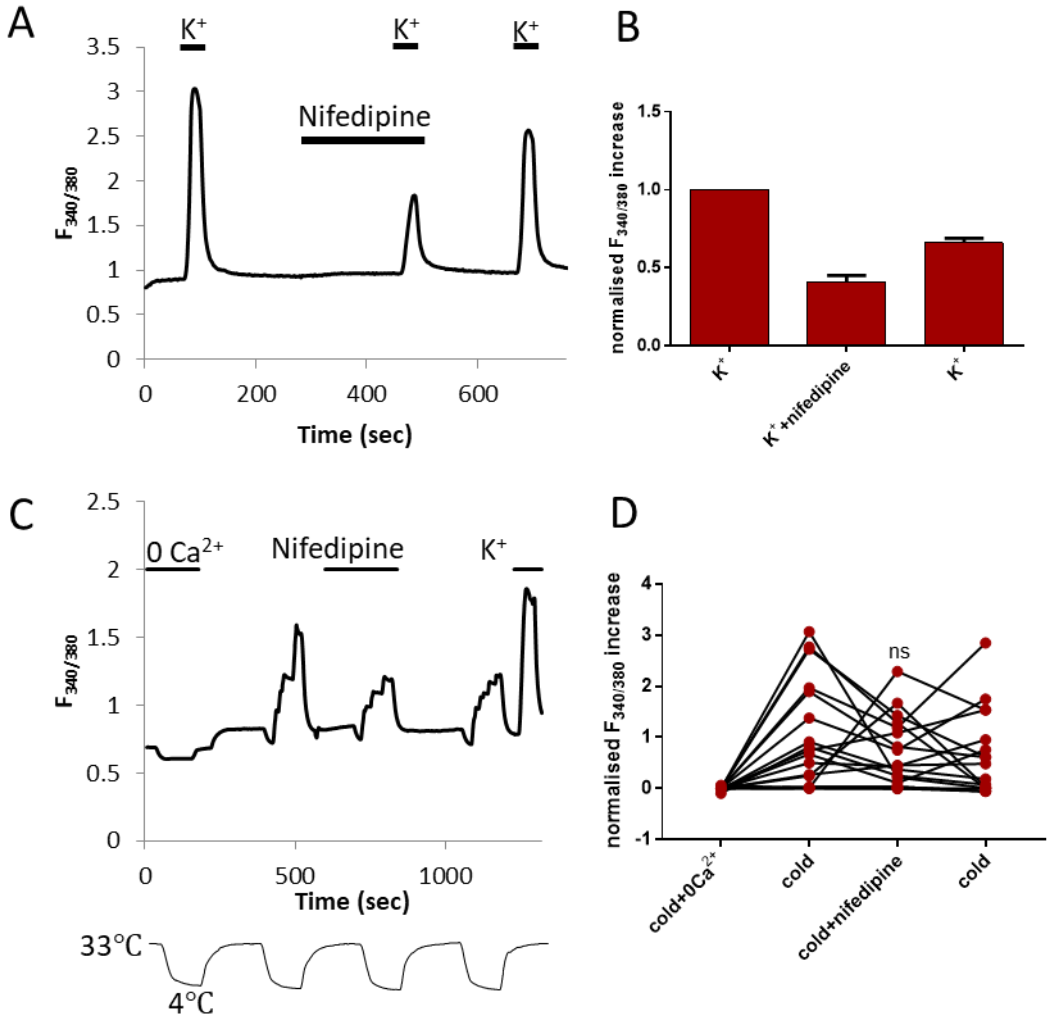

Figure 39 Nifedipine had opposing effects on cold responses in SCG neurons.
A) Representative trace showing the effect of L-type Ca_V channel blocker nifedipine (10µM) on K^+-induced Ca^{2+} influx at 30°C in SCG neurons from adult C57BL/6 mice sacrificed via cervical dislocation and decapitation. B) Bar graph summarising normalised results (mean+SEM) of 20 neurons on one coverslip. Nifedipine caused an inhibition of K^+ responses of >60%. A-B) Data from Dr. Bruno Vilar. C) Representative tracing showing the effect of L-type Ca_V channel blocker nifedipine (5µM) on cold-induced Ca^{2+} influx in SCG neurons from FVB/N ChAT/GFP mouse pups sacrificed via cervical dislocation and decapitation. This experiment was performed after 48h in culture. The dip in the trace that is apparent during the first cold ramp is caused by the intrinsic temperature sensitivity of Fura-2. The temperature trace is shown below. D) Line graph summarising normalised results of 18 cold-sensitive neurons on 8 coverslips, imaged on two separate days. There was no significant difference in cold response amplitude after application of nifedipine as determined by a repeated measures one-way ANOVA and Dunnett's multiple comparisons test. However, nifedipine had a clear effect on some neurons, increasing some responses, and decreasing some responses.

Verapamil is an L-type Ca_V antagonist and at 100µM effectively inhibited K^+-induced Ca^{2+} influx by >85% (Figure 40 A and B). It should therefore effectively block the Ca_V mediated Ca^{2+} influx. If the hypothesis that CICE is also mediated by Ca_V channels is correct, Verapamil would block cold-responses completely. However, Verapamil had no significant effect on mean cold-response amplitude (Figure 40D). This means that CICE is not mediated by a leak from L-type Ca_V channels.

Verapamil showed the same off-target effect as Nifedipine: potentiating small cold-responses (Figure 40C blue trace), and inhibiting large cold-responses, which are presumably mediated by inhibition of K2P channels and subsequent Ca_V activation.

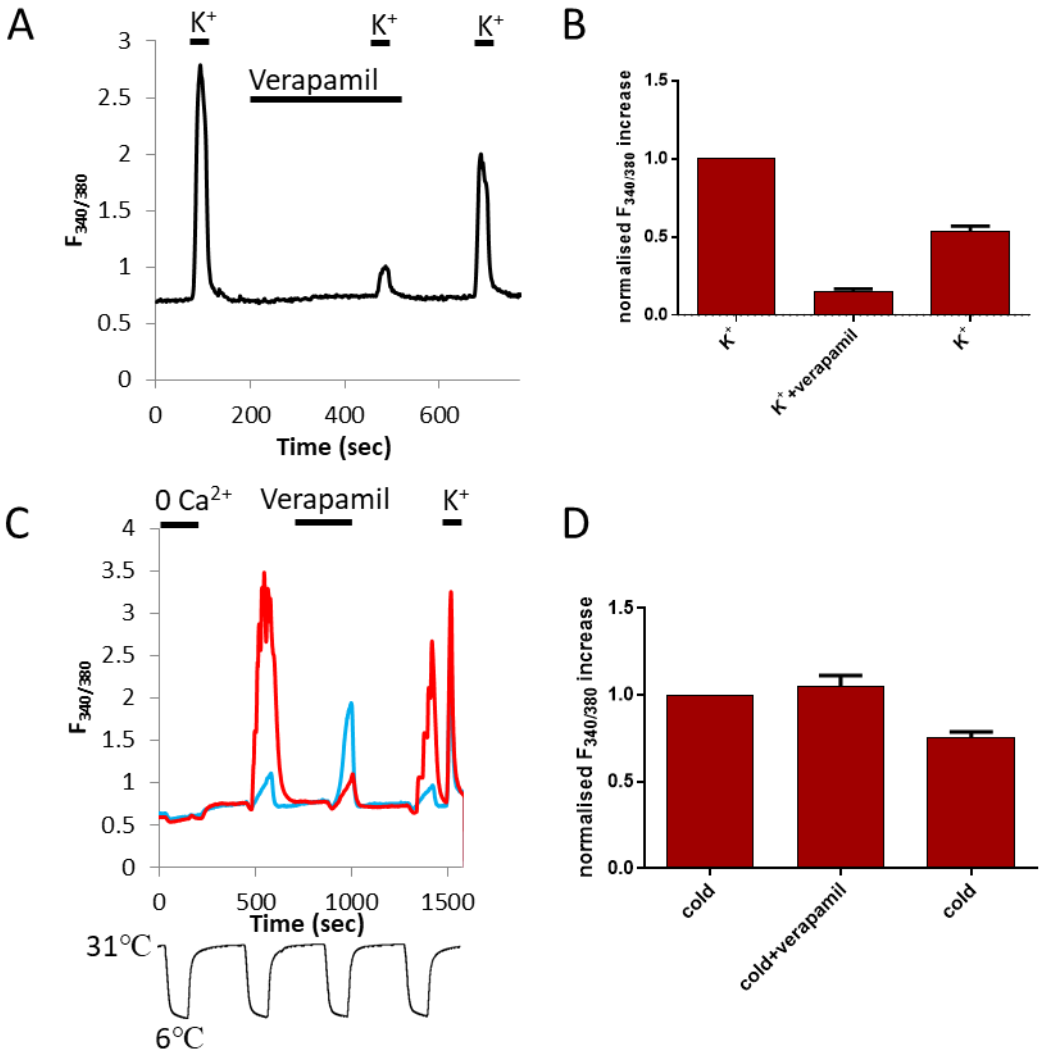

Figure 40 Verapamil had opposing effects on cold responses in SCG neurons.
A) Representative trace showing the effect of L-type Ca_V channel blocker verapamil (100µM) on K^+-induced Ca^{2+} influx at 30°C in SCG neurons from adult C57BL/6 mice sacrificed via cervical dislocation and decapitation. B) Bar graph summarising normalised results (mean+SEM) of 51 neurons on three coverslips. Verapamil caused an inhibition of K^+ responses of >85%. C) Representative tracing showing the effect of L-type Ca_V channel blocker verapamil (100µM) on cold-induced Ca^{2+} influx in SCG neurons from adult C57BL/6 mice sacrificed via cervical dislocation and decapitation. The dip in the trace that is apparent during the first cold ramp is caused by the intrinsic temperature sensitivity of Fura-2. The temperature trace is shown below. Verapamil had opposing effects on some neurons, increasing some responses (blue trace), and decreasing some responses (red trace). D) Bar graph summarising normalised results (mean+SEM) of 277 cold-sensitive neurons on 4 coverslips. A-D) Data from Dr. Bruno Vilar.

If dihydropyridine Ca_V **antagonists** potentiate small cold-responses, perhaps dihydropyridine Ca_V **agonists** inhibit them. This was tested using BayK8644 (30 µM), which is an opener of L-type Ca_V channels (Triggle, Langs and Janis, 1989). Results

show that BayK8644 had no significant effect on mean cold response amplitude (Figure 41).

Like Nifedipine and Verapamil, BayK8644 also had opposing effects on cold responses: inhibiting some responses (e.g. blue trace Figure 41) and potentiating others (e.g. red trace Figure 41). Presumably BayK8644 potentiates the K2P mediated late Ca^{2+} influx, because it is an agonist of Ca_V channels, and inhibits the CICE mechanism. The spiking visible on top of some cold-responses was increased by BayK8644, suggesting that they may be indicative of the K2P-mediated Ca^{2+} influx (red trace in Figure 41).

This effect on CICE seems common to all dihydropyridines, the class of drug that these three compounds belong to. Since Ca_V antagonists Nifedipine and Verapamil failed to block all cold responses and Ca_V agonist BayK8644 failed to increase all cold responses, we can conclude that CICE is not mediated by an increased window current of Ca_V channels in the SCG. The only remaining candidate cold sensor is activation of STIM/Orai channels. All other candidates shown in Figure 25 have now been ruled out.

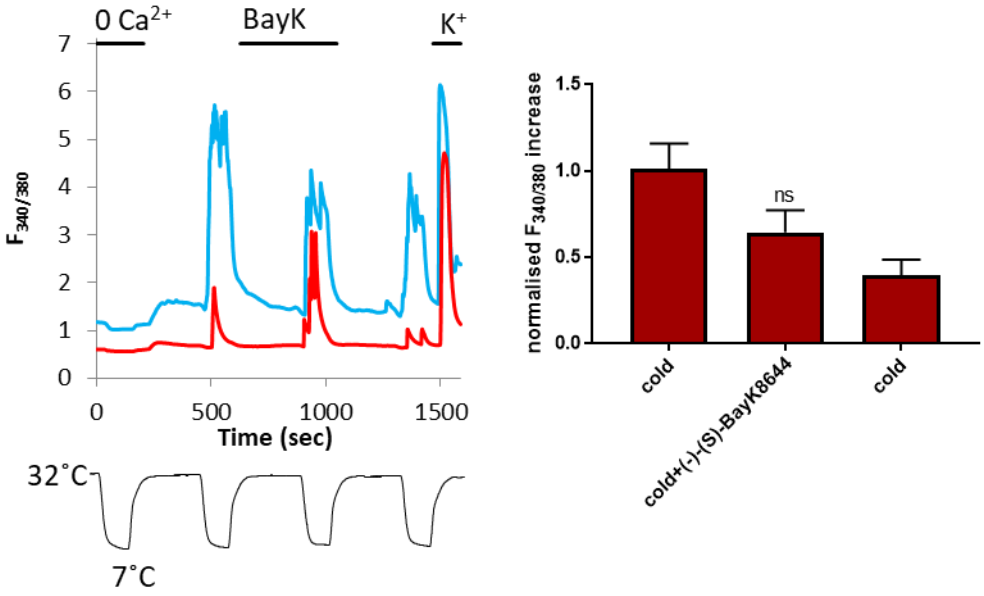

Figure 41 (-)-(S)-BayK8644 had opposing effects on cold responses in SCG neurons.
Left: Representative trace showing the effect of L-type Ca_V channel opener (-)-(S)-BayK8644 (30µM) on cold-induced Ca^{2+} influx in SCG neurons from adult female C57BL/6 mice sacrificed via cervical dislocation and decapitation. The dip in the trace that is apparent during the first cold ramp is caused by the intrinsic temperature sensitivity of Fura-2. The temperature trace is shown below. Right: Line graph summarising normalised results of 45 cold-sensitive neurons on six coverslips. 47% of neurons were cold-sensitive. There was no significant difference in cold response amplitude after application of (-)-(S)-BayK8644 as determined by a repeated measures one-way ANOVA and Dunnett's multiple comparisons test. However, (-)-(S)-BayK8644 had a clear effect on some neurons, potentiating some responses (red trace), and inhibiting some responses (blue trace).

3.3.5 CICE is Mediated by STIM/Orai Channels in SCG Neurons.

Next, we asked whether STIM and Orai, which underlie store-operated Ca^{2+} entry (SOCE), also underlie cold-induced Ca^{2+} entry (CICE). When SCG neurons are cooled, intracellular Ca^{2+} is increased via two mechanisms. CICE, and a separate influx of Ca^{2+} through inhibition of K2P channels and subsequent depolarisation and activation of Ca_V channels.

Three candidate cold-sensors for CICE have so far been ruled out in this chapter. When SCG neurons are cooled, Ca^{2+} is not released from intracellular stores. CICE is not mediated by inhibition of PMCA or by an increased window current through Ca_V channels. The only remaining Ca^{2+} entry pathway that could be mediating responses to cold is the STIM-Orai pathway of store-operated Ca^{2+} entry (Figure 25).

As described in the general introduction, STIM is a Ca^{2+} sensor protein resident in the ER, which binds and opens Orai proteins resident in the plasma membrane to form store-operated channels (SOCE) and refill the intracellular Ca^{2+} stores when emptied. STIM1 contains a thermo-sensor in its c-terminal domain (general introduction section 1.2.1.6). Perhaps STIM1 detects noxious cold and then opens Orai channels to mediate the observed CICE in SCG neurons.

To test this hypothesis, cold ramps were applied to SCG neurons before and after application of a selective Orai antagonist YM58483. The pyrazole derivative YM58483/BTP2 inhibits Orai1-3 (Zitt et al. 2004), inhibits TRPC5 and TRPC3 (He *et al.*, 2005); facilitates TRPM4 (Ryuichi Takezawa *et al.*, 2006), but has no effect on the membrane potential or Ca_V channels (Ishikawa *et al.*, 2003; Xia *et al.*, 2014).

If Orai channels mediate CICE, blocking them would inhibit only part of the cold-responses, because the other part is mediated by K2P inhibition and activation of Ca_V channels, which are not affected by YM58483. Application of YM58483 (3μM) to SCG neurons resulted in a significant 50% reduction in cold-response amplitude (Figure 42). This suggests that STIM and Orai are indeed responsible for CICE.

The frequency histogram in Figure 42D suggests that there are several subpopulations of cold-sensitive SCG neurons: neurons whose cold-responses are blocked by YM58483 (most neurons; blue arrow) presumably mostly express cold-sensitive SOCE channels, and neurons whose cold-responses are unaffected by YM58483 presumably express mostly cold-sensitive K2P channels (red arrow). Some cold-responses were

potentiated by the Orai antagonist (Figure 42D responses>1). The presence of this last group suggests that there is some expression of TRPM4 in SCG neurons, which is facilitated by YM58483. However, no data could be found in the literature to confirm or deny the expression of TRPM4 in sympathetic nerves.

Thus far, all compounds that have significantly decreased cold-response amplitude in SCG neurons (i.e. Cd^{2+}; Gd^{3+}; YM58483) share one property: they are antagonists of the Orai channel (Table 8). This evidence suggests that STIM or Orai are activated by cold in SCG neurons.

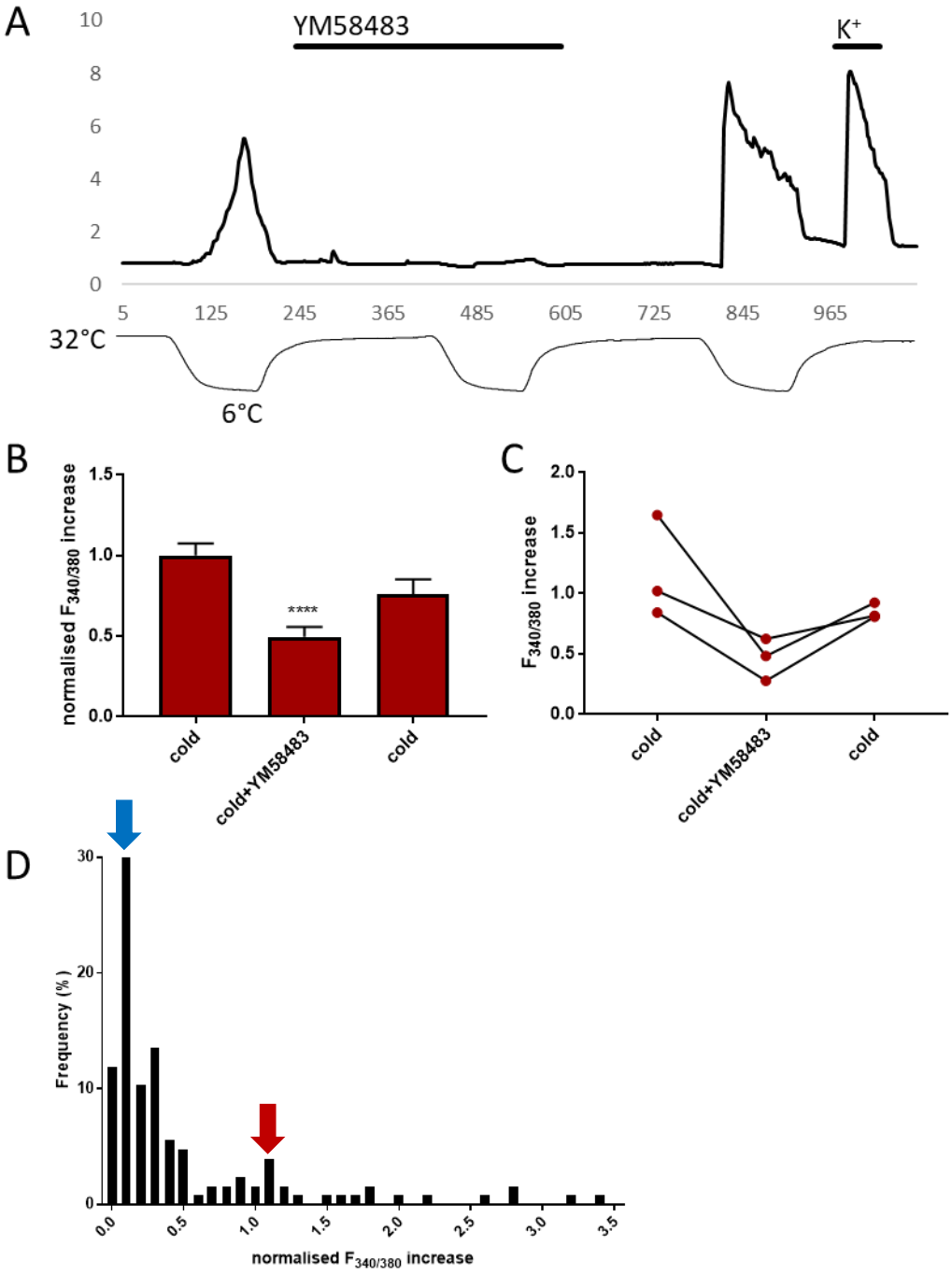

Figure 42 YM58483 inhibited cold responses in SCG neurons.
A) Representative trace showing the effect of Orai channel blocker YM58483 (3μM) on cold-induced Ca^{2+} influx in SCG neurons from adult C57BL/6 mice sacrificed via cervical dislocation and decapitation. The temperature trace is shown below. B) Bar graph summarising normalised results (mean+SEM) of 126 cold-sensitive neurons on 16 coverslips imaged on 3 separate days. YM58483 caused a >50% reduction in cold-response amplitude. There is a significant difference ($p<0.0001$) in cold response amplitude after application of YM58483 as determined by a repeated measures one-way ANOVA and Dunnett's multiple comparisons test. C) Graph summarising results per day. D) Frequency histogram showing normalised cold-response amplitude after application of YM58483. The results suggest two subpopulations: neurons whose cold-responses are reduced after application of YM58483 (blue arrow, mode=0.1) and neurons whose cold-responses are not reduced by YM58483 (red arrow, mode=1.1).

Table 8 Antagonist effects on Ca_V, Orai and cold responses.

	Blocks cold response?	Blocks Orai?	Blocks Ca_V?
Cd^{2+}	✓	✓	✓
Gd^{3+}	✓	✓	✓
Nifedipine	✗	✗	✓
Verapamil	✗	✗	✓
YM58483	✓	✓	✗

Having established that the CICE part of the cold-induced Ca^{2+} influx in SCG neurons is mediated by Orai channels, combined with the knowledge that K2P inhibition-mediated depolarisation and subsequent activation of Ca_V channels also contributes to these cold-response, we tested whether these two mechanisms are sufficient to explain the whole phenomenon of sympathetic cold-sensitivity. Therefore, SCG neurons were perfused with L-type Ca_V antagonist Verapamil (100µM) to block the K2P mechanism and stimulated with a cold ramp in the absence and presence of Orai antagonist YM58483 (3 µM; Figure 43A).

Results show that 34% of SCG neurons responded to cold (with a supra-threshold $F_{340/380}$ increase of >0.2) in the presence of Verapamil. YM58483 fully blocked these cold-responses in the presence of Verapamil (Figure 43B). 31% of cold-insensitive neurons (with cold-response amplitudes of $F_{340/380}$ <0.2) were potentiated by Verapamil (e.g. Figure 43C red trace and all neurons in Figure 43E). YM58483 also fully blocked cold-responses in these neurons (Figure 43E). This suggests that the potentiating effect of Verapamil and the other dihydropyridines tested previously is a direct potentiation of the STIM-Orai channel. The observation that dihydropyridines potentiate Orai channels has since also been made by other scientists in the field (Professor Trebak, unpublished).

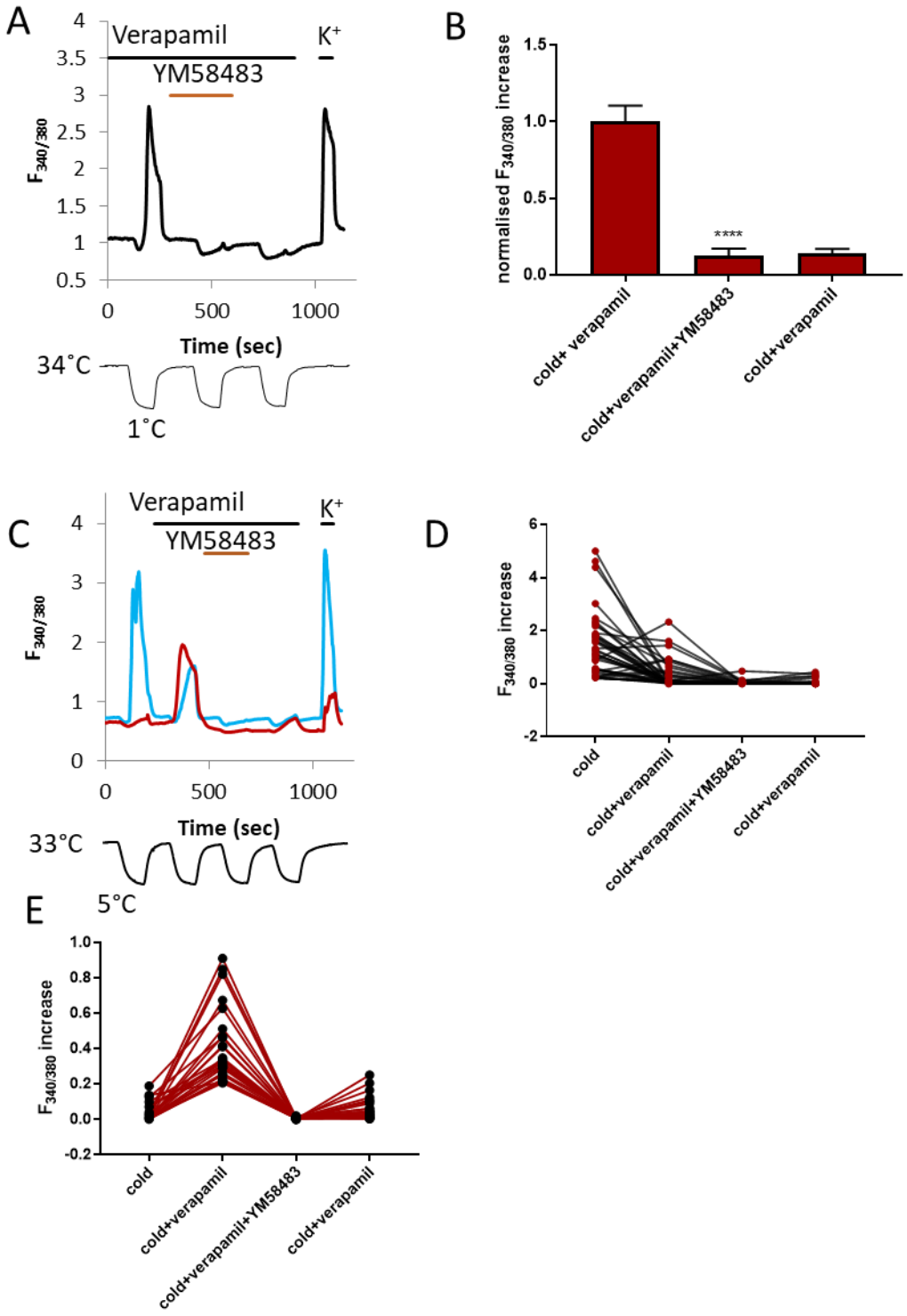

Figure 43 YM58483 completely blocked cold-responses in the presence of Verapamil.
A) Representative trace showing the effect of Orai channel antagonist YM58483 (3μM) on cold responses in the presence of L-type Cav antagonist Verapamil (100μM). B) Bar graph summarising normalised results (mean+SEM) of 117 cold-sensitive neurons imaged on two separate days. YM58483 caused a significant decrease in cold-response amplitude ($p<0.0001$) as determined by a repeated measures one-way ANOVA + Tukey's multiple comparisons test. 34% of SCG neurons responded to cold in the presence of Verapamil with an average amplitude of 1.39. C) Representative traces showing the opposing effects of Verapamil. Cold-responses are potentiated by Verapamil in some neurons (red trace) and inhibited in others (blue trace). The temperature trace is shown below. D) Line graph showing the effect of Verapamil and YM58483 on cold-responses in 48 cold-sensitive SCG neurons. YM58483 fully blocked cold-responses in the presence of Verapamil. E) Line graph showing that cold-insensitive neurons (responses $F_{340/380}<0.2$; n=24) whose responses are potentiated by Verapamil (31% of cold-insensitive neurons) are fully blocked by YM58483.

3.3.6 The Cold-Induced Ca^{2+} Influx is Partly Mediated by STIM-Orai Channels in DRG Neurons

Having established that Orai mediates part of the cold-induced Ca^{2+} influx in SCG neurons, we asked whether STIM-Orai channels also function as cold sensors in DRG neurons. DRG neurons express several cold-sensitive ion channels, including TRPM8, TRPA1, TRPC5, and K2P channels. The SOCE family of proteins (STIM1, STIM2, Orai1, Orai2, and Orai3) are also expressed in DRGs (Lirk *et al.*, 2008; Park and Luo, 2010; Usoskin *et al.*, 2015) and functional mainly in nociceptors (Wei *et al.*, 2017). We hypothesised that these channels also mediate cold-sensitivity in sensory neurons.

To test this, DRG neurons were first stimulated with a cold ramp to 4°C in the absence of extracellular Ca^{2+} to confirm that Ca^{2+} enters the cell through the plasma membrane and is not released from intracellular stores (Figure 44A; first cold ramp). Indeed, no response to cooling is visible in any neurons in this condition. This finding is consistent with reports by others (Reid and M. L. Flonta, 2001; Viana, de la Peña and Belmonte, 2002), but contradicts one study that reports that cooling increases intracellular Ca^{2+} in the absence of extracellular Ca^{2+} in rat DRG neurons (Thut, Wrigley and Gold, 2003). After extracellular Ca^{2+} was added back into the solution, neurons were stimulated with specific agonists for the known and proposed cold sensors TRPM8 (300µM menthol), TRPA1 (50µM AITC), and TRPC5 (100µM Rosiglitazone) to identify a population of "novel" cold-sensitive neurons i.e. not expressing any possibly cold-sensitive TRP channels. These agonists were assumed to be specific for their targets, but may activate other ion channels as well, which may have decreased the percentage of cold-sensitive neurons identified as "novel" in this study. TRP agonist application was followed by cold ramps in the absence and presence of Orai antagonist YM58483 to determine the contribution of STIM-Orai to the cold-responses in these neurons. Note that YM58483 is also a full antagonist of TRPC5 (He *et al.*, 2005), and agonist of TRPM4 (Takezawa et al. 2006) as mentioned previously.

Using this method, three types of cold-sensitive sensory neurons were identified: the light blue trace is representative of a neuron that expresses any known cold-sensitive TRP channel (TRPM8 in this case) and was not inhibited by YM58483. These neurons do not express the STIM-Orai mechanism.

The red trace in Figure 44A is representative of a novel cold-sensitive neuron that does not express any known cold-sensitive TRP channel and was not inhibited by Orai

antagonist YM58483. These neurons do not express the STIM-Orai mechanism but may express the K2P mechanism or another unknown mechanism instead. Babes and colleagues also found a population of cold-sensitive neurons in rat DRG that do not express TRPM8 or TRPA1 and instead expresses a mechanism that causes a large (~700pA) rapidly adapting inward current in response to cooling while neurons were voltage-clamped, which is inhibited by Camphor (Babes, Zorzon and Reid, 2006). Perhaps this is the population represented by the red trace in Figure 44A. This could be tested by repeating the experiment in the presence of Camphor.

The dark blue trace is representative of a novel cold-sensitive neuron that does not express any known cold-sensitive TRP channel but was inhibited by YM58483. The CICE in these neurons must therefore be mediated by Orai channels.

On average, YM58483 had no significant effect on cold-sensitive neurons that expressed TRPM8, TRPA1, or TRPC5 (Figure 44B). YM58483 did cause a significant decrease in cold response amplitude in novel cold-sensitive neurons, which presumably express STIM-Orai channels (Figure 44C).

4% of cold-sensitive neurons were excluded from analysis because they were directly activated by wash-on of YM58483. These neurons presumably expressed TRPM4, which is opened by YM58483.

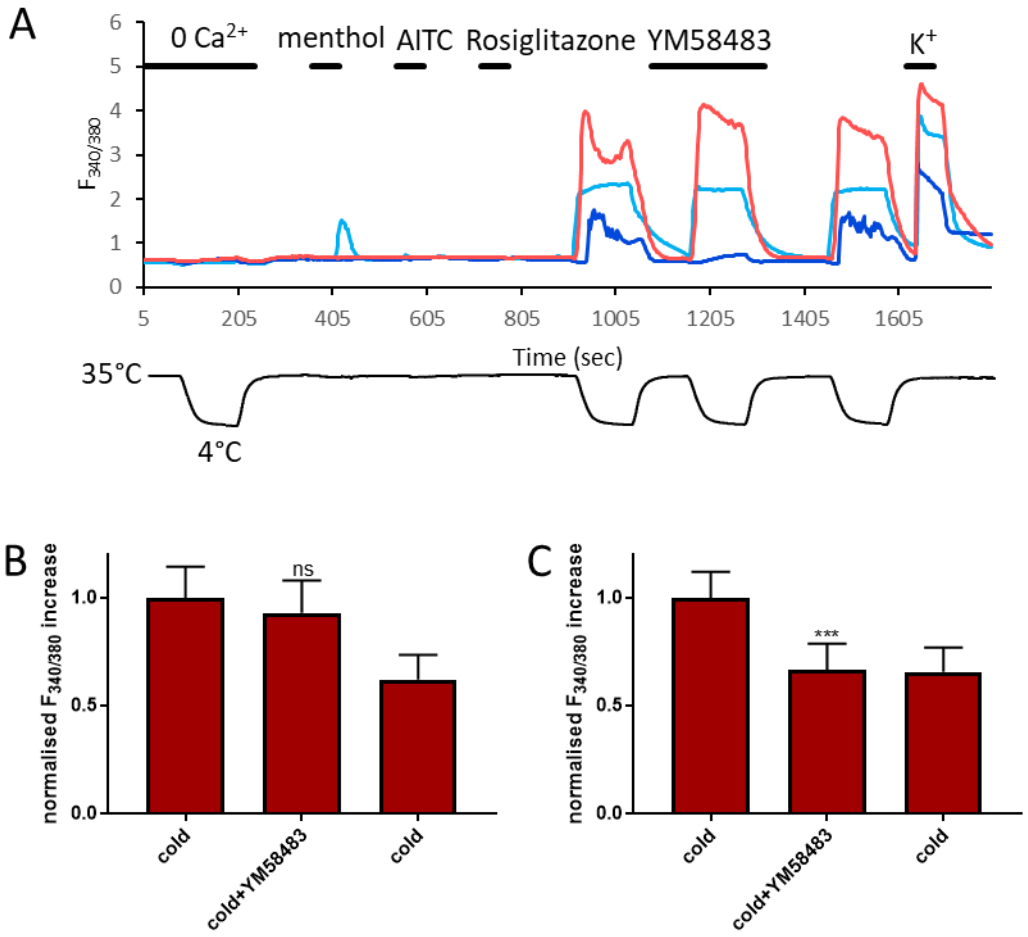

Figure 44 YM58483 inhibited cold responses in DRG neurons.
Representative traces showing the effect of Orai and TRPC5 channel blocker YM58483 (3μM) on cold-induced Ca^{2+} influx in DRG neurons from adult C57BL/6 mice sacrificed via cervical dislocation and decapitation. The temperature trace is shown below. B) Bar graph summarising normalised results (mean+SEM) of 87 cold-sensitive neurons that express either TRPM8 or TRPA1 or TRPC5 imaged on three separate days. YM58483 had no significant effect on cold response amplitude as determined by a repeated measures one-way ANOVA and Dunnett's multiple comparisons test. C) Bar graph summarising normalised results (mean+SEM) of 43 novel cold-sensitive neurons that do not express TRPM8 or TRPA1 or TRPC5 imaged on three separate days. YM58483 caused a >30% reduction in cold-response amplitude. There is a significant difference ($p<0.0001$) in cold response amplitude after application of YM58483 as determined by a repeated measures one-way ANOVA and Dunnett's multiple comparisons test.

Overall, 15% of DRG neurons responded to the 4°C cold ramps (Figure 45A). This percentage is in accordance with other studies (Story *et al.*, 2003; Babes, Zorzon and Reid, 2006; Bautista *et al.*, 2007; Munns, AlQatari and Koltzenburg, 2007; Noël *et al.*, 2009).

Figure 45B shows a subdivision of cold-sensitive DRG neurons by their expression of the three TRP channels tested. 35% of these neurons did not respond to any agonist of TRPM8, TRPA1 or TRPC5 and were therefore considered novel cold-sensitive neurons (Figure 45B). This is in full agreement with previous observations by Munns et

al., who find 33% of cold-sensitive DRG neurons display this novel cold-sensitivity (Munns, AlQatari and Koltzenburg, 2007). In contrast, other groups have found that TRPM8 and TRPA1 are fully responsible for cold responses in the mouse (Yamamoto *et al.*, 2016).

Figure 45B shows that 23% of cold-sensitive DRG neurons expressed TRPM8 (red, green, purple, and orange pie chart sections). Only 5% of cold-sensitive neurons (less than 1% of all neurons tested) co-expressed TRPM8 and TRPA1 (Figure 45B; purple and orange). This low level of co-expression has also been found by others (Story *et al.*, 2003; Munns, AlQatari and Koltzenburg, 2007; Memon *et al.*, 2017). Finally, 31% of cold-sensitive neurons expressed TRPA1; most of these neurons co-expressed TRPC5. Classification of DRG neurons by their expression of these three TRP channels in Figure 45C revealed that TRPM8 expression is more highly correlated with cold-sensitivity than TRPA1 or TRPC5 expression, because most neurons that responded to TRPM8 agonist (menthol) also responded to cold, whereas most neurons that responded to TRPA1 agonist (AITC) or TRPC5 agonist (Rosiglitazone) did not respond to cold Therefore, TRPA1 and TRPC5 may not be directly cold-sensitive. This observation is consistent with many recent reports that TRPA1 is not cold-sensitive (e.g. Vandewauw et al. 2018; Ran et al. 2016; Morenilla-Palao et al. 2014; Knowlton et al. 2010; Chen et al. 2011; de Oliveira et al. 2014). Others have suggested that Ca^{2+} imaging is not sensitive enough to detect TRPA1 cold-sensitivity, and that TRPA1-mediated cold-responses might be missed, because TRPA1 is activated much more strongly by AITC than by cold (Karashima *et al.*, 2009).

If TRPA1 and TRPC5 are not directly cold-sensitive, possibly some of these neurons are cold-sensitive instead because of other cold transduction mechanisms. Perhaps the K2P and STIM/Orai mechanisms are co-expressed in neurons expressing TRPA1 and/or TRPC5. Others have found that STIM1 is co-expressed in 81% of AITC sensitive neurons (Wei *et al.*, 2017).

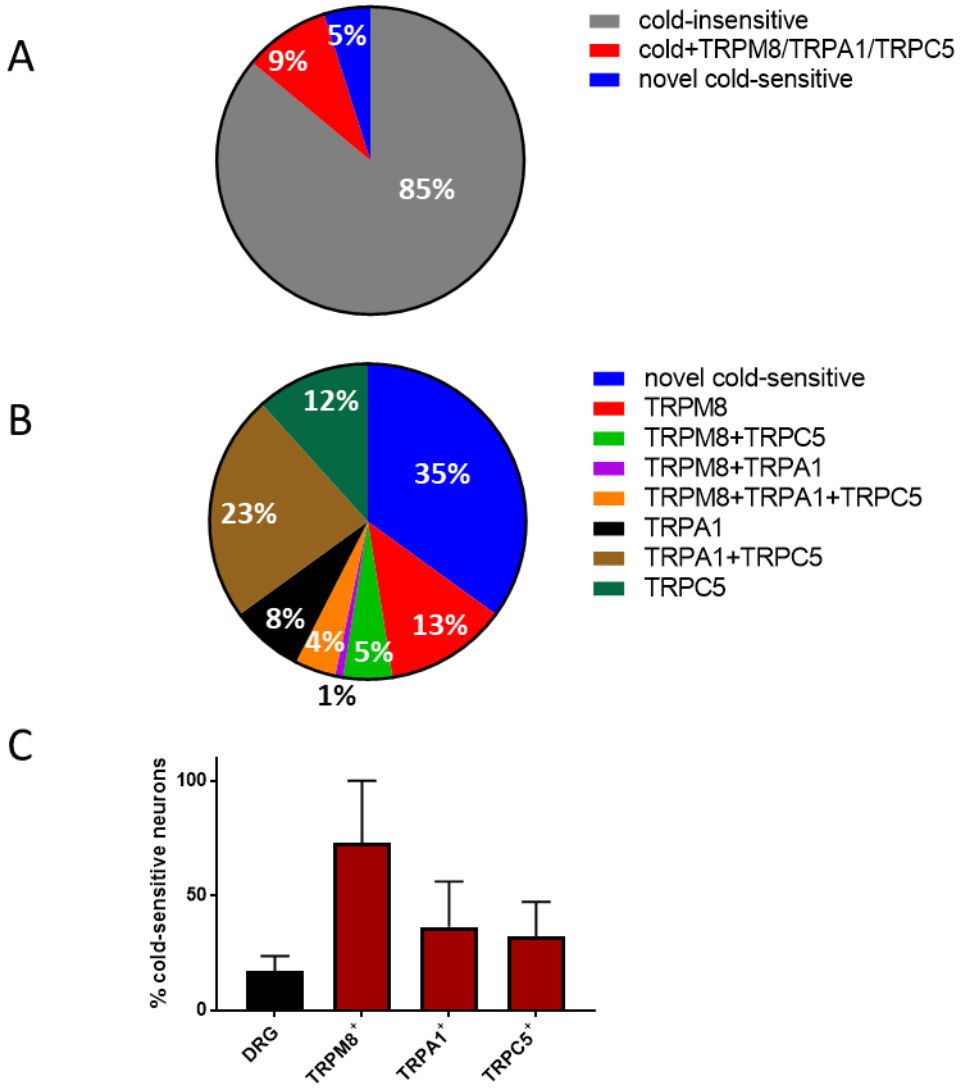

Figure 45 TRPM8 is more highly correlated with cold-sensitivity than TRPA1 and TRPC5.
A) Pie chart showing the percentage of DRG neurons that were both cold-sensitive and expressed either TRPM8, TRPA1, or TRPC5 (red); and novel cold-sensitive DRG neurons that did not express any of these channels (blue). n=859 neurons imaged on three separate days. 5% of DRG neurons expressed a novel cold-sensitive mechanism. B) Pie chart showing the different populations of cold-sensitive neurons by expression of TRPM8, TRPA1, and TRPC5 n=99 neurons imaged on three separate days. 35% of cold-sensitive neurons ded not express TRPM8 or TRPA1 or TRPC5 (blue). C) Bar graph showing the average percentage of cold-sensitive neurons in the whole DRG; in the subpopulation of DRG neurons expressing TRPM8 but not TRPA1 or TRPC5; in the subpopulation of DRG neurons expressing TRPA1, but not TRPM8 or TRPC5; and the subpopulation of DRG neurons expressing TRPC5, but not TRPM8 or TRPA1 (mean+SEM). Cold-sensitivity is more highly correlated with TRPM8 than with TRPA1 or TRPC5. n=3 days.

To examine potential overlap between the Orai mechanism and expression of TRPM8, TRPA1 and TRPC5, frequency histograms were made showing the effect of the Orai blocker YM58483 on normalised cold response amplitudes of each subpopulation (Figure 46). If YM58483 blocks cold responses in these neurons, that suggests a contribution of the Orai mechanism to the response amplitudes.

TRPM8 expressing neurons were the least inhibited by YM58483 (Figure 46B) and novel cold-sensitive neurons (not expressing TRPM8, TRPA1 or TRPC5) were the

most inhibited (Figure 46E). The observation that not all novel cold-sensitive neurons are inhibited by YM58483 is consistent with reports that K2P channels are expressed in these neurons, which would not be blocked by YM58483 (Noël et al. 2009; Madrid et al. 2009).

A large proportion of TRPA1 expressing neurons were also inhibited by YM58483, suggesting co-expression of TRPA1 and STIM/Orai in these neurons (Figure 46C). This may explain why these neurons are cold-sensitive if TRPA1 is not directly activated by cold. Others have also found overlap of TRPA1 and STIM expression (Wei *et al.*, 2017).

Not many cold-responses in TRPC5-expressing neurons were inhibited by YM58483 (Figure 46D). This was surprising because YM58483 is a **full antagonist** of TRPC5 at the concentration used (He *et al.*, 2005). If TRPC5 mediates cold responses in these neurons, they would be blocked by YM58483. The data therefore suggests that TRPC5 is not directly cold-sensitive. This is consistent with reports that TRPC5 knockout mice do not have deficits in cold-sensation (Zimmermann et al. 2011b).

The population of cold-sensitive TRPC5-expressing neurons that do not express TRPM8 or TRPA1 and are not blocked by YM58483 must then express another cold-sensor. We can speculate that this would be the K2P mechanism, as it is not affected by YM58483. One way of confirming this would be to repeat the experiment with Ca_V blocker Verapamil present during one of the cold ramps, to block the Ca^{2+} influx associated with this mechanism.

Figure 46E shows that novel cold-sensitive neurons in the DRG are somewhat normally distributed and there are no clear subpopulations. If these novel neurons would either express the STIM-Orai mechanism or the K2P mechanism, but not co-express these two mechanisms, we would expect one subpopulation to be fully blocked and one subpopulation to be unaffected by YM58483. We can therefore speculate that STIM/Orai and K2P channels are co-expressed in some of these neurons. One way to test this would be to repeat this experiment with a cold ramp in the presence of Ca_V blocker Verapamil and a cold ramp in the presence of Verapamil and Orai blocker YM58483.

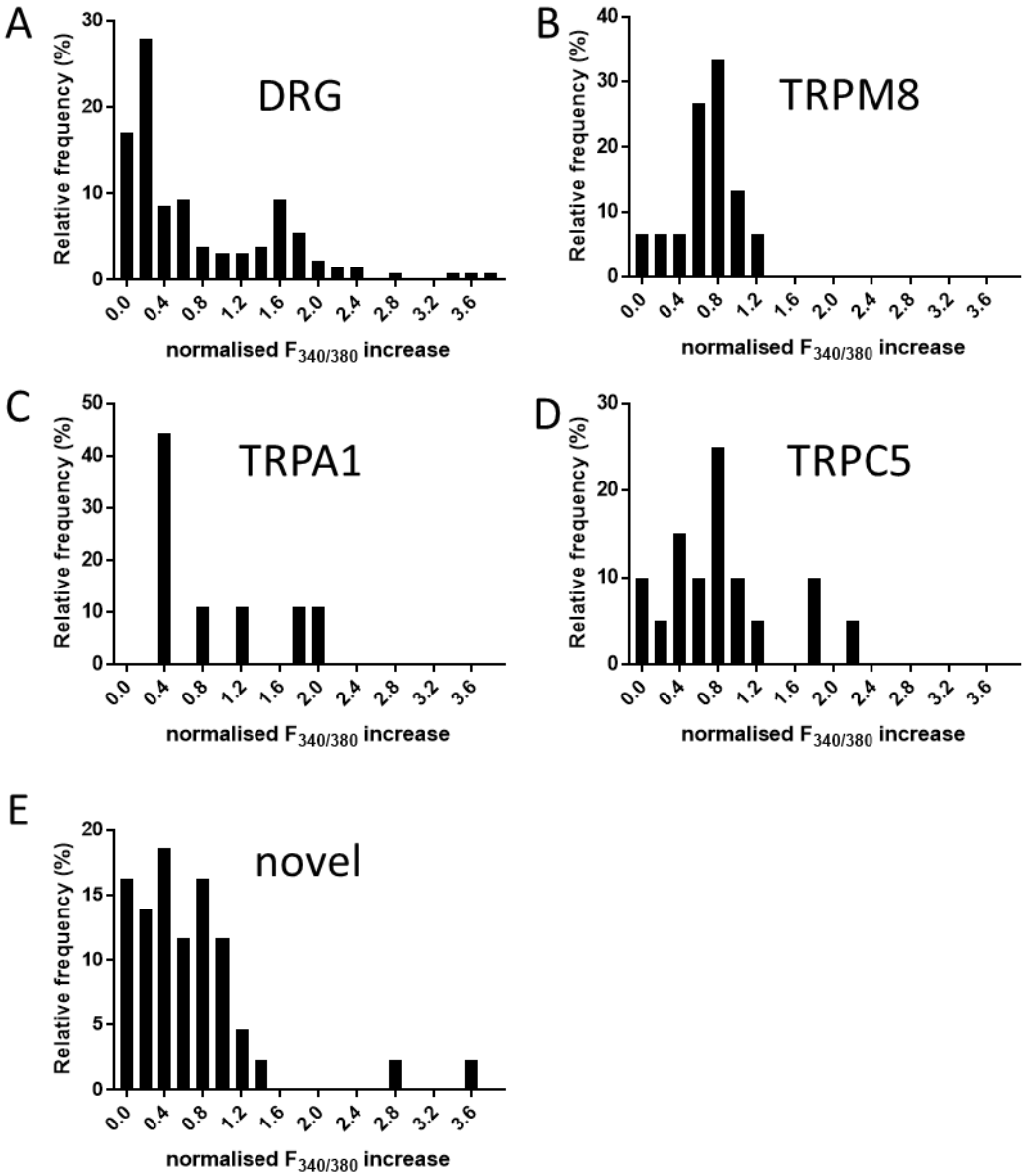

Figure 46 The effect of YM58483 on subpopulations of DRG neurons.
Frequency histograms showing the effect of Orai and TRPC5 channel antagonist YM58483 on normalised cold-response amplitudes of cold-sensitive neurons in the DRG (A; n=129), the subpopulation of cold-sensitive neurons that express TRPM8 but not TRPA1 or TRPC5 (B; n=15), the subpopulation of cold-sensitive neurons that express TRPA1, but not TRPM8 or TRPC5 (C; n=9), the subpopulation of cold-sensitive neurons that expressed TRPC5, but not TRPM8 or TRPA1 (D; n=20), and the subpopulation of cold-sensitive neurons that did not express TRPM8, TRPA1 or TRPC5 (E; n=43). YM58483 potentiated some cold-responses, but not in TRPM8 expressing neurons. YM58483 caused the least inhibition in the subpopulation of cold-sensitive neurons that express TRPM8, but not TRPA1 or TRPC5 (B; mode=0.8). YM58483 fully inhibited TRPC5 at the concentration used, but did not have a large inhibitory effect on the subpopulation of cold-sensitive neurons that expressed TRPC5, but not TRPM8 or TRPA1 (D; mode=0.8). Inhibition of Orai channels in novel cold-sensitive neurons does not reveal distinct populations of novel cold-sensitive neurons (E). The modal response of novel cold-sensitive neurons in the presence of YM58483 is the same as the modal response of neurons that expressed TRPA1, but not TRPM8 or TRPC5 (E and C; mode=0.4). Cold-response amplitudes were corrected for Fura-2 artifacts before normalisation.

Finally, activation thresholds were calculated for each subpopulation of DRG neurons (Figure 47). Activation thresholds were defined as the bath temperature corresponding to the time at which a cell responded to cold with an $F_{340/380}$ increase larger than the mean+3.09SD of the baseline of that cell.

The largest proportion (mode) of cold-sensitive DRG neurons were activated when cooled to 10°C, which shows that many sensory neurons detect noxious cold. Based on the activation threshold of STIM-Orai channels measured in SCG neurons, we expected sensory neurons that express these channels to have a similar activation threshold. Indeed, the average cold activation threshold of novel cold-sensitive DRG neurons was 15.1±1.0℃ (mean±SEM), which is similar to the average cold activation threshold of 12.1±0.50℃ found in SCG neurons (see section 2.3.2).

The population of neurons expressing TRPA1, and the population of neurons expressing the novel cold-sensitive mechanisms had the same mode of 10°C. Again, we can speculate that the cold-sensitivity of these cells is not mediated by TRPA1, but by activation of STIM-Orai channels instead. The modal activation threshold of TRPM8 expressing neurons was 30°C, which is consistent with the literature that reports TRPM8 is activated between 18-32°C (Babes, Zorzon and Reid, 2004).

The modal activation threshold of TRPC5 expressing neurons was 18°C, which is **inconsistent** with reports that TRPC5 is activated by temperatures between 37-26°C (K Zimmermann *et al.*, 2011b). Again, we can speculate that the cold-sensitivity of these cells is not mediated by TRPC5, but by inhibition of K2P channels instead, which show a 20-fold inhibition at 22°C versus 42°C (Noël et al. 2009).

Taken together, the experiments performed on sensory neurons show that there are at least two subpopulations of cold-sensitive neurons in the DRG. One population expresses TRPM8, but not K2P or STIM-Orai channels and senses mild cold. The other population co-expresses the STIM-Orai and K2P mechanisms, and senses noxious cold. Inhibition of K2P channels leads to action potential firing and could contribute to conscious thermosensation, whereas activation of STIM-Orai channels does not affect the membrane potential, so must serve a local function.

Possibly the local rise in Ca^{2+} in these neurons triggers release of inflammatory and/or vasodilatory neuropeptides, such as CGRP. This is likely since STIM1 is expressed in all CGRP positive DRG neurons (Wei *et al.*, 2017). A chemiluminescent enzyme

immunoassay could be used to determine whether CGRP is indeed released from DRG neurons in response to cold.

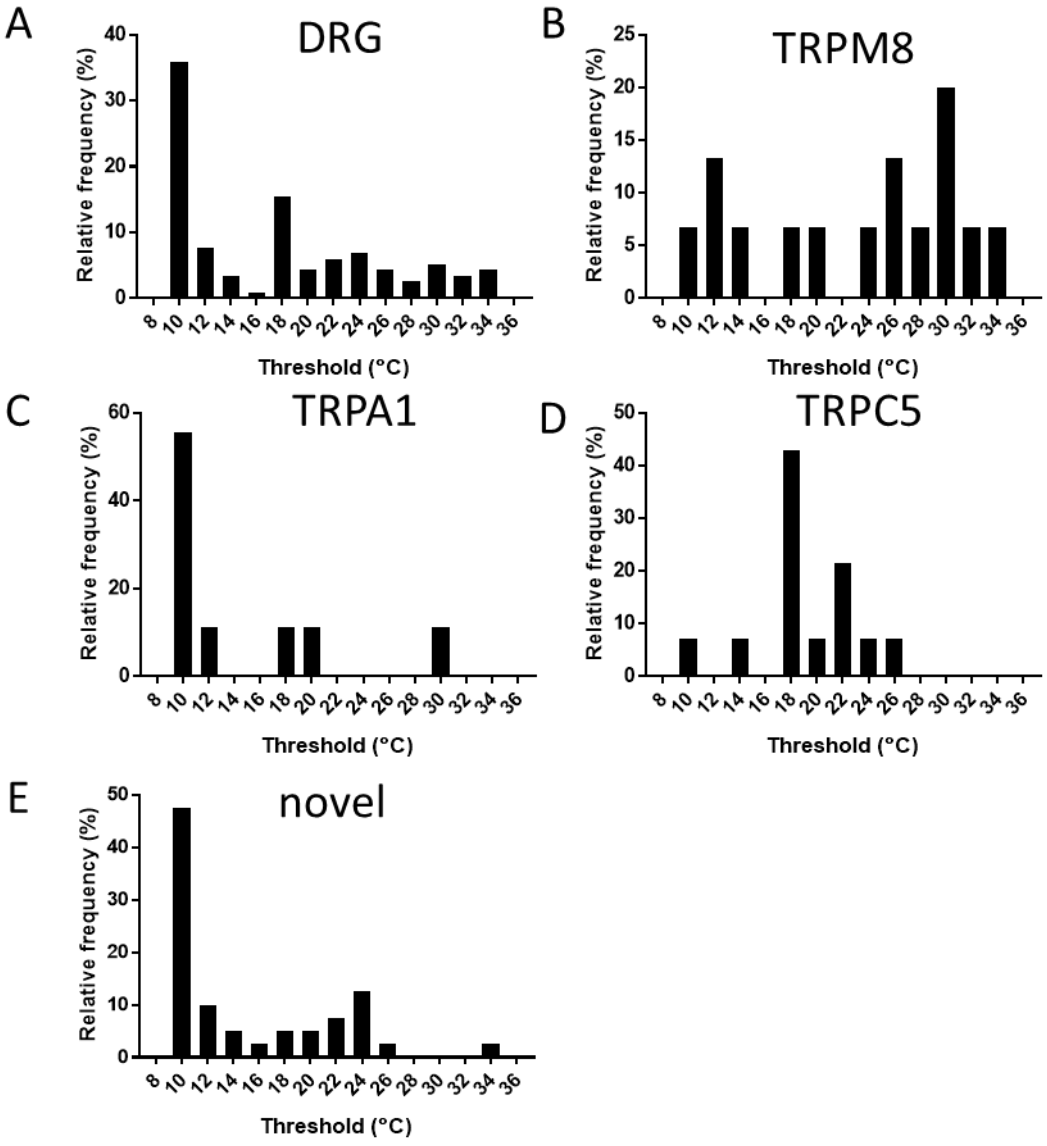

Figure 47 The activation threshold of novel cold-sensitive neurons was most similar to TRPA1 expressing neurons. Frequency histograms showing the temperature activation thresholds of cold-sensitive neurons in the whole population of DRG neurons (A; n=117), the subpopulation of cold-sensitive neurons that expressed TRPM8 but not TRPA1 or TRPC5 (B; n=15), the subpopulation of cold-sensitive neurons that expressed TRPA1, but not TRPM8 or TRPC5 (C; n=8), the subpopulation of cold-sensitive neurons that expressed TRPC5, but not TRPM8 or TRPA1 (D; n=14), and the subpopulation of cold-sensitive neurons that did not express TRPM8, TRPA1 or TRPC5 (E; n=40). The modal activation threshold in the population of novel cold-sensitive neurons (10°C) was the same as in the subpopulation of cold-sensitive neurons that expressed TRPA1, but not TRPM8 or TRPC5.

3.4 Conclusion

The aim of this chapter was to identify the molecular identity of a novel cold-sensor discovered in sympathetic and sensory neurons. Any protein that leads to an increase of intracellular Ca^{2+} could in theory be functioning as a cold sensor (Figure 25).

At the start of this project, several of these proteins had already been ruled out (TRPM8, TRPA1, NCX, NCKX, Ligand-Gated Channels) and it was shown that there are two parts to these cold responses. An **early** cold-induced Ca^{2+} entry (CICE) carried no detectable ionic current, and a **late** influx of Ca^{2+} was mediated by inhibition of K2P channels and subsequent depolarisation and activation of Ca_V channels (Tan et al. unpublished).

Four hypotheses were considered for a candidate cold sensor that could mediate CICE: Ca^{2+} could be released from intracellular stores; intracellular Ca^{2+} could be increased by inhibition of PMCA; Ca^{2+} could enter the cell through an increased window current leak from Ca_V channels; and Ca^{2+} could enter the cell through Orai channels.

Results show that the cold-induced Ca^{2+} influx is not mediated by any known cold-sensitive TRP channel (TRPM8, TRPA1, TRPC5) in the majority (90%) of SCG neurons. The cold-induced Ca^{2+} influx is not caused by Ca^{2+} release from intracellular stores, either directly or indirectly via GPCR activation. In SCG neurons, CICE is not mediated by an increased Ca_V window current. Ca_V channel blockers do decrease cold response amplitude in some neurons, which presumably express the K2P channel mechanism. Ca_V channel blockers also potentiate cold responses, through a direct effect on the Orai channel.

The main finding of this chapter is that CICE is mediated by SOCE channels in SCG and DRG neurons. The combination of Orai-mediated CICE and K2P-mediated late Ca^{2+} influx is sufficient to explain all cold responses in SCG neurons.

Results show that a proportion of cold responses in DRG neurons are mediated by STIM/Orai and support the function of TRPM8 as a cold-sensor. Others have shown the involvement of K2P channels in the population of cold-sensitive DRG neurons that do not express TRPM8 (Viatchenko-Karpinski, Ling and Gu, 2018). Our data does not support the function of TRPA1 and TRPC5 as cold sensors and suggests possible overlap of TRPA1 and STIM/Orai expression.

Data from a recent large-scale single-cell RNA sequencing study can be used to corroborate our findings (Usoskin *et al.*, 2015). Table 9 shows the expression levels of

the genes discussed in this chapter. TRPA1 and STIM1 are both most highly expressed in the population of non-peptidergic neurons. Perhaps STIM1 mediates responses to cold in these neurons instead of TRPA1.

Another way to corroborate our findings would be to detect expression of STIM and Orai in SCG and in DRG by immunohistochemistry, western blot, or in situ hybridization.

Activation of TRPM8 and K2P mediated Ca_V activation are both electrogenic mechanism and trigger action potential firing and can therefore contribute to conscious thermosensation. On the other hand, CICE through Orai channels does not generate much current and can therefore not contribute to conscious thermosensation directly. Possibly it serves a local function, which we will explore in chapter 5.

Table 9 Expression of possible cold sensors in DRG neurons.
Expression of Stim1-2, Orai1-3, TRPA1, TRPM8, TRPC5, TREK1 (Kcnk2), TRAAK (Kcnk4) TREK2 (Kcnk10), CGRP (Calca) in populations of DRG neurons. Data given as percentage of neurons expressing the gene in each population. NF=neurofilament heavy chain-expressing neurons; NP=non-peptidergic neurons; PEP=peptidergic neurons; TH=tyrosine hydroxylase-expressing neurons. Data from Usoskin et al. 2015.

	NF					NP			PEP			
		NF2/3			NF4/5		NP2/3					
Gene	NF1	NF2	NF3	NF4	NF5	NP1	NP2	NP3	PEP1	PEP2	TH	**Colour scheme**
Stim1	23%	27%	8%	14%	15%	32%	25%	50%	3%	6%	25%	0%
Stim2	0%	6%	8%	5%	8%	5%	3%	8%	6%	6%	6%	10%
Orai1	3%	2%	0%	0%	0%	6%	6%	0%	5%	0%	5%	20%
Orai2	3%	2%	25%	9%	12%	10%	9%	0%	14%	18%	8%	30%
Orai3	26%	6%	8%	14%	4%	22%	31%	17%	16%	18%	12%	40%
Trpa1	0%	0%	0%	0%	0%	51%	22%	17%	6%	0%	18%	50%
Trpm8	0%	0%	0%	0%	0%	0%	0%	0%	6%	0%	0%	60%
Trpc5	0%	6%	0%	0%	0%	2%	0%	0%	0%	0%	0%	70%
Kcnk2	3%	4%	0%	0%	0%	0%	0%	0%	20%	6%	0%	80%
Kcnk4	19%	8%	17%	5%	0%	2%	19%	0%	6%	12%	0%	90%
Kcnk10	0%	2%	0%	0%	4%	1%	0%	8%	6%	6%	0%	100%
Calca	0%	0%	8%	0%	0%	20%	88%	8%	78%	100%	0%	

3.5 Limitations

A few things must be kept in mind when interpreting the data in this chapter. First of all, the Fura-2 Ca^{2+} dye used for all experiments buffers intracellular Ca^{2+} (Bootman *et al.*, 2013), and Orai channels are inactivated by Ca^{2+} (Palty, Fu and Isacoff, 2017). Therefore, the Ca^{2+}-buffering properties of Fura-2 may cause a small potentiation of cold responses. Secondly, a recent study has shown that STIM and Orai are upregulated by high glucose (25mM) via calcineurin-NFAT signalling after 72h (Daskoulidou *et al.*, 2015). Neurons used for the experiments in this chapter were cultured in Neurobasal-A medium containing 25mM glucose for 18-24 hours before use. Therefore, it could be possible that cultured neurons have a higher expression of STIM and Orai *in vitro* and display enhanced cold-sensitivity.

The use of neurons in culture carries with it the caveat that the whole cell is stimulated at once. It is not possible to cool just the axon using this method. Therefore, it remains an assumption that the mechanisms studied in this chapter are expressed in the axon terminal as well as the soma. In chapter 6 we will develop a method that allows for the study of these mechanisms in the sympathetic nervous system *in vivo*.

Chapter 4 Does Altering STIM/Orai Expression Affect Cold-Induced Ca^{2+} Entry?

4.1 Introduction

Having established in the previous chapter that CICE is mediated by store-operated calcium entry (SOCE) channels, which consist of STIM and Orai proteins, the aim of this chapter is to determine which isoforms of STIM and Orai are responsible for detecting cold. There are two isoforms of STIM and three isoforms of Orai (Hou *et al.*, 2012). Any of these proteins could be involved e.g. STIM1 could be activated by cold and in turn open Orai1 homomeric channels or STIM2 could be activated by cold and in turn open Orai1/3 heteromeric channels, etc.

To identify the exact molecular identity of the cold sensor in SCG neurons, the RNA interference gene-silencing approach was used to knock down individual SOCE proteins. In tandem, different combinations of STIM and Orai isoforms were overexpressed in rat adrenal pheochromocytoma 12 cells (PC12). These cells can be differentiated into a sympathetic phenotype but are not intrinsically cold-sensitive.

4.2 Materials and Methods

4.2.1 Gene Silencing

ON-TARGET plus small interfering RNA (siRNA, Dharmacon) was used to knock down Orai1,2,3 genes in SCG neurons. siRNA was resuspended in RNase-free siRNA buffer containing 60mM KCl, 6mM HEPES-pH 7.5 and 0.2 mM $MgCl_2$ to produce 20μM stock and stored at -20˚C. siRNA concentration was verified using a Nanodrop ND-1000 UV spectrophotometer (Sinica) at 260nm in combination with Beer's Law $A_{260} = \varepsilon CL$ (ε = extinction coefficient (~372100.1 L/mol x cm); C = concentration of siRNA; L = path length of the cuvette.

C57BL/6J mouse SCG neurons were enzymatically dissociated as described in Chapter 2. Neurons were resuspended in supplemented Nucleofector Solution (Lonza) containing 300nM siRNA or 0.4μg GFP plasmid at room temperature in aliquots of 20,000 – 50,000 neurons each and placed in small cell number (SCN) certified cuvettes (method from Eickholt et al. 2007). GFP plasmid was used for quantification of electroporation efficiency. The control sample was electroporated with non-targeting siRNA (Dharmacon).

Neurons were electroporated using SCN Basic Neuron Programme 6 of a Nucleofector II machine (Amaxa Scientific) to allow the siRNA to enter the cells as per the manufacturer's instructions. Pre-equilibrated supplemented Neurobasal-A medium (as described in chapter 2) was added immediately after electroporation and the cells were then placed in a humidified 37˚C/5%CO_2 incubator for 10 minutes and plated onto coverslips pre-coated as described in chapter 2. Neurons were allowed to adhere for 10-20 minutes in the incubator before wells were filled with cell culture medium. Cells were incubated at 37°C for at least 24 hours post-electroporation before assaying gene knockdown. Immunocytochemistry and calcium imaging were performed as described in Chapter 2.

4.2.1.1 RNA Quantification

After calcium imaging, coverslips were washed 2x with PBS and then total RNA was isolated using the RNeasy Micro Kit (Qiagen) as per the manufacturer's instructions. RNA concentration was quantified using a Nanodrop ND-1000 UV spectrophotometer (Sinica) as described above. Reverse-transcription was performed using a High

Capacity RNA-to-cDNA kit (Thermo Fisher Scientific) as per the manufacturer's instructions.

Expression levels of Gapdh, Orai1, Orai*2*, Orai3, STIM1, STIM*2*, and Store-Operated Ca^{2+} Entry Associated Regulatory Factor (SARAF) were quantified using TaqMan Gene Expression Assays (Applied Biosystems; Table 10) and Reverse-Transcription quantitative Polymerase Chain Reaction (RT-qPCR) in triplicate as per the manufacturer's instructions using a Lightcycler 480II (Roche) machine with the following protocol: preincubation at 95°C for 10min; 45 cycles of amplification at 60-95°C for 30s each at a rate of 2.5°C/s; cooling at 40°C for 30s.

Table 10 Taqman Gene Expression Assays (20x)

Gene	Assay ID
Gapdh	Mm99999915_g1
Orai1	Mm00774349_m1
Orai*2*	Mm04214089_s1
Orai3	Mm01612888_m1
STIM1	Mm00486423_m1
STIM*2*	Mm01223103_m1
SARAF	Mm00509538_m1

4.2.1.*2* Data Analysis

Roche Lightcycler software was used to calculate cycle thresholds (Ct), defined as the second derivative maximum of the curve (the point of greatest rate change). Assuming equal primer efficiency, double delta Ct analysis ($2^{-\Delta\Delta C_t}$) was used to calculate expression fold change between experimental and control conditions: comparing the Ct of each gene (e.g. Orai1) to both the Ct of a housekeeping gene (i.e. Gapdh) in the same sample, and the Ct of that gene (e.g. Orai1) in the control sample (method from Livak & Schmittgen 2001).

4.2.1.3 Optimisation

Initially, adult mice were used for knockdown experiments, which required the cells from 10 mice to be pooled to provide enough cells per electroporation. Therefore, new-born mice were used in later experiments, which greatly improved cell viability.

4.2.2 Overexpression of SOCE Channels in PC12 Cells

4.2.2.1 Plasmid amplification

Bacterial stabs containing plasmids with Orai1, Orai2, Orai3, STIM1, and STIM2 (Addgene; Table 11) were amplified using a HiSpeed Plasmid Midi Kit (Qiagen) according to the manufacturer's instructions.

Table 11 Plasmids

Gene	Vector	Item#
hOrai1	pcDNA3.1	21638
hOrai2	pcDNA3.1	16369
hOrai3	pcDNA3.1	16370
mSTIM1 myc	pcDNA3.1	17732
mSTIM2 myc	pENTR11	17734

h = human; m = mouse; myc = synthetic peptide tag that can be labeled with an antibody

4.2.2.2 HEK293 Cell Culture

Human Embryonic Kidney cells (HEK293, ATCC) that were previously frozen at passage 57 were thawed from liquid nitrogen storage in a 37˚C water bath, centrifuged for 10 minutes at 1000rpm and resuspended in Dulbecco's Modified Eagle Medium (DMEM with L-glutamine, 1000mg/L D-glucose and sodium pyruvate, Invitrogen) and mechanically dissociated and cultured in 25cm^2 cell culture flasks (Fisher Scientific) which had been previously coated for one hour with 40ng/mL laminin (Fisher Scientific) in 0.01% w/v Poly-L-Lysine solution (Sigma). Flasks were kept in a sterilised humid incubator at 37˚C and 5% CO_2.

DMEM cell culture medium had been previously supplemented with 10% v/v foetal bovine serum (FBS, Invitrogen), 1% penicillin/streptomycin (Thermo Fisher Scientific). Every 2-3 days, when grown to 90% confluency, HEK293 cells were detached from the flasks using 0.05% trypsin (Thermo Fisher Scientific) for 5 minutes, centrifuged for 10 minutes at 1000rpm, resuspended in DMEM, and mechanically dissociated. Cells were then passaged to another flask and a portion of cells were seeded on 13mm coverslips (Thermo Fisher Scientific) that had been coated in the same way as the cell culture flasks. Cells were cultured for 18-36 hours before use.

4.2.2.3 Undifferentiated PC12 Cell Culture

Rat adrenal pheochromocytoma 12 cells in 10% DMSO (PC12; Greene & Tischler 1976) were thawed from liquid nitrogen storage in a 37˚C water bath, centrifuged for 10 minutes at 1000rpm and resuspended in RPMI-1640 medium (Sigma-Aldrich) supplemented with 1% (v/v) penicillin-streptomycin (Invitrogen), 1% (v/v) L-glutamine (200mM; Invitrogen), and 10% (v/v) horse serum (Invitrogen), and mechanically dissociated by pipetting up and down 20x using a P200 pipette and plated on 25cm^2 cell culture flasks (Fisher Scientific) which were previously coated for one hour with 1mg/mL Collagen IV from human placenta (Sigma) dissolved in acetic acid and diluted 10x in 0.01% w/v Poly-L-Lysine solution (Sigma), and subsequently washed twice with sterile PBS (Sigma).

Flasks were kept in a sterilised humid incubator at 37˚C and 5% CO_2. 80% of cell culture medium was replaced every 2-3 days. Once a week, when grown to 90% confluency or when starting to form clumps, PC12 cells were detached from the flasks using 0.05% trypsin (Thermo Fisher Scientific) for 5 minutes at 37˚C, centrifuged for 10 minutes at 1000rpm, resuspended in supplemented RPMI, and mechanically dissociated by pipetting up and down 20x using a P200 pipette. 25% of cells were then passaged to another flask and a portion or seeded on 13mm coverslips (Thermo Fisher Scientific) previously coated in the same way as the cell culture flasks. Cells were cultured for 18-36 hours before transfection. PC12 cells can be differentiated into a more sympathetic-like phenotype with trophic factors, but this feature of the cell line was not used for the experiments in this chapter.

4.2.2.4 Transfection of Plasmid DNA into Undifferentiated PC12 Cells Using Lipofectamine LTX Reagent

Plasmid DNA was transfected into undifferentiated PC12 cells using Lipofectamine LTX Reagent (ThermoFisher Scientific) as per the manufacturer's instructions. Undifferentiated cells were used because dividing cells are easier to transfect. Briefly, for each well to be transfected, 0.5µg of total DNA (with STIM, Orai, and mCherry in 2:1:1 ratio) was dissolved in 100µL Opti-MEM Reduced Serum Medium containing 0.5µL PLUS Reagent (ThermoFisher Scientific). Then, 1.75µL Lipofectamine LTX was added and the solution was vortexed at full speed for 5s and incubated for 25min at

room temperature to allow formation of DNA-Lipofectamine LTX complexes and added to the cells.

mCherry was co-transfected into PC12 cells with STIM and Orai to determine which cells were successfully transfected, assuming each DNA-Lipofectamine LTX complex contains DNA for each protein. Cells were incubated at 37°C for 18-24 hours post-transfection before assaying for transgene expression using immunocytochemistry and calcium imaging methods as described in Chapter 2.

4.2.2.5 Optimisation

Initially, GFP was co-transfected into PC12 cells with STIM and Orai to determine which cells were successfully transfected. The GFP fluorescence spectrum overlaps with that of Fura-2, so GFP fluorescence interfered with the calcium imaging signal (Figure 48). Therefore, the red fluorescent protein mCherry was used instead.

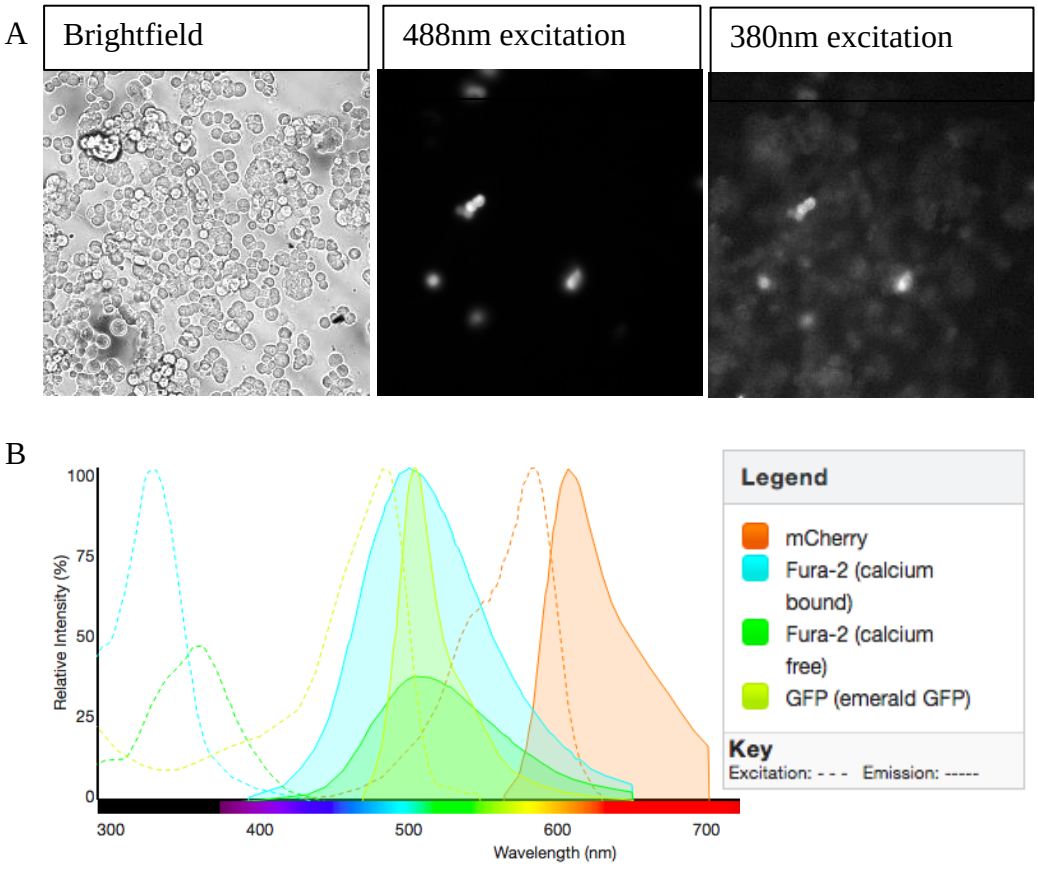

Figure 48 GFP and Fura-2 excitation spectra overlap.
A) Images of GFP overexpression in undifferentiated PC12 cells (not loaded with Fura-2). Left: brightfield image. Middle: excitation at 488nm shows GFP expression. Right: excitation at 380 shows that GFP is visible in the Fura-2 channel and would interfere with the calcium imaging signal. B) The fluorescence excitation spectra (dotted lines / no fill) of Fura-2 and GFP overlap, but Fura-2 and mCherry do not. Figure adapted from www.thermofisher.com/us/en/home/life-science/cell-analysis/labeling-chemistry/fluorescence-spectraviewer.html

4.3 Results and Discussion

4.3.1 Small Interfering RNA-Mediated Knock-Down of Orai Subunits in SCG Neurons

To determine the optimum time-point to perform Ca^{2+} imaging after knock-down, RNA was extracted at 24, 48, and 72h after Orai1 was knocked down. Figure 49A-D shows that Orai1 was knocked down by 47%, 96% and 91% after 24, 48, and 72h respectively. Silencing of Orai1 did not have a large effect on the expression of the other proteins measured.

The largest reduction of Orai1 mRNA was achieved at 48h, but because the protein turnover rate of the Orai subunits is unknown, the delay between knock-down of the mRNA and the resulting protein cannot be estimated. Therefore, 72h was chosen as the time-point for experiments, to allow for the lag in protein turnover. Gene silencing of Orai2 using the same method was unsuccessful and needs further optimisation (Figure 49E).

Figure 49F shows that knock-down of Orai3 was successful, but also affected expression levels of Orai1 and STIM2. This effect has also been observed by others (Prof. Trebak, personal communication).

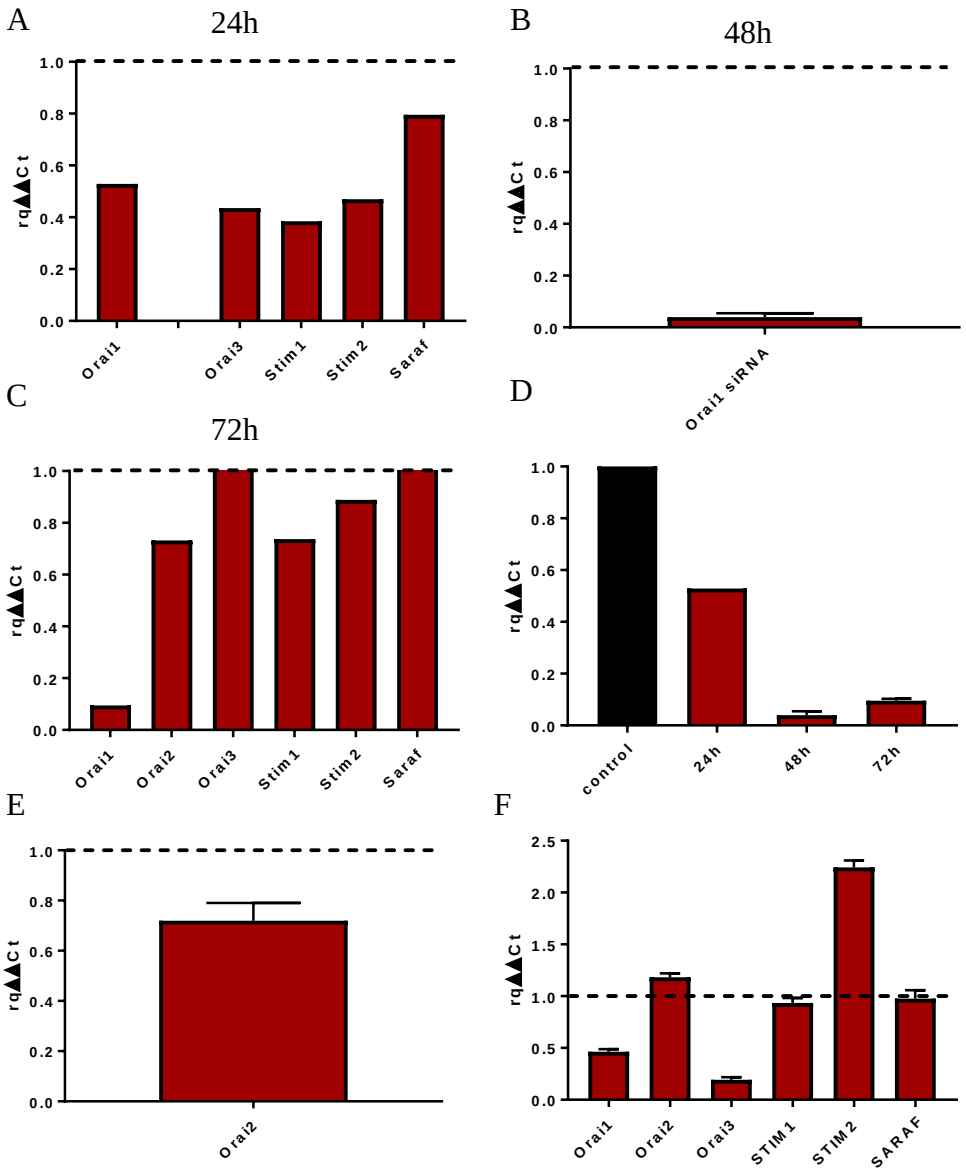

Figure 49 Gene silencing of Orai genes.
Relative quantification (rqΔΔCt) of the mRNA levels of STIM, Orai and SARAF normalised to Gapdh and non-targeting siRNA control sample 24h after electroporation with Orai1 siRNA. There was not enough RNA for Orai2 levels to be measured. n=1 technical replicate for each gene, cells pooled from 10 adult mice. B) Relative quantification of the mRNA levels of Orai1 normalised to Gapdh and non-targeting siRNA control 48h after electroporation with Orai1 siRNA. n=2 technical replicates, cells pooled from 10 adult mice. C) Relative quantification of the mRNA levels of STIM and Orai normalised to Gapdh and non-targeting siRNA control 72h after electroporation with Orai1 siRNA. There was not enough RNA for the other genes to be measured. n = 1 technical replicate, cells pooled from 10 adult mice. D) Bar chart comparing the knock down efficiency of Orai1 siRNA after 24h, 48h and 72h. Effective knock down (>90%) was achieved after 24h and 72h. E) Relative quantification of mRNA levels of Orai2 normalised to Gapdh and non-targeting siRNA control 72h after electroporation with Orai2 siRNA. Knock-down was unsuccessful. There was not enough total RNA for the other genes to be measured. n=3 technical replicates, cells pooled from 10 animals. F) Relative quantification of mRNA levels of STIM, Orai and SARAF compared to Gapdh and non-targeting siRNA control 72h after electroporation with Orai3 siRNA. Knock down of Orai3 was successful. Orai1 is also knocked down. STIM2 expression is increased. n=3 technical replicates, cells pooled from 7 new-born mice.

Ca^{2+} imaging was performed after each knock-down experiment, but comparing the cold-sensitivity of neurons transfected with siRNA for STIM and/or Orai with neurons transfected with non-targeting siRNA did not yield consistent results (data not shown). Therefore, we wondered whether the gene silencing approach was successfully targeting neurons. Since RTqPCR only measures a population average and the SCG contains glia as well as neurons, it was unclear whether gene silencing was succesful in neurons, or merely in glia. Therefore, 5μM arabinofuranosyl-cytosine (Ara-C; Sigma) was added to the cultures 2h after siRNA transfection to inhibit glial cell proliferation. Unfortunately this resulted in undetectable RNA for all proteins tested including the housekeeping gene Gapdh (data not shown). This suggests that the resulting cell number after application of Ara-C was too low to provide a large enough amount of RNA to quantifying gene expression.

Therefore, GFP was electroporated into SCG cells instead of siRNA and cells were stained for GFP and neuronal marker β3tubulin to determine the electroporation efficiency of neurons specifically. Figure 50 shows that most GFP expression did not overlap with β3tubulin expression, which means that the gene silencing approach was probably mainly targeting glial cells and needed to be optimised further.

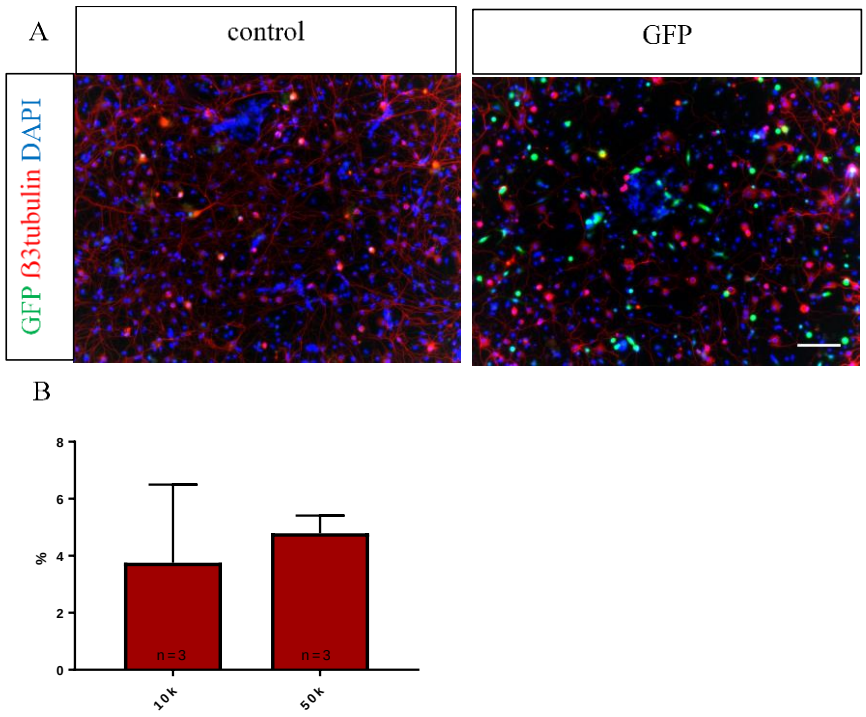

Figure 50 Electroporation with GFP revealed a very low electroporation efficiency.
Representative fluorescence images taken with a 20x objective showing cultured SCG neurons from new-born C57/BL6J mice plated at 50,000 neurons/coverslip that were stained for GFP (green), βIII Tubulin (red), and DNA (blue) to label cells expressing GFP, neurons, and all cell nuclei respectively. SCG neurons were fixed one day after electroporation with GFP plasmid DNA. There was no GFP expression in control (left) as expected. GFP expression in the electroporated sample did not overlap with βIII Tubulin expression in most cells, showing that the electroporation of neurons was mostly unsuccessful. Chicken anti-GFP antibody (1:500) was used in combination with goat anti-chicken Alexa Fluor 488 (1:1000); mouse anti-βIII Tubulin (1:500) was used in combination with goat anti-mouse Alexa Fluor 594 (1:1000); DAPI (1:50,000) was used to stain for DNA in cell nuclei. Scale bar = 50μm. B) Bar chart summarising the electroporation efficiency of neurons at 10,000 neurons per electroporation and 50,000 neurons per electroporation. In both cases electroporation efficiency was very low (~4% of neurons). n = 3 electroporations.

4.3.2 Overexpression of SOCE Channels in PC12 Cells

Because the gene silencing approach was unsuccessful in knocking down STIM/Orai proteins in SCG neurons, we decided to use the opposite approach and overexpress the SOCE channel component proteins STIM1 and Orai1 in a cell line and measure their effect on cold-response amplitude. HEK293 cells are one of the most frequently used cell lines for overexpression experiments. Like almost all cell types, HEK293 cells express SOCE channels (Thul *et al.*, 2017), so HEK293 cells were tested for intrinsic cold-sensitivity first. As shown in Figure 51, HEK293 cells consistently responded to cold ramps with a clear $F_{340/380}$ increase. This makes HEK293 cells less suitable for overexpression of cold-sensitive proteins.

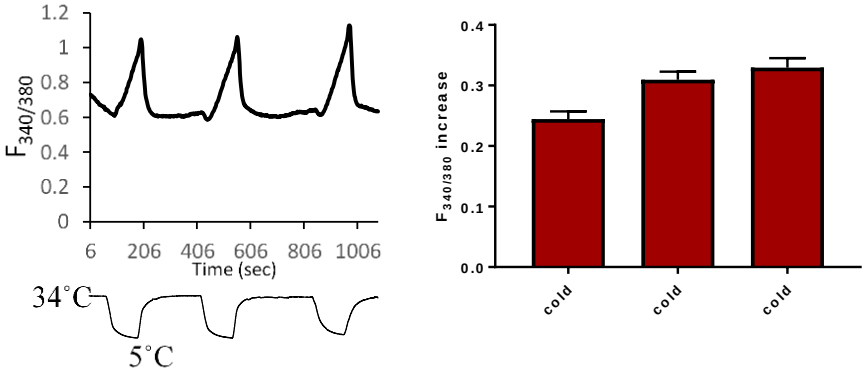

Figure 51 HEK293 cells are intrinsically cold-sensitive
Left: Representative trace showing the effect of cold ramps from 34 to 5°C on [Ca^{2+}] levels in HEK293 cells. The temperature trace is shown below. Right: Graph summarising results of 64 HEK293 cells (mean+SEM). HEK293 cells consistently responded to cold.

Perhaps HEK293 cells express the same cold-sensitive mechanisms as SCG neurons and could be used as a proxy, which would be convenient because HEK293 do not express Ca_V channels (Thul *et al.*, 2017) and would provide an opportunity to study the STIM-Orai mechanism in isolation (without contribution of the K_2P mechanism). To determine whether Ca^{2+} enters through the plasma membrane (like in neurons) or is released from intracellular stores, HEK293 cells were exposed to cold in the absence of extracellular Ca^{2+}.

Figure 52 shows that HEK293 cells release Ca^{2+} from intracellular stores when cooled, evidenced by the rise in intracellular Ca^{2+} in the absence of extracellular Ca^{2+}. This suggests that HEK293 cells use a difference mechanism to respond to cold than SCG neurons do. Therefore, HEK293 cells cannot be used as a proxy for SCG neurons to study the cold-sensitive mechanisms. Cold also causes release of Ca^{2+} from intracellular stores in avian sensory neurons (Yamamoto *et al.*, 2016), mouse olfactory ensheathing glial cells (Stavermann *et al.*, 2012), and HeLa cells (Tseeb *et al.*, 2009). Perhaps the cold-sensitive mechanism in HEK293 cells is similar.

As reviewed in the general introduction section 1.2.1.2, TRPA1 was found to be sensitive to cold below 17˚C when expressed in HEK293 cells (Sawada *et al.*, 2007), but most TRPA1-expressing DRG neurons are not cold-sensitive (Babes, Zorzon and Reid, 2004; Bautista *et al.*, 2007; Munns, AlQatari and Koltzenburg, 2007; Noël *et al.*, 2009; Memon *et al.*, 2017). This suggests that TRPA1 is not directly cold-sensitive.

We report here that HEK293 cells release Ca^{2+} from intracellular stores when cooled, which could activate TRPA1 directly (Doerner *et al.*, 2007), and explain why TRPA1 responds to cold when overexpressed in these cells.

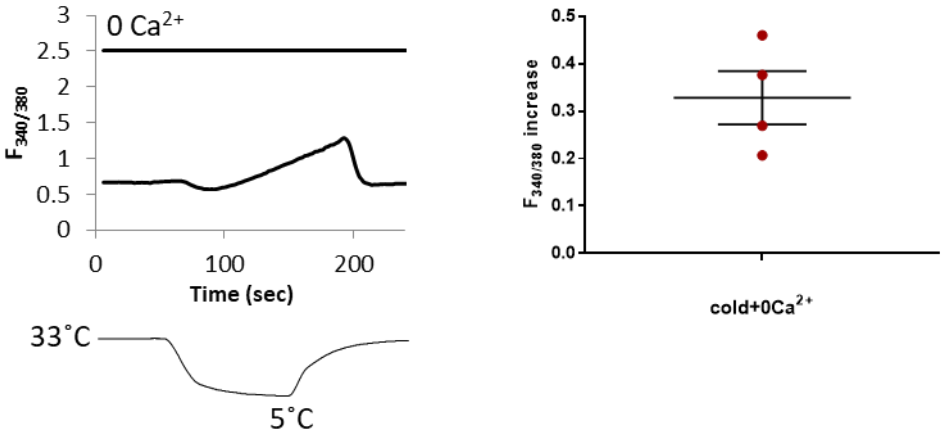

Figure 52 HEK293 cells still responded to cold in 0 Ca^{2+} solution.
Left: Representative trace showing the cold-induced Ca^{2+} increase in HEK293 cells in the absence of extracellular Ca^{2+}. The temperature trace is shown below. Right: Graph summarising results of 471 HEK293 on 4 coverslips (mean+SEM). Unlike neurons, HEK293 cells responded to cold in the absence of extracellular Ca^{2+}.

Next, undifferentiated rat pheochromocytoma (PC12) cells were tested for cold-sensitivity to investigate their suitability as an overexpression system for STIM and Orai proteins. Differentiated PC12 cells are a model of sympathetic neurons, but primarily use TRPC1 (rather than Orai1) for SOCE (Selvaraj, Watt and Singh, 2009), which may make them less cold-sensitive intrinsically.

Figure 53 shows that when undifferentiated PC12 cells were exposed to cold ramps to 6˚C, they displayed only a minor intrinsic cold-sensitivity of $\Delta F_{340/380}$ = 0.18±0.10 (roughly half the size of the average HEK293 cell response in Ca^{2+} free extracellular solution shown in Figure 52). PC12 cells express Ca_V channels and responded to K^+ with a large influx of Ca^{2+} as expected (Figure 53).

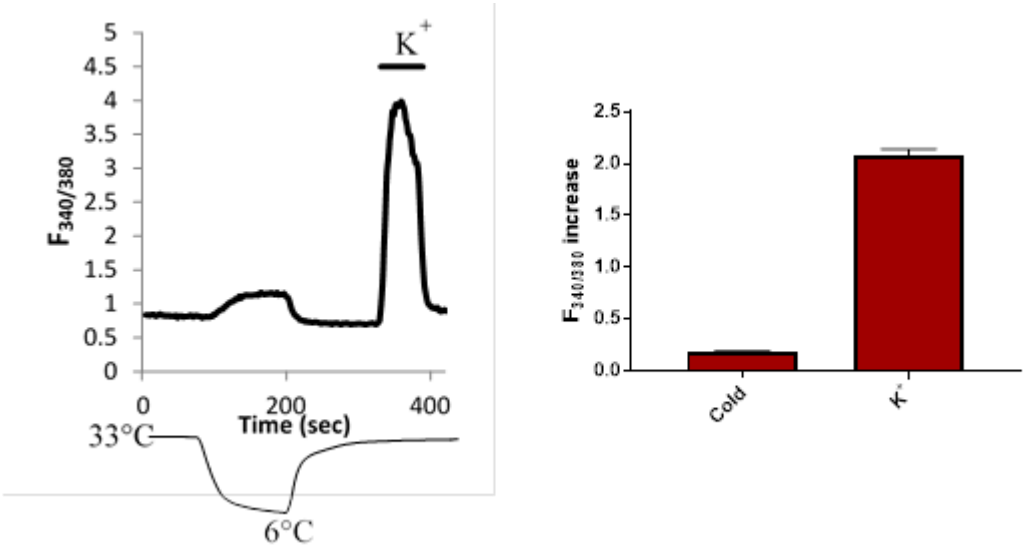

Figure 53 PC12 cells displayed a low intrinsic cold-sensitivity.
Left: Representative trace showing the cold-responses of a PC12 cell. The temperature trace is shown below. Right: Bar graph summarising results of 172 cells (mean+SEM). Cold response amplitude was low and not variable, which makes PC12 cells a suitable cell line for overexpression experiments.

Having demonstrated that PC12 cells display a relatively low intrinsic cold-sensitivity, STIM1 and Orai1 were overexpressed in PC12 cells to examine whether this would increase the cold-response amplitude in these cells. STIM1 and Orai1 were overexpressed in combination with mCherry to label successfully transfected cells.

Results show that 36% of cells were successfully transfected, as evidenced by their expression of mCherry (Figure 54). Cells with a red pixel intensity value of larger than the maximum value (+1) of a control coverslip not transfected with mCherry were defined as expressing mCherry. This method matched well with a manual quantification of the data, namely cells that were counted as red by eye consistently had an average pixel intensity value above the threshold set previously, and cells that were not counted as red had an average pixel intensity value below threshold.

After transfection, cells expressing mCherry/STIM1/Orai1 had a significantly increased cold-response amplitude ($\Delta F_{340/380}$=1.403±0.07) compared to cells on the same coverslip not expressing mCherry ($\Delta F_{340/380}$=0.6485±0.33) (Figure 54). Furthermore, the cold-responses of these cells were ~8 fold higher than untransfected PC12 cells previously tested ($\Delta F_{340/380}$=1.403±0.07 *versus* $\Delta F_{340/380}$ = 0.18±0.10). This data suggests that overexpression of STIM1/Orai1 induces cold-sensitivity and is consistent with our findings in the previous chapter that Orai channels mediate a proportion of cold-responses in SCG and DRG neurons.

If expression of mCherry reliably labelled expression of STIM1 and Orai1, we would expect every cell that expressed mCherry to also express STIM1/Orai, and every cell that did not express mCherry to also not express STIM1/Orai1.

Therefore, we would expect the endogenous cold-response amplitude of untransfected PC12 cells to be the same as the cold-response amplitude of unsuccessfully transfected PC12 cells that do not express mCherry. However, the endogenous mean cold-response amplitude of untransfected PC12 cells ($\Delta F_{340/380}$ = 0.18±0.10) was ~4 fold lower than the mean cold-response amplitude of PC12 cells that did not express mCherry after transfection with STIM1/Orai1/mCherry ($\Delta F_{340/380}$=0.6485±0.33). This suggests that there are some false negatives in the data i.e. cells that overexpress STIM1/Orai1 but not mCherry, perhaps because mCherry does not always co-transfect with STIM/Orai.

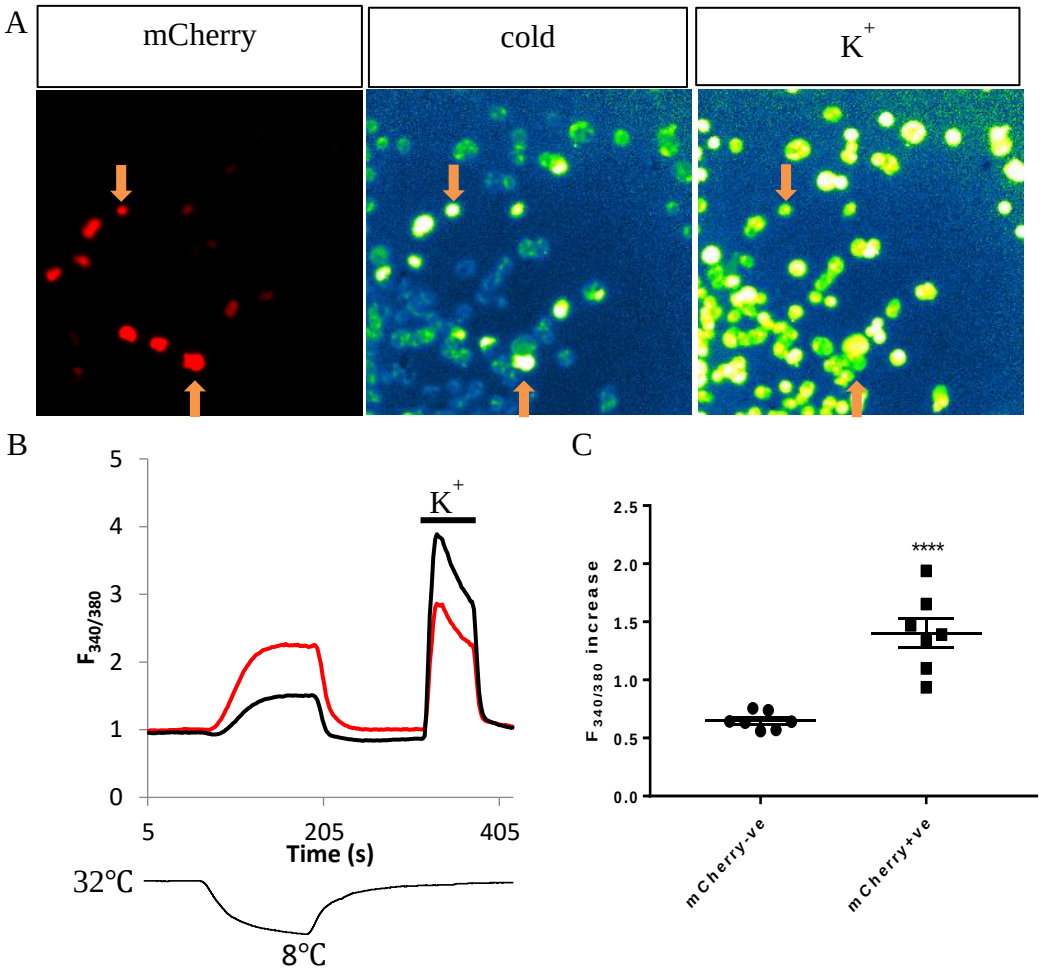

Figure 54 Overexpression of mCherry/STIM1/Orai1 induced cold-sensitivity in PC12 cells after 24h.
A) Fluorescence images showing mCherry expression (left), Fura-2 fluorescence ($F_{340/380}$) during the cold ramp (middle), and during application of K^+ (right). 36% of PC12 cells were successfully transfected. Cells expressing mCherry looked brighter during the cold ramp. The orange arrows mark two examples. B) Average traces showing cold-responses of PC12 cells transfected with mCherry/STIM1/Orai1. The temperature trace is shown below. The black trace is the average response of cells that did not express any mCherry after transfection. The red trace is the average response of cells expressing mCherry and presumably STIM1/Orai1 after transfection. C) Graph showing the average response per coverslip of seven coverslips (mean+SEM). "mCherry-ve" corresponds to the black trace in B. "mCherry+ve" corresponds to the red trace in B. There was a significant difference between the two groups as determined by an unpaired two tailed t-test ($P<0.0001$).

4.4 Conclusion

The aim of this chapter was to determine which isoforms of STIM and Orai mediate CICE. A gene silencing approach was attempted in primary cultures of SCG neurons but needed further optimisation. A gene overexpression approach in PC12 cells proved more fruitful. Differentiated PC12 cells are an immortalised cell culture model of sympathetic neurons *in vitro*. The undifferentiated PC12 cells used in this study exhibited some neuron-like properties already e.g. Ca_V expression, evidenced by their responses to K^+. However, undifferentiated PC12 cells did not display a large endogenous cold-induced Ca^{2+} influx.

Overexpression of STIM1/Orai1/mCherry caused a significant increase in cold-response amplitude. This suggests that either STIM1 or Orai1 can detect cold and expression of both proteins together is sufficient to mediate CICE. Other combinations of STIM and Orai subunits will need to be tested to determine their role in CICE.

4.5 Limitations

The main limitation of both approaches used in this chapter is the lack of a fully reliable measure of protein expression levels after either knock down or overexpression. Measuring mRNA levels in the whole population of SCG cells proved misleading as it became clear that the electroporation protocol targeted glia more than neurons.

We used co-transfection of a fluorescent protein (e.g. mCherry) together with STIM and Orai, which gives some measure of which individual cells have been transfected and is commonly used (e.g. Chiu et al. 2004). However, these genes are not in the same plasmid, so the data may include both false positives and false negatives i.e. cells that express STIM1 but not mCherry, or cells that express mCherry but not STIM1. The STIM1 and STIM2 plasmids we used both contain myc tags, so one way to resolve this issue would be to stain for myc and mCherry to investigate to what extent their expression reliably overlaps after co-transfection.

Chapter 5 A Possible *in vivo* Function of CICE

5.1 Introduction

The observation that sympathetic neurons contain cold transduction mechanisms raises the question of what the function of these mechanisms might be. CICE through Orai channels does not produce a large enough current to affect the membrane potential and produce action potential firing (see section 3.1). Therefore, cold detected by the SOCE system likely serves a local function.

One local effect of extreme cold is a phenomenon called cold-induced vasodilation (CIVD) of blood vessels in the skin (see section 1.1.7). CIVD is known to be mediated locally by nerves in the skin, because it is gradually lost after sympathectomy (Lewis, 1930), but the exact molecular mechanism has not yet been identified. The aim of this chapter is to determine whether sympathetic nerves could serve this function through release of vasodilators.

The Ca^{2+}-dependent enzyme nNOS produces nitric oxide (NO), which is a strong vasodilator (Lee and Stull, 1998). Similarly, the vasodilatory neuropeptide CGRP is released from nerve terminals through Ca^{2+} dependent exocytosis (Douglas, 1974). Both of these processes could be activated by CICE. Therefore, we stained for neuronal nitric oxide synthase (nNOS) and calcitonin gene-related peptide (CGRP) in SCG and SG neurons.

5.2 Materials and Methods

5.2.1 Immunofluorescence

Adult ChAT-GFP mice were used for all experiments in this chapter (see section 2.2.1). The antibodies used for immunofluorescence imaging are listed in Table 12 and Table 13. See chapter 2 for remaining methods relating to immunofluorescence.

Table 12 Primary antibodies

Antibody	**Reference**	**Source**	**Dilution**
Goat anti-nNOS	Ab1376	Abcam	1:1000
Rabbit anti-TH	Ab152	Millipore	1:500
Chicken anti-GFP	Ab13970	Abcam	1:1000
Mouse anti-βIIITubulin	G712A	Promega	1:1000
Rabbit anti-CGRP	C8198	Sigma Aldrich	1:4000
Rabbit anti-nNOS	NP2141	ECM	1:300
Rabbit anti-nNOS	AB5380	Millipore	1:4000
Mouse anti-HCN2	N71/37	Neuromab	1:500

Table 13 Secondary antibodies (all used at 1:1000 dilution)

Antibody	**Reference**	**Source**	**Conjugate**
F(ab')2-Goat anti-Rabbit IgG (H+L)	A11069	Life Technologies	Alexa Fluor® 350
Goat anti-Chicken IgY (H+L)	A11039	Life Technologies	Alexa Fluor® 488
Donkey anti-Goat IgG (H+L)	A11058	Invitrogen	Alexa Fluor® 594
Chicken anti-Rabbit IgG (H+L)	A21441	Invitrogen	Alexa Fluor® 488
Donkey anti-Rabbit IgG (H+L)	A21207	Invitrogen	Alexa Fluor® 594
Goat anti-Mouse IgG (H+L)	A21049	Invitrogen	Alexa Fluor® 350
Goat anti-Mouse IgG2a	A21131	Life Technologies	Alexa Fluor® 488
Donkey anti-Mouse IgG (H+L)	A21202	Life Technologies	Alexa Fluor® 488
F(ab')2-Goat anti-Mouse IgG (H+L)	A11020	Life Technologies	Alexa Fluor® 594

5.3 Results and Discussion

5.3.1 Sympathetic Neurons Express Neuronal Nitric Oxide Synthase

It is well established that noradrenergic sympathetic neurons release noradrenaline to cause blood vessel **constriction** *via* an action on α2 receptors (Grayson, 1950), but whether these neurons might contribute to **vasodilation** remains unclear.

Somatosensory neurons, that have their cell bodies in the DRG, can cause vasodilation by secreting calcitonin gene-related peptide (CGRP) in inflammatory states (Brain *et al.*, 1985). To determine whether sympathetic neurons might use the same mechanism, we stained for the presence of CGRP in sympathetic neurons. Figure 55 shows that while DRG neurons widely express CGRP, sympathetic neurons of the stellate ganglion (SG) do not seem to express CGRP. This makes it unlikely that sympathetic neurons use CGRP to cause vasodilation.

A recent RNA sequencing study of the mouse SG and thoracic ganglia found that CGRP is expressed in only 1% of sympathetic ganglion neurons, consistent with the data presented here (Furlan *et al.*, 2016).

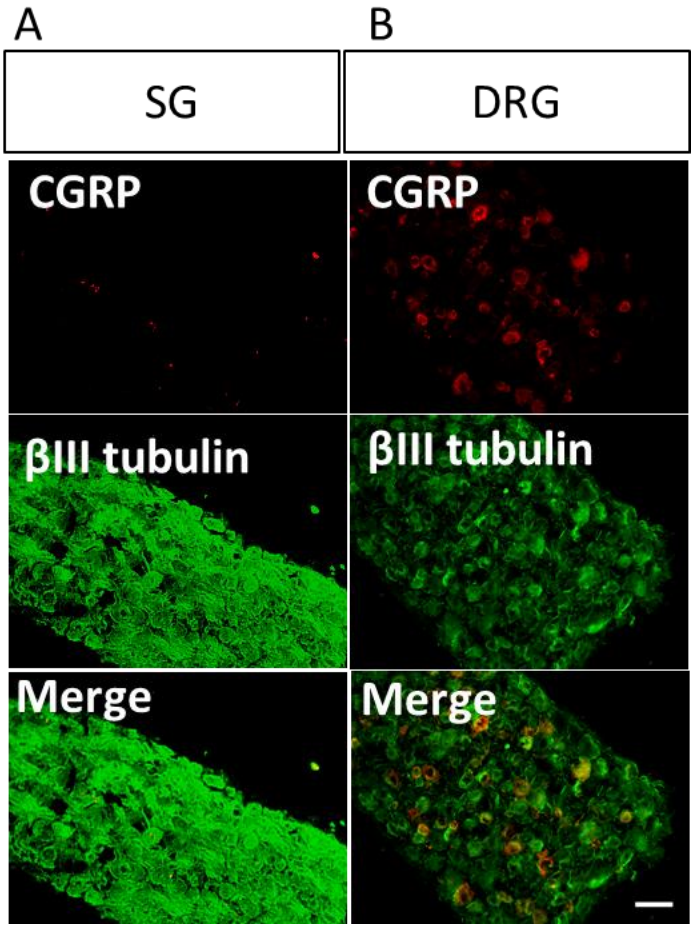

Figure 55 Stellate ganglion (SG) neurons do not express CGRP.
A) Representative immunofluorescence images showing adult mouse SG sections stained for CGRP (red), and βIIItubulin (green). CGRP is not clearly expressed. Rabbit anti-CGRP antibody (1:4000) was used in combination with donkey anti-rabbit Alexa Fluor 594 (1:1000). n=3. B) DRG sections are from the same animal and function as a positive control. CGRP is widely expressed in the DRG. Rabbit anti-CGRP antibody was used in combination with donkey anti-rabbit Alexa Fluor 594 (1:1000); mouse anti-βIII Tubulin (1:1000) was used in combination with goat anti-mouse 488 (1:1000). n=2. Scale bar = 50 μm.

When the skin is not inflamed, a dominant cause of vasodilation is the release of nitric oxide from endothelial cells lining the vascular walls (Quillon 2013). We hypothesised that sympathetic neurons might contribute to vasodilation by releasing additional nitric oxide onto blood vessels. Therefore, we stained the SG with an antibody against neuronal nitric oxide synthase (nNOS), the enzyme that neurons use to synthesize nitric oxide.

A dilution series to determine the optimal concentration of this antibody was performed (Figure 56). DRG are known to contain nNOS in a subset of neurons, and thus function as a positive control. From these results, the dilution factor 1:1000 was chosen for the nNOS antibody because it gives the best signal for the lowest background and was used in all further experiments in this chapter. Unlike CGRP, nNOS is clearly expressed in

preganglionic fibres as well as in neuronal cell bodies of the SCG and SG, but not in glia (Figure 57).

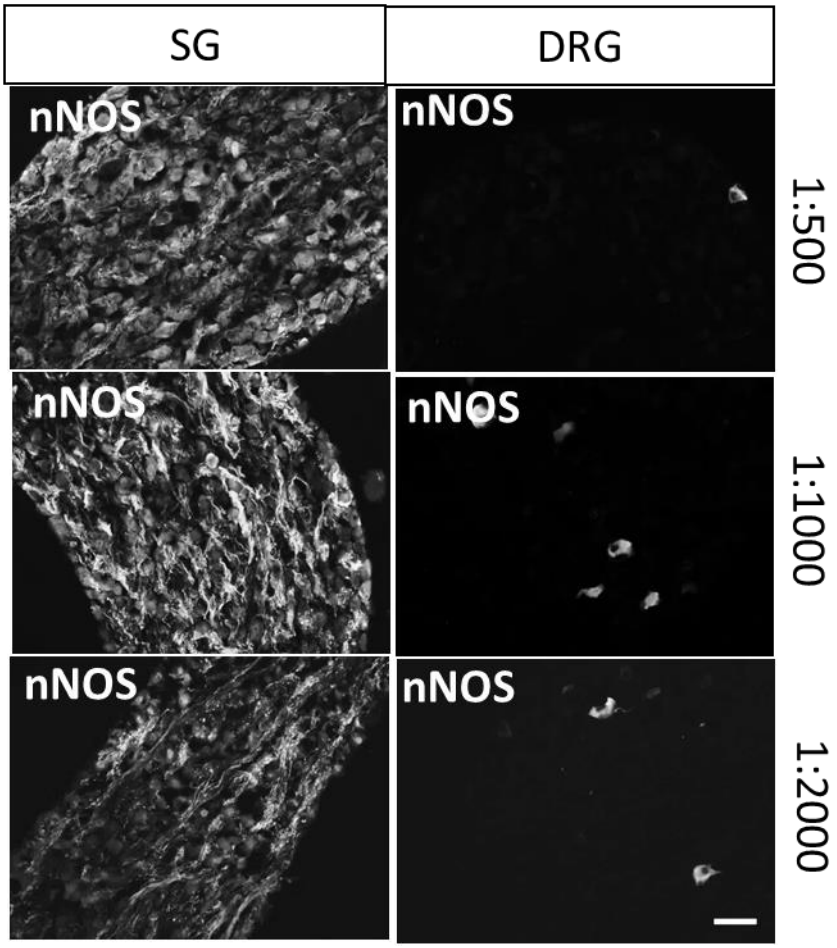

Figure 56 Anti-nNOS antibody dilution series to determine the optimal concentration of antibody.
Representative immunofluorescence images showing adult mouse SG (left) and DRG (right) sections that were stained for nNOS with antibody dilution factor 1:500 (top), 1:1000 (middle), and 1:2000 (bottom). The 1:1000 dilution was used in all further experiments in this chapter. The 1:500 image appears somewhat less bright because fewer preganglionic fibres are present. Goat anti-nNOS antibody was used in combination with donkey anti-goat Alexa Fluor 594 (1:1000); DRG sections are from the same animal and function as a positive control. nNOS is expressed in a subset of DRG neurons. n=1. Scale bar = 50 μm.

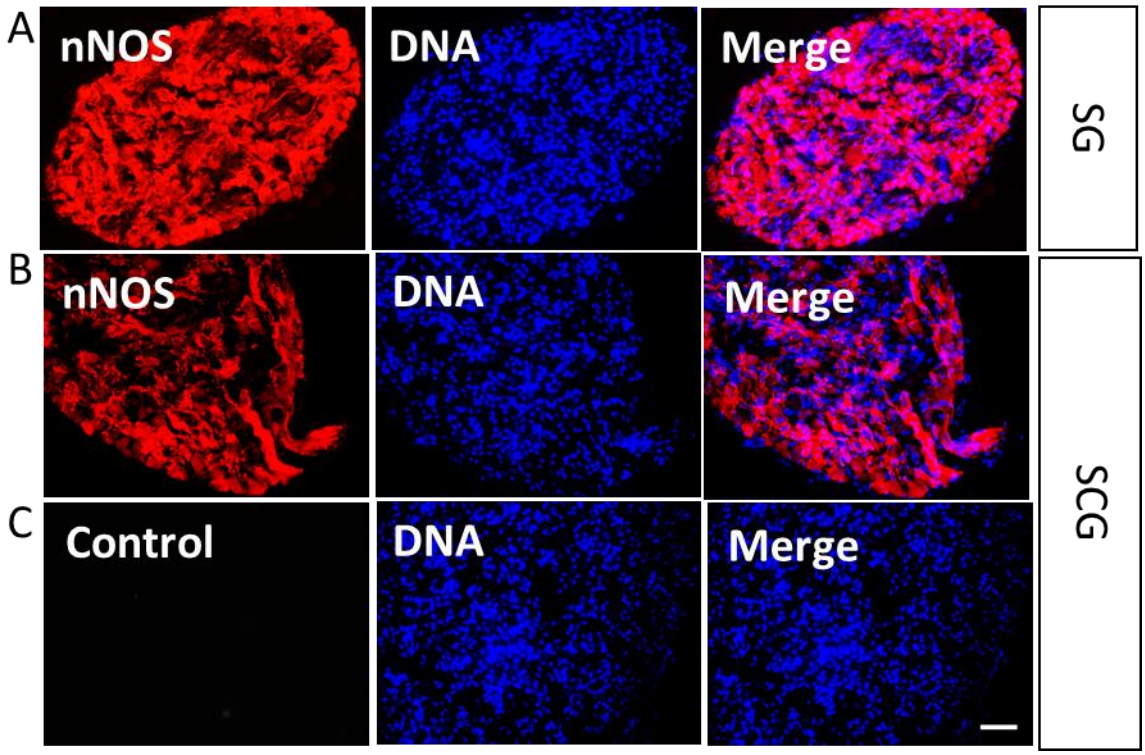

Figure 57 Sympathetic neurons express nNOS in cell bodies and neurites.
Representative immunofluorescence images showing adult mouse SG (A) and SCG (B-C) sections that were stained for nNOS (red) to label nitrergic neurons and DNA (blue) to label cell nuclei. nNOS is expressed in neuronal cell bodies and highly expressed in neurites. Goat anti-nNOS antibody (1:1000) was used in combination with donkey anti-goat Alexa Fluor 594 (1:1000). Nuclei of both neurons and glia are shown by DAPI staining (blue, 1:50000). C) Negative control images of SCG section from the same animal but incubated without primary antibody. n= 4. Scale bar = 50 µm.

To determine the proportion of neurons that express nNOS, we stained for nNOS together with the general neuronal marker βIII Tubulin (Figure 58). Unfortunately, the nNOS antibody we used (manufactured by Abcam) also stained neuronal nuclei. This is likely to be non-specific staining, as nNOS is not normally present in nuclei (Korzhevskii *et al.*, 2007). It seems like nNOS is present in all neurons, but the nuclear staining makes exact quantification impossible. Dissociated sympathetic neurons in culture show the same pattern of staining (Figure 59).

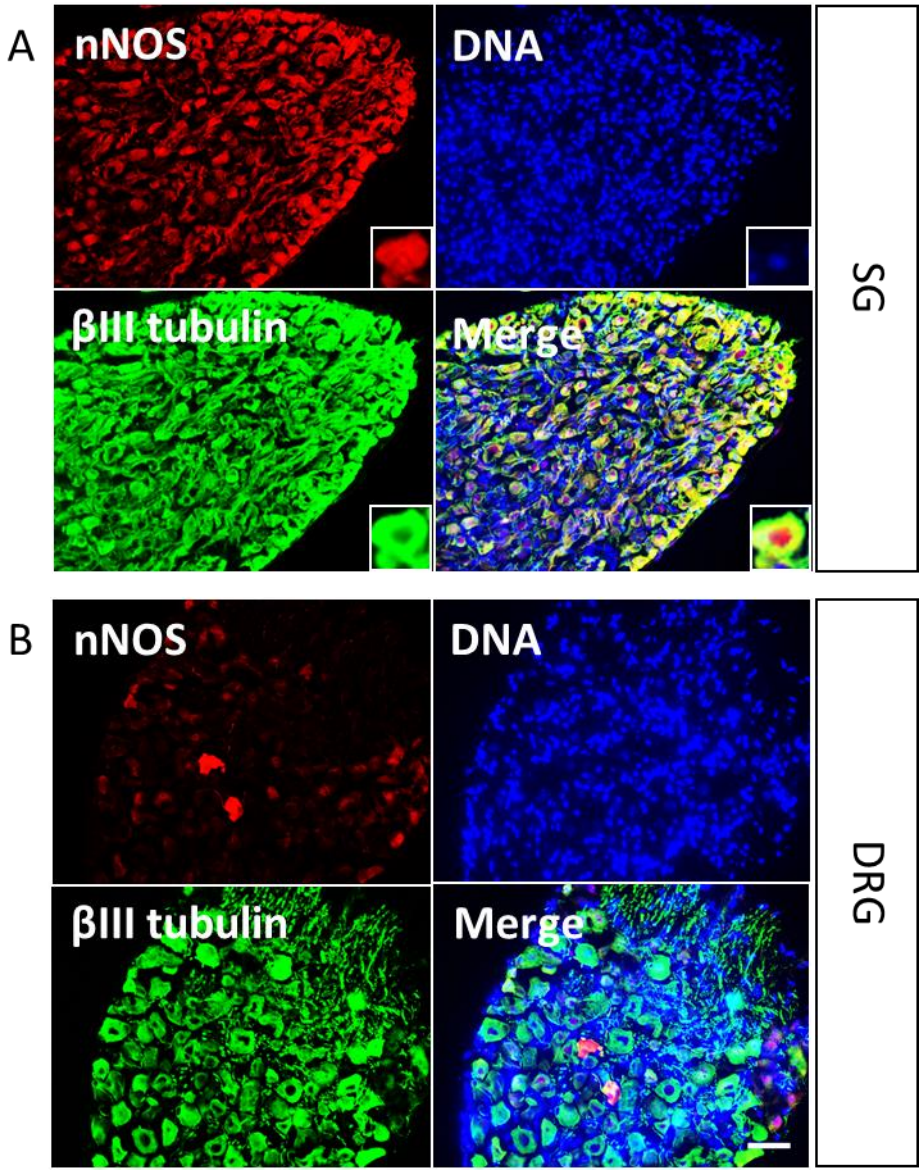

Figure 58 nNOS is widely expressed in sympathetic neurons.
Representative immunofluorescence images showing adult mouse SG (A) and DRG (B) sections that were stained for nNOS (red), and βIII Tubulin (green) to label nitrergic neurons and all neurons respectively. nNOS is widely expressed in neurons of the stellate ganglion, but absent from most glial cells. 3-fold enlarged inserts: nNOS antibody (Abcam) stains nuclei. Goat anti-nNOS antibody (1:1000) was used in combination with donkey anti-goat Alexa Fluor 594 (1:1000); mouse anti-βIII Tubulin (1:1000) was used in combination with goat anti-mouse Alexa Fluor 488 antibody (1:1000). Nuclei of both neurons and glia are shown by DAPI staining (blue, 1:50000). DRG sections are from the same animal and function as a positive control. n=5. Scale bar = 50 μm.

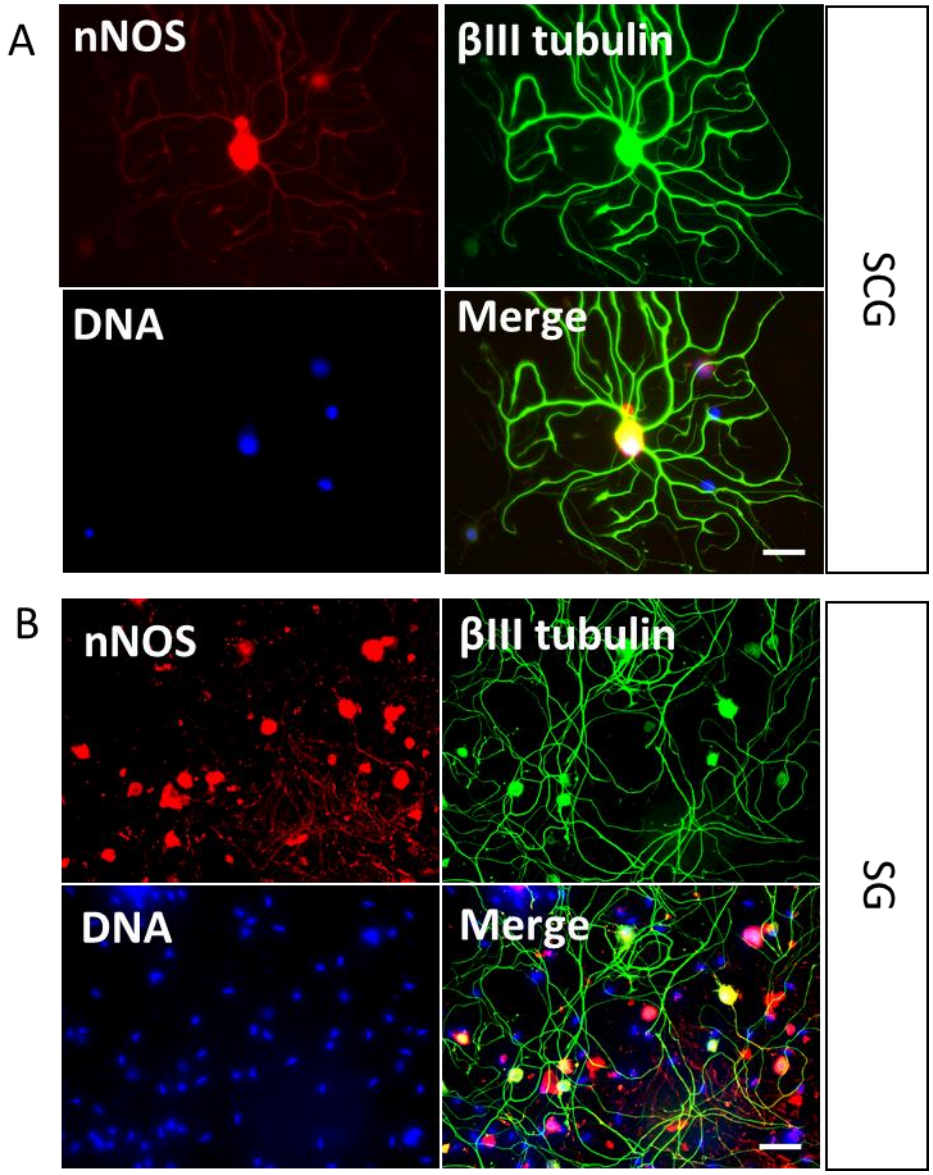

Figure 59 Cultured sympathetic ganglion neurons show the same expression of nNOS as seen in tissue sections. Representative immunofluorescence images showing cultured SCG (A) and SG (B) neurons from adult mice stained with nNOS (red), and βIII Tubulin (green) to label nitrergic neurons and all neurons respectively. nNOS is widely expressed in neurons of the SCG and SG, but absent from most glial cells. Non-specific nuclear stain of the nNOS antibody is visible. Goat anti-nNOS antibody (1:500) was used in combination with donkey anti-goat Alexa Fluor 594 (1:1000); mouse anti-βIII Tubulin (1:500) was used in combination with goat anti-mouse Alexa Fluor 488 antibody (1:1000). Nuclei of both neurons and glia are shown by DAPI staining (blue, 1:50000). n=2. Scale bar = 50 μm.

To determine whether the nNOS stain of cell bodies and fibres was also non-specific, we performed the same staining with nNOS antibodies from two other manufacturers: Millipore and ECM. These antibody samples were a gift from Mr. Carl Hobbs. All three antibodies demonstrate a similar widespread stain for nNOS, showing expression in all noradrenergic and cholinergic SCG neurons, though the nuclear stain is much more obvious with the Abcam antibody (Figure 60). Interestingly, the Abcam antibody does not show a nuclear stain in DRG. This suggests that the nuclear staining is likely to be an artifact, because it is highly antibody and tissue-dependent. The result that all three antibodies show a widespread expression of nNOS shows that sympathetic neurons could indeed release NO into the blood vessels they innervate.

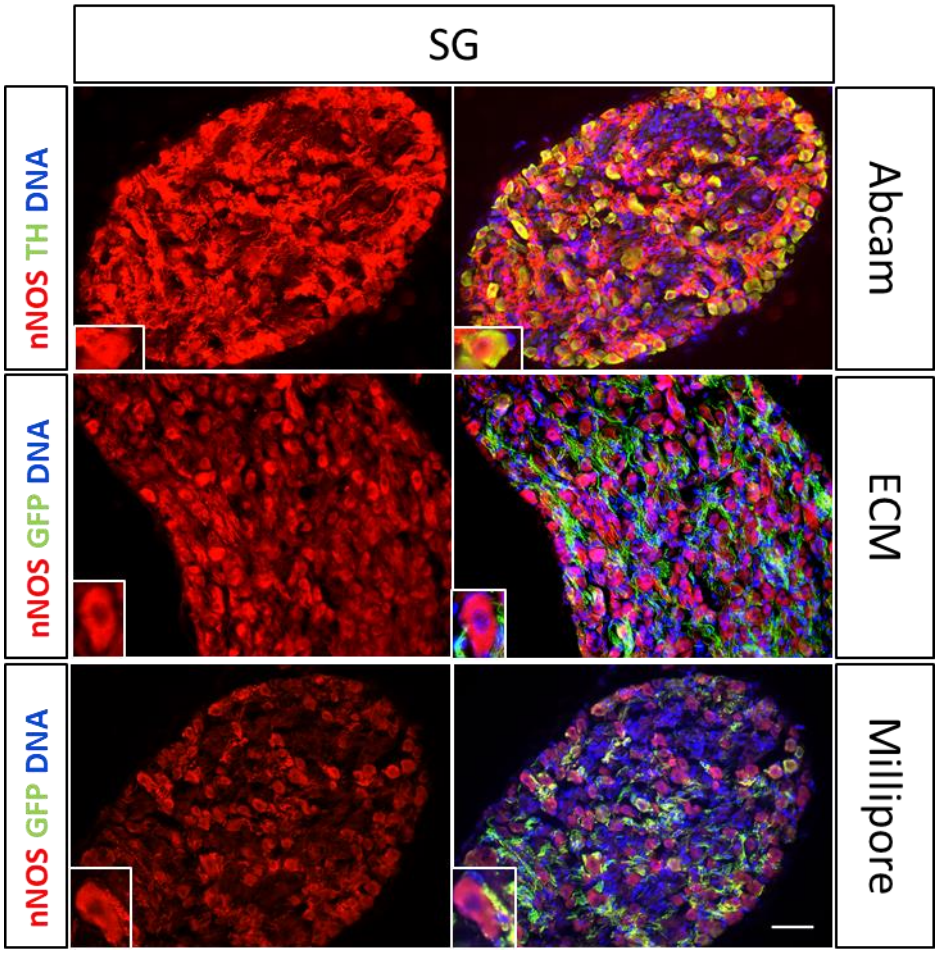

Figure 60 Three antibodies demonstrate similar widespread nNOS immunoreactivity, but the nNOS antibody manufactured by Abcam shows off-target nuclear staining in stellate ganglion neurons.
Representative immunofluorescence images showing adult mouse SG sections that were stained for nNOS with three different antibodies manufactured by Abcam (top), ECM (middle), and Millipore (bottom). nNOS looks widely expressed in SG cell bodies and neurites with all three antibodies, but only the Abcam antibody stains neuronal nuclei. A 3x magnified neuron is shown as an example in the bottom left corner of the images. Abcam goat anti-nNOS antibody (1:1000) was used in combination with donkey anti-goat Alexa Fluor 594 (1:1000). ECM rabbit anti-nNOS antibody (1:300) was used in combination with Alexa Fluor 594 antibody (1:1000). Milipore rabbit anti-nNOS antibody (1:4000) was used in combination with donkey anti-rabbit Alexa Fluor 594 antibody (1:1000). n=1. Scale bar = 50 µm.

The expression of nNOS in postganglionic sympathetic neurons has been controversial. Early studies in rat have found only low expression of NOS in SCG (Dun *et al.*, 1993), or that NOS is only expressed in preganglionic fibres entering the ganglion (Ceccatelli *et al.*, 1994). Others have found that it is only expressed in non-catecholaminergic postganglionic neurons in guinea pig (Fischer, Mayer and Kummer, 1996). A study in dogs found considerable expression of nNOS (Tadaki *et al.*, 1996).

Our finding that nNOS is widely expressed in sympathetic ganglia of the mouse directly contradicts another more recent paper that was published on this topic (Masliukov et al. 2014). This paper reports no expression of nNOS in the SG of mice at any stage of development. Unfortunately, they did not show any data to support their conclusions as the paper in question only states "data not shown". Masliukov et al. used the same antibody for nNOS (Abcam) and looked in the same tissue. The only difference between our immunohistochemistry protocol and the one used by Masliukov et al. was the length of tissue fixation, as they fixed the tissue for two hours in 4% PFA versus ten minutes in our study.

To determine whether this difference explains the different results, we compared nNOS staining on tissue sections that were fixed for two hours to sections that were fixed for ten minutes in 4% PFA as before. Figure 61 shows that prolonged formalin fixation, as used in the Masliukov et al. protocol, has an adverse effect on nNOS antibody staining and both cell body and fibre staining are no longer clearly distinguishable from background. This may explain why they reported nNOS to be absent from mouse sympathetic ganglia.

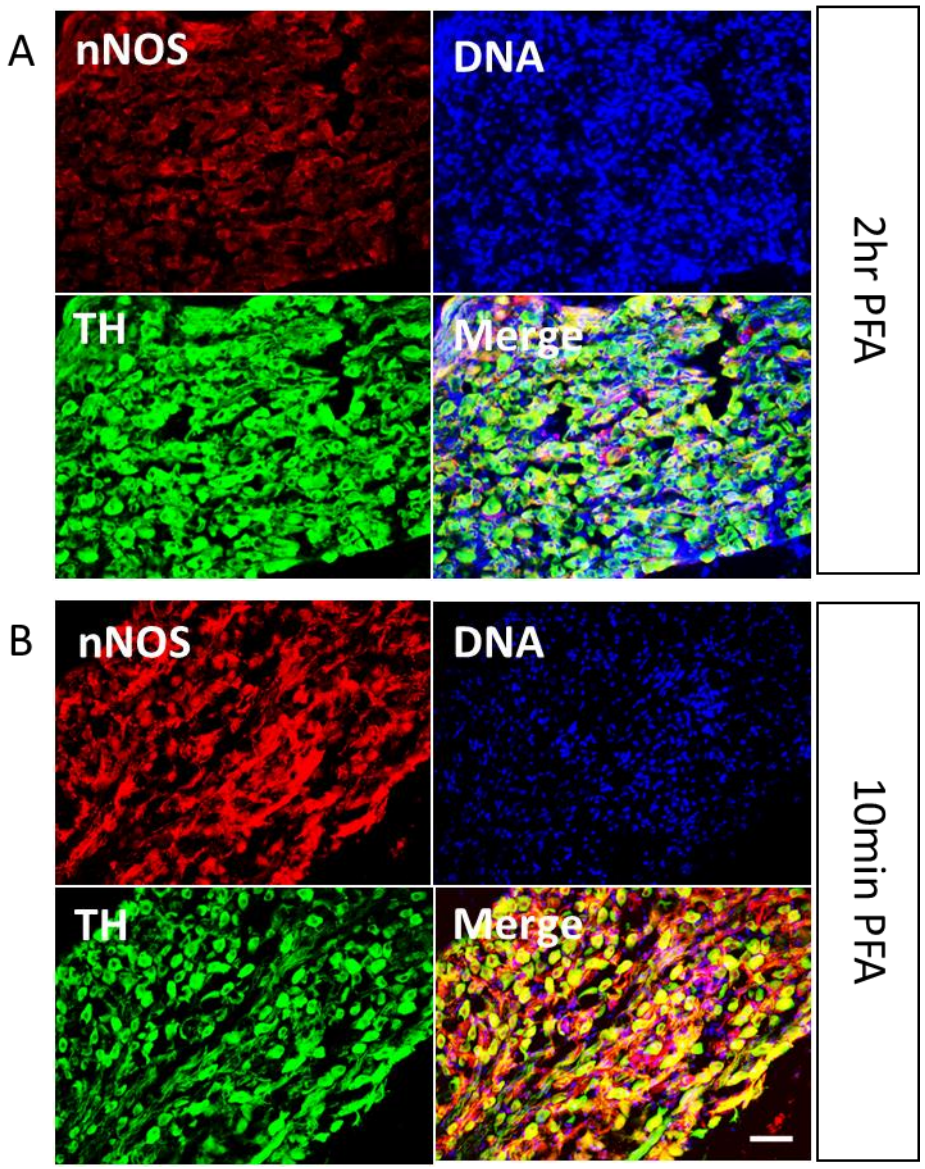

Figure 61 Prolonged formalin fixation has an adverse effect on nNOS antibody staining.
Representative immunofluorescence images showing adult mouse SG sections that were stained for nNOS (red) and TH (green) to label nitrergic and noradrenergic neurons respectively. The section shown in A was fixed in PFA for two hours and the section shown in B was fixed in PFA for 10 minutes according to the standard immunohistochemistry protocol as described in methods. Abcam anti-nNOS antibody staining is greatly affected by fixation time; cell body and neurite staining is no longer clearly visible. Goat anti-nNOS antibody (1:1000) was used in combination with donkey anti-goat Alexa Fluor 594 (1:1000); rabbit anti-TH antibody (1:500) was used in combination with chicken anti-rabbit Alexa Fluor 488 antibody (1:1000). Nuclei of both neurons and glia are shown by DAPI staining (blue, 1:50000). n=1. Scale bar = 50 μm.

Next, we asked whether nNOS is expressed in noradrenergic and/or cholinergic neurons by staining for nNOS in combination with tyrosine hydroxylase (TH), an enzyme in the pathway to noradrenaline synthesis. As shown in Chapter 2 (Figure 17), the images generated using an antibody for the NA-synthesising enzyme dopamine-β-hydoxylase, which is later in the NA synthesis pathway, were of greatly inferior quality to those using the antibody for TH. Therefore, we stained for TH to label noradrenergic neurons.

Most sympathetic ganglion neurons are noradrenergic and considering the large proportion of cells we found to express nNOS, it is perhaps not surprising that we found TH and nNOS to be co-expressed (Figure 62). It was not possible to avoid using the somewhat non-specific Abcam nNOS antibody for this experiment, because of a limitation in the diversity of secondary antibodies available in the lab at the time.

We also found that nNOS is co-expressed in all cholinergic neurons in the SG using the Milipore nNOS antibody (Figure 63). As cholinergic neurons innervate sweat glands, this is consistent with the literature which suggests that NO can enhance sweating (Lee and Mack, 2006). The SG was used to stain for cholinergic neurons, because there are no cholinergic neurons present in SCG (see Figure 14).

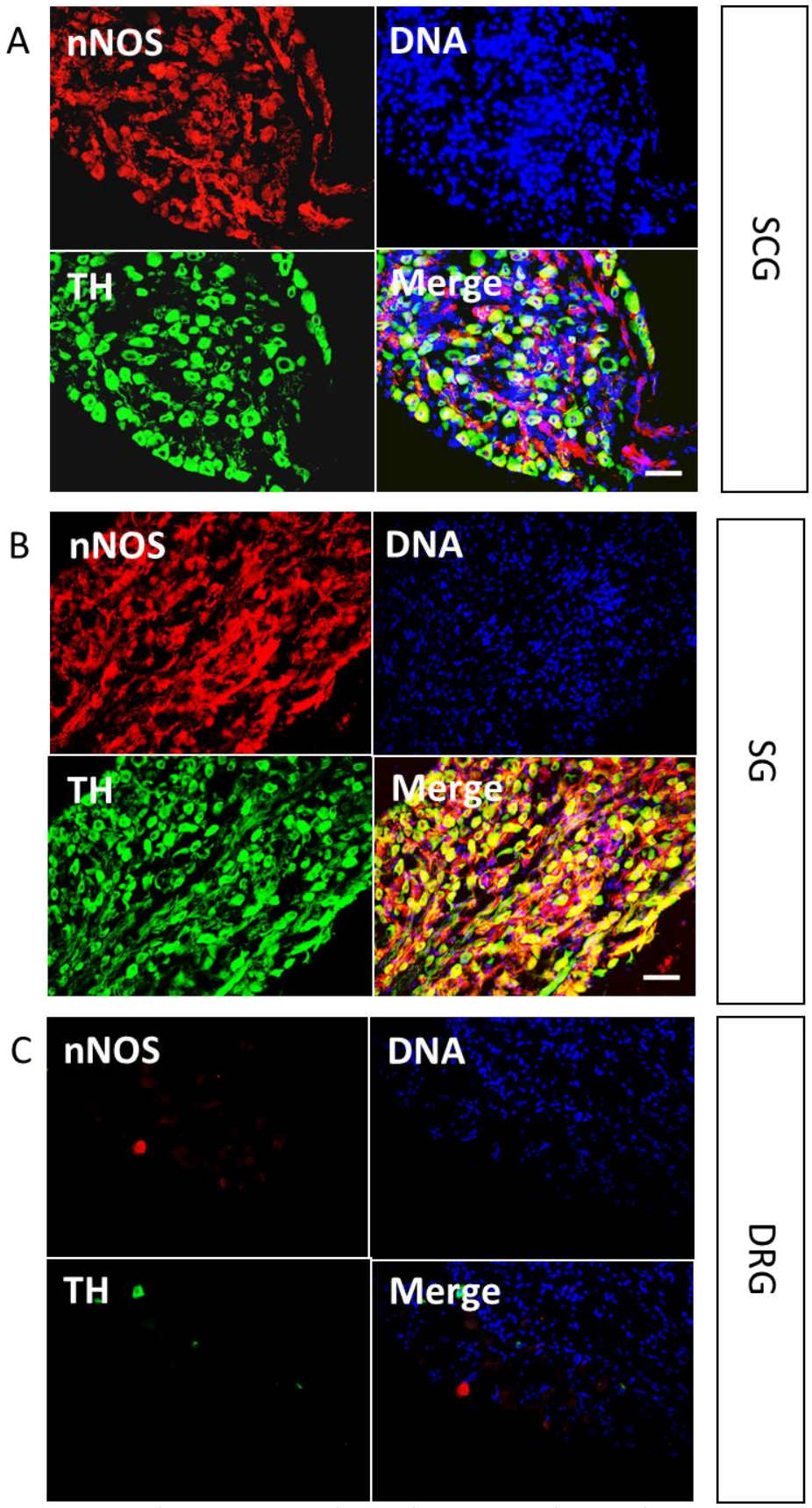

Figure 62 nNOS and TH are coexpressed in noradrenergic sympathetic ganglion neurons.
Representative immunofluorescence images showing adult mouse SCG n=2 (A), SG n=1 (B) and DRG n=2 (C) sections that were stained for nNOS (red) and TH (green) to label nitrergic and noradrenergic neurons respectively. Many noradrenergic cells also express nNOS. Goat anti-nNOS antibody (1:1000) was used in combination with donkey anti-goat Alexa Fluor 594 (1:1000); rabbit anti-TH antibody (1:500) was used in combination with chicken anti-rabbit Alexa Fluor 488 antibody (1:1000). Nuclei of both neurons and glia are shown by DAPI staining (blue, 1:50000). DRG sections are from the same animal and function as a positive control. Scale bar = 50 μm.

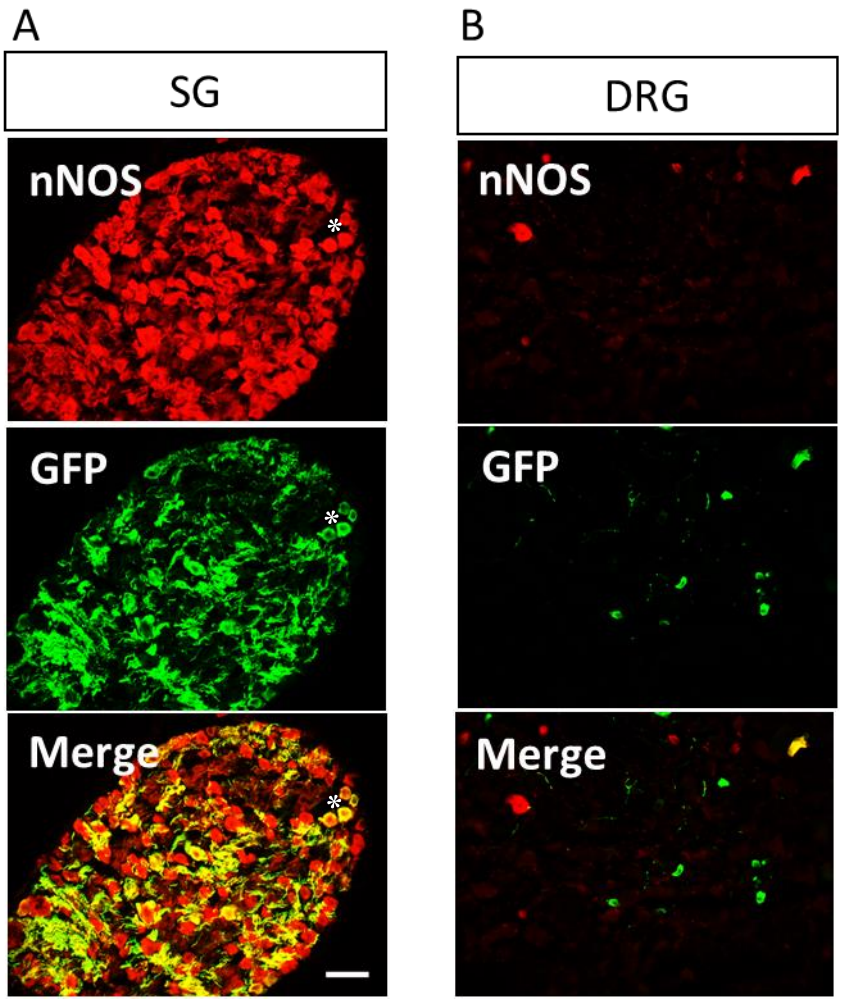

Figure 63 nNOS and ChAT are coexpressed in neurons.
Representative immunofluorescence images showing adult ChAT-GFP mouse SG n=2 (A) and DRG n=1 (B) sections that were stained for nNOS (red) and GFP (green) to label nitrergic and cholinergic neurons respectively. Cholinergic cells also express nNOS. For example, the asterisk is surrounded by four neurons expressing both nNOS and GFP(ChAT). Rabbit anti-nNOS antibody (1:4000, Millipore) was used in combination with donkey anti-rabbit Alexa Fluor 594 (1:1000); chicken anti-GFP antibody (1:1000) was used in combination with goat anti-chicken Alexa Fluor 488 antibody (1:1000). DRG sections are from the same animal and function as a positive control. Scale bar = 50 μm.

Next, we stained for Hyperpolarisation-activated Cyclic Nucleotide-gated Channel 2 (HCN2). This ion channel is a downstream target of nitric oxide via cyclic guanosine monophosphate (cGMP) (Kopp-Scheinpflug, Pigott and Forsythe, 2015) and thus may be part of a negative feedback mechanism in these cells. Figure 64 shows that HCN2 is expressed in a subset of neurons in the SG. It is expressed in both cholinergic and noradrenergic neurons.

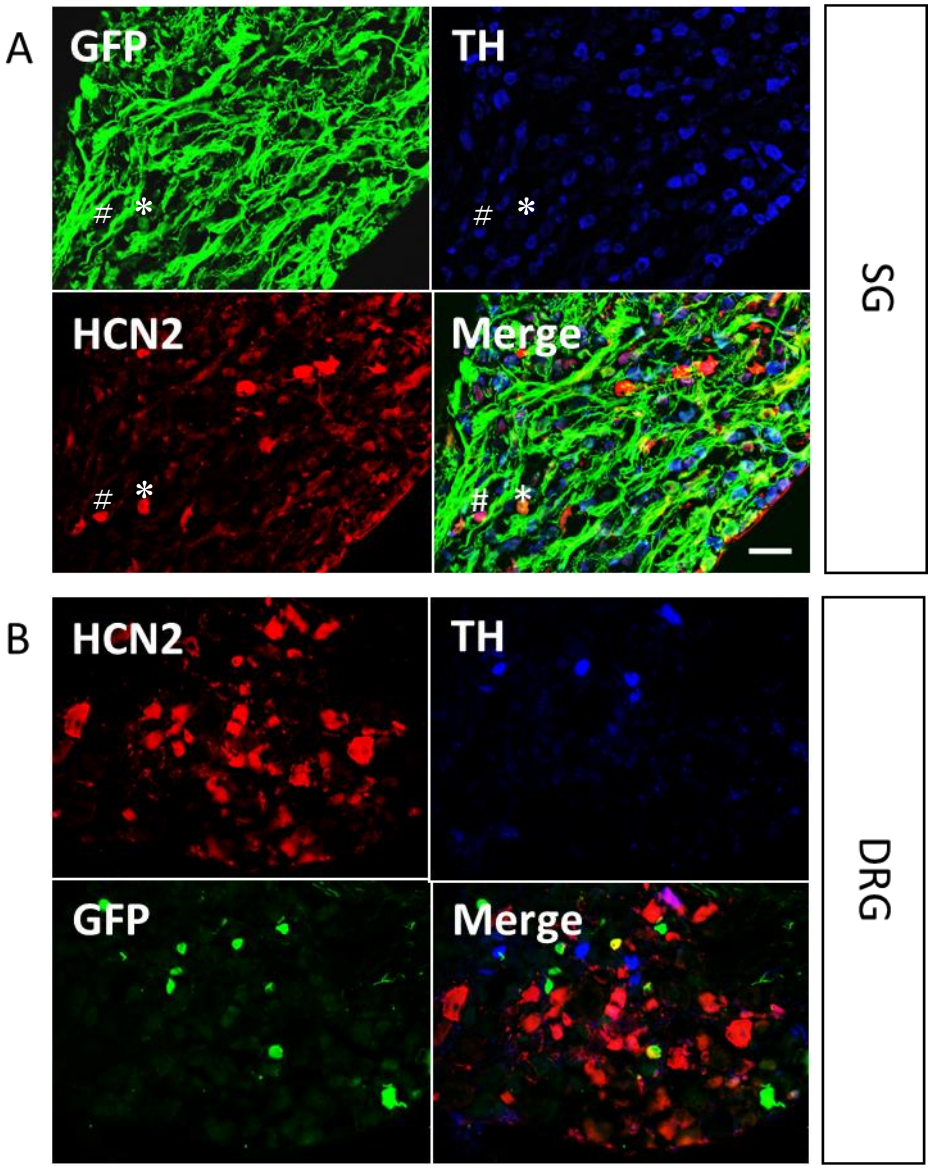

Figure 64 HCN2 is coexpressed with both TH and ChAT in sympathetic neurons.
Fluorescence images showing adult ChAT-GFP mouse SG (A) and DRG (B) sections that were stained for HCN2 (red) and GFP (green) and TH (blue). HCN2 is coexpressed with both ChAT (*) and TH (#) in the SG. Mouse anti-HCN2 antibody (1:500) was used in combination with goat anti-mouse Alexa Fluor 594 (1:1000); chicken anti-GFP antibody (1:1000) was used in combination with goat anti-chicken Alexa Fluor 488 antibody (1:1000); rabbit anti-TH antibody (1:500) was used in combination with goat anti-rabbit Alexa Fluor 350 (1:1000). DRG sections are from the same animal and function as a positive control. n=1. Scale bar = 50 μm.

5.4 Conclusion

The aim of this chapter was to determine if vasodilatory substances (i.e. CGRP and NO) can be produced by sympathetic nerves. This could provide a clue as to the plausibility of our hypothesis, which states that the function of cold transduction mechanisms in sympathetic neurons is to trigger CIVD. Results show that CGRP is widely expressed in DRG neurons but not in SG neurons. A chemiluminescent enzyme immunoassay could be used to determine whether CGRP is released from DRG neurons in response to noxious cold.

The main finding of this chapter is that nNOS is widely expressed in SCG and SG neurons, where it is co-expressed in both noradrenergic and cholinergic neurons. Therefore, cold could potentially trigger vasodilation in the following sequence of events: STIM1 detects cold and opens Orai1 channels → Ca^{2+} enters the cell; binds calmodulin and activates nNOS → nNOS produces NO which freely diffuses into the surrounding vascular smooth muscle tissue and dilates it to prevent frostbite. One way to assess whether sympathetic neurons produce NO in response to cold would be to set up a co-culture system with HEK293 cells that overexpress a fluorescent NO reporter.

Chapter 6 In Vivo Imaging of Sympathetic Neuron Activity Using a Genetically-Encoded Ca^{2+} Indicator

6.1 Introduction

As discussed previously, cultured Superior Cervical Ganglion (SCG) neurons of the sympathetic nervous system can detect temperature using TRPM2, K2P channels and STIM/Orai channels (Tan and McNaughton, 2016; Noël *et al.*, 2009; section 3.3.5). One limitation of the *in vitro* Ca^{2+} imaging system used in previous chapters is that it does not allow for specific temperature stimulation of exclusively the nerve ending. A microfluidics approach with separate chambers for the cell body and nerve ending could be used, but microfluidics chambers cannot accommodate high perfusion speeds.

So far, we have assumed that the temperature-sensitive mechanisms observed in the cell body of neurons in culture are also expressed in the nerve terminal, which is the only part of the neuron that could experience these temperature fluctuations *in vivo*. If the expression of temperature transduction mechanisms is restricted to the cell body, they would never experience the changes in temperature needed to activate these mechanisms under physiological conditions.

There is evidence that cold-transduction in sensory nerve endings in guinea pig trigeminal neurons is not detectable in the cell body (Cabanes, Viana and Belmonte, 2003). However, one recent study in rats has found that heat and cold transduction mechanisms (but not mechanosensory mechanisms) are expressed not just in nerve endings of DRG neurons, but all along the axon (Teliban *et al.*, 2011), so should be detectable in the soma. Another recent study found differential expression of acid sensing mechanisms in cellular compartments of mouse DRG neurons using a microfluidics chamber (Clark *et al.*, 2018). These studies show that the expression of some transduction molecules is restricted to specific cell compartments, while others are not.

Demonstration that the observed temperature transduction mechanisms are not restricted to the cell body will require a method that allows for local temperature stimulation of the sympathetic nerve terminal and signal measurement in the cell body. If we can detect in the cell body a response to local cooling and/or heating of the skin,

this shows that the temperature transduction mechanisms are expressed in the nerve ending.

The sympathetic nervous system is an efferent system and thought to have only motor functions (Buijs 2013), so expression of temperature transduction mechanisms in the nerve terminal may still not be detectable in the cell body if their activation does not result in antidromic action potential firing. The heat-sensitive mechanism of TRPM2 activation and the cold-sensitive mechanism of K2P channel inhibition both lead to changes in membrane potential and can therefore trigger action potentials. In theory, this could mean that information about temperature can be sensed by sympathetic nerve endings in the skin and transmitted to the cell body in an antidromic fashion.

Several studies have shown antidromic action potential firing in sympathetic nerves (Namer *et al.*, 2004; Illigens and Gibbons, 2009). A clinical test called the quantitative sudomotor axon reflex test (QSART) is based on these findings and commonly used to assess sympathetic nerve function in patients that suffer from neuropathy caused by various conditions such as type 2 diabetes and reflex sympathetic dystrophy (Illigens and Gibbons, 2009). This makes our hypothesis that temperature transduction mechanism in the nerve terminal can signal to the cell body not unlikely.

The aim of this chapter is to develop a method that can be used to determine whether heating and cooling of the skin leads to activation of temperature transduction mechanisms in sympathetic nerve terminals, and antidromic action potential firing that could be measured in the cell body. This would show that temperature transduction mechanisms are expressed in sympathetic nerve terminals and would suggest a localised sensory function of the sympathetic nervous system *in vivo*.

To achieve this aim, an *in vivo* optical imaging approach was developed using mice that express a genetically encoded fluorescent Ca^{2+} indicator (GCaMP6s) in central and peripheral neurons to visualise functional responses to peripheral stimulation. This approach had been used by others to image the DRG (Emery *et al.*, 2016; Chisholm *et al.*, 2018), but had not been attempted on the SCG. The DRG are relatively easy to expose and stabilise, since those ganglia are surrounded by bony structures. In contrast, the SCG is located in the neck and surrounded by soft tissue, such as the carotid artery and the trachea. Therefore, movement of the SCG caused by the pulse and respiration of the mouse posed a challenge even in anaesthetised mice. In this chapter, we developed this method that allows for stabilisation and imaging of the SCG.

6.2 Materials and Methods

6.2.1 Animals

1-6 month old female C57/BL6 mice heterozygous for Snap25-2A-GCaMP6s-D (Jackson Labs, Stock No: 025111) were used for all experiments (Madisen *et al.*, 2015). The Snap25-2A-GCaMP6s-D knockin allele has a viral 2A oligopeptide sequence (T2A) that mediates ribosomal skipping and a GCaMP6 slow variant Ca^{2+} indicator (GCaMP6s) inserted downstream of the synaptosomal-associated protein 25 (Snap25) coding region, which codes for a t-SNARE protein involved in vesicular exocytosis and is both exclusive to neurons and constitutively expressed in all neurons.

GCaMP6s is an ultrasensitive detector of single neuronal action potentials with slower decay and response kinetics than other GCaMP6 variants and results in EGFP fluorescence following Ca^{2+} binding e.g. upon neuronal activation (Chen *et al.*, 2013). Snap25-2A-GCaMP6s-D mice are expected to have pan-neuronal expression of GCaMP6s.

The ribosomal skipping sequence in the genetic insert should have allowed for both SNAP25 and GCaMP6s to be fully functional. Nonetheless, the homozygous expression of GCaMP6s resulted in embryonic lethality, which we confirmed by genotyping stillborn pups (data not shown). This lethality was probably due to a malfunction of vesicular exocytosis, which would be compensated for in the heterozygous mice by the second copy of SNAP25. All experiments were performed in accordance with the UK Home Office Animals (Scientific Procedures) Act (1986).

6.2.2 *In vivo* Imaging of Sympathetic Neuron Activity Using GCaMP6s Fluorescence

All experiments in this chapter were performed in collaboration with Dr. Kim Chisholm, who had previously developed a similar method for *in vivo* imaging of DRG using viral transfection of GCaMP (Chisholm *et al.*, 2018).

Urethane (12.5% w/v; 37.5mg/0.3mL IP) was used to anaesthetise the mouse. Depth of anaesthesia was determined using hind limb and corneal reflex activity. Repeated doses of 50% of the previous dose were given every 15-20 minutes until full anaesthesia

was achieved. The mouse was placed on a homeothermic heating mat with a rectal probe (FHC) and its body temperature was maintained at ~37˚C.

The scalp was removed, and the skull was securely glued onto a metal bar using dental cement (Lang Dental) diluted in instant glue. The metal bar was securely clamped in place by a clamp attached to the imaging stage (Figure 65). To place a tracheal catheter, the thorax was shaved, and the skin of the throat was lifted using forceps and cut open using scissors to expose the underlying tissue.

The salivary glands and muscular tissue around the trachea were separated using forceps, and a silk thread (USP size 5; VWR International) was placed around the trachea in a loose knot. Then, the trachea was cut and a 2cm piece of plastic tubing was placed partly inside and fixed in place by fastening the knot. This procedure allowed for spontaneous breathing throughout the recording. Mice were given a 0.5mL subcutaneous injection of sterile saline (0.9%) to ensure hydration for the duration of the experiment (method based on Chisholm et al. 2018).

To expose the SCG, the tracheal catheter was pulled 45˚ to the contralateral side using thread fixed to the stage with masking tape. The skin and digastric muscle were pulled to the ipsilateral side using the same method. Any remaining soft tissue covering the carotid artery was carefully separated using forceps. The SCG is attached dorsally to the bifurcation of the carotid artery (Figure 66), but the anatomy varies greatly between mice and the SCG is not always completely covered by the artery.

Cotton was dipped in saline and stuffed into the cavity underneath the carotid artery to lift the SCG. The SCG was then covered with silicone elastomer (WPI) to prevent tissue dehydration and a 3mm coverslip (thickness:#1; Biochrom) fixed inside a custom-made holder was immediately lowered onto the SCG and kept securely in place using a micromanipulator (Narishige) attached to a custom-made imaging stage (Thor labs) (Figure 65).

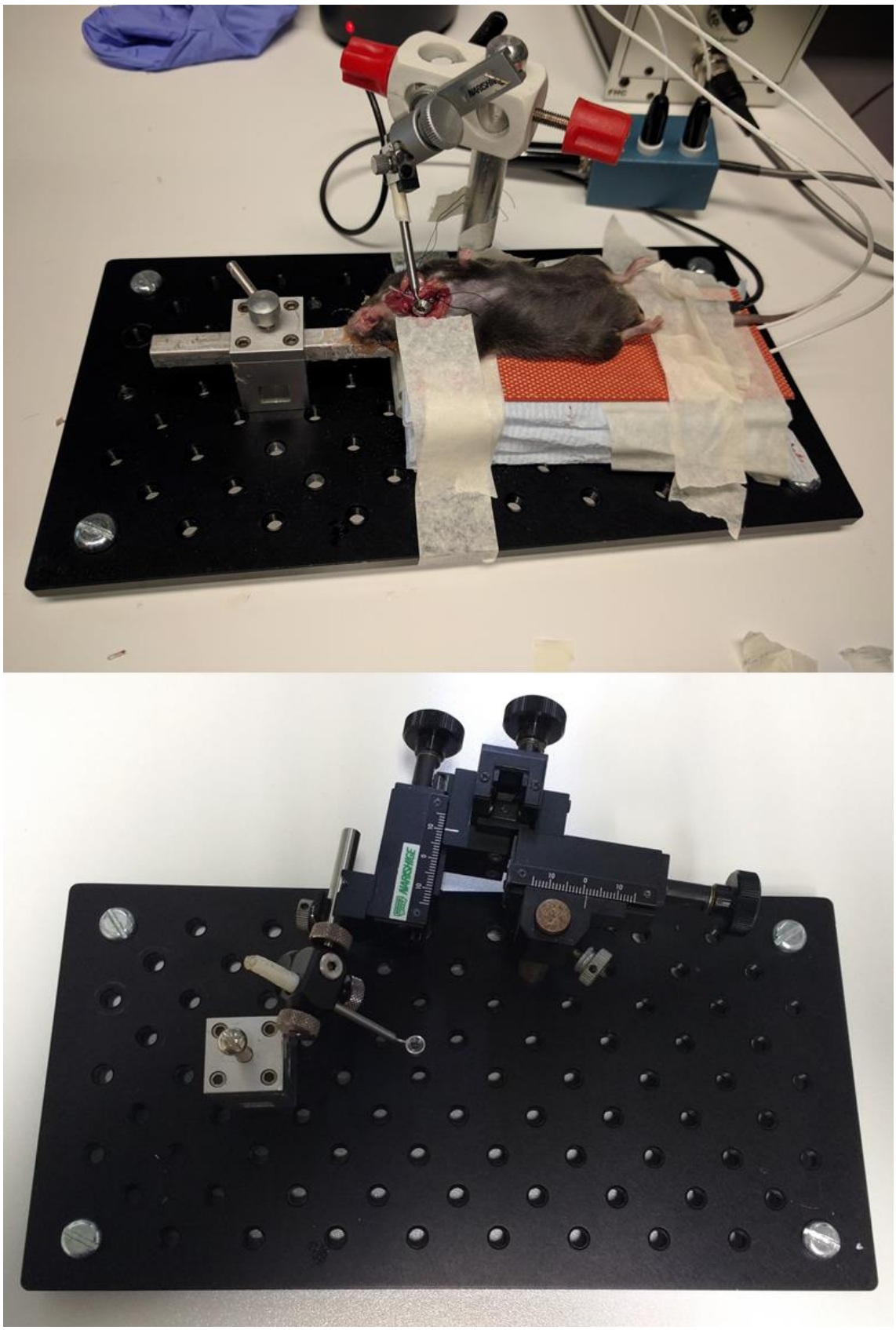

Figure 65 Stabilisation setup.
Top: Picture of the setup used to stabilise the mouse SCG. Bottom: A later iteration of the stage, which includes a micromanipulator.

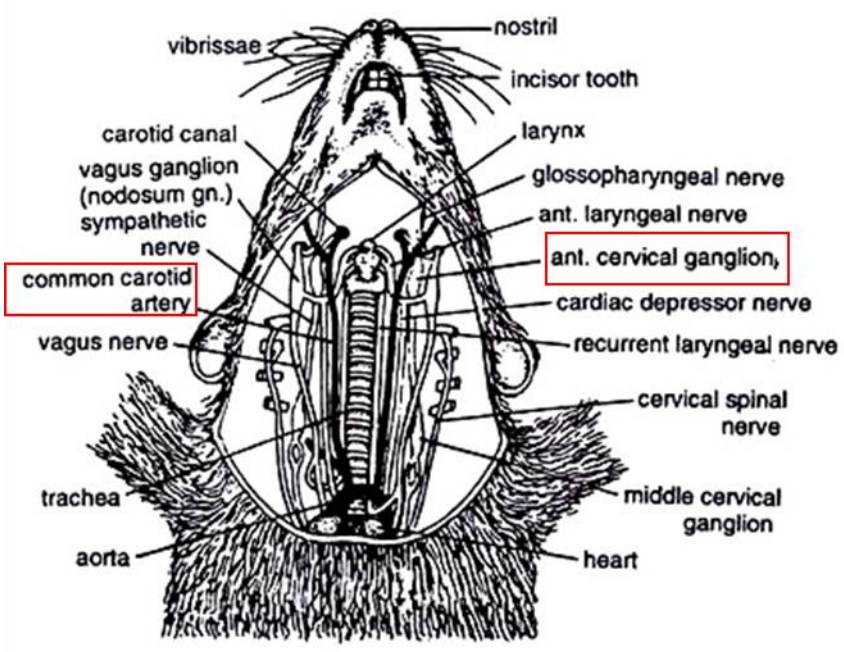

Figure 66 Dissection of the rat neck region.
Ventral view of exposed structures in the neck of a rat, which is similar in anatomy to the mouse. The common carotid artery and anterior cervical ganglion (SCG) are highlighted. The SCG is attached to the dorsal side of the common carotid artery, inferior to its bifurcation. Image adapted from www.biologydiscussion.com/zoology/dissection/dissection-of-rat-with-diagram-zoology/45221

After the SCG was exposed and the coverslip holder was put in place, the entire stabilisation setup was transferred to an Eclipse Ni-E FN upright confocal microscope (Nikon) with a 10x dry objective installed. The sample was excited using a 488nm Argon ion laser and GCaMP6s fluorescence was collected at 500-550nm. Images were acquired at 2 frames per second (a compromise between temporal resolution and file size) at one plane only with a spatial resolution of 512 x 512 pixels and a fully open pinhole to achieve maximum brightness to compensate for the relatively low expression of GCaMP6s in heterozygous mice.

To induce hyperthermia, the homeothermic heating mat was set to 40˚C. To induce hypothermia, the heating mat was set to 30˚C. IP administration of nicotine (15µg/0.3mL; Sigma), an agonist of all postganglionic sympathetic neurons, was used as a positive control (Figure 67). At the end of the experiment, death was induced by clamping the tracheal catheter.

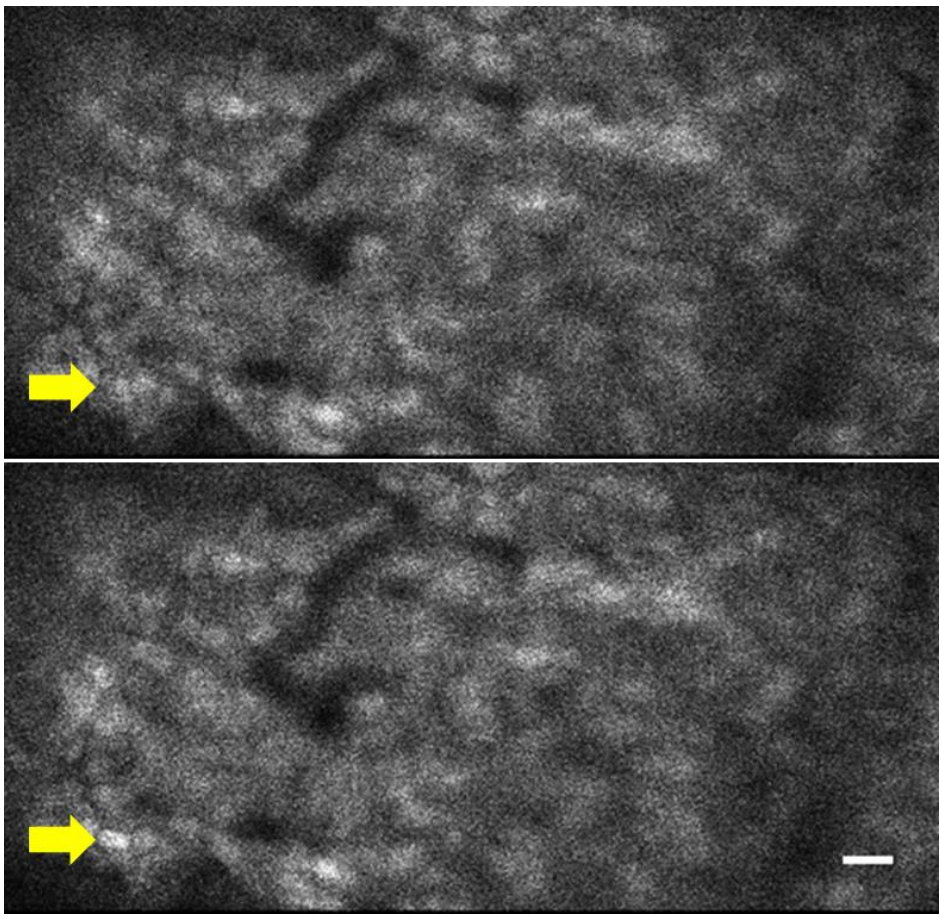

Figure 67 Activity of SCG can be visualised with GCaMP6.
Raw data images of GCaMP6 fluorescence in spontaneously active SCG neurons. Many SCG neurons are visible. The yellow arrows point to a neuron that has a low level of Ca^{2+} in the top image and a high level of Ca^{2+} in the bottom image. Scale bar = 20μm.

6.2.3 Optimisation

The method was optimised in several ways. During the first few attempts, the tracheal catheter filled up with fluid over time and mice died as a result. Therefore, the tracheal catheter was connected to an artificial ventilator (Harvard Apparatus model 587) connected to an oxygen machine (Vet-Tech Solutions). This was later deemed unnecessary when the muscarinic blocker atropine (1μg/0.3mL; IP; Sigma) was injected along with the anaesthetic, which prevented the fluid build-up (Buckley *et al.*, 1989).

Ethanol was applied to the mouse's abdomen to speed up body cooling during induction of hypothermia.

Initially, the SCG was physically separated from the carotid artery to allow for full exposure of the ganglion, but this resulted in the absence of spontaneous activity in the ganglion, possibly because either the blood supply or preganglionic fibres were disrupted.

We also attempted to pull the carotid artery to one side to expose the SCG, which occluded blood flow in the artery and resulted in death of the mouse.

In most experiments, mice died during baseline recording. This was probably because the coverslip holder compressed the carotid artery when it was placed on the SCG and reduced blood flow to the brain. At the time of writing, the method still requires further optimisation to improve the viability of the mice during experiments.

A further optimisation strategy that has not yet been attempted is to place a small metal cuff around the carotid artery, such that when the coverslip holder is pressed onto the SCG, the artery is pressed into the tissue, but not compressed, and blood flow is not inhibited. Another addition to the method would be the use of retrograde tracing (see Chapter 2). This would allow for the labelling of only those neurons that are innervating the skin and not innervating other tissues, such as the salivary glands.

6.2.4 Data Analysis

The alignment function of NIS Elements AR 4.30.01 software was used to correct for drift between images and the remaining image analysis was performed using FIJI (ImageJ) software. Files were down-sampled 8 times to improve signal to noise ratio, resulting in one data point every 4 seconds. This makes detection of single action potentials impossible.

A region of interest (ROI) was selected for each neuron and traces were generated from the average pixel intensity over time for each ROI. An average value of 5 areas of background was subtracted from each ROI. The fluorescence data was then normalised to a baseline taken immediately prior to each stimulus, calculated as ΔF/F.

$$\frac{\Delta F}{F} = \frac{F_t - F_0}{F_0}$$

$$F_t = fluorescence\ at\ time\ t$$

$$F_0 = fluorescence\ average\ over\ a\ baseline\ period$$

Vasoconstrictor neurons of the SCG are known to fire spontaneous bursts of activity (Bartsch, Häbler and Jänig, 1996), which is not affected by urethane anaesthesia in the rat (Häbler *et al.*, 1994). Therefore, SCG neurons that did not show any spontaneous Ca^{2+} spikes during the first baseline period were excluded from analysis.

6.3 Results and Discussion

To validate the method, a preliminary experiment was performed to confirm previously observed properties of SCG neurons. Preganglionic fibres synapsing onto the SCG are cholinergic in nature, and postganglionic SCG neurons contain nicotinic acetylcholine receptors (see general introduction section 1.1.1). Therefore, nicotine can be used as a positive control. Figure 68 A and B shows the effect of IP injection of 15μg/0.3mL nicotine on SCG neurons. The dotted line indicates the time of injection. As expected, normalised mean pixel intensity was increased by nicotine, verifying our methodology for interrogation of SCG neurons.

Next, the mouse was cooled down to a hypothermic state, which should activate vasoconstrictor neurons of the SCG (Bartsch, Häbler and Jänig, 1996). The orange line indicates the period during which the mouse was cooled. Figure 68 (C and D) show that hypothermia indeed increased activity of SCG neurons, in a somewhat delayed fashion. Possibly the vasoconstrictor neurons are not activated until a certain threshold temperature is reached. As expected, hyperthermia had the opposite effect (Figure 68 E and F).

At the end of the experiment, another injection of nicotine was given to determine whether the neurons were still responsive (Figure 68G and H). As expected, nicotine resulted in an increase in GCaMP6s fluorescence in most neurons. Taken together, these results show that GCaMP can be used to visualise SCG neuron activity *in vivo*.

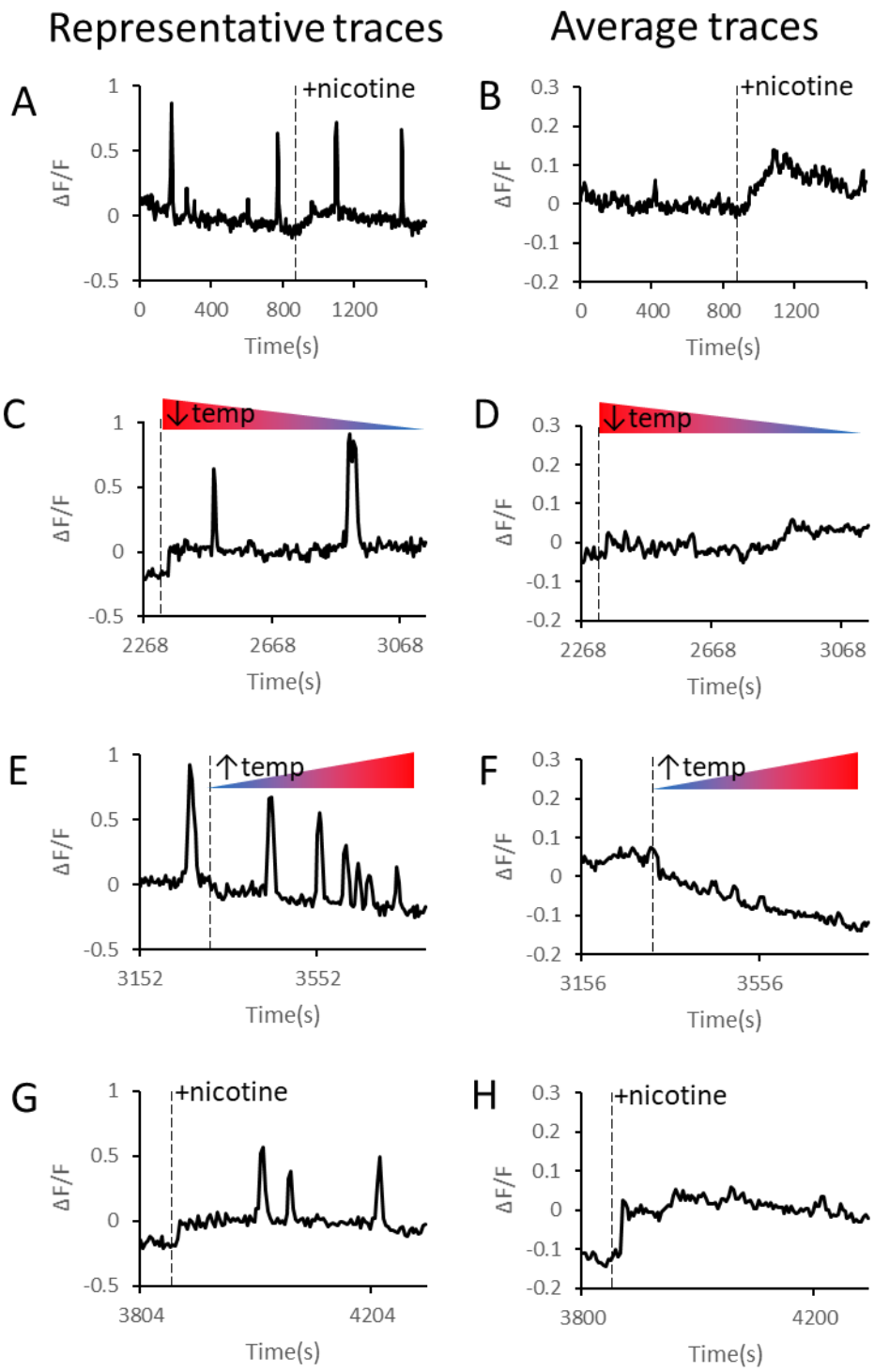

Figure 68 GCaMP-expressing SCG neurons can be visualised in vivo using confocal microscopy.
Representative (A) and average (B) traces showing the response of SCG neurons to IP injection of nicotine (dashed line indicates time of injection). Nicotine increases [Ca^{2+}]. Representative (C) and average (D) traces showing the response of SCG neurons to a decreasing body temperature of 36.2 to 30˚C (dashed line indicates start of cooling period). Hypothermia increases [Ca^{2+}]. Representative (E) and average (F) traces showing the response of SCG neurons to an increasing body temperature of 30 to 40˚C (dashed line indicates start of heating period). Heating decreases [Ca^{2+}]. Representative (G) and average (H) traces showing the response of SCG neurons to a second IP injection of nicotine (dashed line indicates time of injection). SCG neurons are still responsive to nicotine. All representative traces are from the same neuron. Average traces are from 34 neurons.

Figure 69 summarises the effects of the different stimuli on SCG neurons. The effect sizes are small (±0.1), because average pixel intensity is used as a measure. Spike frequency could not be used in its place, because not all spikes are uniform in size and shape.

The line graph on the right of Figure 69 shows the responses of each individual neuron per stimulus. Most neurons showed an increase in GCaMP6s fluorescence in response to acetylcholine receptor agonist nicotine as expected. In contrast, the responses to decreasing body temperature were varied, with some neurons showing a clear increase in GCaMP6s fluorescence and others responding with a decrease in fluorescence. Vasoconstrictor neurons that innervate blood vessels are expected to increase their activity in response to hypothermia. Therefore, it is likely that not all the neurons included in the analysis are vasoconstrictor neurons. Other targets of the SCG include the heart, lungs, and salivary glands. Possibly the neurons that respond to hypothermia with a decrease in activity innervate one of these other tissues.

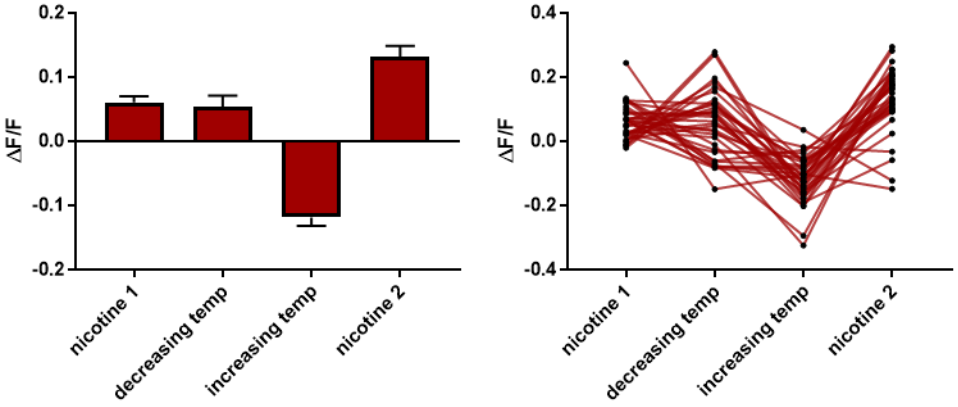

Figure 69 SCG neurons respond to body temperature changes.
Left: Bar graph summarising responses of 34 SCG neurons in the same ganglion to various stimuli. Average fluorescence pixel intensity values (ΔF/F) are normalised to a baseline directly before the start of the stimulus. Right: Line graph showing the response of each cell to each stimulus. While most SCG neurons responded to nicotine in a similar fashion, the responses to hypothermia varied greatly.

6.3.1 Conclusion

The sympathetic nervous system has been extensively studied in the last century using electrophysiological methods. These methods have increased our understanding but did not allow for the simultaneous monitoring of many individual neurons. This chapter has provided a proof-of-concept for a novel method that allows for high-yield data acquisition of the activity of SCG neurons *in vivo*.

The preliminary data presented here suggests that GCaMP6s can accurately measure increases in activity of individual sympathetic neurons in response to both pharmacological agents and physiological stimuli. These results reveal that *in vivo* imaging of the SCG is possible and could be a promising new method for studies of the sympathetic nervous system.

The aim of this chapter was to develop a method that can be used to determine whether cooling and heating of sympathetic nerve terminals leads to afferent action potential firing, which may reveal a sensory function of a part of the peripheral nervous system that has always been thought to be purely motor. Indeed, the method described here can be used to answer such questions in future.

Chapter 7 General Discussion

The aims of this thesis were to identify the molecular mechanism underlying CICE in sympathetic and sensory neurons, and to elucidate its function. More specifically, in Chapter 2 we aimed to correlate the thermal and neurotransmitter phenotype of sympathetic neurons with the use of calcium imaging and immunocytochemistry. Calcium imaging was also used in combination with pharmacology for our second aim to identify the mechanisms underlying cold transduction in the sensory and sympathetic nervous systems in Chapter 3. Several candidates were ruled out before discovering that STIM and Orai form a novel cold-transduction mechanism in peripheral neurons.

The aim of Chapter 4 was to determine which members of the SOCE family are involved through the different approaches of gene silencing and heterologous overexpression. Cold-sensitivity was induced in PC12 cells by overexpression of STIM1 and Orai1 in combination.

We explored in Chapter 5 whether sympathetic neurons could release vasodilators in response to cold using immunohistochemistry and found that nNOS is widely expressed in these neurons.

In Chapter 6 we provided a proof-of-concept for a novel *in vivo* Ca^{2+} imaging method that can be used to observe the activity of hundreds of sympathetic ganglion neurons simultaneously in the mouse.

7.1 Cold Transduction

Cold is sensed by specialised nerve endings in the periphery whose cell bodies reside in the dorsal root (DRG) or trigeminal ganglia. In these nerve endings, a combination of ion channels is responsible for transducing the sensation of cold. Of these ion channels, the cold-sensitivity of TRPM8 has been well established but the role of TRPA1 in cold-sensation remains controversial (see general introduction section 1.2.1.2). Furthermore, a third of the DRG neurons that respond to cold, and almost all cold-sensitive SCG neurons, lack both ion channels (Munns, AlQatari and Koltzenburg, 2007). Therefore, there must be another cold transduction mechanism present in these neurons.

One major aim of this thesis was to discover the molecular identity of this mechanism. We have addressed this question by using an *in vitro* single-cell Ca^{2+} imaging system coupled to a gravity-driven perfusion system that allowed for both temperature and

pharmacological stimulation of the neurons. First, SCG neurons were studied to identify the molecular basis of cold-induced Ca^{2+} influx in these cells. We report that the cold-induced Ca^{2+} influx is mediated by a combination of Orai channels and Ca_V channels in all cold-sensitive SCG neurons (section 3.3.1-3.3.5). Orai channels mediate the part of the Ca^{2+} influx we have named cold-induced Ca^{2+} entry (CICE), and the other part of the Ca^{2+} influx is probably mediated by inhibition of cold-sensitive K2P channels, which indirectly activate Ca_V channels *via* depolarisation of the plasma membrane (see section 3.1).

Orai channels are directly gated by STIM proteins and STIM1 has recently been shown to be temperature-sensitive (Bailong Xiao *et al.*, 2011), so the most likely explanation for CICE through Orai channels is that STIM1 senses cold and subsequently activates Orai channels in the plasma membrane. Another part of the cold-induced Ca^{2+} influx in SCG neurons is mediated by Ca_V channels (section 3.3.4), which are probably activated by a depolarisation resulting from inhibition of cold-sensitive K2P channels (Noël *et al.*, 2009).

Secondly, we found that Orai channels also mediate CICE present in a population of DRG neurons (section 3.3.6). Finally, the cold-sensitivity of STIM1/Orai1 was confirmed *via* overexpression of these proteins in a cell line (section 4.3.2).

7.2 How Can a Ubiquitous Protein Give Rise to a Specialised Function?

The discovery that Orai channels mediate CICE in sympathetic and sensory neurons was surprising, because STIM and Orai proteins are expressed ubiquitously (Uhlen *et al.*, 2015). How can a protein that is expressed in all tissue types be responsible for transducing cold - a property only present in a subset of neurons in the DRG and SCG? Consider glial cells, which have a much higher expression of SOCE channels than neurons do (Kwon *et al.*, 2017). There are many glial cells present in our cultures of both DRG and SCG neurons and yet they do not respond to temperature stimuli (Tan and McNaughton, 2016). What could be the difference between these cell types? Possible explanations include subunit variation due to alternative splicing, alternative translation initiation, post-translational modifications, heteromeric assembly of subunits, and co-assembly with accessory proteins.

The splice-variants of STIM1 have been shown to be cell-type specific (Nelson and Roe, 2018), so cold-sensitive neurons could express a different splice variant of STIM1. It is not likely however, that cold-sensitive neurons express a different splice variant of STIM1, because heterologous overexpression of the most common mouse variant of STIM1 in combination with human Orai1 rendered PC12 cells cold-sensitive (section 4.2.2).

The presence of cell-type specific post-translational modifications of STIM1 may provide a better explanation. For example, STIM1 can be directly activated *via* S-glutathionylation during oxidative stress, which evokes constitutive Ca^{2+} entry independent of intracellular Ca^{2+} stores (Hawkins *et al.*, 2010). STIM1 can also be inhibited *via* S-nitrosylation (Gui *et al.*, 2018). Perhaps one such post-translational modification renders STIM1 cold-sensitive in a subpopulation of sensory and sympathetic neurons. Another possibility is that **cold-insensitive** cells express a protein which inhibits STIM1 cold-sensitivity or inhibits Orai channel activation by STIM1.

7.3 Possible Functions of CICE in DRG Neurons

The cold-induced Ca^{2+} influx through Orai channels does not produce a large enough current to affect the membrane potential and produce action potential firing (Derler *et al.*, 2013). Therefore, expression of this mechanism in sensory nerves is unlikely to contribute to thermosensation in the same manner that the non-selective cationic ion channel TRPM8 might do. This raises the question of what the function of CICE in sensory neurons might be.

Ca^{2+} is a universal second messenger with a plethora of functions in neurons. For example, local increases in $[Ca^{2+}]$ can trigger neurogenic inflammation by vesicular exocytosis of neurotransmitters and neuropeptides, such as Substance P and CGRP (Figure 70); Ca^{2+} can activate enzymes such as kinases and neuronal Nitric Oxide Synthase (nNOS); Ca^{2+} can influence gene transcription; Ca^{2+} can activate calcium-activated potassium channels (K_{Ca}/BK channels); Ca^{2+} can even elicit apoptosis (Brini *et al.*, 2014).

Store-operated Ca^{2+} entry (SOCE) has been implicated in several processes, such as activation of adenylyl cyclase (Cooper, 2015) and PKC (Miyano *et al.*, 2009). More specifically, neuronal SOCE has been implicated in processes such as presynaptic vesicular exocytosis (de Juan-Sanz *et al.*, 2017); activation of nNOS (Zuccolo *et al.*,

2016); activation of Ca^{2+}/calmodulin-dependent protein kinase II (CaMKII) (Sun *et al.*, 2014); long-term potentiation (Baba *et al.*, 2003); and ubiquitination and degradation of transcription factors (Lalonde, Saia and Gill, 2014).

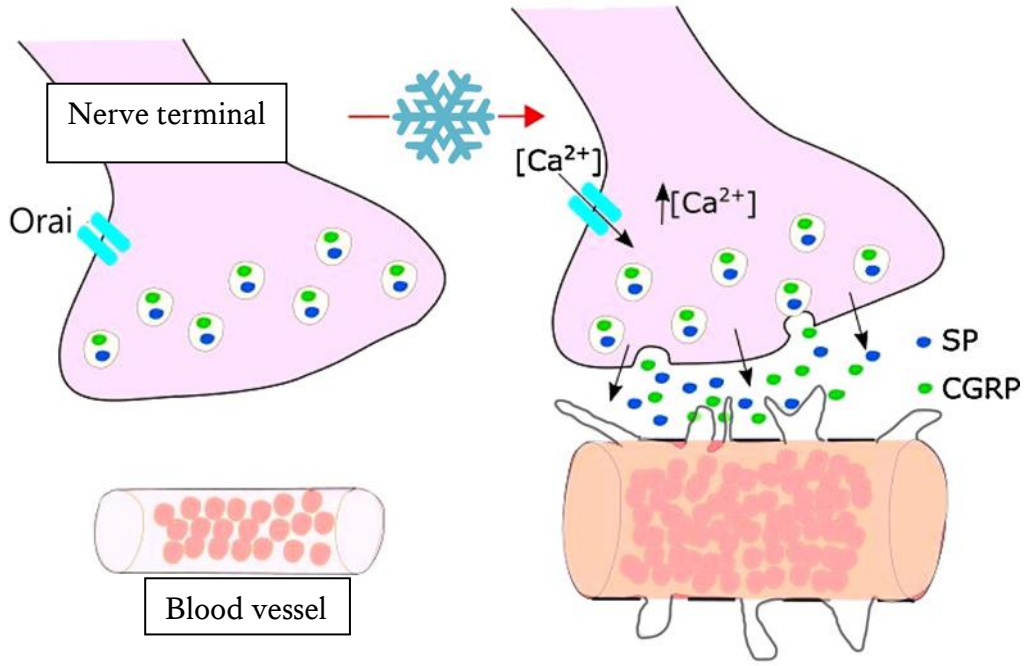

Figure 70 Schematic of neurogenic inflammation in the periphery.
Cold could trigger neurogenic inflammation via activation of Orai channels in C-fibre terminals. The resulting increase in Ca^{2+} could result in exocytosis of neuropeptide-containing vesicles. These inflammatory peptides act on cutaneous blood vessels to induce vasodilation and plasma extravasation. SP= Substance P; CGRP= Calcitonin Gene-Related Peptide. Figure adapted from (Kodji, Aubdool and Brain, 2016).

In sensory neurons, cytoplasmic Ca^{2+} homeostasis is impaired after peripheral nerve injury (Fuchs *et al.*, 2005; Fuchs, Rigaud and Hogan, 2007; Pan *et al.*, 2016) and inflammatory chronic pain and diabetic neuropathy are associated with elevated cytosolic Ca^{2+} (Kostyuk *et al.*, 2001; Huang *et al.*, 2002; Lu and Gold, 2008). Indeed, SOCE has been found to contribute to nociception. Oral administration of Orai antagonist YM58483 produced analgesia and prevented the development of chronic pain in mice (Gao *et al.*, 2013; Qi *et al.*, 2016). This analgesic effect of YM58483 is due to inhibition of Orai1 in dorsal horn neurons, where it functions to increase neuronal excitability *via* activation of protein kinase C which results in a reduced expression of potassium channels (Dou *et al.*, 2017).

The same group found that SOCE is mediated by Orai1/Orai3 in DRG neurons and induces membrane depolarisation and thereby increases excitability of C- and A-fibres (Wei *et al.*, 2017). SOCE is also involved in the production of proinflammatory cytokines in spinal astrocytes (Gao *et al.*, 2016). These findings provide further evidence for a role of SOCE in nociception.

We can combine this information about the function of SOCE with what is known about the effects of cold to form a hypothesis about a possible sensory function of cold-induced Ca^{2+} entry in sensory nerve endings.

Cooling the skin results in thermosensation and/or nociception, depending on the temperature. We can speculate that CICE could be involved in these processes despite a possible lack of effect on the membrane potential if it activates or inhibits another ion channel that does produce a large current.

One such protein is TRPA1, whose role in nociception has been well established, unlike its role in thermosensation (Kwan & Corey 2009). Importantly, TRPA1 can be directly activated by $[Ca^{2+}]_i$ (Doerner *et al.*, 2007; Zurborg *et al.*, 2007) and is co-expressed with STIM1 in nociceptors (Usoskin *et al.*, 2015; Wei *et al.*, 2017). Furthermore, co-immunoprecipitation experiments in immune cells have shown a direct association between TRPA1 and STIM1, as well as TRPA1 and Orai1 (Albarrán *et al.*, 2013). We can therefore hypothesise that CICE activates TRPA1 and use this to explain why some studies find that TRPA1 is activated by cold and others do not.

TRPA1 is highly expressed in sensory neurons, but the majority of TRPA1-expressing DRG neurons are not cold-sensitive (Figure 45; Babes, Zorzon and Reid, 2004; Bautista *et al.*, 2007; Munns, AlQatari and Koltzenburg, 2007; Noël *et al.*, 2009; Memon *et al.*, 2017). This suggests that TRPA1 is not directly activated by cold. However, most of the observed Ca^{2+} influx in cold-sensitive and TRPA1-expressing DRG neurons is in fact mediated by TRPA1, because the amplitude of the cold-induced Ca^{2+} influx in these neurons was decreased after application of a selective TRPA1 antagonist (Memon *et al.*, 2017). To explain these findings, we hypothesise that when STIM1 is activated by cold, it opens Orai channels, which mediate a Ca^{2+} influx that directly gates TRPA1 channels (Figure 70).

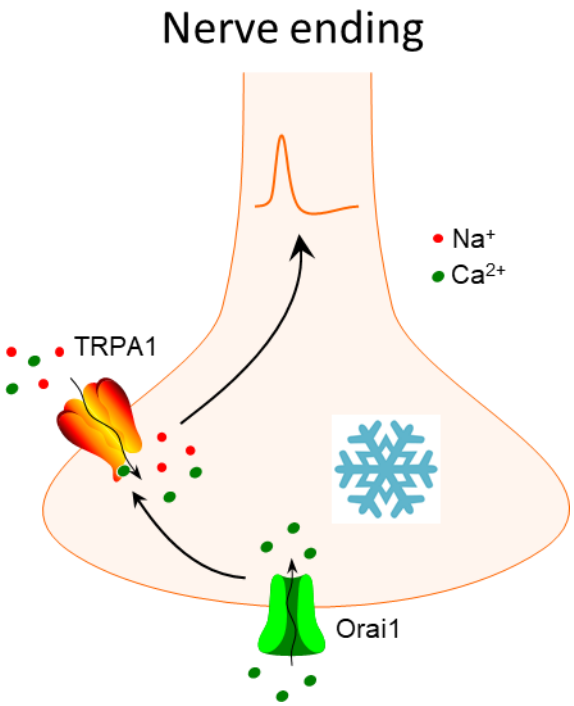

Figure 71 Schematic of TRPA1 hypothesis.
Cold-induced Ca^{2+} entry could open TRPA1 and lead to action potential firing in sensory nerve endings to contribute to conscious thermosensation.

Therefore, CICE in sensory neurons could possibly lead to TRPA1 activation and nociception. We could measure this using patch clamp electrophysiology in DRG neurons as TRPA1 activation would produce a detectable current, unlike Orai channel opening alone. CICE could also modulate all other TRP channels via calmodulin (Wu, Sweet and Clapham, 2010).

7.4 Possible Functions of CICE in SCG Neurons

The hypothalamus receives information about the overall temperature of the body. When body temperature is below its set point, the hypothalamus can activate the sympathetic nervous system to cause vasoconstriction and thus conserve body heat (Wang and Siemens, 2015). When body temperature is above its set point, sympathetic vasoconstrictor tone is lessened and vasodilation is caused by the constant production of nitric oxide in endothelial cells, which will lead to increased dissipation of body heat and lower body temperature (Loscalzo, 2013).

When skin that contains arterio-venous anastomoses (AVAs), such as in the finger or ear, is severely cooled, blood vessels dilate in an attempt to protect the tissue from frostbite, a phenomenon known as CIVD (Daanen and Van Der Struijs, 2005). However, core body temperature homeostasis is given preference over the protection of

local tissue, and CIVD does not happen when the body is hypothermic. The combination of hypothermia and extreme local cold will thus lead to frostbite.

Cold inhibits nerve conduction velocity by 15m/s per 10°C until full block is achieved at noxious cold temperatures of 8-10°C (Franz and Iggo, 1968; Vanggaard, 1975). Therefore, the body has evolved a local cold response mechanism of CIVD that does not require nerve conduction. CIVD could be mediated by sympathetic neurons, which are strongly activated by noxious cold.

Immunohistochemical analysis of the SCG and SG revealed that nNOS is widely expressed in postganglionic sympathetic neurons (see Chapter 5). This shows that sympathetic neurons have the ability to release nitric oxide (NO) and thereby cause neurogenic vasodilation (Taylor, Bishop and Fred, 1993). Neuronal NOS is a Ca^{2+}/calmodulin-dependent protein (Förstermann and Sessa, 2012), so could be activated by the cold-induced Ca^{2+} influx through Orai channels. In fact, sustained endothelial NOS activation has been shown to require SOCE (Kwan, Huang and Yao, 2000; Lin *et al.*, 2000).

Additionally, almost all plants (which also express Ca^{2+} channels and contain an ER that releases Ca^{2+} upon stimulation by IP_3) respond to cold with a rapid increase of NO production by NOS enzymes, which in turn triggers cold acclimatisation processes *via* post-translational modification and changes in gene expression (Puyaubert and Baudouin, 2014). Perhaps sympathetic neurons use a similar strategy.

Thus, we have developed a new hypothesis: we suspect that CICE may be the elusive mechanism behind cold-induced vasodilation (CIVD), which means that activation of Orai channels by local noxious cold may cause sympathetic neurons to release nitric oxide and cause vasodilation in order to protect the skin from frostbite (Figure 72). Cold-induced Orai channel opening causes a slow rise in Ca^{2+} and would lead to nitric oxide synthesis and subsequent vasodilation, whereas action potential input from the hypothalamus would cause a rapid rise in Ca^{2+} and lead to exocytosis of vesicles containing noradrenaline and subsequent vasoconstriction (when nerve conduction is not inhibited). The consequence of the Ca^{2+} rise could also depend on its specific location in the cell, as local Ca^{2+} is known to form nanodomains with local effects (Kar *et al.*, 2014).

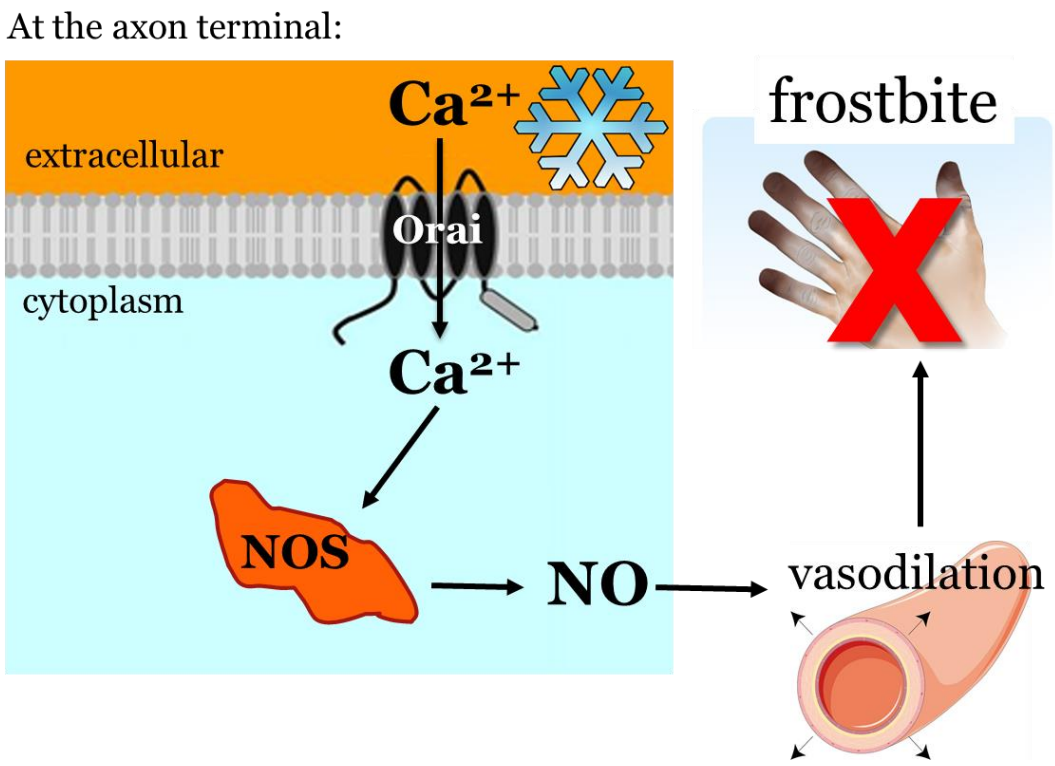

Figure 72 Schematic of CIVD hypothesis.
NOS= neuronal nitric oxide synthase; NO = nitric oxide.

The noradrenergic sympathetic neuron has two different inputs: action potentials originating in the hypothalamus (CNS) and local increases in calcium resulting from activation of Orai channels. The CNS will stimulate the efferent sympathetic nerve when core body temperature is too low, but nerve conduction will be inhibited by local cold. The opening of Orai channels will stimulate the nerve when local noxious cold is detected by STIM/Orai.

The nerve also has different and opposing outputs i.e. exocytosis of vesicles containing noradrenaline (NA), and synthesis of nitric oxide (NO). Depending on the output, the innervated blood vessel will either contract or dilate. Vasoconstriction will result in conservation of heat and core body temperature increase; vasodilation will result in heat dissipation and core body temperature decrease. When the skin is extremely cold, vasodilation will protect the tissue from damage, and vasoconstriction will lead to frostbite.

Figure 73 incorporates the hypothesis listed above in a simplified model of thermoregulation. While it is presented as a truth table and logic circuit, one must keep in mind that neuronal systems are not binary. Therefore, it is best to interpret *1* as *more* and *0* as *less*, rather than *on* and *off*.

			Input		Output			
	T_{core}	T_{skin}	CNS	Orai	NA	NO	Result	Outcome
A	cold	neutral	1	0	1	0	vasoconstriction	↑T_{core}
B	warm	neutral	0	0	0	0	vasodilation	↓ T_{core}
C	neutral	cold	0	1	0	1	CIVD	no frostbite
D	cold	cold	1	1	1	0	vasoconstriction	frostbite

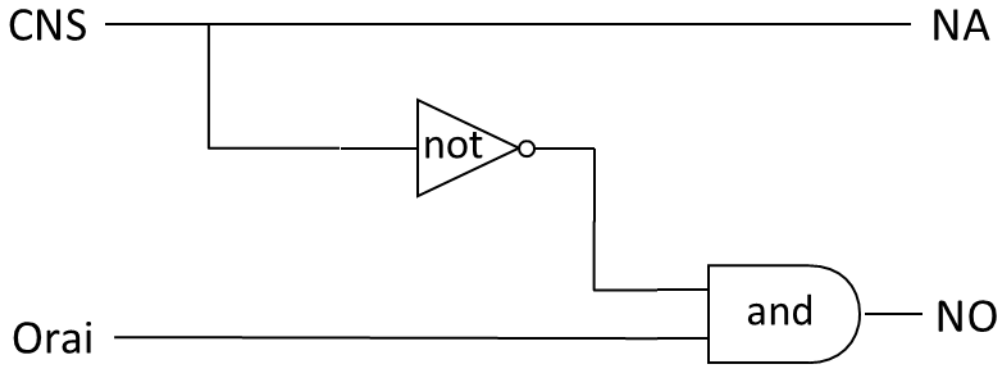

Figure 73 Truth table and logic circuit of thermoregulation hypothesis.
A) Low body temperature but neutral skin temperature. Hypothalamic input causes a large rise in calcium; NA is released and causes vasoconstriction which leads to increased body temperature. **B)** High body temperature and neutral skin temperature. The sympathetic nerve is inactive and baseline tonic vasodilation is mediated by endothelial release of nitric oxide and leads to decreased body temperature. **C)** High body temperature but skin noxious cold. Orai channel activation causes a slow rise in Ca^{2+}, which is not enough to cause NA exocytosis but high enough to cause nitric oxide synthesis and subsequent vasodilation to protect to the tissue from frostbite. **D)** Low body temperature and local extreme cold. CNS input causes a fast rise in Ca^{2+}. NA is released and causes vasoconstriction which leads to increased body temperature. Increasing core body temperature is given preference over local tissue health and may result in frostbite. The logic circuit at the bottom shows a direct connection between CNS input and NA release. It also shows a connection between local Orai-mediated input and NO release. However, for NO to be released, CNS input must be 'off'. Readers that are not familiar with logic circuits are referred to Appendix A.

7.5 Conclusions and Future Directions

In conclusion, this thesis has contributed to the advancement of knowledge about thermosensation by showing that STIM and Orai channels underlie a novel cold transduction mechanism in peripheral neurons. Going forward, it will be important to determine whether these proteins are involved in thermosensation, nociception, neurogenic inflammation, or CIVD.

The involvement of STIM1 in these processes could be tested with the use of a STIM1 knockout mouse. Since a global knockout of STIM1 results in perinatal lethality (Mancarella, Wang and Gill, 2011), a tissue-specific knockout of STIM1 would have to be generated. This can be achieved by employing the Cre-Lox recombination system. For example crossing a mouse that expresses cre-recombinase in peripheral neurons,

such as the Wnt1-Cre mouse (Danielian *et al.*, 1998), with a mouse whose STIM1 gene is flanked by *LoxP* sites (Oh-Hora *et al.*, 2008).

Such a STIM1 conditional knockout mouse could then be tested for deficits in nociception, thermosensation, and thermoregulation using available standardised tests such as the cold plate test, acetone test, thermal place preference test, or thermal stress test. Deficits in CIVD responses can be tested with the use of Laser Doppler Flowmetry.

7.6 Medical Significance

If the SOCE system is expressed in vasomotor nerves and responsible for CIVD this makes STIM and Orai potential targets of therapeutic interest. For example, a cream that activates this process could be applied to the skin of people suffering from Raynaud's phenomenon to induce reperfusion of the affected fingers (see general introduction section 1.1.8).

Raynaud's is typically treated with dihydropyridine Ca_V blockers such as Nifedipine, which acts directly on the smooth muscle, but can cause many side effects, such as tachycardia and oedema (Musa and Qurie, 2018). Notably, we have found that these drugs potentiate Orai-mediated cold responses (section 3.3.4). Possibly part of their therapeutic effect is mediated by these channels rather than their intended target. Regardless, a more specific agonist of the vasodilatory response would be preferred.

Another treatment for Raynaud's phenomenon is the application of topical nitrates to cause vasodilation of the affected area. Unfortunately, these drugs are systemically absorbed and cause side effects such as hypotension. A potentially better treatment would include topical application of a specific Orai channel agonist, which could result in local vasodilation. This novel drug would circumvent all above problems and could also have potential applications for soldiers training in arctic conditions or mountain climbers to prevent frostbite.

STIM1 has been shown to play a role in presynaptic exocytosis as mentioned previously. If the SOCE system is expressed in sympathetic BAT nerves and the increase in Ca^{2+} enhances NA exocytosis it could be involved in thermogenesis. This makes the SOCE system a potential therapeutic target in the prevention and treatment of obesity, which is caused by an imbalance between energy intake and expenditure; BAT thermogenesis requires a large energy expenditure. Local activation of SOCE in sympathetic BAT nerves could increase the amount of fat that is burned in the body and would result in a

lower body weight, thus decreasing the health risk associated with excess body fat and obesity-related metabolic syndrome, without causing the cardiovascular side effects associated with a global activation of the sympathetic nervous system.

Further studies are needed to determine the feasibility of the therapeutic opportunities proposed here.

Bibliography

Albarrán, L., Lopez, J. J., Dionisio, N., Smani, T., Salido, G. M. and Rosado, J. A. (2013) 'Transient receptor potential ankyrin-1 (TRPA1) modulates store-operated Ca2+entry by regulation of STIM1-Orai1 association', *Biochimica et Biophysica Acta - Molecular Cell Research*, 1833(12), pp. 3025–3034. doi: 10.1016/j.bbamcr.2013.08.014.

Alkadhi, K. a (2008) 'Rhythmic discharge induced by temperature variation and drugs in isolated sympathetic ganglia.', *Clin Exp Hypertens*, 30(7), pp. 497–510. doi: 10.1080/10641960802251867.

Alloui, A., Zimmermann, K., Mamet, J., Duprat, F., Noel, J., Chemin, J., Guy, N., Blondeau, N., Voilley, N., Rubat-Coudert, C., Borsotto, M., Romey, G., Heurteaux, C., Reeh, P., Eschalier, A. and Lazdunski, M. (2006) 'TREK-1, a K+ channel involved in polymodal pain perception', *EMBO J.* 2006/05/06, 25(11), pp. 2368–2376. doi: 10.1038/sj.emboj.7601116.

Almeida, M. C., Hew-Butler, T., Soriano, R. N., Rao, S., Wang, W., Wang, J., Tamayo, N., Oliveira, D. L., Nucci, T. B., Aryal, P., Garami, A., Bautista, D., Gavva, N. R. and Romanovsky, A. A. (2012) 'Pharmacological blockade of the cold receptor TRPM8 attenuates autonomic and behavioral cold defenses and decreases deep body temperature', *Journal of Neuroscience*. 2012/02/11, 32(6), pp. 2086–2099. doi: 10.1523/jneurosci.5606-11.2012.

Anderson, C. R., Bergner, A. and Murphy, S. M. (2006) 'How many types of cholinergic sympathetic neuron are there in the rat stellate ganglion?', *Neuroscience*, 140(2), pp. 567–576. doi: 10.1016/j.neuroscience.2006.02.021.

Andersson, D. A., Chase, H. W. and Bevan, S. (2004) 'TRPM8 activation by menthol, icilin, and cold is differentially modulated by intracellular pH', *J Neurosci*. 2004/06/11, 24(23), pp. 5364–5369. doi: 10.1523/jneurosci.0890-04.2004.

Andersson, D. A., Gentry, C., Moss, S. and Bevan, S. (2009) 'Clioquinol and pyrithione activate TRPA1 by increasing intracellular Zn2+', *Proceedings of the National Academy of Sciences*, 106(20), pp. 8374–8379. doi: 10.1073/pnas.0812675106.

Apostolova, G. and Dechant, G. (2009) 'Development of neurotransmitter phenotypes in sympathetic neurons', *Auton Neurosci*, 151(1), pp. 30–38. doi:

10.1016/j.autneu.2009.08.012.

Arnold, W. P., Mittal, C. K., Katsuki, S. and Murad, F. (1977) 'Nitric oxide activates guanylate cyclase and increases guanosine 3':5'-cyclic monophosphate levels in various tissue preparations.', *Proceedings of the National Academy of Sciences of the United States of America*, 74(8), pp. 3203–3207. doi: 10.1073/pnas.74.8.3203.

Askwith, C. C., Benson, C. J., Welsh, M. J. and Snyder, P. M. (2001) 'DEG/ENaC ion channels involved in sensory transduction are modulated by cold temperature.', *Proceedings of the National Academy of Sciences of the United States of America*, 98(11), pp. 6459–6463. doi: 10.1073/pnas.111155398.

Aubdool, A. A., Graepel, R., Kodji, X., Alawi, K. M., Bodkin, J. V., Srivastava, S., Gentry, C., Heads, R., Grant, A. D., Fernandes, E. S., Bevan, S. and Brain, S. D. (2014) 'TRPA1 is essential for the vascular response to environmental cold exposure', *Nature Communications*. Nature Publishing Group, 5, pp. 1–13. doi: 10.1038/ncomms6732.

Baba, A., Yasui, T., Fujisawa, S., Yamada, R. X., Yamada, M. K., Nishiyama, N., Matsuki, N. and Ikegaya, Y. (2003) 'Activity-evoked capacitative Ca2+ entry: implications in synaptic plasticity.', *The Journal of neuroscience : the official journal of the Society for Neuroscience*, 23(21), pp. 7737–7741. doi: 23/21/7737 [pii].

Babes, A., Zorzon, D. and Reid, G. (2004) 'Two populations of cold-sensitive neurons in rat dorsal root ganglia and their modulation by nerve growth factor', *European Journal of Neuroscience*, 20(9), pp. 2276–2282. doi: 10.1111/j.1460-9568.2004.03695.x.

Babes, A., Zorzon, D. and Reid, G. (2006) 'A novel type of cold-sensitive neuron in rat dorsal root ganglia with rapid adaptation to cooling stimuli', *Eur J Neurosci*, 24(3), pp. 691–698. doi: 10.1111/j.1460-9568.2006.04941.x.

Bandell, M., Story, G. M., Hwang, S. W., Viswanath, V., Eid, S. R., Petrus, M. J., Earley, T. J. and Patapoutian, A. (2004) 'Noxious cold ion channel TRPA1 is activated by pungent compounds and bradykinin', *Neuron*, 41(6), pp. 849–857. doi: 10.1016/S0896-6273(04)00150-3.

Bartness, T. J., Vaughan, C. H. and Song, C. K. (2010) 'Sympathetic and sensory innervation of brown adipose tissue', *Int J Obes (Lond)*. 2010/10/12, 34 Suppl 1, pp. S36-42. doi: 10.1038/ijo.2010.182.

Bartsch, T., Häbler, H. J. and Jänig, W. (1996) 'Functional properties of postganglionic sympathetic neurones supplying the submandibular gland in the anaesthetized rat',

Neuroscience Letters, 214(2–3), pp. 143–146. doi: 10.1016/0304-3940(96)12910-4.

Bautista, D. M., Jordt, S. E., Nikai, T., Tsuruda, P. R., Read, A. J., Poblete, J., Yamoah, E. N., Basbaum, A. I. and Julius, D. (2006) 'TRPA1 mediates the inflammatory actions of environmental irritants and proalgesic agents', *Cell*. 2006/03/28, 124(6), pp. 1269–1282. doi: 10.1016/j.cell.2006.02.023.

Bautista, D. M., Siemens, J., Glazer, J. M., Tsuruda, P. R., Basbaum, A. I., Stucky, C. L., Jordt, S. E. and Julius, D. (2007) 'The menthol receptor TRPM8 is the principal detector of environmental cold', *Nature*. 2007/06/01, 448(7150), pp. 204–208. doi: 10.1038/nature05910.

Beech, D. J. (2007) 'Canonical transient receptor potential 5', *Handb Exp Pharmacol*. 2007/01/16, (179), pp. 109–123. doi: 10.1007/978-3-540-34891-7_6.

Behrendt, H. J., Germann, T., Gillen, C., Hatt, H. and Jostock, R. (2004) 'Characterization of the mouse cold-menthol receptor TRPM8 and vanilloid receptor type-1 VR1 using a fluorometric imaging plate reader (FLIPR) assay', *Br J Pharmacol*. 2004/02/06, 141(4), pp. 737–745. doi: 10.1038/sj.bjp.0705652.

Biagi, B. A. and Enyeart, J. J. (1990) 'Gadolinium blocks low- and high-threshold calcium currents in pituitary cells.', *Am J Physiol*, 259(3 Pt 1), pp. C515-20. doi: 10.1152/ajpcell.1990.259.3.C515.

Blix, M. (1882) 'Experimentela bidrag till losning af fragan om hudnervernas specifika energi', *Uppsala Lakfor Forh*, 18, pp. 87–102.

Bockenhauer, D., Zilberberg, N. and Goldstein, S. A. N. (2001) 'KCNK2: reversible conversion of a hippocampal potassium leak into a voltage-dependent channel', *Nature Neuroscience*. Nature Publishing Group, 4(5), pp. 486–491. doi: 10.1038/87434.

Bootman, M. D., Rietdorf, K., Collins, T., Walker, S. and Sanderson, M. (2013) 'Ca2+-sensitive fluorescent dyes and intracellular Ca2+ imaging', *Cold Spring Harbor Protocols*, 8, pp. 83–99. doi: 10.1101/pdb.top066050.

Boughter, J. D. and Gilbertson, T. A. (1999) *From Channels to Behavior: Minireview An Integrative Model of NaCl Taste or transducin), in turn, causes an increase in phosphodi-esterase activity, resulting in decreased levels of cAMP, ultimately leading to an increase in Ca 2 influx. In addi*, *Neuron*.

Boulant, J. A. and Dean, J. B. (1986) 'Temperature receptors in the central nervous system.', *Annual review of physiology*, 48(1), pp. 639–54. doi: 10.1146/annurev.ph.48.030186.003231.

Brain, S. D., Petty, R. G., Lewis, J. D. and Williams, T. J. (1990) 'Cutaneous blood flow responses in the forearms of Raynaud's patients induced by local cooling and intradermal injections of CGRP and histamine.', *British Journal of Clinical Pharmacology*, 30(6), pp. 853–859. doi: 10.1111/j.1365-2125.1990.tb05451.x.

Brain, S. D., Williams, T. J., Tippins, J. R., Morris, H. R. and MacIntyre, I. (1985) 'Calcitonin gene-related peptide is a potent vasodilator', *Nature*, 313(5997), pp. 54–56. doi: 10.1038/313054a0.

Brengelmann, G. L., Freund, P. R., Rowell, L. B., Olerud, J. E. and Kraning, K. K. (1981) 'Absence of active cutaneous vasodilation associated with congenital absence of sweat glands in humans.', *The American journal of physiology*, 240(4), pp. H571–H575. doi: 10.1152/ajpheart.1981.240.4.H571.

Brenner, D. S., Golden, J. P., Vogt, S. K., Dhaka, A., Story, G. M. and Gereau, R. W. (2014) 'A dynamic set point for thermal adaptation requires phospholipase C-mediated regulation of TRPM8 in vivo', *Pain*. International Association for the Study of Pain, 155(10), pp. 2124–2133. doi: 10.1016/j.pain.2014.08.001.

Brini, M., Calì, T., Ottolini, D. and Carafoli, E. (2014) 'Neuronal calcium signaling: Function and dysfunction', *Cellular and Molecular Life Sciences*, 71(15), pp. 2787–2814. doi: 10.1007/s00018-013-1550-7.

Buckley, N. J., Bonner, T. I., Buckley, C. M. and Brann, M. R. (1989) 'Antagonist binding properties of five cloned muscarinic receptors expressed in CHO-K1 cells', *Mol Pharmacol*, 35(4), pp. 469–476.

Buijs, R. M. (2013) 'The autonomic nervous system: A balancing act', *Handbook of Clinical Neurology*. Elsevier, 117, pp. 1–11. doi: 10.1016/B978-0-444-53491-0.00001-8.

Bullard, R. W., Banerjee, M. R. and Mac Intyre, B. A. (1967) 'The role of the skin in negative feedback regulation of eccrine sweating', *International Journal of Biometeorology*. Springer-Verlag, 11(1), pp. 93–104. doi: 10.1007/BF01424278.

Cabanes, C., Viana, F. and Belmonte, C. (2003) 'Differential thermosensitivity of sensory neurons in the guinea pig trigeminal ganglion.', *Journal of neurophysiology*, 90(4), pp. 2219–2231. doi: 10.1152/jn.00299.2003.

del Camino, D., Murphy, S., Heiry, M., Barrett, L. B., Earley, T. J., Cook, C. A., Petrus, M. J., Zhao, M., D'Amours, M., Deering, N., Brenner, G. J., Costigan, M., Hayward, N. J., Chong, J. A., Fanger, C. M., Woolf, C. J., Patapoutian, A. and Moran,

M. M. (2010) 'TRPA1 Contributes to Cold Hypersensitivity', *Journal of Neuroscience*, 30(45), pp. 15165–15174. doi: 10.1523/JNEUROSCI.2580-10.2010.

Cane, K. N. and Anderson, C. R. (2009) 'Generating diversity: Mechanisms regulating the differentiation of autonomic neuron phenotypes', *Auton Neurosci*, 151(1), pp. 17–29. doi: 10.1016/j.autneu.2009.08.010.

Caspani, O. and Heppenstall, P. A. (2009) 'TRPA1 and cold transduction: an unresolved issue?', *The Journal of general physiology*, 133(3), pp. 245–249. doi: 10.1085/jgp.200810136.

Caterina, M. J. (2007) 'Transient receptor potential ion channels as participants in thermosensation and thermoregulation', *Am J Physiol Regul Integr Comp Physiol*. 2006/09/16, 292(1), pp. R64-76. doi: 10.1152/ajpregu.00446.2006.

Ceccatelli, S., Lundberg, J. M., Zhang, X., Aman, K. and Hökfelt, T. (1994) 'Immunohistochemical demonstration of nitric oxide synthase in the peripheral autonomic nervous system.', *Brain Research*, 656(2), pp. 381–395.

Chen, F. (1996) 'Hand and finger skin temperatures in convective and contact cold exposure', *European Journal of Applied Physiology and Occupational Physiology*, 72(4), pp. 372–379. doi: 10.1007/BF00599699.

Chen, J., Joshi, S. K., DiDomenico, S., Perner, R. J., Mikusa, J. P., Gauvin, D. M., Segreti, J. A., Han, P., Zhang, X. F., Niforatos, W., Bianchi, B. R., Baker, S. J., Zhong, C., Simler, G. H., McDonald, H. A., Schmidt, R. G., McGaraughty, S. P., Chu, K. L., Faltynek, C. R., Kort, M. E., Reilly, R. M. and Kym, P. R. (2011) 'Selective blockade of TRPA1 channel attenuates pathological pain without altering noxious cold sensation or body temperature regulation', *Pain*. 2011/03/16, 152(5), pp. 1165–1172. doi: 10.1016/j.pain.2011.01.049.

Chen, T.-W., Wardill, T. J., Sun, Y., Pulver, S. R., Renninger, S. L., Baohan, A., Schreiter, E. R., Kerr, R. A., Orger, M. B., Jayaraman, V., Looger, L. L., Svoboda, K. and Kim, D. S. (2013) 'Ultrasensitive fluorescent proteins for imaging neuronal activity.', *Nature*, 499(7458), pp. 295–300. doi: 10.1038/nature12354.

Cheng, K. T., Ong, H. L., Liu, X. and Ambudkar, I. S. (2013) 'Contribution and Regulation of TRPC Channels in Store-Operated Ca2+Entry', *Current Topics in Membranes*. Academic Press, 71, pp. 149–179. doi: 10.1016/B978-0-12-407870-3.00007-X.

Chisholm, K. I., Khovanov, N., Lopes, D. M., Russa, F. La and McMahon, S. B. (2018)

'Large Scale in Vivo Recording of Sensory Neuron Activity with GCaMP6', *eNeuro*, p. ENEURO.0417-17.2018. doi: 10.1523/ENEURO.0417-17.2018.

Chiu, Y., Cao, H., Jacque, J., Stevenson, M. and Rana, T. M. (2004) 'Inhibition of Human Immunodeficiency Virus Type 1 Replication by RNA Interference Directed against Human Transcription Elongation Factor P-TEFb (CDK9 / CyclinT1)', *Journal of Virology*, 78(5), pp. 2517–29. doi: 10.1128/JVI.78.5.2517.

Cho, H., Yang, Y. D., Lee, J., Lee, B., Kim, T., Jang, Y., Back, S. K., Na, H. S., Harfe, B. D., Wang, F., Raouf, R., Wood, J. N. and Oh, U. (2012) 'The calcium-activated chloride channel anoctamin 1 acts as a heat sensor in nociceptive neurons', *Nature Neuroscience*. Nature Publishing Group, 15(7), pp. 1015–1021. doi: 10.1038/nn.3111.

Chuang, H. H., Neuhausser, W. M. and Julius, D. (2004) 'The super-cooling agent icilin reveals a mechanism of coincidence detection by a temperature-sensitive TRP channel', *Neuron*. 2004/09/15, 43(6), pp. 859–869. doi: 10.1016/j.neuron.2004.08.038.

Chubb, D. P. and Anderson, C. R. (2010) 'The relationship of the birth date of rat sympathetic neurons to the target they innervate', *Dev Dyn*, 239(3), pp. 897–904. doi: 10.1002/dvdy.22240.

Clark, A. J., Menendez, G., AlQatari, M., Patel, N., Arstad, E., Schiavo, G. and Koltzenburg, M. (2018) 'Functional imaging in microfluidic chambers reveal sensory neuron sensitivity is differentially regulated between neuronal regions', *Pain*, 159(7), p. 1. doi: 10.1097/j.pain.0000000000001145.

Colburn, R. W., Lubin, M. Lou, Stone, D. J., Wang, Y., Lawrence, D., D'Andrea, M. R. R., Brandt, M. R., Liu, Y., Flores, C. M. and Qin, N. (2007) 'Attenuated Cold Sensitivity in TRPM8 Null Mice', *Neuron*, 54(3), pp. 379–386. doi: 10.1016/j.neuron.2007.04.017.

Conti, V., Russomanno, G., Corbi, G., Izzo, V., Vecchione, C. and Filippelli, A. (2013) 'Adrenoreceptors and nitric oxide in the cardiovascular system', *Frontiers in Physiology*, 4 NOV(November), pp. 1–11. doi: 10.3389/fphys.2013.00321.

Cooper, D. M. F. (2015) 'Store-operated Ca2+-entry and adenylyl cyclase', *Cell Calcium*. Elsevier Ltd, 58(4), pp. 368–375. doi: 10.1016/j.ceca.2015.04.004.

Coste, B., Mathur, J., Schmidt, M., Earley, T. J., Ranade, S., Petrus, M. J., Dubin, A. E. and Patapoutian, A. (2010) 'Piezo1 and Piezo2 are essential components of distinct mechanically activated cation channels', *Science*. 2010/09/04, 330(6000), pp. 55–60. doi: 10.1126/science.1193270.

Craig, A. D. (2002) 'How do you feel? Interoception: the sense of the physiological condition of the body', *Nat Rev Neurosci*. 2002/08/03, 3(8), pp. 655–666. doi: 10.1038/nrn894.

Craig, A. D. (2003) 'Interoception: The sense of the physiological condition of the body', *Current Opinion in Neurobiology*. Nature Publishing Group, 13(4), pp. 500–505. doi: 10.1016/S0959-4388(03)00090-4.

Daanen, H. a and Ducharme, M. B. (2000) 'Axon reflexes in human cold exposed fingers.', *European journal of applied physiology*, 81(3), pp. 240–244. doi: 10.1007/s004210050037.

Daanen, H. a M. and Van Der Struijs, N. R. (2005) 'Resistance index of frostbite as a predictor of cold injury in arctic operations', *Aviation Space and Environmental Medicine*, 76(12), pp. 1119–1122.

Danielian, P. S., Muccino, D., Rowitch, D. H., Michael, S. K. and McMahon, A. P. (1998) 'Modification of gene activity in mouse embryos in utero by a tamoxifen-inducible form of Cre recombinase', *Current Biology*. Cell Press, 8(24), pp. 1323-S2. doi: 10.1016/S0960-9822(07)00562-3.

Daskoulidou, N., Zeng, B., Berglund, L. M., Jiang, H., Chen, G. L., Kotova, O., Bhandari, S., Ayoola, J., Griffin, S., Atkin, S. L., Gomez, M. F. and Xu, S. Z. (2015) 'High glucose enhances store-operated calcium entry by upregulating ORAI/STIM via calcineurin-NFAT signalling', *Journal of Molecular Medicine*, 93(5), pp. 511–521. doi: 10.1007/s00109-014-1234-2.

Davis, F. M., Goulding, E. H., D'Agostin, D. M., Janardhan, K. S., Cummings, C. A., Bird, G. S., Eddy, E. M. and Putney, J. W. (2016) 'Male infertility in mice lacking the store-operated Ca2+channel Orai1', *Cell Calcium*. Elsevier Ltd, 59(4), pp. 189–197. doi: 10.1016/j.ceca.2016.02.007.

Dehaven, W. I., Jones, B. F., Petranka, J. G., Smyth, J. T., Tomita, T., Bird, G. S. and Putney, J. W. (2009) 'TRPC channels function independently of STIM1 and Orai1', *Journal of Physiology*, 587(10), pp. 2275–2298. doi: 10.1113/jphysiol.2009.170431.

Derler, I., Schindl, R., Fritsch, R., Heftberger, P., Riedl, M. C., Begg, M., House, D. and Romanin, C. (2013) 'The action of selective CRAC channel blockers is affected by the Orai pore geometry', *Cell Calcium*. Elsevier Ltd, 53(2), pp. 139–151. doi: 10.1016/j.ceca.2012.11.005.

Dhaka, A., Murray, A. N., Mathur, J., Earley, T. J., Petrus, M. J. and Patapoutian, A.

(2007) 'TRPM8 is required for cold sensation in mice', *Neuron*. 2007/05/08, 54(3), pp. 371–378. doi: 10.1016/j.neuron.2007.02.024.

Ding, Z., Gomez, T., Werkheiser, J. L., Cowan, A. and Rawls, S. M. (2008) 'Icilin induces a hyperthermia in rats that is dependent on nitric oxide production and NMDA receptor activation', *Eur J Pharmacol*. 2007/11/03, 578(2–3), pp. 201–208. doi: 10.1016/j.ejphar.2007.09.030.

DiPasquale, D. M., Buono, M. J. and Kolkhorst, F. W. (2003) 'Effect of skin temperature on the cholinergic sensitivity of the human eccrine sweat gland.', *The Japanese journal of physiology*. 2004/03/25, 53(6), pp. 427–430. doi: 10.2170/jjphysiol.53.427.

Doerner, J. F., Gisselmann, G., Hatt, H. and Wetzel, C. H. (2007) 'Transient receptor potential channel A1 is directly gated by calcium ions', *Journal of Biological Chemistry*, 282(18), pp. 13180–13189. doi: 10.1074/jbc.M607849200.

Dou, Y., Xia, J., Gao, R., Gao, X., Munoz, F. M., Wei, D., Tian, Y., Barrett, J. E., Ajit, S., Meucci, O., Putney, J. W., Dai, Y. and Hu, H. (2017) 'Orai1 plays a crucial role in central sensitization by modulating neuronal excitability', *The Journal of Neuroscience*, 38(4), pp. 3007–17. doi: 10.1523/JNEUROSCI.3007-17.2017.

Douglas, W. W. (1974) 'Involvement of calcium in exocytosis and the exocytosis--vesiculation sequence.', *Biochemical Society symposium*, (39), pp. 1–28.

Dun, N. J., Dun, S. L., Wu, S. Y. and Forstermann, U. (1993) 'Nitric oxide synthase immunoreactivity in rat superior cervical ganglia and adrenal glands', *Neuroscience Letters*, 158(1), pp. 51–54.

Dunham, J. P., Leith, J. L., Lumb, B. M. and Donaldson, L. F. (2010) 'Transient receptor potential channel A1 and noxious cold responses in rat cutaneous nociceptors', *Neuroscience*. Elsevier Inc., 165(4), pp. 1412–1419. doi: 10.1016/j.neuroscience.2009.11.065.

Eickholt, B. J., Ahmed, A. I., Davies, M., Papakonstanti, E. A., Pearce, W., Starkey, M. L., Bilancio, A., Need, A. C., Smith, A. J. H., Hall, S. M., Hamers, F. P., Giese, K. P., Bradbury, E. J. and Vanhaesebroeck, B. (2007) 'Control of axonal growth and regeneration of sensory neurons by the p110δ PI 3-kinase', *PLoS ONE*, 2(9), pp. 1–9. doi: 10.1371/journal.pone.0000869.

Emery, E. C., Luiz, A. P., Sikandar, S., Magnusdottir, R., Dong, X. and Wood, J. N. (2016) 'In vivo characterization of distinct modality-specific subsets of somatosensory

neurons using GCaMP', *Science Advances*, 2(11), pp. e1600990–e1600990. doi: 10.1126/sciadv.1600990.

Enyedi, P. and Czirjak, G. (2010) 'Molecular background of leak K+ currents: two-pore domain potassium channels', *Physiol Rev*. 2010/04/16, 90(2), pp. 559–605. doi: 10.1152/physrev.00029.2009.

Everaerts, W., Gees, M., Alpizar, Y. A., Farre, R., Leten, C., Apetrei, A., Dewachter, I., van Leuven, F., Vennekens, R., De Ridder, D., Nilius, B., Voets, T. and Talavera, K. (2011) 'The Capsaicin Receptor TRPV1 Is a Crucial Mediator of the Noxious Effects of Mustard Oil', *Current Biology*. Cell Press, 21(4), pp. 316–321. doi: 10.1016/J.CUB.2011.01.031.

Fajardo, O., Meseguer, V., Belmonte, C. and Viana, F. (2008) 'TRPA1 Channels Mediate Cold Temperature Sensing in Mammalian Vagal Sensory Neurons: Pharmacological and Genetic Evidence', *Journal of Neuroscience*, 28(31), pp. 7863–7875. doi: 10.1523/JNEUROSCI.1696-08.2008.

Feng, M., Grice, D. M., Faddy, H. M., Nguyen, N., Leitch, S., Wang, Y., Muend, S., Kenny, P. A., Sukumar, S., Roberts-Thomson, S. J., Monteith, G. R. and Rao, R. (2010) 'Store-independent activation of orai1 by SPCA2 in mammary tumors', *Cell*. Elsevier Ltd, 143(1), pp. 84–98. doi: 10.1016/j.cell.2010.08.040.

Feske, S., Gwack, Y., Prakriya, M., Srikanth, S., Puppel, S. H., Tanasa, B., Hogan, P. G., Lewis, R. S., Daly, M. and Rao, A. (2006) 'A mutation in Orai1 causes immune deficiency by abrogating CRAC channel function', *Nature*, 441(7090), pp. 179–185. doi: 10.1038/nature04702.

Fischer, A., Mayer, B. and Kummer, W. (1996) 'Nitric oxide synthase in vagal sensory and sympathetic neurons innervating the guinea-pig trachea', *Journal of the Autonomic Nervous System*, 56(3), pp. 157–160. doi: 10.1016/0165-1838(95)00085-2.

Flouris, A. D. and Cheung, S. S. (2010) 'On the origins of cold-induced vasodilation', *European Journal of Applied Physiology*, 108(6), pp. 1281–1282. doi: 10.1007/s00421-009-1324-y.

Förstermann, U. and Sessa, W. C. (2012) 'Nitric oxide synthases: Regulation and function', *European Heart Journal*, 33(7), pp. 829–837. doi: 10.1093/eurheartj/ehr304.

Franz, D. N. and Iggo, A. (1968) 'Conduction Failure in Myelinated and Non-Myelinated Axon at Low Temperatures', *the Journal of Physiology*, 199, pp. 319–345.

Fuchs, A., Lirk, P., Stucky, C., D, P., Abram, S. E. and Hogan, Q. H. (2005)

'Concentrations in Sensory Neurons of Rats', (6).

Fuchs, A., Rigaud, M. and Hogan, Q. H. (2007) 'Painful nerve injury shortens the intracellular Ca2+ signal in axotomized sensory neurons of rats', *Anesthesiology*, 107(1), pp. 106–116. doi: 10.1097/01.anes.0000267538.72900.68.

Furlan, A., La Manno, G., Lübke, M., Häring, M., Abdo, H., Hochgerner, H., Kupari, J., Usoskin, D., Airaksinen, M. S., Oliver, G., Linnarsson, S. and Ernfors, P. (2016) 'Visceral motor neuron diversity delineates a cellular basis for nipple- and pilo-erection muscle control', *Nature Neuroscience*, 19(10), pp. 1331–1340. doi: 10.1038/nn.4376.

Gao, R., Gao, X., Xia, J., Tian, Y., Barrett, J. E., Dai, Y. and Hu, H. (2013) 'Potent analgesic effects of a store-operated calcium channel inhibitor', *Pain*. International Association for the Study of Pain, 154(10), pp. 2034–2044. doi: 10.1016/j.pain.2013.06.017.

Gao, X., Xia, J., Munoz, F. M., Manners, M. T., Pan, R., Meucci, O., Dai, Y. and Hu, H. (2016) 'STIMs and Orai1 regulate cytokine production in spinal astrocytes', *Journal of Neuroinflammation*. Journal of Neuroinflammation, 13(1), pp. 1–13. doi: 10.1186/s12974-016-0594-7.

Gatto, C., Hale, C. C., Xu, W. and Milanick, M. A. (1995) 'Eosin, a Potent Inhibitor of the Plasma Membrane Ca Pump, Does Not Inhibit the Cardiac Na-Ca Exchanger', *Biochemistry*, 34(3), pp. 965–972. doi: 10.1021/bi00003a031.

Gavva, N. R., Davis, C., Lehto, S. G., Rao, S., Wang, W. and Zhu, D. X. (2012) 'Transient receptor potential melastatin 8 (TRPM8) channels are involved in body temperature regulation', *Mol Pain*. 2012/05/11, 8, p. 36. doi: 10.1186/1744-8069-8-36.

Geiser, F. (2004) 'Metabolic Rate and Body Temperature Reduction During Hibernation and Daily Torpor', *Annual Review of Physiology*. Annual Reviews , 66(1), pp. 239–274. doi: 10.1146/annurev.physiol.66.032102.115105.

Gentry, C., Andersson, D. A. and Bevan, S. (2015) 'TRPA1 mediates the hypothermic action of acetaminophen', *Scientific Reports*. Nature Publishing Group, 5(1), p. 12771. doi: 10.1038/srep12771.

Gibbins, I. L. (1991) 'Vasomotor, pilomotor and secretomotor neurons distinguished by size and neuropeptide content in superior cervical ganglia of mice', *Journal of the Autonomic Nervous System*, 34(2–3), pp. 171–183. doi: 10.1016/0165-1838(91)90083-F.

Goldstein, S. A., Bayliss, D. A., Kim, D., Lesage, F., Plant, L. D. and Rajan, S. (2005) 'International Union of Pharmacology. LV. Nomenclature and molecular relationships of two-P potassium channels', *Pharmacol Rev*. 2005/12/31, 57(4), pp. 527–540. doi: 10.1124/pr.57.4.12.

Grayson, J. (1950) '' Cold and Warmth Vasoconstrictor Responses in the Skin of Man', pp. 167–176.

Green, B. G. and Frankmann, S. P. (1988) 'The effect of cooling on the perception of carbohydrate and intensive sweeteners', *Physiology & Behavior*. Elsevier, 43(4), pp. 515–519. doi: 10.1016/0031-9384(88)90127-8.

Greene, L. A. and Tischler, A. S. (1976) 'Establishment of a Noradrenergic Clonal Line of Rat Adrenal Pheochromocytoma Cells Which Respond to Nerve Growth-Factor', *Proceedings of the National Academy of Sciences of the United States of America*. National Acad Sciences, 73(7), pp. 2424–2428. doi: DOI 10.1073/pnas.73.7.2424.

Grigoriev, I., Gouveia, S. M., van der Vaart, B., Demmers, J., Smyth, J. T., Honnappa, S., Splinter, D., Steinmetz, M. O., Putney, J. W., Hoogenraad, C. C. and Akhmanova, A. (2008) 'STIM1 Is a MT-Plus-End-Tracking Protein Involved in Remodeling of the ER', *Current Biology*, 18(3), pp. 177–182. doi: 10.1016/j.cub.2007.12.050.

Grossmann, L., Gorodetskaya, N., Teliban, A., Baron, R. and Jänig, W. (2009) 'Cutaneous afferent C-fibers regenerating along the distal nerve stump after crush lesion show two types of cold sensitivity', *European Journal of Pain*. European Federation of Chapters of the International Association for the Study of Pain, 13(7), pp. 682–690. doi: 10.1016/j.ejpain.2008.09.004.

Grybko, M. J., Hahm, E. T., Perrine, W., Parnes, J. A., Chick, W. S., Sharma, G., Finger, T. E. and Vijayaraghavan, S. (2011) 'A transgenic mouse model reveals fast nicotinic transmission in hippocampal pyramidal neurons', *Eur J Neurosci*, 33(10), pp. 1786–1798. doi: 10.1111/j.1460-9568.2011.07671.x.

Gui, L., Zhu, J., Lu, X., Sims, S. M., Lu, W. Y., Stathopulos, P. B. and Feng, Q. (2018) 'S-Nitrosylation of STIM1 by Neuronal Nitric Oxide Synthase Inhibits Store-Operated Ca2 +Entry', *Journal of Molecular Biology*. Elsevier Ltd, 430(12), pp. 1773–1785. doi: 10.1016/j.jmb.2018.04.028.

Guidry, G. and Landis, S. C. (2000) 'Absence of cholinergic sympathetic innervation from limb muscle vasculature in rats and mice', *Autonomic Neuroscience: Basic and Clinical*, 82, pp. 97–108. doi: 10.1016/S0165-1838(00)00094-1.

Häbler, H. J., Jänig, W., Krummel, M. and Peters, O. A. (1994) 'Reflex patterns in postganglionic neurons supplying skin and skeletal muscle of the rat hindlimb', *J Neurophysiol*, 72(5), pp. 2222–2236. doi: 10.1152/jn.1994.72.5.2222.

HALE, A. R. and BURCH, G. E. (1960) 'The arteriovenous anastomoses and blood vessels of the human finger. Morphological and functional aspects.', *Medicine*, 39, pp. 191–240.

Harding, S. D., Sharman, J. L., Faccenda, E., Southan, C., Pawson, A. J., Ireland, S., Gray, A. J. G., Bruce, L., Alexander, S. P. H., Anderton, S., Bryant, C., Davenport, A. P., Doerig, C., Fabbro, D., Levi-Schaffer, F., Spedding, M. and Davies, J. A. (2018) 'The IUPHAR/BPS Guide to PHARMACOLOGY in 2018: Updates and expansion to encompass the new guide to IMMUNOPHARMACOLOGY', *Nucleic Acids Research*. Oxford University Press, 46(D1), pp. D1091–D1106. doi: 10.1093/nar/gkx1121.

Harraz, O. F. and Altier, C. (2014) 'STIM1-mediated bidirectional regulation of Ca(2+) entry through voltage-gated calcium channels (VGCC) and calcium-release activated channels (CRAC).', *Frontiers in cellular neuroscience*, 8(February), p. 43. doi: 10.3389/fncel.2014.00043.

Hawkins, B. J., Irrinki, K. M., Mallilankaraman, K., Lien, Y. C., Wang, Y., Bhanumathy, C. D., Subbiah, R., Ritchie, M. F., Soboloff, J., Baba, Y., Kurosaki, T., Joseph, S. K., Gill, D. L. and Madesh, M. (2010) 'S-glutathionylation activates STIM1 and alters mitochondrial homeostasis', *Journal of Cell Biology*, 190(3), pp. 391–405. doi: 10.1083/jcb.201004152.

He, L. P., Hewavitharana, T., Soboloff, J., Spassova, M. A. and Gill, D. L. (2005) 'A functional link between store-operated and TRPC channels revealed by the 3,5-bis(trifluoromethyl)pyrazole derivative, BTP2', *Journal of Biological Chemistry*, 280(12), pp. 10997–11006. doi: 10.1074/jbc.M411797200.

Heurteaux, C., Guy, N., Laigle, C., Blondeau, N., Duprat, F., Mazzuca, M., Lang-Lazdunski, L., Widmann, C., Zanzouri, M., Romey, G. and Lazdunski, M. (2004) 'TREK-1, a K+ channel involved in neuroprotection and general anesthesia.', *The EMBO journal*. EMBO Press, 23(13), pp. 2684–95. doi: 10.1038/sj.emboj.7600234.

Hirota, S., Pertens, E. and Janssen, L. J. (2007) 'The reverse mode of the Na(+)/Ca(2+) exchanger provides a source of Ca(2+) for store refilling following agonist-induced Ca(2+) mobilization.', *American journal of physiology. Lung cellular and molecular*

physiology, 292(2), pp. L438-47. doi: 10.1152/ajplung.00222.2006.

Hirst, G. D. and McLachlan, E. M. (1984) 'Post???natal development of ganglia in the lower lumbar sympathetic chain of the rat.', *The Journal of Physiology*. Wiley/Blackwell (10.1111), 349(1), pp. 119–134. doi: 10.1113/jphysiol.1984.sp015147.

Hobai, I. A., Bates, J. A., Howarth, F. C. and Levi, A. J. (1997) 'Inhibition by external Cd2+ of Na/Ca exchange and L-type Ca channel in rabbit ventricular myocytes.', *The American journal of physiology*, 272(5 Pt 2), pp. H2164-72.

Horowitz, M., Kenny, G. P., McAllen, R. M. and van Marken Lichtenbelt, W. D. (2015) 'Thermal physiology in a changing thermal world', *Temperature*, 2(1), pp. 22–26. doi: 10.1080/23328940.2015.1017088.

Hoth, M. and Penner, R. (1992) 'Depletion of intracellular calcium stores activates a calcium current in mast cells', *Nature*, 355(6358), pp. 353–356. doi: 10.1038/355353a0.

Hou, X., Pedi, L., Diver, M. and Long, S. B. (2012) 'Crystal Structure of the Calcium Release – Activated Calcium Channel Orai', *Science*, (November), pp. 1–10.

Huang, T. J., Sayers, N. M., Fernyhough, P. and Verkhratsky, A. (2002) 'Diabetes-induced alterations in calcium homeostasis in sensory neurones of streptozotocin-diabetic rats are restricted to lumbar ganglia and are prevented by neurotrophin-3', *Diabetologia*. Springer-Verlag, 45(4), pp. 560–570. doi: 10.1007/s00125-002-0785-x.

Iftinca, M. C. (2011) 'Neuronal T-type calcium channels: what's new? Iftinca: T-type channel regulation.', *Journal of medicine and life*, 4(2), pp. 126–38.

Iftinca, M., McKay, B. E., Snutch, T. P., McRory, J. E., Turner, R. W. and Zamponi, G. W. (2006) 'Temperature dependence of T-type calcium channel gating', *Neuroscience*, 142(4), pp. 1031–1042. doi: 10.1016/j.neuroscience.2006.07.010.

Iggo, A. and Muir, A. R. (1969) 'The structure and function of a slowly adapting touch corpuscle in hairy skin.', *The Journal of physiology*, 200(3), pp. 763–96.

Illigens, B. M. W. and Gibbons, C. H. (2009) 'Sweat testing to evaluate autonomic function', *Clinical Autonomic Research*. Steinkopff-Verlag, 19(2), pp. 79–87. doi: 10.1007/s10286-008-0506-8.

Isekutz, B., Hetenyi, G. and Diosy, A. (1950) 'Contributions to the physiology of sweat secretion.', *Archives internationales de pharmacodynamie et de therapie*, 83(1), pp. 133–42.

Ishikawa, J., Ohga, K., Yoshino, T., Takezawa, R., Ichikawa, A., Kubota, H. and

Yamada, T. (2003) 'A Pyrazole Derivative, YM-58483, Potently Inhibits Store-Operated Sustained Ca2+ Influx and IL-2 Production in T Lymphocytes', *The Journal of Immunology*, 170(9), pp. 4441–4449. doi: 10.4049/jimmunol.170.9.4441.

Ivanov, K. P. (2006) 'The development of the concepts of homeothermy and thermoregulation', *Journal of Thermal Biology*. Pergamon, 31(1–2 SPEC. ISS.), pp. 24–29. doi: 10.1016/j.jtherbio.2005.12.005.

Jang, Y., Lee, Y., Kim, S. M., Yang, Y. D., Jung, J. and Oh, U. (2012) 'Quantitative analysis of TRP channel genes in mouse organs', *Arch Pharm Res*. 2012/11/10, 35(10), pp. 1823–1830. doi: 10.1007/s12272-012-1016-8.

Jaquemar, D., Schenker, T. and Trueb, B. (1999) 'An ankyrin-like protein with transmembrane domains is specifically lost after oncogenic transformation of human fibroblasts', *J Biol Chem*. 1999/03/06, 274(11), pp. 7325–7333.

Johnson, J. M., Brengelmann, G. L., Hales, J. R., Vanhoutte, P. M. and Wenger, C. B. (1986) 'Regulation of the cutaneous circulation.', *Federation proceedings*, 45(13), pp. 2841–2850.

Johnson, J. M., Minson, C. T. and Kellogg, D. L. (2014) 'Cutaneous vasodilator and vasoconstrictor mechanisms in temperature regulation', *Comprehensive Physiology*, 4(1), pp. 33–89. doi: 10.1002/cphy.c130015.

Jordt, S. E., Bautista, D. M., Chuang, H. H., McKemy, D. D., Zygmunt, P. M., Hogestatt, E. D., Meng, I. D. and Julius, D. (2004) 'Mustard oils and cannabinoids excite sensory nerve fibres through the TRP channel ANKTM1', *Nature*. 2004/01/09, 427(6971), pp. 260–265. doi: 10.1038/nature02282.

de Juan-Sanz, J., Holt, G. T., Schreiter, E. R., de Juan, F., Kim, D. S. and Ryan, T. A. (2017) 'Axonal Endoplasmic Reticulum Ca2+Content Controls Release Probability in CNS Nerve Terminals', *Neuron*. Cell Press, 93(4), p. 867–881.e6. doi: 10.1016/j.neuron.2017.01.010.

Julius, D. (2013) 'TRP channels and pain', *Annu Rev Cell Dev Biol*. 2013/10/09, 29, pp. 355–384. doi: 10.1146/annurev-cellbio-101011-155833.

Kang, D., Choe, C. and Kim, D. (2005) 'Thermosensitivity of the two-pore domain K+ channels TREK-2 and TRAAK', *J Physiol*. 2005/01/29, 564(Pt 1), pp. 103–116. doi: 10.1113/jphysiol.2004.081059.

Kang, D., Choe, C. and Kim, D. (2005) 'Thermosensitivity of the two-pore domain K + channels TREK-2 and TRAAK', *J Physiol*. 2005/01/29, 5641(Pt 1), pp. 103–116.

doi: 10.1113/jphysiol.2004.081059.

Kar, P., Samanta, K., Kramer, H., Morris, O., Bakowski, D. and Parekh, A. B. (2014) 'Dynamic assembly of a membrane signaling complex enables selective activation of NFAT by orai1', *Current Biology*, 24(12), pp. 1361–1368. doi: 10.1016/j.cub.2014.04.046.

Karashima, Y., Talavera, K., Everaerts, W., Janssens, A., Kwan, K. Y., Vennekens, R., Nilius, B. and Voets, T. (2009) 'TRPA1 acts as a cold sensor in vitro and in vivo', *Proceedings of the National Academy of Sciences*. National Academy of Sciences, 106(4), pp. 1273–1278. doi: 10.1073/pnas.0808487106.

Keatinge, W. R. (1957) 'The effect of general chilling on the vasodilator response to cold.', *The Journal of physiology*, 139(3), pp. 497–507.

Kellogg, D. L., Hodges, G. J., Orozco, C. R., Phillips, T. M., Zhao, J. L. and Johnson, J. M. (2007) 'Cholinergic mechanisms of cutaneous active vasodilation during heat stress in cystic fibrosis', *Journal of Applied Physiology*. American Physiological Society, 103(3), pp. 963–968. doi: 10.1152/japplphysiol.00278.2007.

Kellogg, D. L., Johnson, J. M. and Kosiba, W. a (1989) 'Selective abolition of adrenergic vasoconstrictor responses in skin by local iontophoresis of bretylium.', *The American journal of physiology*. American Physiological Society Bethesda, MD , 257(5 Pt 2), pp. H1599–H1606. doi: 10.1152/ajpheart.1989.257.5.H1599.

Kellogg, D. L., Zhao, J. L. and Wu, Y. (2008) 'Neuronal nitric oxide synthase control mechanisms in the cutaneous vasculature of humans in vivo', *Journal of Physiology*. American Physiological Society, 586(3), pp. 847–857. doi: 10.1113/jphysiol.2007.144642.

Kellogg, D. L., Zhao, J. L., Wu, Y. and Johnson, J. M. (2010) 'VIP/PACAP receptor mediation of cutaneous active vasodilation during heat stress in humans', *Journal of Applied Physiology*. American Physiological Society Bethesda, MD, 109(1), pp. 95–100. doi: 10.1152/japplphysiol.01187.2009.

Ketchum, K. A., Joiner, W. J., Sellers, A. J., Kaczmarek, L. K. and Goldstein, S. A. N. (1995) 'A new family of outwardly rectifying potassium channel proteins with two pore domains in tandem', *Nature*. Nature Publishing Group, 376(6542), pp. 690–695. doi: 10.1038/376690a0.

Kimura, K., Takeuchi, H., Yuri, K. and Wakayama, I. (2013) 'Effects of nitric oxide synthase inhibition on cutaneous vasodilation in response to acupuncture stimulation in

humans', *Acupuncture in Medicine*. American Physiological SocietyBethesda, MD , 31(1), pp. 74–80. doi: 10.1136/acupmed-2012-010177.

Knowlton, W. M., Bifolck-Fisher, A., Bautista, D. M. and McKemy, D. D. (2010) 'TRPM8, but not TRPA1, is required for neural and behavioral responses to acute noxious cold temperatures and cold-mimetics in vivo', *Pain*. 2010/06/15, 150(2), pp. 340–350. doi: 10.1016/j.pain.2010.05.021.

Kochegarov, A. A. (2003) 'Pharmacological modulators of voltage-gated calcium channels and their therapeutical application', *Cell Calcium*, 33(3), pp. 145–162. doi: 10.1016/S0143-4160(02)00239-7.

Kodji, X., Aubdool, A. A. and Brain, S. D. (2016) 'Evidence for physiological and pathological roles for sensory nerves in the microvasculature and skin', *Current Research in Translational Medicine*. Elsevier Masson SAS, 64(4), pp. 195–201. doi: 10.1016/j.retram.2016.09.002.

Kopp-Scheinpflug, C., Pigott, B. M. and Forsythe, I. D. (2015) 'Nitric oxide selectively suppresses IH currents mediated by HCN1-containing channels', *Journal of Physiology*, 593(7), pp. 1685–1700. doi: 10.1113/jphysiol.2014.282194.

Korzhevskii, D. E., Otellin, V. A., Grigor'ev, I. P., Petrova, E. S., Gilerovich, E. G. and Zin'kova, N. N. (2007) '[Immunocytochemical demonstration of neuronal NO-synthase in rat brain cells]', *Morfologiia*, 132(4), pp. 77–80.

Kostyuk, E., Voitenko, N., Kruglikov, I., Shmigol, A., Shishkin, V., Efimov, A. and Kostyuk, P. (2001) 'Diabetes-induced changes in calcium homeostasis and the effects of calcium channel blockers in rat and mice nociceptive neurons', *Diabetologia*. Springer-Verlag, 44(10), pp. 1302–1309. doi: 10.1007/s001250100642.

Kwan, H., Huang, Y. and Yao, X. C. N.-C. (2000) 'Store-operated calcium entry in vascular endothelial cells is inhibited by cGMP via a protein kinase G-dependent mechanism', *J Biol Chem*, 275(10), pp. 6758–6763.

Kwan, K. Y., Allchorne, A. J., Vollrath, M. A., Christensen, A. P., Zhang, D. S., Woolf, C. J. and Corey, D. P. (2006) 'TRPA1 contributes to cold, mechanical, and chemical nociception but is not essential for hair-cell transduction', *Neuron*. 2006/04/25, 50(2), pp. 277–289. doi: 10.1016/j.neuron.2006.03.042.

Kwan, K. Y. and Corey, D. P. (2009) 'Burning Cold: Involvement of TRPA1 in Noxious Cold Sensation', *The Journal of General Physiology*. 2009/02/25, 133(3), pp. 251–256. doi: 10.1085/jgp.200810146.

Kwon, J., An, H., Sa, M., Won, J., Shin, J. I. and Lee, C. J. (2017) 'Orai1 and Orai3 in Combination with Stim1 Mediate the Majority of Store-operated Calcium Entry in Astrocytes', *Experimental Neurobiology*, 26(1), p. 42. doi: 10.5607/en.2017.26.1.42.

de la Peña, E., Mälkiä, A., Cabedo, H., Belmonte, C. and Viana, F. (2005) 'The contribution of TRPM8 channels to cold sensing in mammalian neurones', *Journal of Physiology*, 567(2), pp. 415–426. doi: 10.1113/jphysiol.2005.086546.

Lalonde, J., Saia, G. and Gill, G. (2014) 'Store-Operated Calcium Entry Regulates Transcription Factor Sp4 in Resting Neurons', *Science signaling*, 7(328), pp. 1–14.

Landsberg, L. (2012) 'Core temperature: a forgotten variable in energy expenditure and obesity?', *Obesity Reviews*. Wiley/Blackwell (10.1111), 13, pp. 97–104. doi: 10.1111/j.1467-789X.2012.01040.x.

Lee, K. and Mack, G. W. (2006) 'Role of nitric oxide in methacholine-induced sweating and vasodilation in human skin.', *Journal of applied physiology (Bethesda, Md. : 1985)*, 100(4), pp. 1355–1360. doi: 10.1152/japplphysiol.00122.2005.

Lee, S. J. and Stull, J. T. (1998) 'Calmodulin-dependent regulation of inducible and neuronal nitric-oxide synthase', *Journal of Biological Chemistry*, 273(42), pp. 27430–27437. doi: 10.1074/jbc.273.42.27430.

Lesage, F., Terrenoire, C., Romey, G. and Lazdunski, M. (2000) 'Human TREK2, a 2P domain mechano-sensitive K+ channel with multiple regulations by polyunsaturated fatty acids, lysophospholipids, and Gs, Gi, and Gq protein-coupled receptors', *J Biol Chem*. 2000/07/06, 275(37), pp. 28398–28405. doi: 10.1074/jbc.M002822200.

Lewis, T. (1930) 'Observations upon the reactions of the vessels of the human skin to cold', *Heart*, 15(2), pp. 177–208.

Li, X. J., Blackshaw, S. and Snyder, S. H. (1994) 'Expression and localization of amiloride-sensitive sodium channel indicate a role for non-taste cells in taste perception.', *Proceedings of the National Academy of Sciences of the United States of America*. National Academy of Sciences, 91(5), pp. 1814–8. doi: 10.1073/PNAS.91.5.1814.

Lim, S., Honek, J., Xue, Y., Seki, T., Cao, Z., Andersson, P., Yang, X., Hosaka, K. and Cao, Y. (2012) 'Cold-induced activation of brown adipose tissue and adipose angiogenesis in mice', *Nat Protoc*. 2012/03/03, 7(3), pp. 606–615. doi: 10.1038/nprot.2012.013.

Lin, S., Fagan, K. A., Li, K., Shaul, P. W., Cooper, D. M. F. and Rodman, D. M. (2000)

'Sustained Endothelial Nitric-oxide Synthase Activation Requires Capacitative Ca 2 Entry *', *Biochemistry*, 275(24), pp. 17979–17985.

Lin, W., Finger, T. E., Rossier, B. C. and Kinnamon, S. C. (1999) 'Epithelial Na+ channel subunits in rat taste cells: Localization and regulation by aldosterone', *The Journal of Comparative Neurology*. Wiley-Blackwell, 405(3), pp. 406–420. doi: 10.1002/(SICI)1096-9861(19990315)405:3<406::AID-CNE10>3.0.CO;2-F.

Lirk, P., Poroli, M., Rigaud, M., Fuchs, A., Fillip, P., Huang, C. Y., Ljubkovic, M., Sapunar, D. and Hogan, Q. (2008) 'Modulators of calcium influx regulate membrane excitability in rat dorsal root ganglion neurons', *Anesthesia and Analgesia*, 107(2), pp. 673–685. doi: 10.1213/ane.0b013e31817b7a73.

Livak, K. J. and Schmittgen, T. D. (2001) 'Analysis of relative gene expression data using real-time quantitative PCR and the 2-ΔΔCT method', *Methods*, 25(4), pp. 402–408. doi: 10.1006/meth.2001.1262.

Lloyd, D. P. C. (1961) 'Temperature and the Action of Sweat Glands', *Proceedings of the National Academy of Sciences*. National Academy of Sciences, 47(3), pp. 358–362. doi: 10.1073/pnas.47.3.358.

Long, R. R. (1977) 'Sensitivity of cutaneous cold fibers to noxious heat: paradoxical cold discharge.', *Journal of neurophysiology*. American Physiological Society Bethesda, MD , 40(3), pp. 489–502. doi: 10.1152/jn.1977.40.3.489.

Loscalzo, J. (2013) 'The identification of nitric oxide as endothelium-derived relaxing factor', *Circulation Research*, 113(2), pp. 100–103. doi: 10.1161/CIRCRESAHA.113.301577.

Low, P. A. (1993) 'Evaluation of autonomic function in the autonomic disorders', *Journal of the Autonomic Nervous System*. Elsevier, 43, pp. 27–29. doi: 10.1016/0165-1838(93)90143-I.

Loy, B., Apostolova, G., Dorn, R., McGuire, V. a, Arthur, J. S. C. and Dechant, G. (2011) 'p38{alpha} and p38{beta} Mitogen-Activated Protein Kinases Determine Cholinergic Transdifferentiation of Sympathetic Neurons.', *The Journal of neuroscience : the official journal of the Society for Neuroscience*, 31(34), pp. 12059–12067. doi: 10.1523/JNEUROSCI.0448-11.2011.

Lu, B. and Fivaz, M. (2016) 'Neuronal SOCE: Myth or Reality?', *Trends in Cell Biology*, 26(12), pp. 890–893. doi: 10.1016/j.tcb.2016.09.008.

Lu, S. G. and Gold, M. S. (2008) 'Inflammation-induced increase in evoked calcium

transients in subpopulations of rat dorsal root ganglion neurons', *Neuroscience*. Pergamon, 153(1), pp. 279–288. doi: 10.1016/j.neuroscience.2008.02.006.

Ma, X. Y., Yu, J. M., Zhang, S. Z., Liu, X. Y., Wu, B. H., Wei, X. L., Yan, J. Q., Sun, H. L., Yan, H. T. and Zheng, J. Q. (2011) 'External Ba2+ block of the two-pore domain potassium channel TREK-1 defines conformational transition in its selectivity filter', *J Biol Chem*. 2011/10/04, 286(46), pp. 39813–39822. doi: 10.1074/jbc.M111.264788.

MacIntyre, B. A., Bullard, R. W., Banerjee, M. and Elizondo, R. (1968) 'Mechanism of enhancement of eccrine sweating by localized heating.', *Journal of Applied Physiology*, 25(3), pp. 255–260. doi: 10.1152/jappl.1968.25.3.255.

Macpherson, L. J., Hwang, S. W., Miyamoto, T., Dubin, A. E., Patapoutian, A. and Story, G. M. (2006) 'More than cool: promiscuous relationships of menthol and other sensory compounds', *Mol Cell Neurosci*. 2006/07/11, 32(4), pp. 335–343. doi: 10.1016/j.mcn.2006.05.005.

Madisen, L., Garner, A. R., Shimaoka, D., Chuong, A. S., Klapoetke, N. C., Li, L., van der Bourg, A., Niino, Y., Egolf, L., Monetti, C., Gu, H., Mills, M., Cheng, A., Tasic, B., Nguyen, T. N., Sunkin, S. M., Benucci, A., Nagy, A., Miyawaki, A., Helmchen, F., Empson, R. M., Knöpfel, T., Boyden, E. S., Reid, R. C., Carandini, M. and Zeng, H. (2015) 'Transgenic mice for intersectional targeting of neural sensors and effectors with high specificity and performance', *Neuron*, 85(5), pp. 942–958. doi: 10.1016/j.neuron.2015.02.022.

Madrid, R., de la Pena, E., Donovan-Rodriguez, T., Belmonte, C. and Viana, F. (2009) 'Variable Threshold of Trigeminal Cold-Thermosensitive Neurons Is Determined by a Balance between TRPM8 and Kv1 Potassium Channels', *Journal of Neuroscience*, 29(10), pp. 3120–3131. doi: 10.1523/JNEUROSCI.4778-08.2009.

Maingret, F., Lauritzen, I., Patel, A. J., Heurteaux, C., Reyes, R., Lesage, F., Lazdunski, M. and Honore, E. (2000) 'TREK-1 is a heat-activated background K(+) channel', *EMBO J.* 2000/06/03, 19(11), pp. 2483–2491. doi: 10.1093/emboj/19.11.2483.

Majeed, Y., Bahnasi, Y., Seymour, V. A. L., Wilson, L. A., Milligan, C. J., Agarwal, A. K., Sukumar, P., Naylor, J. and Beech, D. J. (2011) 'Rapid and contrasting effects of rosiglitazone on transient receptor potential TRPM3 and TRPC5 channels.', *Molecular pharmacology*, 79(6), pp. 1023–30. doi: 10.1124/mol.110.069922.

Mak, S., Zhang, X. and McNaughton, P. (2010) 'Thermosensation', *Encyclopedia of*

Life Sciences.

Mamasuew, K., Michalakis, S., Breer, H., Biel, M. and Fleischer, J. (2010) 'The cyclic nucleotide-gated ion channel CNGA3 contributes to coolness-induced responses of Grueneberg ganglion neurons', *Cellular and Molecular Life Sciences*. SP Birkhäuser Verlag Basel, 67(11), pp. 1859–1869. doi: 10.1007/s00018-010-0296-8.

Mancarella, S., Wang, Y. and Gill, D. L. (2011) 'STIM1 senses both Ca 2 + and heat', *Nature Publishing Group*. Nature Publishing Group, 7(6), pp. 344–345. doi: 10.1038/nchembio.587.

Manteniotis, S., Lehmann, R., Flegel, C., Vogel, F., Hofreuter, A., Schreiner, B. S. P., Altmüller, J., Becker, C., Schöbel, N., Hatt, H. and Gisselmann, G. (2013) 'Comprehensive RNA-Seq expression analysis of sensory ganglia with a focus on ion channels and GPCRs in trigeminal ganglia', *PLoS ONE*, 8(11), pp. 1–30. doi: 10.1371/journal.pone.0079523.

van Marken Lichtenbelt, W. D., Vanhommerig, J. W., Smulders, N. M., Drossaerts, J. M., Kemerink, G. J., Bouvy, N. D., Schrauwen, P. and Teule, G. J. (2009) 'Cold-activated brown adipose tissue in healthy men', *N Engl J Med*. 2009/04/10, 360(15), pp. 1500–1508. doi: 10.1056/NEJMoa0808718.

Masliukov, P. M. (2013) 'Neurotransmitters in the sympathetic nervous system: Developmental aspects', *Brain Research Journal*, 6(2), pp. 149–170.

Masliukov, P. M., Emanuilov, A. I., Madalieva, L. V, Moiseev, K. Y., Bulibin, A. V, Korzina, M. B., Porseva, V. V, Korobkin, A. A. and Smirnova, V. P. (2014) 'Development of nNOS-positive neurons in the rat sensory and sympathetic ganglia', *Neuroscience*, 256(0), pp. 271–281. doi: http://dx.doi.org/10.1016/j.neuroscience.2013.10.013.

Masliukov, P. M., Emanuilov, A. I., Moiseev, K., Nozdrachev, A. D., Dobrotvorskaya, S. and Timmermans, J.-P. (2015) 'Development of non-catecholaminergic sympathetic neurons in para- and prevertebral ganglia of cats', *International Journal of Developmental Neuroscience*, 40, pp. 76–84. doi: 10.1016/j.ijdevneu.2014.12.004.

Masliukov, P. M., Konovalov, V. V, Emanuilov, A. I. and Nozdrachev, A. D. (2012) 'Development of neuropeptide Y-containing neurons in sympathetic ganglia of rats', *Neuropeptides*, 46(6), pp. 345–352. doi: http://dx.doi.org/10.1016/j.npep.2012.08.003.

McBurney, D. H., Collings, V. B. and Glanz, L. M. (1973) 'Temperature dependence

of human taste responses', *Physiology & Behavior*. Elsevier, 11(1), pp. 89–94. doi: 10.1016/0031-9384(73)90127-3.

McCorry, L. K. (2007) 'Physiology of the autonomic nervous system', *American Journal of Pharmaceutical Education*, 71(4). doi: 10.5688/aj710478.

McKemy, D. D., Neuhausser, W. M. and Julius, D. (2002) 'Identification of a cold receptor reveals a general role for TRP channels in thermosensation', *Nature*. 2002/03/08, 416(6876), pp. 52–58. doi: 10.1038/nature719.

Mcnamara, T. C., Keen, J. T., Simmons, G. H., Alexander, L. M. and Wong, B. J. (2014) 'Endothelial nitric oxide synthase mediates the nitric oxide component of reflex cutaneous vasodilatation during dynamic exercise in humans', *Journal of Physiology*. Wiley/Blackwell (10.1111), 592(23), pp. 5317–5326. doi: 10.1113/jphysiol.2014.272898.

Medhurst, A. D., Rennie, G., Chapman, C. G., Meadows, H., Duckworth, M. D., Kelsell, R. E., Gloger II and Pangalos, M. N. (2001) 'Distribution analysis of human two pore domain potassium channels in tissues of the central nervous system and periphery', *Brain Res Mol Brain Res*. 2001/02/13, 86(1–2), pp. 101–114.

Memon, T., Chase, K., Leavitt, L. S., Olivera, B. M. and Teichert, R. W. (2017) 'TRPA1 expression levels and excitability brake by KVchannels influence cold sensitivity of TRPA1-expressing neurons', *Neuroscience*. IBRO, 353, pp. 76–86. doi: 10.1016/j.neuroscience.2017.04.001.

Miljanich, G. P. and Ramachandran, J. (1995) 'Antagonists of neuronal calcium channels: structure, function, and therapeutic implications', *Annu Rev Pharmacol Toxicol*, 35(1), pp. 707–734. doi: 10.1146/annurev.pa.35.040195.003423.

Miller, R. J. (1991) 'The Control of Neuronal Ca++ Homeostasis', *Progress in neurobiology*, 37, pp. 255–285. doi: 10.1016/0301-0082(91)90028-Y.

Miura, S., Takahashi, K., Imagawa, T., Uchida, K., Saito, S., Tominaga, M. and Ohta, T. (2013) 'Involvement of TRPA1 activation in acute pain induced by cadmium in mice', *Molecular Pain*, 9(1), pp. 1–10. doi: 10.1186/1744-8069-9-7.

Miyano, K., Tang, H. Bin, Nakamura, Y., Morioka, N., Inoue, A. and Nakata, Y. (2009) 'Paclitaxel and vinorelbine, evoked the release of substance P from cultured rat dorsal root ganglion cells through different PKC isoform-sensitive ion channels', *Neuropharmacology*. Elsevier Ltd, 57(1), pp. 25–32. doi: 10.1016/j.neuropharm.2009.04.001.

Morenilla-Palao, C., Luis, E., Fernandez-Pena, C., Quintero, E., Weaver, J. L., Bayliss, D. a and Viana, F. (2014) 'Ion Channel Profile of TRPM8 Cold Receptors Reveals a Role of TASK-3 Potassium Channels in Thermosensation', *Cell*, pp. 1571–1582. doi: 10.1016/j.celrep.2014.08.003.

Mori, N., Kurata, M., Yamazaki, H., Hosokawa, H., Nadamoto, T., Inoue, K. and Fushiki, T. (2013) 'Intragastric Administration of Allyl Isothiocyanate Reduces Hyperglycemia in Intraperitoneal Glucose Tolerance Test (IPGTT) by Enhancing Blood Glucose Consumption in Mice', *Journal of Nutritional Science and Vitaminology*. Center for Academic Publications Japan, 59(1), pp. 56–63. doi: 10.3177/jnsv.59.56.

Morrison, S. F. (2004) 'Central pathways controlling brown adipose tissue thermogenesis.', *News in physiological sciences : an international journal of physiology produced jointly by the International Union of Physiological Sciences and the American Physiological Society*, 19, pp. 67–74. doi: 10.1152/nips.01502.2003.

Morrison, S. F. (2011) '2010 Carl Ludwig Distinguished Lectureship of the APS Neural Control and Autonomic Regulation Section: Central neural pathways for thermoregulatory cold defense', *Journal of Applied Physiology*, 110(5), pp. 1137–1149. doi: 10.1152/japplphysiol.01227.2010.

Morrison, S. F. (2016) 'Central neural control of thermoregulation and brown adipose tissue', *Autonomic Neuroscience: Basic and Clinical*. Elsevier B.V., 196, pp. 14–24. doi: 10.1016/j.autneu.2016.02.010.

Munns, C., AlQatari, M. and Koltzenburg, M. (2007) 'Many cold sensitive peripheral neurons of the mouse do not express TRPM8 or TRPA1.', *Cell Calcium*, 41, pp. 331–342. doi: 10.1016/j.ceca.2006.07.008.

Musa, R. and Qurie, A. (2018) *Raynauds Disease (Raynauds Phenomenon, Raynauds Syndrome)*, *StatPearls*. StatPearls Publishing.

Nadal, A., Fuentes, E., Pastor, J. and McNaughton, P. A. (1995) 'Plasma albumin is a potent trigger of calcium signals and DNA synthesis in astrocytes.', *Proceedings of the National Academy of Sciences of the United States of America*, 92(5), pp. 1426–30. doi: 10.1073/pnas.92.5.1426.

Nadel, E. R., Bullard, R. W. and Stolwijk, J. A. (1971) 'Importance of skin temperature in the regulation of sweating', *J Appl Physiol*. 1971/07/01, 31(1), pp. 80–87.

Nagata, K. (2005) 'Nociceptor and Hair Cell Transducer Properties of TRPA1, a Channel for Pain and Hearing', *Journal of Neuroscience*, 25(16), pp. 4052–4061. doi:

10.1523/JNEUROSCI.0013-05.2005.

Nagatsu, T., Levitt, M. and Udenfriend, S. (1964) 'Tyrosine Hydroxylase', *The Journal of biological chemistry*, 239(September), pp. 2910–2917.

Namer, B., Bickel, A., Krämer, H., Birklein, F. and Schmelz, M. (2004) 'Chemically and electrically induced sweating and flare reaction', *Autonomic Neuroscience: Basic and Clinical*. Elsevier, 114(1–2), pp. 72–82. doi: 10.1016/j.autneu.2004.06.007.

Narouze, S., Vydyanathan, A. and Patel, N. (2007) 'Ultrasound-guided stellate ganglion block successfully prevented esophageal puncture.', *Pain physician*, 10(6), pp. 747–752.

Nelms, J. D. and Soper, D. J. G. (1962) 'Cold vasodilatation and cold acclimatization in the hands of British fish filleters', *J Appl Physiol*, 17(3), pp. 444–448.

Nelson, H. A. and Roe, M. W. (2018) 'Molecular physiology and pathophysiology of stromal interaction molecules', *Experimental Biology and Medicine*. SAGE PublicationsSage UK: London, England, 243(5), pp. 451–472. doi: 10.1177/1535370218754524.

Noël, J., Zimmermann, K., Busserolles, J., Deval, E., Alloui, A., Diochot, S., Guy, N., Borsotto, M., Reeh, P., Eschalier, A., Lazdunski, M., Noel, J., Zimmermann, K., Busserolles, J., Deval, E., Alloui, A., Diochot, S., Guy, N., Borsotto, M., Reeh, P., Eschalier, A. and Lazdunski, M. (2009) 'The mechano-activated K+ channels TRAAK and TREK-1 control both warm and cold perception', *EMBO J*, 28(9), pp. 1308–1318. doi: 10.1038/emboj.2009.57.

Noël, J., Zimmermann, K., Busserolles, J. J. J., Deval, E., Alloui, A., Diochot, S., Guy, N., Borsotto, M., Reeh, P., Eschalier, A., Lazdunski, M., Noel, J., Zimmermann, K., Busserolles, J. J. J., Deval, E., Alloui, A., Diochot, S., Guy, N., Borsotto, M., Reeh, P., Eschalier, A., Lazdunski, M., Noël, J., Zimmermann, K., Busserolles, J. J. J., Deval, E., Alloui, A., Diochot, S., Guy, N., Borsotto, M., Reeh, P., Eschalier, A. and Lazdunski, M. (2009) 'The mechano-activated K+ channels TRAAK and TREK-1 control both warm and cold perception', *The EMBO journal*, 28(9), pp. 1308–1318. doi: 10.1038/emboj.2009.57.

Ogawa, T. (1970) 'Local effect of skin temperature on threshold concentration of sudorific agents.', *Journal of applied physiology*, 28(1), pp. 18–22. doi: 10.1152/jappl.1970.28.1.18.

Ogawa, T. and Asayama, M. (1986) 'Quantitative analysis of the local effect of skin

temperature on sweating.', *The Japanese journal of physiology*. THE PHYSIOLOGICAL SOCIETY OF JAPAN, 36(2), pp. 417–422. doi: 10.2170/jjphysiol.36.417.

Ogawa, T. and Sugenoya, J. (1993) 'Pulsatile sweating and sympathetic sudomotor activity', *Japanese Journal of Physiology*. THE PHYSIOLOGICAL SOCIETY OF JAPAN, pp. 275–289. doi: 10.2170/jjphysiol.43.275.

Oh-Hora, M., Yamashita, M., Hogan, P. G., Sharma, S., Lamperti, E., Chung, W., Prakriya, M., Feske, S. and Rao, A. (2008) 'Dual functions for the endoplasmic reticulum calcium sensors STIM1 and STIM2 in T cell activation and tolerance.', *Nature Immunology*. Nature Publishing Group, 9(4), pp. 432–443. doi: 10.1038/ni1574.

Okada, T., Shimizu, S., Wakamori, M., Maeda, A., Kurosaki, T., Takada, N., Imoto, K. and Mori, Y. (1998) 'Molecular cloning and functional characterization of a novel receptor-activated TRP Ca2+ channel from mouse brain', *J Biol Chem*. 1998/05/30, 273(17), pp. 10279–10287.

de Oliveira, C., Garami, A., Lehto, S. G., Pakai, E., Tekus, V., Pohoczky, K., Youngblood, B. D., Wang, W., Kort, M. E., Kym, P. R., Pinter, E., Gavva, N. R. and Romanovsky, A. A. (2014) 'Transient receptor potential channel ankyrin-1 is not a cold sensor for autonomic thermoregulation in rodents', *J Neurosci*. 2014/03/29, 34(13), pp. 4445–4452. doi: 10.1523/jneurosci.5387-13.2014.

Oliver, A. E., Baker, G. A., Fugate, R. D., Tablin, F. and Crowe, J. H. (2000) 'Effects of temperature on calcium-sensitive fluorescent probes', *Biophys J*, 78(4), pp. 2116–2126. doi: 10.1016/S0006-3495(00)76758-0.

Palty, R., Fu, Z. and Isacoff, E. Y. (2017) 'Sequential Steps of CRAC Channel Activation', *Cell Reports*. ElsevierCompany., 19(9), pp. 1929–1939. doi: 10.1016/j.celrep.2017.05.025.

Pan, B., Guo, Y., Wu, H., Park, J., Trinh, V. N., Luo, Z. D. and Hogan, Q. H. (2016) 'gated Ca 2 1 channel subtypes in sensory neurons after nerve injury', 157, pp. 2068–2080.

Parekh, A. B. and Putney, J. W. (2005) 'Store-operated calcium channels', *Physiological reviews*, 85(2), pp. 757–810. doi: 10.1152/physrev.00057.2003.

Park, C. Y., Shcheglovitov, A. and Dolmetsch, R. (2010) 'The CRAC channel activator STIM1 binds and inhibits L-type voltage-gated calcium channels.', *Science (New York, N.Y.)*. American Association for the Advancement of Science, 330(6000), pp. 101–5.

doi: 10.1126/science.1191027.

Park, J. F. and Luo, Z. D. (2010) 'Calcium channel functions in pain processing', *Channels*. Taylor & Francis, 4(6), pp. 510–517. doi: 10.4161/chan.4.6.12869.

Peier, A. M., Moqrich, A., Hergarden, A. C., Reeve, A. J., Andersson, D. A., Story, G. M., Earley, T. J., Dragoni, I., McIntyre, P., Bevan, S. and Patapoutian, A. (2002) 'A TRP channel that senses cold stimuli and menthol', *Cell*. 2002/03/15, 108(5), pp. 705–715.

Pereira, V., Busserolles, J., Christin, M., Devilliers, M., Poupon, L., Legha, W., Alloui, A., Aissouni, Y., Bourinet, E., Lesage, F., Eschalier, A., Lazdunski, M. and Noël, J. (2014) 'Role of the TREK2 potassium channel in cold and warm thermosensation and in pain perception', *Pain*, 155(12), pp. 2534–2544. doi: 10.1016/j.pain.2014.09.013.

Pereira, V., Busserolles, J., Christin, M., Devilliers, M., Poupon, L., Legha, W., Alloui, A., Aissouni, Y., Bourinet, E., Lesage, F., Eschalier, A., Lazdunski, M., Noël, J. and Noel, J. (2014) 'Role of the TREK2 potassium channel in cold and warm thermosensation and in pain perception', *Pain*. International Association for the Study of Pain, 155(12), pp. 2534–2544. doi: 10.1016/j.pain.2014.09.013.

Philipp, S., Hambrecht, J., Braslavski, L., Schroth, G., Freichel, M., Murakami, M., Cavalie, A. and Flockerzi, V. (1998) 'A novel capacitative calcium entry channel expressed in excitable cells', *EMBO J*. 1998/08/04, 17(15), pp. 4274–4282. doi: 10.1093/emboj/17.15.4274.

Pollema-Mays, S. L., Centeno, M. V, Ashford, C. J., Apkarian, A. V and Martina, M. (2013) 'Expression of background potassium channels in rat DRG is cell-specific and down-regulated in a neuropathic pain model', *Mol Cell Neurosci*. 2013/09/03, 57, pp. 1–9. doi: 10.1016/j.mcn.2013.08.002.

Prakriya, M. and Lewis, R. S. (2015) 'Store-Operated Calcium Channels', *Physiological reviews*, 95(4), pp. 1383–1436. doi: 10.1152/physrev.00020.2014.

Price, M. P., Lewin, G. R., McIlwrath, S. L., Cheng, C., Xie, J., Heppenstall, P. A., Stucky, C. L., Mannsfeldt, A. G., Brennan, T. J., Drummond, H. A., Qiao, J., Benson, C. J., Tarr, D. E., Hrstka, R. F., Yang, B., Williamson, R. A. and Welsh, M. J. (2000) 'The mammalian sodium channel BNC1 is required for normal touch sensation', *Nature*. Nature Publishing Group, 407(6807), pp. 1007–1011. doi: 10.1038/35039512.

Putney, J. W. (1986) 'A model for receptor-regulated calcium entry', *Cell Calcium*, 7(1), pp. 1–12. doi: 10.1016/0143-4160(86)90026-6.

Puyaubert, J. and Baudouin, E. (2014) 'New clues for a cold case: Nitric oxide response to low temperature', *Plant, Cell and Environment*, 37(12), pp. 2623–2630. doi: 10.1111/pce.12329.

Qi, Z., Wang, Y., Zhou, H., Liang, N., Yang, L., Liu, L. and Zhang, W. (2016) 'The Central Analgesic Mechanism of YM-58483 in Attenuating Neuropathic Pain in Rats', *Cellular and Molecular Neurobiology*. Springer US, 36(7), pp. 1035–1043. doi: 10.1007/s10571-015-0292-5.

Ran, C., Hoon, M. A. and Chen, X. (2016) 'The coding of cutaneous temperature in the spinal cord', *Nature Neuroscience*, 19(July), pp. 1–11. doi: 10.1038/nn.4350.

Rand, R. P., Burton, A. C. and Ing, T. (1965) 'the Tail of the Rat, in Temperature Regulation and Acclimatization', *Canadian Journal of Physiology and Pharmacology*. NRC Research Press Ottawa, Canada , 43(2), pp. 257–267. doi: 10.1139/y65-025.

Reid, G. (2005) 'ThermoTRP channels and cold sensing: What are they really up to?', *Pflugers Archiv European Journal of Physiology*, 451(1), pp. 250–263. doi: 10.1007/s00424-005-1437-z.

Reid, G., Babes, A. and Pluteanu, F. (2002) 'A cold- and menthol-activated current in rat dorsal root ganglion neurones: properties and role in cold transduction', *The Journal of Physiology*. Wiley/Blackwell (10.1111), 545(2), pp. 595–614. doi: 10.1113/jphysiol.2002.024331.

Reid, G. and Flonta, M.-L. (2001) 'Cold current in thermoreceptive neurons', *Nature*. Nature Publishing Group, 413(6855), pp. 480–480. doi: 10.1038/35097164.

Reid, G. and Flonta, M. (2001) 'Thermoreceptive Neurons', *October*, 413(October), pp. 2001–2001.

Reid, G. and Flonta, M. L. (2001) 'Cold transduction by inhibition of a background potassium conductance in rat primary sensory neurones', *Neuroscience Letters*, 297(3), pp. 171–174. doi: 10.1016/S0304-3940(00)01694-3.

Riccio, A., Medhurst, A. D., Mattei, C., Kelsell, R. E., Calver, A. R., Randall, A. D., Benham, C. D. and Pangalos, M. N. (2002) 'mRNA distribution analysis of human TRPC family in CNS and peripheral tissues', *Brain Res Mol Brain Res*. 2003/01/18, 109(1–2), pp. 95–104.

Rohács, T., Lopes, C. M. B., Michailidis, I. and Logothetis, D. E. (2005) 'PI(4,5)P2regulates the activation and desensitization of TRPM8 channels through the TRP domain', *Nature Neuroscience*, 8(5), pp. 626–634. doi: 10.1038/nn1451.

Romanovsky, A. A. (2007) 'Thermoregulation: some concepts have changed. Functional architecture of the thermoregulatory system', *Am J Physiol Regul Integr Comp Physiol*, 292(1), pp. R37-46. doi: 10.1152/ajpregu.00668.2006.

Rossato, M., Granzotto, M., Macchi, V., Porzionato, A., Petrelli, L., Calcagno, A., Vencato, J., De Stefani, D., Silvestrin, V., Rizzuto, R., Bassetto, F., De Caro, R. and Vettor, R. (2014) 'Human white adipocytes express the cold receptor TRPM8 which activation induces UCP1 expression, mitochondrial activation and heat production', *Mol Cell Endocrinol*. 2013/12/18, 383(1–2), pp. 137–146. doi: 10.1016/j.mce.2013.12.005.

Roussel, C., Erneux, T., Schiffmann, S. N. and Gall, D. (2006) 'Modulation of neuronal excitability by intracellular calcium buffering: From spiking to bursting', *Cell Calcium*, 39(5), pp. 455–466. doi: 10.1016/j.ceca.2006.01.004.

Ruit, K. G., Osborne, P. A., Schmidt, R. E., Johnson Jr., E. M. and Snider, W. D. (1990) 'Nerve growth factor regulates sympathetic ganglion cell morphology and survival in the adult mouse', *J Neurosci*, 10(7), pp. 2412–2419. doi: 10.1523/JNEUROSCI.10-07-02412.1990.

Ruskin, D. N., Anand, R. and LaHoste, G. J. (2007) 'Menthol and nicotine oppositely modulate body temperature in the rat', *Eur J Pharmacol*. 2007/02/17, 559(2–3), pp. 161–164. doi: 10.1016/j.ejphar.2007.01.006.

Saito, S., Banzawa, N., Fukuta, N., Saito, C. T., Takahashi, K., Imagawa, T., Ohta, T. and Tominaga, M. (2014) 'Heat and noxious chemical sensor, chicken TRPA1, as a target of bird repellents and identification of its structural determinants by multispecies functional comparison', *Molecular Biology and Evolution*, 31(3), pp. 708–722. doi: 10.1093/molbev/msu001.

Sawada, Y., Hosokawa, H., Hori, A., Matsumura, K. and Kobayashi, S. (2007) 'Cold sensitivity of recombinant TRPA1 channels', *Brain Res*. 2007/06/26, 1160, pp. 39–46. doi: 10.1016/j.brainres.2007.05.047.

Scholze, a, Plant, T., Dolphin, A. C. and Nürnberg, B. (2001) 'Functional expression and characterization of a voltage-gated CaV1.3 (alpha1D) calcium channel subunit from an insulin-secreting cell line.', *Molecular endocrinology (Baltimore, Md.)*, 15(7), pp. 1211–21. doi: 10.1210/mend.15.7.0666.

Selvaraj, S., Watt, J. A. and Singh, B. B. (2009) 'TRPC1 inhibits apoptotic cell degeneration induced by dopaminergic neurotoxin MPTP/MPP+', *Cell Calcium*, 46(3),

pp. 209–218. doi: 10.1016/j.ceca.2009.07.008.

Shibasaki, M., Wilson, T. E. and Crandall, C. G. (2006) 'Neural control and mechanisms of eccrine sweating during heat stress and exercise', *J Appl Physiol*, 100(5), pp. 1692–1701. doi: 10.1152/japplphysiol.01124.2005.

Silva, J. E. (2006) 'Thermogenic Mechanisms and Their Hormonal Regulation', *Physiological Reviews*. American Physiological Society, 86(2), pp. 435–464. doi: 10.1152/physrev.00009.2005.

Smiles, K. A., Elizondo, R. S. and Barney, C. C. (1976) 'Sweating responses during changes of hypothalamic temperature in the rhesus monkey', *Journal of applied physiology (Bethesda, Md. : 1985)*. 1976/05/01, 40(5), pp. 653–657.

Smith, C. J. and Johnson, J. M. (2016) 'Responses to hyperthermia. Optimizing heat dissipation by convection and evaporation: Neural control of skin blood flow and sweating in humans', *Autonomic Neuroscience: Basic and Clinical*. Elsevier B.V., 196, pp. 25–36. doi: 10.1016/j.autneu.2016.01.002.

Smith, M. P., Beacham, D., Ensor, E. and Koltzenburg, M. (2004) 'Cold-sensitive, menthol-insensitive neurons in the murine sympathetic nervous system.', *Neuroreport*. 2004/06/15, 15(9), pp. 1399–403. doi: 10.1097/01.wnr.0000126559.35631.54.

Smyth, J. T., Beg, A. M., Wu, S., Putney, J. W. and Rusan, N. M. (2012) 'Phosphoregulation of STIM1 leads to exclusion of the endoplasmic reticulum from the mitotic spindle', *Current Biology*, 22(16), pp. 1487–1493. doi: 10.1016/j.cub.2012.05.057.

Spealman, C. R. (1945) 'Effect of Ambient Air Temperature and of Hand Temperature on Blood Flow in Hands', *American Journal of Physiology-Legacy Content*, 145(2), pp. 218–222. doi: 10.1152/ajplegacy.1945.145.2.218.

Spray, D. C. (1986) 'Cutaneous temperature receptors.', *Annual review of physiology*, 48(1), pp. 625–38. doi: 10.1146/annurev.ph.48.030186.003205.

Stavermann, M., Buddrus, K., St. John, J. A., Ekberg, J. A. K., Nilius, B., Deitmer, J. W. and Lohr, C. (2012) 'Temperature-dependent calcium-induced calcium release via InsP3receptors in mouse olfactory ensheathing glial cells', *Cell Calcium*. Elsevier Ltd, 52(2), pp. 113–123. doi: 10.1016/j.ceca.2012.04.017.

Stebe, S., Schellig, K., Lesage, F., Breer, H. and Fleischer, J. (2013) 'The Thermosensitive Potassium Channel TREK-1 Contributes to Coolness-Evoked Responses of Grueneberg Ganglion Neurons', *Cell Mol Neurobiol*. 2013/10/09. doi:

10.1007/s10571-013-9992-x.

Stokes, A., Wakano, C., Koblan-Huberson, M., Adra, C. N., Fleig, A. and Turner, H. (2006) 'TRPA1 is a substrate for de-ubiquitination by the tumor suppressor CYLD', *Cell Signal*. 2006/02/28, 18(10), pp. 1584–1594. doi: 10.1016/j.cellsig.2005.12.009.

Story, G. M., Peier, A. M., Reeve, A. J., Eid, S. R., Mosbacher, J., Hricik, T. R., Earley, T. J., Hergarden, A. C., Andersson, D. A., Hwang, S. W., McIntyre, P., Jegla, T., Bevan, S. and Patapoutian, A. (2003) 'ANKTM1, a TRP-like channel expressed in nociceptive neurons, is activated by cold temperatures', *Cell*. 2003/03/26, 112(6), pp. 819–829.

Su, C. and Su, C. (2013) 'Rhythmic sympathetic nerve discharges in an in vitro neonatal rat brain stem-spinal cord preparation Rhythmic sympathetic nerve discharges in an in vitro neonatal rat brain stem-spinal cord preparation', *Journal of Applied Physiology*. American Physiological SocietyBethesda, MD , 87(3), pp. 1066–1074. doi: 10.1152/jappl.1999.87.3.1066.

Sun, S., Zhang, H., Liu, J., Popugaeva, E., Xu, N. J., Feske, S., White, C. L. and Bezprozvanny, I. (2014) 'Reduced synaptic STIM2 expression and impaired store-operated calcium entry cause destabilization of mature spines in mutant presenilin mice', *Neuron*. Elsevier Inc., 82(1), pp. 79–93. doi: 10.1016/j.neuron.2014.02.019.

Tadaki, N., Tanaka, M., Hisa, Y., Uno, T., Okamura, H., Koike, S. and Ibata, Y. (1996) 'Nitrergic innervation of the rat larynx measured by nitric oxide synthase immunohistochemistry and NADPH-diaphorase histochemistry', *Annals of Otology, Rhinology and Laryngology*, 105(7), pp. 550–554. doi: 10.1177/000348949610500711.

Tajino, K., Matsumura, K., Kosada, K., Shibakusa, T., Inoue, K., Fushiki, T., Hosokawa, H. and Kobayashi, S. (2007) 'Application of menthol to the skin of whole trunk in mice induces autonomic and behavioral heat-gain responses', *Am J Physiol Regul Integr Comp Physiol*. 2007/09/01, 293(5), pp. R2128-35. doi: 10.1152/ajpregu.00377.2007.

Takaki, F., Nakamuta, N., Kusakabe, T. and Yamamoto, Y. (2015) 'Sympathetic and sensory innervation of small intensely fluorescent (SIF) cells in rat superior cervical ganglion', *Cell and Tissue Research*, 359(2), pp. 441–451. doi: 10.1007/s00441-014-2051-1.

Takezawa, R., Cheng, H., Beck, A., Ishikawa, J., Launay, P., Kubota, H., Kinet, J.-P. P., Fleig, A., Yamada, T. and Penner, R. (2006) 'A pyrazole derivative potently inhibits

lymphocyte Ca2+ influx and cytokine production by facilitating transient receptor potential melastatin 4 channel activity.', *Molecular pharmacology*. 2006/01/13, 69(4), pp. 1413–1420. doi: 10.1124/mol.105.021154.

Takezawa, R., Cheng, H., Beck, A., Ishikawa, J., Launay, P., Kubota, H., Kinet, J. P., Fleig, A., Yamada, T. and Penner, R. (2006) 'A pyrazole derivative potently inhibits lymphocyte Ca2+ influx and cytokine production by facilitating transient receptor potential melastatin 4 channel activity', *Mol Pharmacol*. 2006/01/13, 69(4), pp. 1413–1420. doi: 10.1124/mol.105.021154.

Tan, C.-H. (2014) 'Identification of novel thermosensitive mechanisms', Ph.D, University of Cambridge.

Tan, C.-H. and McNaughton, P. A. (2016) 'The TRPM2 ion channel is required for sensitivity to warmth', *Nature*. Nature Publishing Group, 536(7617), pp. 460–463. doi: 10.1038/nature19074.

Tattersall, G. J., Sinclair, B. J., Withers, P. C., Fields, P. A., Seebacher, F., Cooper, C. E. and Maloney, S. K. (2012) 'Coping with thermal challenges: Physiological adaptations to environmental temperatures', *Comprehensive Physiology*, 2(3), pp. 2151–2202. doi: 10.1002/cphy.c110055.

Taylor, D. K., Bubier, J. a., Silva, K. a. and Sundberg, J. P. (2012) 'Development, Structure, and Keratin Expression in C57BL/6J Mouse Eccrine Glands', *Veterinary Pathology*, 49(November 2011), pp. 146–154. doi: 10.1177/0300985811430511.

Taylor, W. F., Bishop, S. and Fred, W. (1993) 'A role for nitric thermoregulatory oxide in active vasodilation', *Am J Physiol (Heart Circ Physiol)*, 264(33), pp. 1355–1359.

Teliban, A., Bartsch, F., Struck, M., Baron, R. and Jänig, W. (2011) 'Axonal thermosensitivity and mechanosensitivity of cutaneous afferent neurons', *European Journal of Neuroscience*, 33(1), pp. 110–118. doi: 10.1111/j.1460-9568.2010.07471.x.

Thastrup, O., Cullen, P. J., Drøbak, B. K., Hanley, M. R. and Dawson, a P. (1990) 'Thapsigargin, a tumor promoter, discharges intracellular Ca2+ stores by specific inhibition of the endoplasmic reticulum Ca2(+)-ATPase.', *Proceedings of the National Academy of Sciences of the United States of America*, 87(7), pp. 2466–2470. doi: 10.1073/pnas.87.7.2466.

Thomas, R. C. (2009) 'The plasma membrane calcium ATPase (PMCA) of neurones is electroneutral and exchanges 2 H+ for each Ca2+ or Ba2+ ion extruded.', *The Journal of physiology*, 587(Pt 2), pp. 315–27. doi: 10.1113/jphysiol.2008.162453.

Thompson, J. L. and Shuttleworth, T. J. (2013) 'How Many Orai's Does It Take to Make a CRAC Channel?', *Scientific Reports*, 3(1), p. 1961. doi: 10.1038/srep01961.

Thompson, M. A., Pabelick, C. M. and Prakash, Y. S. (2009) 'Role of STIM1 in regulation of store-operated Ca2+ influx in pheochromocytoma cells', *Cellular and Molecular Neurobiology*, 29(2), pp. 193–202. doi: 10.1007/s10571-008-9311-0.

Thul, P. J., Åkesson, L., Wiking, M., Mahdessian, D., Geladaki, A., Ait Blal, H., Alm, T., Asplund, A., Björk, L., Breckels, L. M., Bäckström, A., Danielsson, F., Fagerberg, L., Fall, J., Gatto, L., Gnann, C., Hober, S., Hjelmare, M., Johansson, F., Lee, S., Lindskog, C., Mulder, J., Mulvey, C. M., Nilsson, P., Oksvold, P., Rockberg, J., Schutten, R., Schwenk, J. M., Sivertsson, Å., Sjöstedt, E., Skogs, M., Stadler, C., Sullivan, D. P., Tegel, H., Winsnes, C., Zhang, C., Zwahlen, M., Mardinoglu, A., Pontén, F., von Feilitzen, K., Lilley, K. S., Uhlén, M. and Lundberg, E. (2017) 'A subcellular map of the human proteome', *Science*, 356(6340), p. eaal3321. doi: 10.1126/science.aal3321.

Thut, P. D., Wrigley, D. and Gold, M. S. (2003) 'Cold transduction in rat trigeminal ganglia neurons in vitro', *Neuroscience*, 119(4), pp. 1071–1083. doi: 10.1016/S0306-4522(03)00225-2.

Tooyama, I. and Kimura, H. (2000) 'A protein encoded by an alternative splice variant of choline acetyltransferase mRNA is localized preferentially in peripheral nerve cells and fibers', *Journal of Chemical Neuroanatomy*, 17(4), pp. 217–226. doi: 10.1016/S0891-0618(99)00043-5.

Triggle, D. J., Langs, D. A. and Janis, R. A. (1989) 'Ca2+ Channel ligands: Structure-function relationships of the 1,4-dihydropyridines', *Medicinal Research Reviews*, 9(2), pp. 123–180. doi: 10.1002/med.2610090203.

Tsantoulas, C., Lainez, S., Wong, S., Mehta, I., Vilar, B. and McNaughton, P. A. (2017) 'Hyperpolarization-activated cyclic nucleotide-gated 2 (hcn2) ion channels drive pain in mouse models of diabetic neuropathy', *Science Translational Medicine*, 9(409), p. 6072. doi: 10.1126/scitranslmed.aam6072.

Tsavaler, L., Shapero, M. H., Morkowski, S. and Laus, R. (2001) 'Trp-p8, a novel prostate-specific gene, is up-regulated in prostate cancer and other malignancies and shares high homology with transient receptor potential calcium channel proteins', *Cancer Research*. 2001/04/28, 61(9), pp. 3760–3769.

Tseeb, V., Suzuki, M., Oyama, K., Iwai, K. and Ishiwata, S. (2009) 'Highly

thermosensitive Ca $^{2+}$ dynamics in a HeLa cell through IP $_3$ receptors', *HFSP Journal*, 3(2), pp. 117–123. doi: 10.2976/1.3073779.

Ugawa, S., Minami, Y., Guo, W., Saishin, Y., Takatsuji, K., Yamamoto, T., Tohyama, M. and Shimada, S. (1998) 'Receptor that leaves a sour taste in the mouth', *Nature*. Nature Publishing Group, 395(6702), pp. 555–556. doi: 10.1038/26882.

Uhlen, M., Fagerberg, L., Hallstrom, B. M., Lindskog, C., Oksvold, P., Mardinoglu, A., Sivertsson, A., Kampf, C., Sjostedt, E., Asplund, A., Olsson, I., Edlund, K., Lundberg, E., Navani, S., Szigyarto, C. A.-K., Odeberg, J., Djureinovic, D., Takanen, J. O., Hober, S., Alm, T., Edqvist, P.-H., Berling, H., Tegel, H., Mulder, J., Rockberg, J., Nilsson, P., Schwenk, J. M., Hamsten, M., von Feilitzen, K., Forsberg, M., Persson, L., Johansson, F., Zwahlen, M., von Heijne, G., Nielsen, J. and Ponten, F. (2015) 'Tissue-based map of the human proteome', *Science*, 347(6220), pp. 1260419–1260419. doi: 10.1126/science.1260419.

Umemiya, M. and Berger, a J. (1995) 'Single-channel properties of four calcium channel types in rat motoneurons.', *The Journal of neuroscience : the official journal of the Society for Neuroscience*, 15(March), pp. 2218–2224.

Uno, H. (1977) 'Sympathetic innervation of the sweat glands and piloarrector muscles of macaques and human beings', *J Invest Dermatol*. 1977/07/01, 69(1), pp. 112–120.

Usoskin, D., Furlan, A., Islam, S., Abdo, H., Lönnerberg, P., Lou, D., Hjerling-Leffler, J., Haeggström, J., Kharchenko, O., Kharchenko, P. V., Linnarsson, S. and Ernfors, P. (2015) 'Unbiased classification of sensory neuron types by large-scale single-cell RNA sequencing', *Nature Neuroscience*. Nature Publishing Group, 18(1), pp. 145–153. doi: 10.1038/nn.3881.

Vanbeaumont, W. and Bullard, R. W. (1965) 'Sweating: Direct Influence of Skin Temperature.', *Science (New York, N.Y.)*. 1965/03/19, 147(3664), pp. 1465–7.

Vandewauw, I., De Clercq, K., Mulier, M., Held, K., Pinto, S., Van Ranst, N., Segal, A., Voet, T., Vennekens, R., Zimmermann, K., Vriens, J. and Voets, T. (2018) 'A TRP channel trio mediates acute noxious heat sensing', *Nature*. Nature Publishing Group. doi: 10.1038/nature26137.

Vandewauw, I., Owsianik, G. and Voets, T. (2013) 'Systematic and quantitative mRNA expression analysis of TRP channel genes at the single trigeminal and dorsal root ganglion level in mouse', *BMC Neurosci*. BMC Neuroscience, 14, p. 21. doi: 10.1186/1471-2202-14-21.

Vanggaard, L. (1975) 'Physiological reactions to wet-cold.', *Aviation, space, and environmental medicine*, 46(1), pp. 33–36.

Viana, F., de la Peña, E. and Belmonte, C. (2002) 'Specificity of cold thermotransduction is determined by differential ionic channel expression.', *Nature neuroscience*, 5(3), pp. 254–260. doi: 10.1038/nn809.

Viatchenko-Karpinski, V., Ling, J. and Gu, J. G. (2018) 'Characterization of temperature-sensitive leak K+ currents and expression of TRAAK, TREK-1, and TREK2 channels in dorsal root ganglion neurons of rats', *Molecular Brain*. Molecular Brain, 11(1), p. 40. doi: 10.1186/s13041-018-0384-5.

Vig, M., Peinelt, C., Beck, A., Koomoa, D. L., Rabah, D., Koblan-Huberson, M., Kraft, S., Turner, H., Fleig, A., Penner, R. and Kinet, J. P. (2006) 'CRACM1 is a plasma membrane protein essential for store-operated Ca 2+ entry', *Science*, 312(5777), pp. 1220–1223. doi: 10.1126/science.1127883.

Voets, T., Droogmans, G., Wissenbach, U., Janssens, A., Flockerzi, V. and Nilius, B. (2004) 'The principle of temperature-dependent gating in cold- and heat-sensitive TRP channels', *Nature*. 2004/08/13, 430(7001), pp. 748–754. doi: 10.1038/nature02732.

Waldmann, R., Bassilana, F., de Weille, J., Champigny, G., Heurteaux, C. and Lazdunski, M. (1997) 'Molecular cloning of a non-inactivating proton-gated Na+ channel specific for sensory neurons.', *The Journal of biological chemistry*. American Society for Biochemistry and Molecular Biology, 272(34), pp. 20975–8. doi: 10.1074/JBC.272.34.20975.

Waldmann, R., Champigny, G., Bassilana, F., Heurteaux, C. and Lazdunski, M. (1997) 'A proton-gated cation channel involved in acid-sensing', *Nature*. Nature Publishing Group, 386(6621), pp. 173–177. doi: 10.1038/386173a0.

Wang, F., Bélanger, E., Côté, S. L., Desrosiers, P., Prescott, S. A., Côté, D. C. and De Koninck, Y. (2018) 'Sensory Afferents Use Different Coding Strategies for Heat and Cold', *Cell Reports*. Cell Press, 23(7), pp. 2001–2013. doi: 10.1016/J.CELREP.2018.04.065.

Wang, H. and Siemens, J. (2015) 'TRP ion channels in thermosensation, thermoregulation and metabolism', *Temperature*, (May), pp. 00–00. doi: 10.1080/23328940.2015.1040604.

Wang, Y., Deng, X., Mancarella, S., Hendron, E., Eguchi, S., Soboloff, J., Tang, X. D. and Gill, D. L. (2010) 'The calcium store sensor, STIM1, reciprocally controls Orai and

Ca <inf>V</inf>1.2 channels', *Science*, 330(6000), pp. 105–109. doi: 10.1126/science.1191086.

Wang, Y., Deng, X., Mancarella, S., Hendron, E., Eguchi, S., Soboloff, J., Tang, X. D. and Gill, D. L. (2010) 'The Calcium Store Sensor, STIM1, Reciprocally Controls Orai and CaV1.2 Channels', *Science*, 330(6000), pp. 105–109. doi: 10.1126/science.1191086.

Wei, D., Mei, Y., Xia, J. and Hu, H. (2017) 'Orai1 and Orai3 Mediate Store-Operated Calcium Entry Contributing to Neuronal Excitability in Dorsal Root Ganglion Neurons', *Frontiers in Cellular Neuroscience*, 11(December), p. 400. doi: 10.3389/fncel.2017.00400.

Weihe, E., Schutz, B., Hartschuh, W., Anlauf, M., Schafer, M. K. and Eiden, L. E. (2005) 'Coexpression of cholinergic and noradrenergic phenotypes in human and nonhuman autonomic nervous system', *J Comp Neurol*, 492(3), pp. 370–379. doi: 10.1002/cne.20745.

Williams, M. E., Marubio, L. M., Deal, C. R., Hans, M., Brust, P. F., Philipson, L. H., Miller, R. J., Johnson, E. C., Harpold, M. M. and Ellis, S. B. (1994) 'Structure and functional characterization of neuronal alpha 1E calcium channel subtypes.', *The Journal of biological chemistry*, 269(35), pp. 22347–22357.

Winter, Z., Gruschwitz, P., Eger, S., Touska, F. and Zimmermann, K. (2017) 'Cold Temperature Encoding by Cutaneous TRPA1 and TRPM8-Carrying Fibers in the Mouse', *Frontiers in Molecular Neuroscience*, 10(June). doi: 10.3389/fnmol.2017.00209.

Wu, L.-J., Sweet, T.-B. and Clapham, D. E. (2010) 'International Union of Basic and Clinical Pharmacology. LXXVI. Current Progress in the Mammalian TRP Ion Channel Family', *Pharmacological Reviews*. American Society for Pharmacology and Experimental Therapeutics, 62(3), pp. 381–404. doi: 10.1124/pr.110.002725.

Xia, J., Pan, R., Gao, X., Meucci, O. and Hu, H. (2014) 'Native store-operated calcium channels are functionally expressed in mouse spinal cord dorsal horn neurons and regulate resting calcium homeostasis.', *The Journal of physiology*, 592(Pt 16), pp. 3443–61. doi: 10.1113/jphysiol.2014.275065.

Xiao, B., Coste, B., Mathur, J. and Patapoutian, A. (2011) 'Temperature-dependent STIM1 activation induces Ca(2)+ influx and modulates gene expression', *Nat Chem Biol*. Nature Publishing Group, 7(6), pp. 351–358. doi: 10.1038/nchembio.558.

Xu, S.-Z. Z., Zeng, F., Boulay, G., Grimm, C., Harteneck, C. and Beech, D. J. (2005)

'Block of TRPC5 channels by 2-aminoethoxydiphenyl borate: a differential, extracellular and voltage-dependent effect.', *British journal of pharmacology*. 2005/04/05, 145(4), pp. 405–14. doi: 10.1038/sj.bjp.0706197.

Yamamoto, A., Takahashi, K., Saito, S., Tominaga, M. and Ohta, T. (2016) 'Two different avian cold-sensitive sensory neurons: Transient receptor potential melastatin 8 (TRPM8)-dependent and -independent activation mechanisms', *Neuropharmacology*. Elsevier Ltd, 111, pp. 130–141. doi: 10.1016/j.neuropharm.2016.08.039.

Yamashita, M., Yeung, P. S. W., Ing, C. E., McNally, B. A., Pomès, R. and Prakriya, M. (2017) 'STIM1 activates CRAC channels through rotation of the pore helix to open a hydrophobic gate', *Nature Communications*, 8. doi: 10.1038/ncomms14512.

Yang, X. R., Lin, M. J., McIntosh, L. S. and Sham, J. S. (2006) 'Functional expression of transient receptor potential melastatin- and vanilloid-related channels in pulmonary arterial and aortic smooth muscle', *Am J Physiol Lung Cell Mol Physiol*. 2006/01/10, 290(6), pp. L1267-76. doi: 10.1152/ajplung.00515.2005.

Ye, L., Wu, J., Cohen, P., Kazak, L., Khandekar, M. J., Jedrychowski, M. P., Zeng, X., Gygi, S. P. and Spiegelman, B. M. (2013) 'Fat cells directly sense temperature to activate thermogenesis', *Proc Natl Acad Sci U S A*, 110(30), pp. 12480–12485. doi: 10.1073/pnas.1310261110.

Yeromin, A. V., Zhang, S. L., Jiang, W., Yu, Y., Safrina, O. and Cahalan, M. D. (2006) 'Molecular identification of the CRAC channel by altered ion selectivity in a mutant of Orai', *Nature*, 443(7108), pp. 226–229. doi: 10.1038/nature05108.

Zhang, L., Jones, S., Brody, K., Costa, M. and Brookes, S. J. (2004) 'Thermosensitive transient receptor potential channels in vagal afferent neurons of the mouse', *Am J Physiol Gastrointest Liver Physiol*. 2004/01/17, 286(6), pp. G983-91. doi: 10.1152/ajpgi.00441.2003.

Zhang, S. L., Yeromin, A. V, Zhang, X. H., Yu, Y., Safrina, O., Penna, A., Roos, J., Stauderman, K. a and Cahalan, M. D. (2006) 'Genome-wide RNAi screen of Ca 2+ influx identifies genes that regulate Ca 2+ release-activated Ca 2+ channel activity', *Proceedings of the National Academy of Sciences of the United States of America*, 103, pp. 9357–9362. doi: 10.1073/pnas.0603161103.

Zhang, X., Gonzalez-Cobos, J. C., Schindl, R., Muik, M., Ruhle, B., Motiani, R. K., Bisaillon, J. M., Zhang, W., Fahrner, M., Barroso, M., Matrougui, K., Romanin, C. and Trebak, M. (2013) 'Mechanisms of STIM1 Activation of Store-Independent

Leukotriene C4-Regulated Ca2+ Channels', *Molecular and Cellular Biology*, 33(18), pp. 3715–3723. doi: 10.1128/MCB.00554-13.

Zimmermann, K., Leffler, A., Babes, A., Cendan, C. M., Carr, R. W., Kobayashi, J. I., Nau, C., Wood, J. N. and Reeh, P. W. (2007) 'Sensory neuron sodium channel Nav1.8 is essential for pain at low temperatures', *Neuroforum*, 13(3), pp. 100–101. doi: 10.1038/nature05880.

Zimmermann, K., Lennerz, J. K., Hein, A., Link, A. S., Kaczmarek, J. S., Delling, M., Uysal, S., Pfeifer, J. D., Riccio, A. and Clapham, D. E. (2011) 'Transient receptor potential cation channel, subfamily C, member 5 (TRPC5) is a cold-transducer in the peripheral nervous system', *Proc Natl Acad Sci U S A*. 2011/10/26, 108(44), pp. 18114–18119. doi: 10.1073/pnas.1115387108.

Zimmermann, K., Lennerz, J. K., Hein, A., Link, A. S., Kaczmarek, J. S., Delling, M., Uysal, S., Pfeifer, J. D., Riccio, A. and Clapham, D. E. (2011a) 'Transient receptor potential cation channel, subfamily C, member 5 (TRPC5) is a cold-transducer in the peripheral nervous system', *Proc Natl Acad Sci U S A*. 2011/10/26, 108(44), pp. 18114–18119. doi: 10.1073/pnas.1115387108.

Zimmermann, K., Lennerz, J. K., Hein, A., Link, A. S., Kaczmarek, J. S., Delling, M., Uysal, S., Pfeifer, J. D., Riccio, A. and Clapham, D. E. (2011b) 'Transient receptor potential cation channel, subfamily C, member 5 (TRPC5) is a cold-transducer in the peripheral nervous system', *Proc Natl Acad Sci U S A*, 108(44), pp. 18114–18119. doi: 10.1073/pnas.1115387108.

Zitt, C., Strauss, B., Schwarz, E. C., Spaeth, N., Rast, G., Hatzelmann, A. and Hoth, M. (2004) 'Potent Inhibition of Ca2+ Release-activated Ca2+ Channels and T-lymphocyte Activation by the Pyrazole Derivative BTP2', *Journal of Biological Chemistry*, 279(13), pp. 12427–12437. doi: 10.1074/jbc.M309297200.

Zuccolo, E., Bottino, C., Diofano, F., Poletto, V., Codazzi, A. C., Mannarino, S., Campanelli, R., Fois, G., Marseglia, G. L., Guerra, G., Montagna, D., Laforenza, U., Rosti, V., Massa, M. and Moccia, F. (2016) 'Constitutive Store-Operated Ca(2+) Entry Leads to Enhanced Nitric Oxide Production and Proliferation in Infantile Hemangioma-Derived Endothelial Colony-Forming Cells.', *Stem cells and development*. Mary Ann Liebert, Inc. 140 Huguenot Street, 3rd Floor New Rochelle, NY 10801 USA , 25(4), pp. 301–19. doi: 10.1089/scd.2015.0240.

Zurborg, S., Yurgionas, B., Jira, J. A., Caspani, O. and Heppenstall, P. A. (2007) 'Direct

activation of the ion channel TRPA1 by Ca2+', *Nature Neuroscience*, 10(3), pp. 277–279. doi: 10.1038/nn1843.

Zweifach, A. and Lewis, R. S. (1993) 'Mitogen-Regulated Ca2+ Current of T-Lymphocytes Is Activated by Depletion of Intracellular Ca2+ Stores', *Proceedings of the National Academy of Sciences of the United States of America*, 90(13), pp. 6295–6299.

Appendix A. Basic Logic Gates

Table 14 Basic logic gates.
Table adapted from www.educationscotland.gov.uk/.../LogicGateImages_tcm4-719119.ppt

<table>
<tr><th>Logic</th><th>Schematic</th><th>Truth table</th><th>English expression</th></tr>
<tr><td>NOT</td><td> 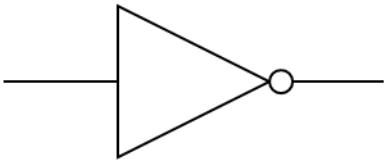 </td><td><table><tr><th>Input</th><th>Output</th></tr><tr><td>0</td><td>1</td></tr><tr><td>1</td><td>0</td></tr></table></td><td>The output is the opposite of the input.</td></tr>
<tr><td>AND</td><td> 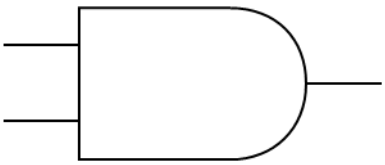 </td><td><table><tr><th>Input</th><th>Input</th><th>Output</th></tr><tr><td>0</td><td>0</td><td>0</td></tr><tr><td>0</td><td>1</td><td>0</td></tr><tr><td>1</td><td>0</td><td>0</td></tr><tr><td>1</td><td>1</td><td>1</td></tr></table></td><td>The only time the output is positive is when both inputs are positive.</td></tr>
</table>